ENERGY LABORATORY

MASSACHUSETTS INSTITUTE
OF TECHNOLOGY

TITAN: AN ADVANCED THREE DIMENSIONAL COUPLED NEUTRONIC/THERMAL-HYDRAULICS CODE FOR LIGHT WATER NUCLEAR REACTOR CORE ANALYSIS

by

D. P. Griggs, M. S. Kazimi and A. F. Henry

Energy Laboratory

and

Department of Nuclear Engineering

Massachusetts Institute of Technology
Cambridge, Mass. 02139

TITAN: AN ADVANCED THREE DIMENSIONAL COUPLED NEUTRONIC/THERMAL-HYDRAULICS CODE FOR LIGHT WATER NUCLEAR REACTOR CORE ANALYSIS

by

D. P. Griggs, M. S. Kazimi and A. F. Henry

June 1984

Sponsored by

Long Island Lighting Company
Northeast Utilities Service Company
Yankee Atomic Electric Company

under

MIT Energy Laboratory Electric Utility Program

Report No. MIT-EL 84-011

TITAN: AN ADVANCED THREE-DIMENSIONAL COUPLED NEUTRONICS/THERMAL-HYDRAULICS CODE FOR LIGHT WATER NUCLEAR REACTOR CORE ANALYSIS

by

Dan P. Griggs, Mujid S. Kazimi, Allan F. Henry

ABSTRACT

The accurate analysis of nuclear reactor transients frequently requires that neutronics, thermal-hydraulics and feedback be included. A number of coupled neutronics/thermal-hydraulics codes have been developed for this purpose. Of these, only a few combine three-dimensional neutronics and thermal-hydraulics, and these are either not generally available or too expensive for many applications of interest. Therefore, TITAN, a coupled code combining state-of-the-art three-dimensional neutronics and thermal-hydraulics models, was developed and tested.

The three-dimensional nodal neutronics code QUANDRY and the three-dimensional two-fluid thermal-hydraulics code THERMIT are combined into TITAN. Steady-state and transient coupling methodologies based upon a tandem structure were devised and implemented. Additional models for nuclear feedback, equilibrium xenon and direct moderator heating were added. TITAN was tested using a boiling water two channel problem and the coupling methodologies were shown to be effective. Simulated turbine trip transients and several control rod withdrawal transients were analyzed with good results. Sensitivity studies indicated that the time-step size can affect transient results significantly.

TITAN was also applied to a quarter core PWR problem based on a real reactor geometry. The steady-state results were compared to a solution produced by MEKIN-B and poor agreement between the horizontal power shapes was found. Calculations with various mesh spacings showed that the mesh spacings in the MEKIN-B analysis were too large to produce accurate results with a finite difference method. The TITAN results were shown to be reasonable. A pair of control rod ejection accidents were also analyzed with TITAN.

The computing time requirements for these analyses were less than 1 hour c.p.u. time on a large mainframe computer. This is reasonable for a severe transient in a large reactor.

A comparison of the TITAN PWR control rod ejection results with results from coupled point kinetics/thermal-hydraulics analyses showed that the point kinetics method used (adiabatic method for contol rod reactivities, steady-state flux shape for core-averaged reactivity feedback) underpredicted the power excursion in one case and overpredicted it in the other. It was therefore concluded that point kinetics methods should be used with caution and that three-dimensional codes like TITAN are superior for analyzing PWR control rod ejection transients.

Publications of the TITAN Project

Papers

1. D. P. Griggs, M. S. Kazimi and A. F. Henry, "TITAN: An Advanced Three-Dimensional Neutronics/Thermal-Hydraulics Code for LWR Safety Analysis," Proc. ANS Conf. on Advances in Reactor Physics and Core Thermal Hydraulics, Sept. 21-24, 1982, Kiamesha Lake, NY.

2. D. Griggs, C. Tsai, A. Henry and M. Kazimi, "TITAN: An Advanced Three Dimensional Coupled Code," Trans. Am. Nucl. Soc. 46, pp. 1984.

Technical Reports

1. D. P. Griggs, A. F. Henry and M. S. Kazimi, "Development of a Three-Dimensional Two-Fluid Code with Transient Neutronic Feedback for LWR Applications," MIT-EL 81-013, Energy Laboratory, M.I.T., April 1981 (NTIS #PB-82-180 217).

2. D. P. Griggs, M. S. Kazimi, and A. F. Henry, "Advanced Methods Development of LWR Transient Analysis, Final Report: 1981 - 1982," E-Lab Report No. MIT-EL 82-021, May 1982.

3. C. K. Tsai, D. P. Griggs, M. S. Kazimi and A. F. Henry, "Development and Quarter Core PWR Rod Ejection Accident Application of the TITAN Code, Final Report: 1982 - 1983," Energy Laboratory Report No. MIT-EL 83-007, June 1983.

4. C. K. Tsai, M. S. Kazimi and A. F. Henry, "TITAN Code Development for Application to a PWR Steam Line Break Accident," MIT-EL 84-014, July 1984.

5. D. P. Griggs, M. S. Kazimi and A. F. Henry, " TITAN: An Advanced Three Dimensional Coupled Neutronic/Thermal-Hydraulics Code for Light Water Nuclear Reactor Core Analysis," MIT-EL 84-011, June 1984.

ACKNOWLEDGEMENTS

This report is based on the Ph.D. thesis submitted by the first author to the Department of Nuclear Engineering at M.I.T.

Shih-Ping Kao and Chon-Kwo Tsai made significant contributions to this effort. Kao installed the original direct moderator heating model and updated the heat transfer package. Tsai improved the geometric flexibility of TITAN, prepared the PWR input data and performed some initial steady-state and rod ejection analyses. Thanks to them for these contributions.

Dr. Kord S. Smith of Argonne National Laboratory-West performed several QUANDRY calculations, thereby saving us time and expense. These calculations are significant in this work, so the author is grateful for Dr. Smith's help.

The author are grateful for the research and personal financial support which was provided by the following companies: Boston Edison Company, Long Island Lighting Company, Northeast Utilities Service Company, Public Service Electric and Gas Company, and Yankee Atomic Electric Company. The assistance of the M.I.T. Energy Laboratory in interfacing with the sponsors is also acknowledged. The first author is also grateful for personal financial support provided by the M.I.T. Department of Nuclear Engineering and especially by his parents, Mr. and Mrs. John J. Griggs.

The support staff of the M.I.T. Nuclear Engineering Department also made a significant contribution to this thesis. Particular thanks to

Gail Jacobson for her expert typing and cooperative spirit during the preparation of the manuscript. Additional typing contributions were made by Mary Shaffer and Marybeth Ferretti. Rachel Morton offered valuable assistance regarding computer systems and programming. The author is grateful for all these contributions.

Thanks to Chon-Kwo Tsai and Robert W. Green for their assistance with graphics. Also, thanks to E.P.M., Inc. for the use of graphics equipment.

TABLE OF CONTENTS

LIST OF FIGURES

LIST OF TABLES

DEDICATION

This thesis is lovingly dedicated to my parents, who were always there when I needed them and who gave generously of their financial resources so that this work could be completed.

CHAPTER 1: INTRODUCTION

1.1 Research Objectives and Scope

The objective of the current work is the development and assessment of a state of the art three-dimensional coupled neutronics/thermal-hydraulics code for the analysis of light water reactor transients. The code has been named TITAN, an acronym for three-dimensional integrated thermal-hydraulics and neutronics.

The development of TITAN involved the merging of existing codes for neutron kinetics and thermal-hydraulics and the addition of coupling logic and other models. The three-dimensional steady-state and transient nodal diffusion code QUANDRY [S-1] was selected for the neutronics portion of TITAN. The three-dimensional steady-state and transient, two-fluid code THERMIT [K-1] was selected for the thermal-hydraulics portion. QUANDRY and THERMIT are discussed in Chapter 3.

The application and assessment of TITAN involved several secondary objectives that may be summarized as follows:

1. To devise and implement a coupling methodology for TITAN.
2. To demonstrate the feasibility and proper implementation of the coupling methodology.
3. To compare results obtained with TITAN to those obtained with comparable coupled codes.
4. To perform sensitivity studies in order to assess selected modeling options.
5. To investigate the need for full space-time analysis of reactor transients.
6. To assess the computing time required to perform steady-state and transient analyses.

These objectives were addressed through TITAN analyses of a small BWR-type test problem and a larger PWR model. The BWR-type test problem was used to demonstrate the coupling methodology and for sensitivity studies. Steady-state and various transient analyses were performed for this problem. The PWR model was used to analyze a severe reactivity transient, the control rod ejection accident. The need for full space-time analytical capability was investigated by performing a point kinetics analysis of two PWR control rod ejection accidents.

1.2 Approaches to Reactor Safety Analysis

1.2.1 Reactor Safety

The fundamental goal of nuclear reactor safety is to protect the public from exposure to the radioactive by-products of the fission process. This goal is addressed by a design philosophy called defense-in-depth in which multiple barriers are placed between the radioactive elements and the public. For a light water reactor (LWR), the greatest amount of the radioactivity is produced directly in the fuel pellets. This radioactivity is segregated from the public by three levels of barriers, namely, the fuel cladding, the reactor pressure vessel and the containment building. Maintaining the integrity of these three barriers for both normal and off-normal conditions is the primary task of nuclear reactor safety engineering. It is during certain off-normal occurrences that the barriers could be threatened. The LWR design approach is that the consequences of all anticipated transients and several postulated accidents be mitigated by conservative design and engineered safety features.

1.2.2 The Role of Computer Codes

In order to insure that the safety goal can be met, it is necessary to assess the consequences of various accident scenarios. Because of the impracticality and undesirability of actually testing power plants under accident conditions, analytical simulations are performed using computer programs (often called codes). These computer codes attempt to simulate the important physical processes through numerical solutions of systems of mathematical equations, empirical correlations and tabular data. Computer codes are tools which can be used to predict the response of a nuclear reactor (or component thereof) to some situation of interest. As a result, the codes have become central to the design, safety analysis and licensing of nuclear power plants.

The ideal analysis of LWR transients requires computer codes capable of modeling diverse physical processes and their interactions. These processes include neutron physics, fluid dynamics, heat transfer, structural mechanics, materials behavior, chemical reactions and electronics. The complexity of the involved phenomena and the detail with which they often must be treated makes an all-encompassing, fully-integrated transient analysis code impractical if not impossible. In practice, codes have been developed to address a portion of the problem, the assumption being made that the remainder can be reasonably decoupled or neglected in the analysis. The subdivisions of the problem tend to be placed at the natural boundaries of the system. Thus, fuel performance codes (and experimental data) can provide the fuel failure criteria needed for core thermal-hydraulics analyses, and reactor system codes can produce the transient steam releases needed for containment analysis codes. These subdivisions do not impair the accuracy of the

analysis as long as no significant interactions are neglected.

1.2.3 Coupled Neutronics/Thermal-Hydraulics Codes

Within the core, the integrity of the fuel is the primary concern. This integrity can be assured if the transient balance between power production and heat removal is sufficient to prevent fuel melting or cladding damage. Very often the analysis of core transients has been subdivided into an analysis of the power production in the core and a separate analysis of the heat removal. This subdivision does not reflect geometrical boundaries, rather it reflects the assumption of independence between the processes involved. From a thermal-hydraulics perspective, the assumption is that the power generation is independent of the heat removal. The equivalent assumption from the reactor physics perspective is that the reactor criticality is independent of the power production. Many codes have been developed which can model the core neutronics and predict the time-dependent power production. Similarly, many codes have been developed to calculate the time-dependent heat removal in the reactor core.

The assumed independence of neutronic and thermal-hydraulic processes does not necessarily imply the independence of neutronic and thermal-hydraulic analyses, however. The thermal-hydraulics code requires that the space- and time-dependent heat source (fission rate) be supplied. The neutronics code requires some knowledge of the temperatures and densities of the important core materials in order to determine the nuclear cross sections. Furthermore, the assumption of independence requires that several potentially important interaction mechanisms be neglected. These interaction mechanisms are known as feedback effects because they make the power generation dependent on the heat removal.

Feedback effects have also been defined as those processes whereby the reactor operating conditions affect the criticality of the core [D-1]. The criticality of the core is dependent on, among other things, the atomic densities of the core and the probabilities of the various interactions of core materials with neutrons. Feedback effects imply that as the power level changes, the core atomic densities and/or nuclear interaction probabilities also change. When feedback effects are included in a core analysis, the power generation and heat removal (criticality) are linked together in a closed loop, as shown in Figure 1.1.

1.3 Nuclear/Thermal-Hydraulic Feedback Mechanisms

1.3.1 Introduction

The core of an operating nuclear reactor is an environment in which many important nuclear reactions combine to create a balance between the production and destruction of neutrons. Changes in the temperatures and densities of core materials affect this balance by modifying the relative reaction rates of the competing nuclear reactions. The impact of these changes may be quantified in terms of global parameters such as core power or core (average) temperature coefficients of reactivity. Such parameters are useful for the discussion of gross reactor behavior. However, since the global parameters are the net effect of several different mechanisms, it is necessary to consider the individual mechanisms in order to understand the global behavior. Furthermore, the individual feedback mechanisms may have pronounced spatial distributions within the core. These considerations motivate the examination of the basic feedback mechanisms in some detail.

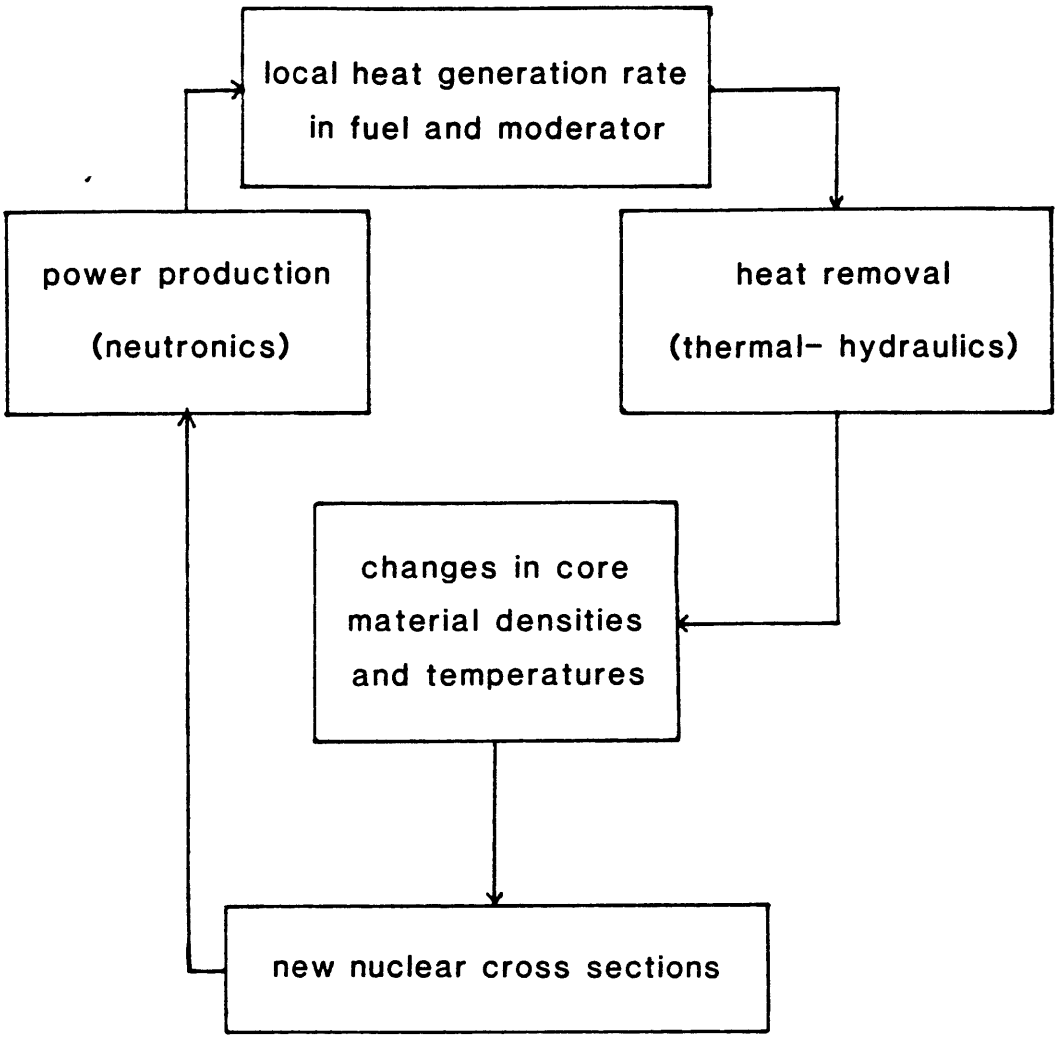

Figure 1.1 Schematic of a Reactor Core Feedback Loop

Yasinsky [Y-1] has classified the feedback mechanisms as consisting of two types:

1. Pure temperature effects, which involve the microscopic reactor properties,
2. Composition effects, which involve the density of the reactor materials.

This classification requires that the feedback mechanisms be examined at a very fundamental level, since changes in density and temperature of reactor materials usually occur simultaneously. Hence, the assessment of a pure temperature effect requires a change in temperature at constant density, while the pure density effect requires a change in density at constant temperature. This is the framework for the discussion that follows. It should be noted that composition effects can also be construed to include changes in isotopic composition due to nuclear reactions. These include the depletion of fissile material and the production of fission products. These composition effects are not considered here, since they do not arise directly from the heat removal process and are therefore not contributors to thermal-hydraulic feedback.

1.3.2 Nuclear Doppler Effect

The temperature of the fuel contributes to the thermal-hydraulic feedback through the nuclear Doppler effect. This important feedback mechanism is a consequence of the existence of resonances in the neutron cross section and the lumping of the fuel into rods.

The probability that a neutron will interact with a target nucleus is dependent on the kinetic energy of the neutron or, more precisely, on the relative speeds of the neutron and target. Some nuclides react very strongly and selectively with neutrons having particular speeds

relative to their nuclei. These points in the neutron energy spectrum where the microscopic cross sections are very large are known as resonances. The cross sections at these resonance energies may be several orders of magnitude higher than at surrounding neutron energies. The effect of a particular resonance is often seen for a very narrow energy range, leading to sharp peaks in the cross section energy dependence. Nuclides may exhibit resonances for neutron capture, scattering, or fission reactions. The fertile isotope U^{238} exhibits large neutron capture resonances for neutron energies in the epithermal region, while fissile isotopes have resonances for both capture and fission. The absorption of neutrons by non-fissile species in the fuel competes with the fission process and therefore affects the core reactivity.

The nuclear Doppler effect arises because the target nuclei belong to atoms which are not stationary, but move continuously as a result of their thermal kinetic energy. This thermal motion is dependent on the temperature of the material, increasing as the temperature increases. The motion of the target nuclei produces relative speeds which may be greater or less than the speed of an approaching neutron. Indeed, the thermal motion is significant enough that even a monoenergetic beam of neutrons impinging on a target would seem to have a continuous energy spectrum [L-1]. For neutrons having energies close to that of a resonance, the thermal motion of the nuclei may be significant in determining whether a neutron will fall in the range of the resonance.

Changes in the fuel temperature produce changes in the thermal motion of the atoms, affecting the probability that a given neutron will be absorbed in a resonance. When the cross section is averaged over

the motions of the nuclei, the shape of the resonances is effectively shortened and widened. This phenomenon, illustrated in Fig. 1.2, is known as Doppler broadening and is analogous to the Doppler shift of the frequencies of light and sound waves reflecting off moving targets. Figure 1.2 shows that the broadening increases as the temperature increases, resulting in a decrease in the cross section for energies close to the peak and an increase in the cross section for other energies around the peak. The net effect of the broadening depends on the integral of the cross section over the resonance and on the energy spectrum of the neutrons. In general, the integral of the cross section over the energy width of the resonance will change with temperature [D-1]. However, for the resonances of interest and the temperatures encountered in reactors, the change is rather small and it is usually assumed that the resonance integral is a constant. Thus, if the resonance absorbers are uniformly distributed in the reactor and relatively dilute in concentration, the broadening of resonances has no reactivity effect [T-1].

The reactivity effect of the Doppler broadening occurs because the lumping together of the resonance absorbers in the fuel causes a depression in the neutron flux, both spatially and at certain energies. These flux depressions are most pronounced for the energies of the absorption resonances because the resonance cross sections are so large that relatively few neutrons at those energies escape being absorbed in the outer part of the fuel. This effect is known as resonance self-shielding. As the temperature of the fuel increases, the effective width of the resonances increases while the peak cross section decreases. Nevertheless, the density of resonance absorbers in the fuel is so great that any neutron having an energy in the range of

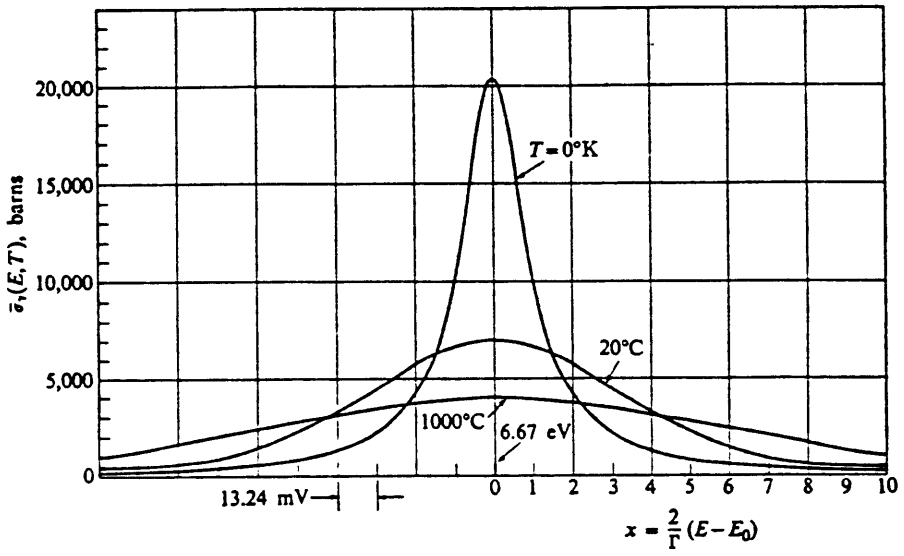

Figure 1.2 Doppler Broadening of the Capture

Cross Section of U^{238} at the 6.67 eV Resonance L-2

the resonance is absorbed. Thus, an increase in the fuel temperature results in a net increase in the resonance absorption of neutrons and a decrease in reactivity.

This negative fuel temperature feedback is very important because it helps make a reactor stable against power excursions. Another important aspect of this mechanism is its rapid response to power changes. Since almost all of the power is produced in the fuel, the temperature responds rapidly to power changes and the feedback effect is quickly felt. Hence, the fuel temperature feedback mechanism is often called prompt feedback. The magnitude of the feedback from changes in the fuel temperature is much greater than that contributed by changes in the temperature of the metal cladding, so that usually only the fuel feedback is modeled [L-3]. The fuel temperature also has a slight effect on the thermal neutron energy spectrum, but this is quite small in comparison to the impact on resonance absorption [L-3].

1.3.3 Moderator Temperature Feedback

The moderator temperature can also be an important source of reactivity feedback. The neutrons produced by fission (either directly or by decay of fission products) undergo collisions with the moderator until they are absorbed (in the fuel, structure, or moderator) or lost by leakage. The neutrons approach (but never attain) thermal equilibrium with the moderator atoms, resulting in an energy distribution which is approximately that of the classic Maxwell-Boltzmann distribution in the thermal range plus an inverse-energy distribution in the slowing-down range [L-3]. The Maxwellian distribution has a characteristic temperature close to that of the moderator, so that a change in moderator temperature produces an approximately equal change in the

characteristic temperature and, hence, in the mean thermal neutron energy [T-1]. Thus, an increase in the moderator temperature results in an increase in the mean energy of the thermal neutrons and produces a slightly harder spectrum. Unlike the fuel temperature effect, the moderator temperature feedback mechanism does not involve resonance absorption [L-3]. In addition, the moderator absorption cross section is insensitive to changes in the thermal neutron spectrum. Rather, the reactivity impact of moderator temperature changes occurs because of the energy dependence of the ratio of fuel fission to capture cross sections for thermal neutrons. In particular, the hardening or softening of the thermal spectrum affects the ratio of fissions to absorption in fissile material and the relative absorptions in fissile and non-fissile materials. The reactivity impact of a moderator temperature change is negative for the principal fissile materials found in LWRs, U-235 and Pu-239. As in fuel temperature feedback, this tends to increase the stability of a nuclear reactor since an increase in power produces a negative moderator temperature reactivity feedback effect.

1.3.4 Moderator Density Feedback

The second category of feedback effects involves changes in the atomic compositions within the reactor caused by changes in the power production and heat removal. As previously mentioned, changes in atomic composition produced by nuclear reactions are not categorized as feedback effects. The amount of fuel and structural material in a core is essentially constant, while the amount of coolant/moderator can vary significantly under accident conditions. Consequently, the most

significant contributor to atomic composition feedback is a change in the density of the moderator and/or coolant. The thermal expansion of the moderator/coolant is much more significant than that of the other core materials and the possibility of boiling provides a dramatic mechanism for changing the atomic composition. In LWRs, the water serves both as coolant and moderator, so two competing mechanisms contribute to the density feedback. A decrease in the moderator density leads to a decrease in the absorption of thermal neutrons by the moderator, a positive reactivity effect. Conversely, a decrease in the moderator density reduces the moderation rate of fast neutrons, resulting in a hardening of the spectrum. The ratio of epithermal to thermal neutron flux is increased and the shape of the epithermal distribution may also be changed [T-1]. The thermal spectrum also tends to move away from equilibrium with the moderator as the ratio of moderator to fuel atoms decreases [L-3].

The spectrum changes associated with a decrease in moderator density produce several different effects. A small increase in fast fission occurs because neutrons are not removed from the high energy regions as effectively. A far more significant effect is that the slowing down of neutrons past the resonance energies is less effective, leading to an increase in resonance absorption in the fuel. For neutrons which reach thermal energies, the hardening of the thermal spectrum produces changes in the relative production and destruction of neutrons in the fuel (as discussed previously for moderator temperature feedback).

The net reactivity impact of these competing processes depends on the relative absorption/moderation characteristics of the moderator and the relative volumes occupied by the fuel and moderator. Water is a better moderator than absorber so that the decrease in absorption in the moderator is usually more than offset by the spectrum changes and the reactivity effect of a decrease in moderator density is negative. However, it is possible for the fuel and moderator in a reactor to be arranged such that the optimum atomic ratio of moderator to fuel is exceeded, leading to an "overmoderated" lattice. This is illustrated in Figure 1.3. Under these circumstances, a decrease in the moderator density leads to a positive reactivity impact. However, LWRs are usually undermoderated, so the reactivity impact of decreased moderator density is negative. This is particularly important in a BWR, which uses the strong feedback from boiling as a primary control mechanism.

The use of soluble boron in the moderator of a pressurized water reactor (PWR) changes the moderator density feedback somewhat. The soluble boron is a neutron absorber used to control the excess reactivity present at the beginning of a fuel cycle. This effectively changes the relative absorption/moderation characteristics of the moderator, since a decrease in the water density also produces a decrease in boron concentration. This causes the reactivity impact of a decrease in moderator density to be less negative or, in some cases, can cause it to be positive.

A final impact of moderator density on reactivity involves control rods. The reactivity worth of a control rod is approximately proportional to the thermal migration length of the surrounding lattice [L-1].

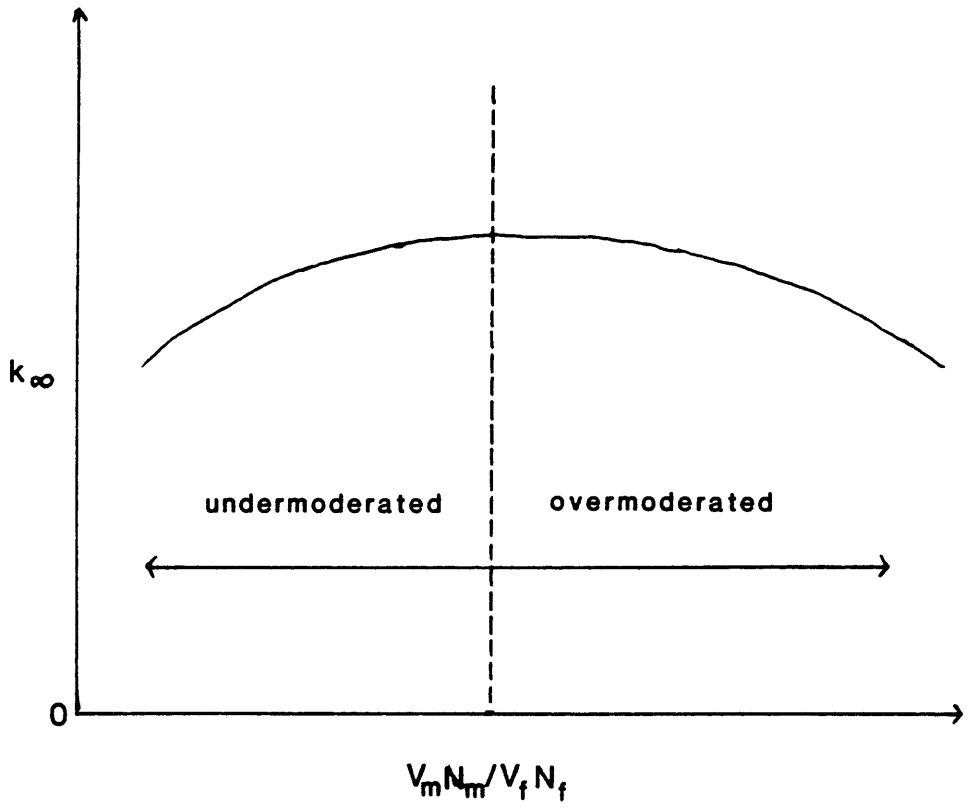

Figure 1.3 Effect of Moderator-to-fuel Atom Ratio on Multiplication Constant for an Infinite Reactor L-3

(The thermal migration length is the square root of the sum of the squares of the slowing-down length and the thermal diffusion length.) The migration length increases as the moderator density decreases. Thus, a control rod becomes more effective as the density of the surrounding moderator decreases. Therefore, the presence of a control rod makes the reactivity change due to a decrease in moderator density more negative.

1.3.5 Other Feedback Effects

Changes in the density of fuel and structural materials can also have a reactivity impact. The thermal expansion of the fuel and structure can lead to an increased core volume, leading to decreased reactivity because of greater neutron leakage. For large power reactors this leakage effect is usually quite small. The expansion of the fuel and cladding can also change the atomic composition if the coolant does not expand the same amount. Both of these effects are usually neglected for thermal reactors, but may be significant in fast reactors. One type of fuel composition feedback that is often considered in LWRs is fuel rod bowing. Radial flux gradients produce a non-uniform thermal expansion of the fuel rod which cause the assemblies to bow in the direction of the gradient (usually toward the center of the core). This affects the local atomic composition and, hence, the reactivity. Changes in fuel rod bowing are usually neglected during transient analyses.

1.4 Applications of Coupled Analysis with Feedback

Some or all of the feedback mechanisms described previously are often neglected in reactor analyses. Presumably, the assumption is made

that this results in acceptably small and/or conservative errors. Such assumptions are valid for certain types of reactor conditions, particularly when the objective of the analysis is to demonstrate compliance with licensing requirements rather than to produce realistic results. Neglecting feedback altogether can be justified when the power level in a reactor is very low. Under these conditions the implied independence of the criticality determination from the power level is valid [L-3]. Feedback may also be unimportant when the nuclear chain reaction is shut down, as in a successful scram. For example, feedback is quite appropriately neglected in the analysis of a large break loss of coolant accident, since the loss of moderator effectively terminates the nuclear chain reaction. The power produced by the decay of fission products and actinides is not affected by feedback.

Some rapid reactivity insertion transients have been analyzed accounting only for fuel temperature feedback. These analyses assume an adiabatic heatup for one or more representative fuel rods. This is justified when the time constant for the conduction of heat to the coolant is large compared to the duration of the reactivity insertion and the Doppler effect is large compared to the moderator feedback mechanisms. This type of analysis yields conservative results and therefore may be quite appropriate for licensing applications.

Even though feedback effects can sometimes be wholly or partially neglected, there exist many transients for which coupled neutronics/thermal-hydraulics codes are needed. These transients may be categorized as either neutronically or thermal-hydraulically driven, depending on the initiating event. For a PWR, feedback effects should be considered for any reactivity insertion accident [T-2]. The ejection or

uncontrolled withdrawal of a control rod (or rods) is an example of such an accident. The PWR rod drop accident, in which a withdrawn control rod accidentally drops into the core, may also require feedback to be modeled. In this accident, the reactor power decreases and the flux shape is perturbed, possibly causing an increase in some of the core peaking factors. Without protective action, the automatic control system automatically withdraws other control rods to restore the initial power level [I-1]. This could lead to DNB, depending on the perturbed power shape.

The steamline break accident is an example of a thermal-hydraulically driven PWR transient requiring a coupled analysis [M-1]. It is usually assumed that the cooldown of the primary coolant is combined with the failure of the most reactive control rod to scram. Certainly, the analysis of an anticipated transient without scram (ATWS) requires a coupled code with feedback.

The boiling water reactor (BWR) provides even more situations which require consideration of feedback effects. The feedback caused by the boiling of the moderator is a fundamental control mechanism of a BWR. As a result, feedback should be included in nearly all BWR analyses [Z-1]. Reactivity transients such as the control rod withdrawal accident are strongly affected by both fuel temperature and moderator density feedback [C-1]. Thermal-hydraulic transients in which a delayed or partial scram occurs require the modeling of feedback. Examples of such transients are the failure of a feedwater heater or the startup of an inactive, cold recirculation loop. Overpressurization transients such as the turbine trip event also fall into this category. As in the PWR, a coupled analysis is required for any ATWS event [D-2].

It has also been shown that the interaction of neutronics and thermal-hydraulics is significant in the analysis of density-wave oscillations, affecting the stability margin of BWRs [P-1].

The discussion in this section shows that, while a coupled neutronics/thermal-hydraulics analysis with feedback is not necessary for many transients of interest, the type and number of transients for which coupled analysis is desirable or even necessary are of sufficient importance to motivate the development of computer codes capable of performing such analyses. As the desire for more realistic analytical tools increases, the need for improved coupled codes will likewise increase. The current work is a response to this need.

CHAPTER 2: APPROACHES TO COUPLED NEUTRONIC/ THERMAL-HYDRAULIC ANALYSIS

2.1 Overview of Existing Coupled Codes

2.1.1 Introduction

The importance of feedback in the analysis of reactor transients was recognized early in the history of commercial nuclear power. Accordingly, computer codes capable of modeling feedback effects have been developed and applied for at least twenty years. More than fifty such codes of varying sophistication have been reported in the literature. Diamond [D-2] has identified two general types of coupled codes. The first type accounts for fuel depletion and fission product buildup. They may be applied to steady-state analyses during a given fuel cycle and to slow transients such as those caused by changing xenon concentration. Codes of this type which permit a fully three-dimensional representation of the core are frequently called core simulators.

The second type of coupled codes are called core dynamics codes. They combine time-dependent thermal-hydraulics and neutron kinetics along with the appropriate feedback mechanisms. Such codes are used for analyses of accidents and operational transients. They may represent the reactor core in either one, two or three dimensions and usually are also capable of calculating steady-state conditions. Core dynamics codes have been developed for application to LWRs, LMFBRs, gas cooled reactors and heavy water reactors. In addition to the two general types of coupled codes, there are some codes which combine neutronics with very simple approximate feedback models. An example is the CYCLOPS code [B-1], which has a fuel temperature feedback model

but does not have a model for the coolant thermal-hydraulics or feedback. These codes may be applicable to some of the same transients as the more complex core dynamics codes.

A review of the existing coupled neutronics/thermal-hydraulics codes has been performed in order to assess their capabilities and limitations. The review enabled the current work to benefit from the experience gained with the other codes. It also serves to give a perspective on the current work, illustrating the unique status of TITAN among existing core dynamics codes. Core simulators were not included in the review, nor were codes having simplified feedback representations. Appendix A contains detailed summary descriptions of the thirty-three codes reviewed. Included in this group are many of the publicly available LWR and liquid metal fast breeder reactor (LMFBR) core dynamics codes, as well as a few proprietary codes for which open literature descriptions are available. An overview of this review is presented here.

2.1.2 Coupled Code Reactor Models

Table 2.1 summarizes the important features of the coupled codes reviewed. TITAN is included for comparison purposes. The table reveals that the existing coupled codes have a wide spectrum of capabilities and applications. Of the thirty-three codes, twenty-seven are applicable to PWRs, sixteen are applicable to BWRs, and ten are applicable to LMFBRs. Fifteen of the codes can perform both PWR and BWR analyses. However, nine of these do not permit the modeling of open channels with cross-flow. Nevertheless, these codes are considered applicable to certain PWR analyses [C-2]. Five of the codes are applicable to

Table 2.1

Comparison of Coupled Neutronics/Thermal-hydralics Codes

		Neutronics										Thermal-hydraulics						
		Reactor Type			Dimensions				Energy Groups			Dimensions		Two-Phase Flow				LOOP
Code	Ref.	PWR	BWR	LMFBR	PK	1	2	3	1	2	*	1D	3D	NB	HEM	#	TF	
NOWIG	Y-2	X			X					X		X		X				
FORE	G-1	X		X	X						X	X		X				
FORE-II	F-1	X		X	X						X	X		X				
"FORE-III"	H-1	X		X	X						X	X		X				
CHIC-KIN	R-1	X	X		X						X	X			X			
PARET	O-1	X	X		X						X	X			X			
NAIADQ	D-3	X	X		X						X	X				X		
THIOD-K	D-4	X	X		X						X	X					X	
THERMIT-3	D-4	X	X		X						X	X	X				X	

Key: PK - Point Kinetics; NB - No Boiling; HEM - Homogeneous Equilibrium Model; TF - Two-Fluid Model

*energy groups irrelevant for point kinetics code

#NAIADQ - homogeneous non-equilibrium model

Table 2.1 (continued)

		Reactor Type			Neutronics									Thermal-hydraulics				
					Dimensions				Energy Groups			Dimensions		Two-Phase Flow				LOOP
Code	Ref.	PWR	BWR	LMFBR	PK	1	2	3	1	2	*	1D	3D	NB	HEM	#	TF	
WIGL2	H-2	X				X				X		X		X				
WIGL3	V-1	X				X				X		X		X				
ALMOS	F-2	X	X			X				X		X			X			X
RETRANO2	M-2	X	X			X				X		X				X		X
TWIGL	Y-3	X					X			X		X		X				
ADEP	D-5	X				X	X		X	X	X	X		X				
CONSTANZA(R,Z)	V-2	X		X			X			X	X	X		X				
RADYVAR	K-2	X					X		X	X	X	X		X				
COTRAN	P-2	X	X				X		X			X			X			

Key: PK - Point Kinetics; NB - No Boiling; HEM - Homogeneous Equilibrium Model; TF - Two-Fluid Model.

*ADEP - arbitrary number of groups; COSTANZA(R,Z), COSTANZA-CYINDRICAL - up to 10 groups; RADYVAR - up RADYVAR - up to 6 groups.

RETRANO2 - equilibrium with dynamic slip.

Table 2.1 (continued)

		Neutronics										Thermal-hydraulics						
		Reactor Type			Dimensions				Energy Groups			Dimensions		Two-Phase Flow				LOOP
Code	Ref.	PWR	BWR	LMFBR	PK	1	2	3	1	2	*	1D	3D	NB	HEM	#	TF	
BNL-TWIGL	D-6	X	X				X			X		X			X			
QUANDRY	S-1	X					X	X		X		X		X				
MEKIN	B-2	X	X					X	X	X		X	X		X			
MEKIN-B	A-1	X	X					X	X	X		X	X		X			
BWKIN	M-3	X	X					X	X	X		X	X		X			
HERMITE	R-2	X	X			X	X	X	X	X	X	X	X		X			
CRONOS	K-3	X	X					X			X	X			X			
ANTI	L-4	X	X					X	X			X	X			X		
RAMONA-3B	W-1		X					X			X	X				X		X

Key: PK - Point Kinetics: NB - No Boiling: HEM - Homogeneous Equilibrium Model: TF - Two-Fluid Model

*HERMITE - up to 4 groups: RAMONA-3B - 1 1/2 group model.

#ANTI - drift flux model; RAMONA-3B - non-equilibrium with slip model.

Table 2.1 (continued)

		Neutronics										Thermal-hydraulics						
		Reactor Type			Dimensions				Energy Groups			Dimensions		Two-Phase Flow				LOOP
Code	Ref.	PWR	BWR	LMFBR	PK	1	2	3	1	2	*	1D	3D	NB	HEM	#	TF	
TITAN	——	X	X					X		X		X	X				X	
FREADM-1	F-3			X	X						X	X		X				X
SAS1A	C-3			X	X						X	X		X				X
SAS2A	D-7			X	X						X	X		X				X
SAS3A	S-3			X	X						X	X		X				X
COSTANZA-CYL.	A-2			X		X				X	X	X		X				
FX2-TH	S-2			X		X	X		X	X	X	X		X				

Key: PK - Point Kinetics; NB - No Boiling; HEM - Homogeneous Equilibrium Model; TF - Two-Fluid Model

*enery groups irrelevant for point kinetics code; COSTANZA-CYLINDRICAL - up to 10 groups; FX2-TH - up to 4 groups.

either PWRs or LMFBRs. This is possible because the codes allow fluid properties and heat transfer correlations to be supplied. The geometrical representations possible with the codes range from a single channel to a full core. Seven codes can also model the reactor loop, including four which are strictly for LMFBRs, one which is strictly for BWRs, and two which are either PWRs or BWRs.

2.1.3 Coupled Code Neutronics Models

All the coupled codes reviewed use some formulation of the neutron diffusion equations or the point kinetics approximation for their neutronics models. Point kinetics is used in thirteen codes, five used one-dimensional diffusion theory, seven used two-dimensional diffusion theory and eight used three-dimensional diffusion theory. Most of the diffusion theory codes represent two prompt energy groups and six delayed precursor groups. The numerical solution techniques included finite difference, finite element and nodal methods.

2.1.4 Coupled Code Thermal-Hydraulics Models

The thermal-hydraulic models of the coupled codes used several techniques to calculate the reactor conditions. Twenty-three codes assume water as the coolant, five assume sodium, and five can analyze any single phase coolant. Twenty-seven of the codes assume one-dimensional flow in solving the coolant conservation equations, while the fluid dynamics models of the remaining six codes can analyze three-dimensional flow fields. The treatment of two-phase flow is another distinguishing feature of the coupled codes. Seventeen of the codes are applicable only to single phase flows, ten used a homogeneous equilibrium model (HEM) for two-phase flow, and the remaining six

use more advanced models. Several of the codes include models for subcooled boiling as well as critical heat flux correlations. The sophistication of the heat transfer and fluid flow calculations varies greatly among the codes, but all of them use a lumped parameter approach for the coolant. In this approach, the parameters determining the thermodynamic state of the coolant are assumed to be uniform within fixed control volumes. Both the lumped parameter and the distributed parameter approach are applied to the solution of the fuel rod heat conduction problem. In the simplest model, the fuel rod is treated as a single lumped heat capacity region. In the most complex models, a one-dimensional (radial) finite difference solution for the fuel pellet, gap, and cladding heat conduction equations with temperature-dependent thermal properties, gap conductance models and elaborate fuel/coolant heat transfer models are used. These differences can be significant, since the fuel temperatures, coolant temperatures and coolant densities are the primary feedback parameters.

2.1.5 Coupling Methodologies

The coupling between neutronics and thermal-hydraulics models is another important basis for comparison of the codes reviewed. Judged upon this basis, the codes are all remarkably similar. All the codes have their neutronics and thermal-hydraulics calculations performed separately with the feedback information passed between the two segments. This tandem coupling method involves the assumption that the feedback can be modeled as discrete step changes rather than continuous smoother functions of time and space. The integration carrying the thermal-hydraulics and neutronics forward in time is

performed assuming no feedback beyond the step change at the old time. In no case does a code attempt to solve the neutronics and thermal-hydraulics equations simultaneously. The codes using point kinetics couple the neutronics to the thermal-hydraulics via a reactivity feedback loop. This type of code requires the specification of reactivity feedback coefficients to enable changes in core thermal-hydraulic conditions to be translated into changes in the core neutronics. An exception to this is the NOWIG code [Y-2], which uses a neutron cross section model to determine the changes in reactivity due to thermal-hydraulic feedback. The coupled codes using spatial neutronics models also use cross section models for the thermal-hydraulic feedback. The most common feedback parameters are fuel temperature, coolant temperature and coolant density or void fraction. The cross section models usually assume that a given cross section can be approximated as a polynomial function (often linear) of the feedback parameters. A few codes use a tabular cross section library and an interpolation routine to account for changes in core thermal-hydraulics.

2.1.6 Summary

This overview indicates that different models are used in the existing codes, but does not address the limitations in accuracy or applicability implied by the various models. The next two sections address these questions for the neutronics and thermal-hydraulics models, respectively.

2.2 Assessment of Neutronics Models for Coupled Codes

2.2.1 Diffusion Theory

The neutronics model is very significant in determining the applicability, the accuracy, and the economy of a coupled code. All the codes reviewed used either the space-time neutron diffusion equations or the point reactor kinetics equations. The continuous-energy diffusion equation can be obtained from the rigorous Boltzmann transport equation when the diffusion theory approximation (Fick's Law) is applied [H-3]. For diffusion theory to be valid, the neutrons should behave like a gas diffusing through a porous medium. Mathematically, the angular distribution of the neutrons should be fairly uniform. In nuclear reactors, diffusion theory is generally valid except within or very near to strongly absorbing regions and near or outside of external boundaries.

The most rigorous neutronics models found in coupled codes consist of formulations of the three-dimensional time-dependent few group neutron diffusion and delayed neutron precursor equations. The delayed precursors are not all explicitly considered; rather, a few (typically one to six) equivalent precursor groups having atom densities, decay constants and neutron fractions representative of the entire population are used. Many codes use a less general, one or two-dimensional formulation of the diffusion equations (referred to herein as lower order methods). This requires the assumption that the spatial derivatives in the directions not modeled are zero. A two-dimensional neutronics model may represent the flux shape in a cylindrical (r,θ) or Cartesian plane (x,y), or the axial and radial flux shape in an

axisymmetric cylinder (r,z), or the axial and transverse flux shape in a symmetric slab (x,z). Similarly, a one-dimensional neutronics model may represent either the radial (r or x) or axial flux shape (z) in a reactor.

2.2.2 Point Kinetics

The point reactor kinetics model is the simplest and most restrictive neutronics model used in coupled codes. It is also the most widely used model for core transient analyses. The point kinetics equations describe the transient behavior of a reactor in terms of a few global parameters. These equations can be obtained rigorously from the time-dependent continuous-energy diffusion equations and delayed precursor equations by integrating over the volume of the reactor and the total range of neutron energies. By representing the flux as the product of an amplitude function and a shape function, the point kinetics parameters can be formally defined and the point equations obtained [H-3]:

$$\frac{dT(t)}{dt} = \frac{\rho-\beta}{\Lambda} T(t) + \sum_{i=1}^{I} \lambda_i C_i(t) + Q(t) \qquad (1.1)$$

$$\frac{dC_i(t)}{dt} = \frac{\beta_i}{\Lambda} T(t) - \lambda_i C_i(t) \qquad (i = 1,2,\ldots,I) \ , \qquad (1.2)$$

where

$T(t)$ = time-dependent amplitude function,

$C_i(t)$ = time-dependent concentration of the "i"-th delayed neutron precursor group,

$Q(t)$ = time-dependent rate of production of neutrons from "external" source

ρ = reactivity,

β = effective delayed neutron fraction,

Λ = prompt-neutron lifetime, and

λ_i = decay constant of the "i"-th delayed neutron precursor group.

The simplicity of these equations belies the fact that the time-dependent spatial part of the flux (the shape function) is needed in order to evaluate the reactivity, the effective delayed neutron fraction and the prompt-neutron lifetime. It is therefore necessary to make assumptions about the flux shape function in order to gain any benefit from the point formulation. The main assumption usually made is that the time-dependent shape function can be replaced by some time-independent shape function, often the initial unperturbed flux shape. Any other flux shape could be used if judged to be closer to the expected actual transient flux shape. This assumption can be justified for many perturbations on the grounds that the flux shape does in fact change little from the steady-state. In addition, the effective delayed neutron fractions can be reasonably considered time-independent in any case [H-3]. The time dependence of the prompt-neutron lifetime is also usually neglected, though this can result in serious errors for very fast transients with significant flux shape changes. Hence, the assumption of a time-independent shape function is most significant in the determination of the reactivity. The reactivity and the "external" neutron source, if any, are the driving forces behind the transient reactor behavior calculated with point kinetics. The reactivity is usually calculated via a first-order

perturbation theory definition which neglects the terms involving the product of the flux shape changes and the cross section changes. The use of adjoint flux weighting eliminates the first-order terms involving the flux shape changes, thus minimizing the error in the assumption of a time-independent shape function. Nevertheless, the second order terms can only be neglected if the perturbations are small. Practically, this method cannot be expected to yield adequate results for any transient in which flux shape changes are significant. In addition, the steady-state flux shape must be obtained by some auxiliary means. For coupled codes, the total reactivity calculation includes contributions from the thermal-hydraulics calculation via "reactivity coefficients" which are multiplied by changes in reactor material temperatures and densities. These coefficients may be global or have some spatial association. The feedback reactivity of individual regions is sometimes weighted by the square of the flux level in the region. In any event, the reactivity coefficients must also be determined by auxiliary means.

2.2.3 Limitations of Neutronics Models

2.2.3.1 General Remarks

The lower order neutronics models are less general and potentially less accurate than a three-dimensional neutronics model. Lower order methods have often been used for transient analyses in violation of the underlying assumptions of the methods. This has been justified on the grounds that the results were "conservative" because the analyses erred on the side of safety. The lower order methods have been investigated rather extensively in order to demonstrate their conservatism and to assess the magnitude of their errors.

2.2.3.2 Limitations of Point Kinetics

The point kinetics method has been quite heavily investigated because it is both the most restrictive and the most used method. This is the only method in which the spatial response of the neutron population is ignored. Yasinsky [Y-1] has identified three conditions for which point kinetics may be inaccurate:

1) an asymmetric perturbation of the reactor,
2) a reactor core which is large, and
3) a reactor core which is loosely coupled.

Any reactor subjected to a spatially non-uniform perturbation will experience spatially non-uniform transient adjustments in its neutron population [F-4]. These adjustments can have a significant effect on the course of reactor transients, particularly when feedback is present. Furthermore, the magnitude of the changes in flux shape due to local perturbations is directly proportional to reactor size [F-4]. A core which is large neutronically is one which has dimensions many times the neutron diffusion length. A loosely coupled core is one in which a perturbation at one point in the reactor takes several neutron lifetimes to be felt significantly at other points [Y-1]. In addition, the point method may not be satisfactory for large reactivity changes [M-2]. The transients for which point kinetics could be appropriate are therefore characterized as follows:

1) no significant flux tilting,
2) small, tightly coupled cores, and
3) small reactivity perturbations.

Point kinetics may also give satisfactory results for transients in which the reactor is immediately scrammed [M-2].

The application of point kinetics to a reactivity insertion transient in the absence of feedback was investigated by Yasinsky and Henry [Y-4]. A series of numerical investigations were performed to compare point kinetics to space-time kinetics. Two simple slab cores with material compositions typical of LWRs were used. A 240 cm thick core represented a loosely coupled reactor, while a 60 cm thick core represented a tightly coupled reactor. Both prompt critical and below prompt critical transients were initiated by asymmetric changes in the fission cross sections designed to accentuate non-separable space-time effects. The transients were analyzed by a standard point kinetics approach and also by the adiabatic method [H-4]. In the adiabatic method, it is assumed that the dynamic flux shape function may be adequately approximated by the static flux shape corresponding to the perturbed state of the reactor. This neglects the effect of the delayed neutrons; thus, the shape changes too rapidly and the reactivity is overestimated (in the absence of feedback) [Y-1]. A one-dimensional "exact" solution for the transients was obtained with the WIGLE [C-4] code.

A prompt critical transient was simulated for both reactors by step increases in the fission cross sections in a portion of the core followed by a ramp decrease of the same parameters. The WIGLE results showed substantial flux tilting for the large core and much less for the small core. The large core presented a very severe challenge for the conventional point kinetics method: a large, loosely coupled core perturbed asymmetrically with a large instantaneous reactivity insertion.

As might be expected, the point kinetics prediction of this transient was very poor. Figure 2.1 shows the time behavior of both the reactivity and amplitude functions for the prompt critical transient in the large core, as calculated by the three different methods. The point method is shown to be strikingly inadequate, consistently underpredicting the reactivity and underpredicting the maximum amplitude of the transient by four orders of magnitude. The adiabatic approximation is much better, though it overpredicts both the reactivity and the amplitude.

Figure 2.2 shows the time-dependent reactivity and amplitude function for the prompt critical transient in the small core. For this problem, the relatively small and tightly coupled core showed much less flux tilting than did the large core. It would therefore be expected that the performance of point kinetics would be improved over the large core results. Figure 2.2 verifies that this expectation was realized, although the improvement was not sufficient to recommend the method. As in the large core, the reactivity and amplitude function calculated with point kinetics were consistently below those values calculated with space-time kinetics. The maximum of the amplitude function is underestimated by a factor of four. The adiabatic approximation slightly over-predicted the reactivity and overpredicts the maximum amplitude by more than a factor of two. The improvement offered by the adiabatic method was much more significant for the large core.

Perhaps the most significant result is that the conventional point kinetics method yielded non-conservative results for both the large and the small core. Yasinsky and Henry concluded:

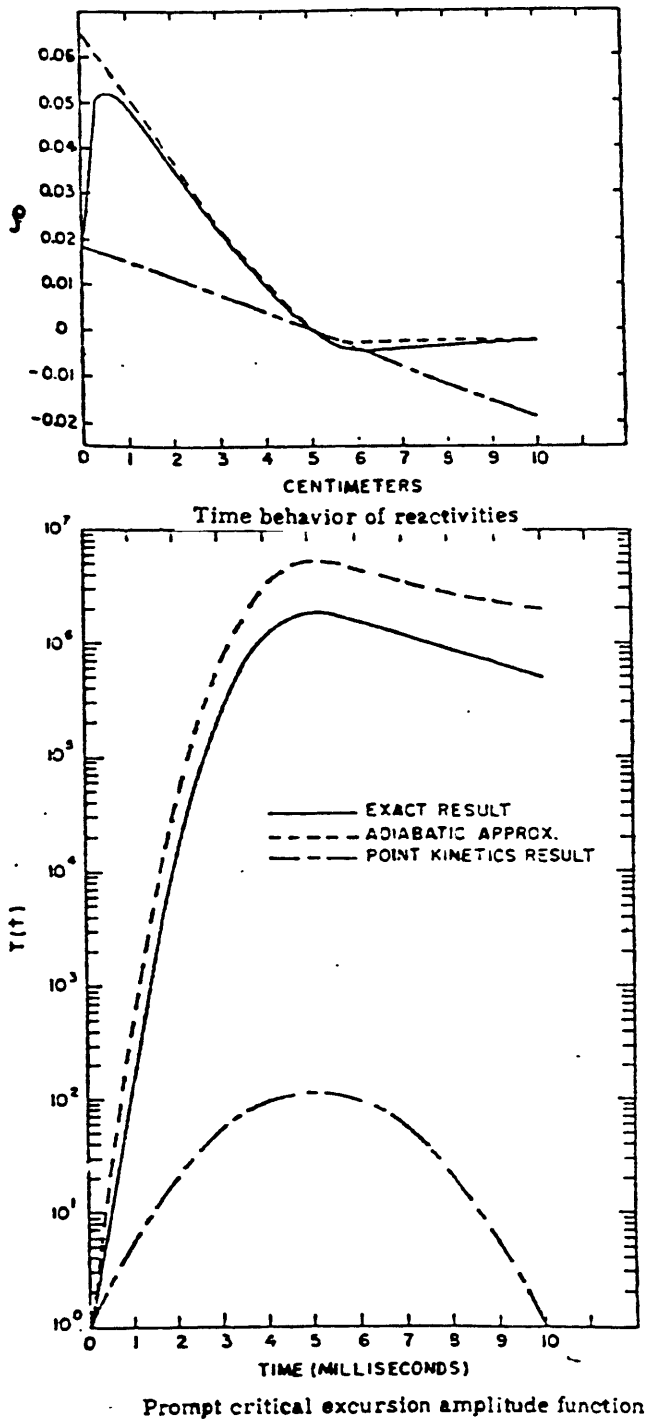

Figure 2.1 Assessment of Point Kinetics for Prompt Critical

Transient with No Feedback ,Large Core Y-4

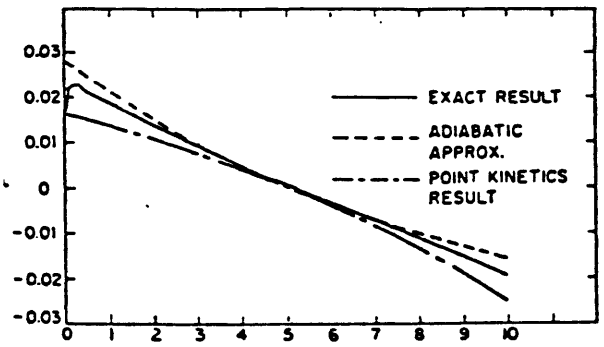

Time behavior of reactivities for a 60-cm core.

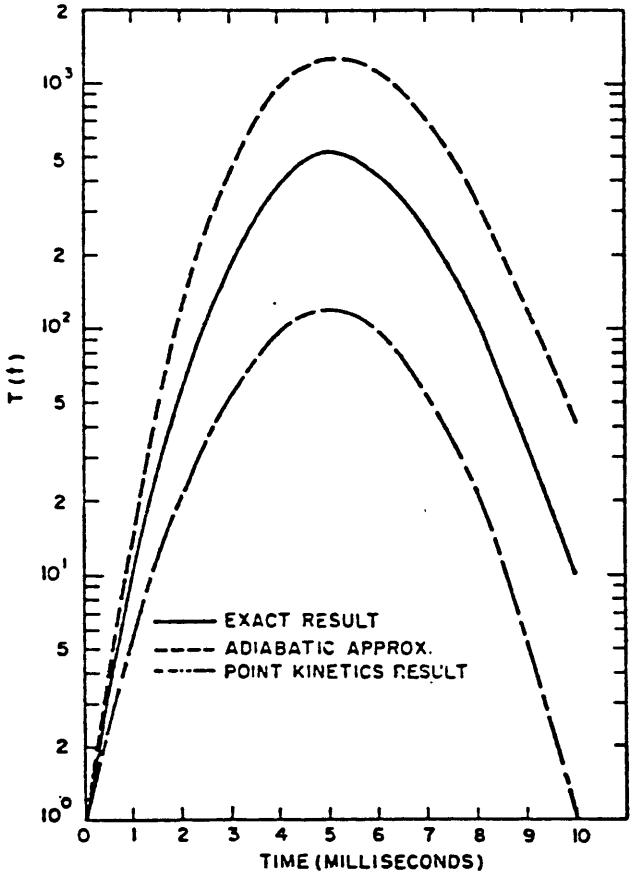

Prompt critical excursion amplitude function $T(t)$ for 60 cm core.

Figure 2.2 Assessment of Point Kinetics for Prompt Critical Transient with No Feedback, Small Core Y-2

> "... the fact that the error in the conventional point method is intrinsically so great for the large core lends considerable support to the view that this model should never be used to analyze prompt excursions in large reactors."

A below prompt critical transient was also analyzed with point kinetics, spatial kinetics and the adiabatic approximation for the two slab cores. Each core was perturbed by a localized ramp increase in the fission cross sections. For the large core, the point kinetics method was again quite unsatisfactory. The point kinetics method significantly underestimated the reactivity, the amplitude function and the flux as well as overestimating the asymptotic period. The adiabatic approximation was much better, yielding conservatively high values for reactivity, neutron flux and amplitude. The point kinetics results were acceptable only for the ramp excursion in the small core. The error in amplitude and period was no greater than 10%, though the error was again non-conservative. The adiabatic approximation was much better than point kinetics for this analysis, too.

The main conclusions to be drawn from this study are:

1) The point kinetics yields a very poor representation of the neutronics behavior of large cores.

2) Point kinetics may be adequate for small, tightly coupled reactors.

3) The adiabatic approximation was generally better then point kinetics and was consistently conservative.

4) The point kinetics method was consistently non-conservative.

Numerical investigations illustrating the importance of flux shape changes and feedback in reactor transient behavior were performed by Johnson et al., [J-1]. A small (60 cm) slab core was analyzed with point kinetics and with the one-dimensional diffusion theory code WIGLE [C-4].

Transients were initiated by a localized step change in fission cross section in a region of the core. Feedback was simulated by changing the thermal absorption cross section in proportion to the power generated in the three core regions. Three different cases were analyzed using different combinations of positive and negative feedback coefficients. The feedback coefficients were selected to give equal feedback for all three cases when the steady-state flux shape was used. Hence, all three cases would yield the same result with the point kinetics model and any differences in the results would be because of changes in the flux shape.

Figure 2.3 shows the power as a function of time obtained from these calculations. The figure shows that flux shape changes and the resulting feedback effects were significant in determining the transient power history. It is also notable that the point kinetics power calculations were non-conservative in comparison with those calculated by the space-time methods.

Yasinsky [Y-5] performed an assessment of the accuracy of various point kinetics approaches for asymmetric rod ejection accidents with feedback. Three different one-dimensional reactor representations were analyzed with five different point kinetics schemes and the resultant time-dependent total core power and peak fuel temperatures were compared. The five point kinetics schemes included:

1) the standard method,

2) the adiabatic method,

3) using the static solution of the perturbed reactor in the presence of feedback,

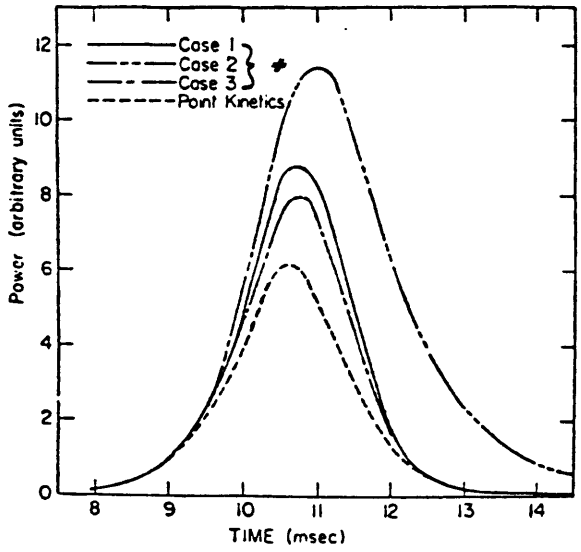

* Cases 1,2,3 with 1-D Diffusion Theory

----- Cases 1,2,3 with point kinetics

Figure 2.3 Power Excursions Computed by Space-time

Diffusion Theory and by Point Kinetics J-1

4) and 5) using the adiabatic flux shape for the external reactivity calculation and the flux shapes of 3) and 1), respectively, for the feedback reactivity.

An "exact" space-time solution for each transient was obtained with the WIGL2 code [H-2]. All the analyses used the same fuel temperature and coolant density feedback models so that any differences between the point kinetics and space-time results were due to errors in the flux shapes used in the point kinetics models.

It was found that "classical" point kinetics was consistently unable to calculate satisfactorily either peak power or peak fuel temperature. These key parameters were always underestimated, often by as much as a factor of three. The other methods were neither consistently conservative nor accurate for the transients considered. Methods two and three overestimated both external and feedback reactivity, but predicted powers and fuel temperatures which were sometimes low and sometimes high. Point method four was the most accurate, though it was neither consistently conservative nor non-conservative. Point method five generally overestimated the feedback reactivity and was the most consistently conservative of the methods. However, their conservatism came at the expense of very poor accuracy.

Figure 2.4 shows a typical set of time-dependent reactor power and fuel temperature as calculated by the different methods. All methods except point kinetics #5 underpredict the maximum power. Three of the five methods underpredict the maximum fuel temperature. The maximum fuel temperature calculated by method 5 (not shown) was very high -- 1610 °F. These results led Yasinsky to conclude:

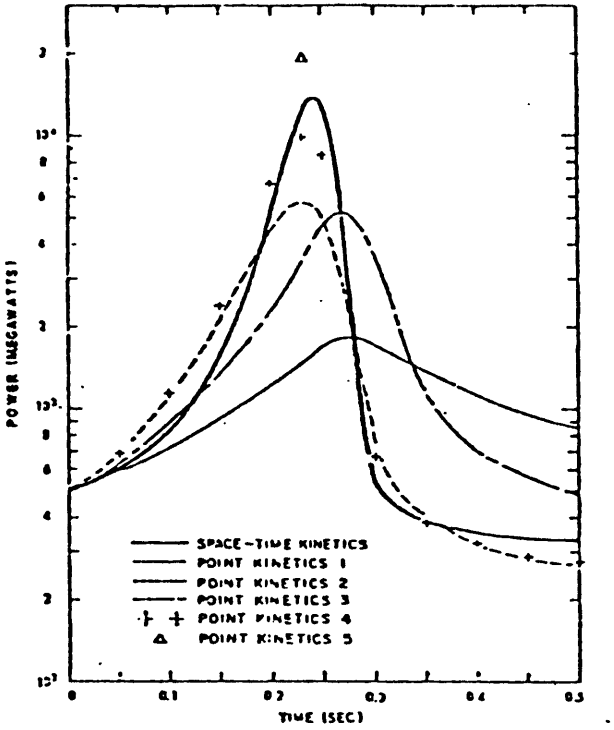

Power for Reactor C rod-ejection accident 1.

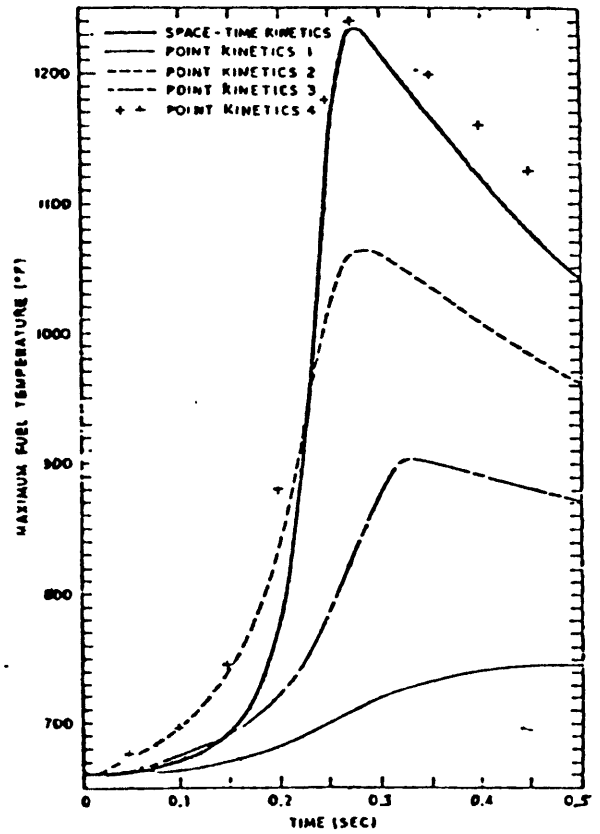

Maximum fuel temperature for Reactor C rod-ejection accident 1.

Figure 2.4 Assessment of Point Kinetics for Rod Ejection Transient with Feedback Y-5

> "In general we have seen that the accuracy of a point model, for rapid, nonseparable transients of the type studied here, is extremely dependent on the specifics of the particular model used (i.e., on the shape functions used). It appears difficult to assume that a given method is conservative; nor can we judge the accuracy of the method a priori."

Hence, the inclusion of feedback complicates the determination of whether a point kinetics model can be used for reactor dynamic analysis.

Another comparison of point kinetics and space-time kinetics was carried out by Dubois [D-8]. The objective of the study was to determine whether three-dimensional neutronics calculations were necessary to obtain conservative results for rapid, localized reactivity insertion transients. Two one-dimensional formulations and a classical point kinetics model were applied to a bare, cubical, uranium metal fueled light water reactor. The reactivity insertion was caused by rapid insertion of a fuel rod bundle into the core. The only feedback mechanism modeled was the thermal expansion of the fuel rods, which were assumed to heat up adiabatically. A large core (240 cm) and a small core (60 cm) were analyzed for both symmetric and asymmetric reactivity insertions. The one-dimensional "x" analyses assumed a constant flux shape in the perpendicular vertical plane, while the one-dimensional "z" analyses assumed a constant flux shape in the horizontal plane.

The "x" model predicted substantial changes in the flux shape and suggested an accident of greater consequences than did the point kinetics and "z" models. This conclusion was true for both symmetric and asymmetric insertions into both large and small cores. The "z" model predicted very little change in the flux shape and therefore essentially

the same response as the point model. This illustrates the point that a one-dimensional model can be as poor as a point kinetics model for accidents which violate the assumptions of the model.

The differences in the three methods were less pronounced for the smaller core. The only analysis for which there was good agreement among the three methods was the symmetric insertion into the small core. The main conclusion drawn from the study was that these lower-order kinetics methods were inappropriate for the analysis of super-prompt critical excursions. Dubois asserted that the significant flux shape changes observed rendered all three methods non-conservative because flux shape changes were neglected in at least two dimensions. It was therefore concluded that three-dimensional neutronics analyses were essential for this type of transient.

Finally, one investigation of point kinetics and spatial kinetics did show that lower order methods can give accurate results when properly applied. Cook [C-5] compared point kinetics, one-dimensional kinetics and three-dimensional kinetics analyses of an idealized homogeneous cube reactor. A zero current boundary condition on the outer surfaces of the reactor produced a uniform flux throughout the cube. A super-prompt critical transient was initiated by an instantaneous uniform perturbation of the neutron capture cross section. The transient was terminated by fuel temperature feedback. The results showed that all three methods were in excellent agreement. This serves to illustrate that point kinetics is a valid model for transients that are consistent with the inherent assumptions of the method.

The numerical investigations reviewed reveal some of the limitations of point kinetics. To summarize, they showed that the model is

inadequate for transients with large changes in the flux shape and questionable for large reactivity insertions. Flux tilting was shown to be more of a problem in large, loosely coupled cores than in small, tightly coupled cores. The error in point kinetics analyses was exacerbated when perturbations were asymmetric. These conclusions were found to hold whether or not feedback was included.

The conclusions drawn from the numerical investigations are generally valid for large commercial LWRs as well. The issue of point kinetics versus spatial kinetics for power plant safety analysis has been extensively investigated. Diamond [D-2] put forth the general criterion that spatial kinetics is needed for any transient in which the power distribution changes rapidly in time. This criterion can only be useful when the transient reactor response is known prior to performing the analysis. As a result, analyses have been performed to identify the modeling requirements of various reactor transients. Accordingly, a discussion of appropriate neutronic models for specific PWR and BWR transients follows.

Reactor transients may be grouped into those which are initiated by thermal-hydraulic perturbations and those which are initiated by reactivity perturbations. Spatial kinetics are not necessary for most PWR thermal-hydraulic transients [D-2]. However, important exceptions to this rule are transients in which the scram system is assumed to fail wholly (i.e., ATWS) or in part. Spatial kinetics are also required for any transient which produces a time-varying distribution of coolant inlet temperatures.

The steamline break accident is a particularly important example which encompasses both of these characteristics. The depressurization of the affected steam generator secondary side results in increased heat transfer and a cooldown of the primary water in that loop. The coolant entering the core is cooler, on the average, than nominal operating conditions and the distribution is uneven, resulting in an asymmetric positive reactivity insertion. The reactor coolant pumps may be tripped, so that there is concurrent a loss of flow. The accident triggers an early scram, but it is usually assumed that the highest worth control rod sticks and remains out of the core. For this accident, the local distortion of the flux shape is very important in determining whether damage occurs. A point kinetics model cannot properly account for these local effects [T-2]. The time-dependent flux has a highly nonuniform spatial distribution which is greatly affected by the local feedback, primarily the coolant temperature [R-3].

Bian et al., compared a point kinetics analysis to a three-dimensional analysis of a main steamline break accident [B-3]. They found that the three-dimensional method resulted in a larger initial power increase than did the point kinetics method. The flux peaking in the vicinity of the missing control rod was less pronounced in the three-dimensional calculation than in the point kinetics calculation. As a result, DNB was predicted with point kinetics but not with three-dimensional kinetics.

An analysis of a loss of feedwater ATWS with point kinetics and three-dimensional kinetics also showed the importance of higher order methods [B-3]. In this accident, the loss of heat removal

capability results in a primary system heatup and overpressurization. The core power level decreases as Doppler and moderator density feedback mechanisms respond to the system heatup. The time-dependent reactor power calculated with three-dimensional neutronics was consistently lower than that calculated with point kinetics. As a result, the maximum system pressure attained was reduced by 2.41 MPa (350 psi).

The change in flux shape associated with many PWR reactivity transients is significant enough to call into question the use of point kinetics. The control rod ejection and the control rod drop accidents are two examples of such transients. The control rod ejection accident is caused by a failure in the housing of the control rod drive mechanism. The high pressure coolant in the core ejects the control rod assembly to its fully withdrawn position, resulting in a large insertion of reactivity. The control rod ejection causes a large, rapid power excursion which is terminated by Doppler feedback. The point kinetics method is frequently used to analyze this accident. The Doppler feedback calculations are normally based upon the steady-state flux shapes. Hence, the effect of local flux peaking in the region from which the control rod was ejected is not accounted for in the feedback calculation. As a result, the Doppler reactivity feedback is considerably underestimated and the increase in reactor power is overestimated.

Bian developed a method for incorporating the effect of local flux peaking on the Doppler feedback in a point kinetics code [B-4]. In this method, steady-state calculations are used to approximate the change in Doppler reactivity caused by the flux shape changes. A

comparison of results obtained with classical and reactivity weighted point kinetics methods and three-dimensional kinetics for two control rod ejection accidents was presented. A super-prompt critical excursion from hot zero power and a sub-prompt critical excursion from hot full power were analyzed with the three methods. Only Doppler feedback was included in the analyses.

For the super-prompt critical transient, the time-dependent reactor power predicted with the weighted point kinetics technique agreed well with the three-dimensional results. However, the classical point kinetics model considerably overestimated the peak reactor power and the integrated energy release. The energy release at the hot spot was 63% higher for the weighted point method and 500% higher for the classical point method. For the sub-prompt critical transient, neither point kinetics model yielded satisfactory results for the reactor power history. The time-dependent powers calculated by the point kinetics methods were consistently higher than the three-dimensional results. The integrated whole core and hot spot energy releases were significantly higher for both point methods.

The conclusion to be drawn from these analyses is that point kinetics methods yield generally inaccurate, though conservative, results for PWR control rod ejection accidents. The reactivity weighting method was consistently better than the classical point kinetics method, but only produced good agreement with the three-dimensional model for the global power history in the supercritical transient case. It is clear that proper treatment of changes in the local flux shape can substantially reduce the predicted consequences

of the accident. As a result, a three-dimensional analysis of the PWR control rod ejection is highly desirable, if not necessary.

Similarly, the PWR rod drop accident requires that spatial effects be included in the neutronics analysis. In this accident, the coupling between a withdrawn control rod and its control rod drive mechanism fails, causing the rod to drop into the core and assume its fully inserted position. Depending on the location of the control rod, this may produce a significant flux maldistribution, leading to increased local power peaking and, possibly, to DNB [T-2]. As in the rod ejection accident, a three-dimensional analysis is recommended for the rod drop accident.

Many BWR transients can only be properly modeled with spatial kinetics. As in the PWR, the BWR rod withdrawal accident produces significant flux shape changes and a higher order method is called for [D-2]. In addition, many thermal-hydraulic transients require spatial kinetics models. In particular, ATWS events or events in which a incomplete scram occurs require spatial kinetics. Overpressurization transients can produce changes in the flux shape which cannot be modeled with point kinetics. Transients which result in changes in the distribution of coolant inlet temperatures, such as the loss of a feedwater heater or the inadvertent startup of a cold recirculation loop, require spatial kinetics.

The BWR turbine trip event causes a rise in core pressure, collapsing the steam voids and initiating an increase in the reactor power. Reactor scram is initiated some time after the power level increase has begun. A comparison of actual plant data and analytical results for a BWR turbine trip was performed by Moberg et al. [M-4].

The point kinetics method has been compared to a one-dimensional model for a BWR transient in which the temperature of the inlet coolant temperature was decreased as a function of time, as in the failure of a feedwater heater [F-5]. The reduction of the core inlet temperature by 5 °K resulted in an increase in the core average moderator density and, hence, an increase in core power. The two analyses were performed with the identical thermal-hydraulic feedback models, so that any differences obtained were due to the neutronics models.

The increase in reactor power calculated with point kinetics was higher than that calculated with one-dimensional kinetics. However, the one-dimensional model predicted a much larger increase in the local power at the peak axial location. The increase in fuel centerline temperature at this location was nearly 200 °K greater than predicted by the point kinetics model. It was therefore concluded that at least a one-dimensional method was required for this type of transient.

In summary, theoretical arguments and analytical assessments indicate that the point kinetics method should be used with care. Transients involving rapid changes in flux shape should be analyzed with spatial kinetics. As previously discussed, methods have been developed to improve on the classical point kinetics approach [Y-5, H-4,H-5,B-4,R-4,L-5]. However, these methods can neither produce consistently accurate results nor can they readily be demonstrated to be consistently conservative [F-4]. Therefore, coupled codes using the point model to describe the core neutronics are limited in their applicability and accuracy. A general rule is that any code which relies upon a point kinetics model should be limited to analyzing

transients in which the flux shape is known to change very slowly or to remain nearly constant during the course of the transient.

2.2.3.3 Limitations of Lower Order Spatial Neutronics

The lower order spatial kinetics models also have been assessed to determine their accuracy and applicability. A one- or two-dimensional model will generally be adequate if the flux shape remains constant in the directions not calculated by the model. The BWR turbine trip accident results in a flux shape change which is predominantly in the axial direction. It is not surprising, then, that a one-dimensional axial neutronics model has been shown to be adequate for this transient [M-4,C-6,C-7]. Similarly, the withdrawal of a centrally located control rod in either a BWR or PWR produces flux shape changes which are axisymmetric in the horizontal plane. Consequently, such transients can be adequately analyzed with a two-dimensional cylindrical neutronics model.

The lower order spatial kinetics methods should be limited to those transients which do not violate the assumptions about flux shape inherent in them. This was demonstrated by an analytical investigation. A comparison of one-, two- and three-dimensional neutronics analyses with feedback was performed for a pair of BWR rod withdrawal transients [B-5]. The reactor was represented by a one-dimensional radial (r) model, by two-dimensional cylindrical (r,z) and planar (x,y) models, and by a three-dimensional (x,y,z) model. An adiabatic fuel rod model provided Doppler feedback in all cases. Symmetric and asymmetric super-prompt critical transients were initiated by ramp reductions of neutron absorption cross sections, simulating the rapid withdrawal of control rods.

For the asymmetric rod withdrawal, the three-dimensional analysis yielded the highest value of the thermal flux, the highest fuel temperature and the lowest total feedback. Figure 2.5 shows the time-dependent thermal flux at the peak location as calculated by the four neutronics models. The maximum thermal fluxes calculated with the (x,y), (r,z) and (r) models were approximately 40%, 45% and 60% lower, respectively, then the three-dimensional result. A secondary increase in the thermal flux prior to scram was absent in the (x,y) case and less pronounced in the (r,z) and (r) cases. The two-dimensional methods underpredicted the maximum fuel temperature by approximately 570 °K (17.1%), while the one-dimensional method was low by approximately 980 °K (29.4%). Only the three-dimensional analysis indicated that fuel melting would result. Hence, all of the lower order spatial methods were non-conservative for the symmetric rod withdrawal analysis.

Similar conclusions were obtained from a comparison of three-dimensional and two-dimensional (x,y) methods for a symmetric rod withdrawal transient. The conclusion was drawn, therefore, that a full three-dimensional analysis of fast transients in LWR cores is necessary. A subsidiary conclusion was that modeling off-center control rods by an "equivalent" central control rod may lead to non-conservative results.

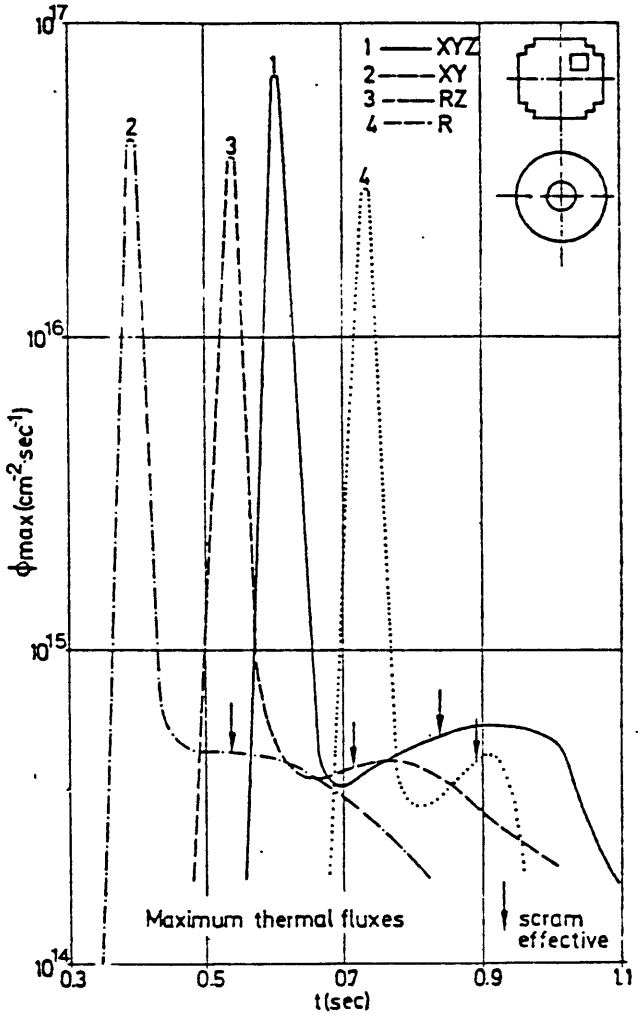

Case I: comparison of maximum thermal fluxes in various geometries.

Figure 2.5 Effect of Multi-dimensional Modeling on Reactivity Insertion Transient B-5

2.2.3.4 Summary

In summary, the various neutronics models used in coupled codes with all produce useful results when properly applied. The utility of lower order methods is that they can produce accurate or at least conservative results for many reactor transients of interest. However, these applications must be selected carefully in order to ensure that the particular code can perform well. As a result, codes using lower order neutronics models cannot be applied as generally as can codes using three-dimensional neutronics. Furthermore, there are many reactor accidents which are most appropriately analyzed in three dimensions. These include PWR and BWR rod withdrawal accidents, PWR rod drop accidents, PWR steamline break accidents, ATWS and partial scram events and others. These accidents are significant for reactor safety and licensing and provide motivation for the development of coupled codes with three-dimensional neutronics models.

2.3 Thermal-Hydraulics Models for Coupled Codes

2.3.1 Overview

The thermal-hydraulics model of a coupled code should fulfill two objectives. The first objective is to calculate accurately the parameters used for feedback to the neutronics calculation. This enables the correct time- and space-dependent power generation to be calculated. Typically, the thermal-hydraulics model must calculate fuel temperatures, coolant temperatures and coolant densities, averaged over control volumes consistent with the neutronics model.

The second objective is to calculate accurately the response of the core to changes in power generation, flow rate, pressure or temperature. The focus in this task is on the safety related parameters such as peak cladding temperature, peak fuel centerline temperature and minimum critical heat flux (CHF)/departure from nucleate boiling (DNB) ratios. Since this second objective involves determining whether the maximum or minimum values of certain parameters fall within acceptable limits, the thermal-hydraulics should be modeled with as much detail as possible. All of the important physical processes affecting both the feedback parameters and the safety parameters must be included in the thermal-hydraulics model in order to satisfy these two objectives.

The coupled neutronics/thermal-hydraulics codes reviewed attempt to satisfy the objectives on many different levels. For some, the thermal-hydraulics model is primarily a vehicle for providing the feedback parameters. The thermal-hydraulics models of such codes are therefore quite simple. Other codes combine a very detailed thermal-hydraulics model with relatively simple neutronics model. Here the emphasis is on the safety parameters, so that an approximate, conservative calculation of the time-dependent heat generation can be tolerated as long as the limits are not violated. The specific models for fluid flow and heat transfer used in coupled codes are quite varied; all contain approximations and compromises which limit their accuracy and generality of application. The purpose of this subsection is to discuss some of the models used, their limitations and the significance of those limitations.

2.3.2 Adiabatic Fuel Rod Models

There exists one category of coupled codes which was not reviewed because they do not model the coolant. These codes contain a model for the fuel rod which assumes no heat transfer from the fuel to its surroundings. This adiabatic fuel model is used for very rapid reactivity transients where it is assumed that the time scale of the transient is smaller than the time required for heat to be conducted out of the fuel. Consequently, the nuclear Doppler effect is the only feedback mechanism modeled. It is assumed that the reactivity insertion will cause a rapid increase in reactor power which is terminated by Doppler feedback. A reactor scram usually follows after the power burst.

Neglecting the heat transfer to the coolant and the coolant feedback mechanisms is assumed to be conservative when such methods are used. Obviously, an accurate calculation of the cladding temperature or the occurrence of critical heat flux is not obtained. This type of analysis is usually applied to the PWR rod ejection accident or the BWR rod withdrawal accident.

The significance of neglecting the moderator in the analysis of the BWR rod withdrawal transient has been investigated extensively [C-1,C-8,C-9,C-10]. The assumption that moderator feedback can be ignored was found to be a poor one, since the energy produced is deposited in the fuel for a period of three to four seconds [C-1]. This time period allows heat to be conducted into the coolant with considerable

reduction in the peak power and peak fuel enthalpy. Moderator feedback also results from the direct deposition of energy in the coolant by gamma ray absorption and neutron thermalization. Direct moderator heating provides an instantaneous feedback mechanism which can be important for certain initial conditions. Heat conduction through the fuel is the primary mechanism contributing to moderator feedback when the reactor is at power because the thermal time constant of the fuel is small. Conversely, when the reactor is at hot zero power, the thermal time constant of the fuel is large, the coolant is near saturation, and direct moderator heating produces rapid moderator feedback [C-8].

A comparison of analyses with and without moderator feedback for BWR rod withdrawal accidents with various initial conditions showed that the peak power and the peak fuel enthalpy were reduced by a factor of two or more when moderator feedback was included [C-9]. In one example, the inclusion of moderator feedback reduced the peak power from 9.0 GW to 2.0 GW, reduced the peak fuel enthalpy from 78 cal/g to 42 cal/g, and obviated the initiation of a scram [C-1].

Even though it is conservative to neglect moderator feedback, the magnitude of the conservatism has significant ramifications. Analyses neglecting feedback have calculated a maximum control rod worth of 2% in order to satisfy the peak fuel enthalpy limit of 280 cal/g [C-9]. This limit on control rod worth has been achieved by complex procedures

for control rod insertion and withdrawal, with the result being a loss in operational flexibility [C-9]. Hence, it was concluded that the effects of moderator feedback are too important to be neglected in the analysis of the BWR rod withdrawal accident. Since this is one of the few transients for which an adiabatic fuel temperature feedback model could be applied, it is clear that coupled codes not containing actual thermal-hydraulics models are of very limited usefulness.

2.3.3 Limitations in Reactor Geometry Representations

Among the most obvious limitations of some coupled codes is the lack of geometrical detail with which the core can be modeled. The typical core representation involves vertial flow channels which are divided axially into control volumes. Some coupled codes limit the number of channels to only a few, perhaps even to a single average channel. The number of axial divisions is also limited in some codes. A few of the codes reviewed assumed that the reactor modeled is axisymmetric. For these codes, the reactor is represented as a number of concentric rings, each having one average flow channel. All such simplified geometrical representations reduce the scope of applicability of the codes and can lead to non-conservative results. For example, the need for spatial detail in the thermal-hydraulics model was examined for the PWR steamline break accident [S-4,R-3].

Rohan and Wagner [R-3] showed that local feedback effects considerably affected the overall core reactivity under steamline break conditions. Figure 2.6 shows a comparison of reactivities based upon local feedback models in spatial calculations with reactivities based upon less sophisticated methods using core average fuel and moderator conditions. The feedback based on local conditions was shown to have a significantly greater negative reactivity effect than the average feedback method.

Sun et al. [S-4] performed a dynamic analysis of a PWR steamline break accident using a coupled point kinetics/thermal-hydraulics code. Two-dimensional and three-dimensional static calculations were performed to determine the variation of core reactivity with core average feedback parameters. Figure 2.7 shows a comparison of the time-dependent reactor power calculated with and without full three-dimensional feedback in the reactivity coefficients. The results indicated that the accident is very sensitive to the detail with which the thermal-hydraulic feedback was modeled. For the analysis which used reactivities based upon two-dimensional calculations, the point kinetics model predicted that the reactor would regain criticality, ultimately attaining a power level that was 9% of the pre-accident power. However, the analysis using reactivities based upon three-dimensional calculations predicted that the core would remain subcritical at power levels consistent with the core reactivity and decay heat content. These analyses indicate that a thermal-hydraulics model capable of calculating local conditions (i.e., a three-dimensional model) is important for the PWR steamline break accident.

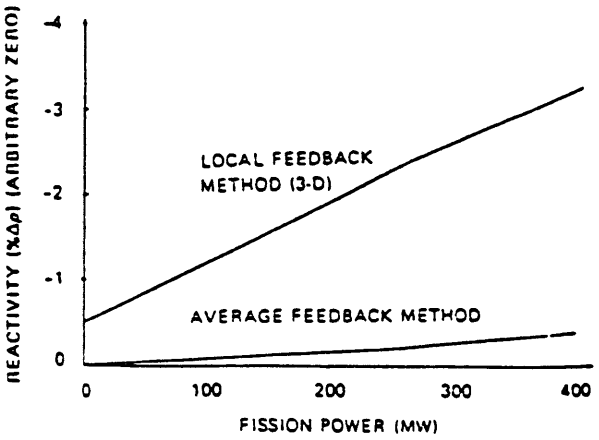

Comparison of reactivity as a function of fission power under steam-line break conditions.

Figure 2.6 Effect of THree-dimensional Feedback on Core Reactivity for Steamline Break Conditions R-3

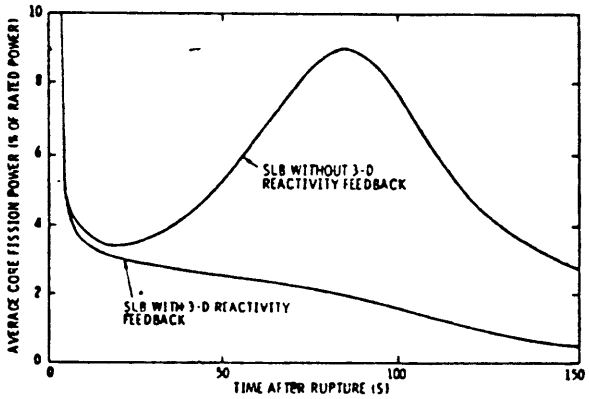

Average core fission power for a CE 2560-MW(th) plant during steam generator outlet nozzle break accident at full load initial conditions with concurrent of loss of off-site power.

Figure 2.7 Effect of Three-dimensional Feedback on Steamline Break Transient S-4

Most of the coupled codes are restricted to modeling the reactor core. This means that boundary conditions replacing the remainder of the loop must be supplied. A few of the codes have models for the pressure vessel and loop (or parts thereof) which can supply appropriate time-dependent boundary conditions. However, these loop models are frequently representative of a particular type of reactor, thus limiting the code applications to that type.

2.3.4 Limitations of One-Dimensional Flow Models

Many coupled codes have fluid dynamics solutions which will only permit one-dimensional fluid flow. This means that the flow channels must be modeled as hydraulically isolated from each other. In a BWR, each fuel assembly is surrounded by a metal "channel" or "can" which prevents coolant flow to the adjacent fuel assemblies. Hence, flow channels corresponding to one or more BWR fuel assemblies can be described reasonably by one-dimensional models. However, the assumption of one-dimensional flow might not be valid if the fuel assemblies are subdivided into flow channels. The fuel assemblies in a PWR are not hydraulically isolated from each other, so a one-dimensional closed channel model is of questionable validity. Nevertheless, closed channel models have been used to analyze steady-state and transient conditions for PWRs.

The appropriateness of using closed channel models for PWRs has been addressed by several authors [R-3,C-2,M-1,K-4,L-4]. The closed channel model was found to be adequate for nominal steady-state conditions [R-3,L-4]. However, for any transient which involves conditions far removed from the nominal operating conditions and, in

particular, when large radial gradients in power, pressure, coolant density, temperature or flow exist, a three-dimensional flow model permitting the exchange of mass, momentum and energy between adjacent channels is appropriate.

A comparison of an open channel model with subcooled boiling to a closed channel model with no subcooled boiling was made for various PWR core heatup transients [C-2]. For accidents without scram or accidents initiated while scrammed, the open channel/subcooled boiling model calculated a higher minimum departure from nucleate boiling ratio (MDNBR) and lower fuel centerline temperatures. As a result, the margins between the calculated safety parameters and the limits on these parameters was increased. However, little difference between the two models was seen for accidents resulting in a scram.

A comparison of open and closed channel steady-state analyses for the stuck rod configuration has also been performed [K-4]. The open channel method predicted considerably less voiding in the vicinity of the stuck rod than did the closed channel method. The open channel calculation also showed less flux peaking and a higher MDNBR. Moreover, the k_{eff} of the "open" core was higher than that of the "closed" core, giving the potential for a higher power rise during the steamline break transient. It was concluded that the results were quite sensitive to the choice of open or closed channel modeling. Motley and Morita [M-1] asserted that the closed channel model is inaccurate for a steamline break analysis, possibly predicting non-conservative reactivity and power peaking.

Finally, the issue of closed versus open channel models was examined for a PWR control rod ejection transient [L-4]. The difference in models had little impact on the time-dependent reactor power. However, the void content of the hottest channel was reduced by a factor of two when the open channel model was used. Hence, the open channel model can have a significant impact on local phenomena even when the gross core behavior is unaffected. If a PWR analysis is concerned with detailed results, an open channel model should be used.

2.3.5 Two-Phase Flow Models

Among the important limitations inherent in many coupled neutronics/thermal-hydraulics codes are those related to the treatment of two-phase flow conditions. The moderator density, one of the basic feedback parameters, can vary a great deal when a change of phase occurs. Hence, the proper treatment of boiling and condensation can be very important for coupled codes. Indeed, the effect of the "voids" created by boiling is the major thermal-hydraulic feedback mechanism which must be modeled in BWRs [Z-1]. For steady-state analysis, the power distribution and the core criticality are strongly influenced by the presence of two-phase moderator. During a transient, the changing void distribution is a primary source of reactivity, and also affects the worth of control rods. For example, the turbine trip event is initiated by changes in the void distribution. The increase in pressure causes condensation of some of the vapor, increasing the moderator density and causing the reactor power to rise. A scram is usually initiated quickly. If the scram is delayed, the power would be limited by the combination of feedback due to an increase in fuel temperature and a decrease in moderator density. The feedback contribution of moderator

density is more important than that of the fuel temperature during the early part of the transient [F-2]. Therefore, the treatment of two-phase flow is of primary importance in the analysis of a BWR.

A PWR normally has little or no boiling present in the core. Nevertheless, boiling can occur during transients and provide a very strong negative feedback. Subcooled boiling is particularly important for PWRs. The proper treatment of two-phase flow is also necessary in order to determine the heat transfer from the fuel to the coolant and to calculate the pressure drop. Hence, the fuel temperature feedback effect is indirectly dependent on the accurate calculation of two-phase flow.

Despite the importance of two-phase flow, seventeen of the thirty-three codes reviewed were not capable of modeling two-phase flow. None of these codes could be applied to a BWR (ten of the seventeen were primarily or exclusively for LMFBR analysis). Most of the remaining codes use some variation of the homogeneous equilibrium model (HEM), in which two-phase flow is assumed to be a homogeneous mixture with the liquid and vapor in thermal equilibrium with each other. The two phases are also assumed to move with the same velocity or to have a constant velocity ratio (slip ratio). There are many situations in nuclear reactors in which the assumptions inherent in the homogeneous equilibrium model are unrealistic. This model is most appropriate at low qualities, when vapor bubbles are dispersed throughout the liquid, and at very high qualities when droplets of liquid are suspended in the vapor. It is least appropriate for the annular flow

regimes often encountered in BWRs [R-5]. If slip is not modeled, the buoyancy of the vapor bubbles is neglected and counter-current flow cannot be described. The assumption of equal phase temperatures means that subcooled boiling cannot be modeled, but must be treated by correlation. The dryout flow regime in which droplets of saturated liquid are suspended in superheated vapor also cannot be modeled when equilibrium is assumed. Nevertheless, codes using the homogeneous equilibrium model can give adequate results when prudently applied.

In a few cases, coupled codes used two-phase flow models which relax one or more of the HEM assumptions. The RETRAN 02 code uses a variation of HEM in which a differential equation describing the relative velocities between the phases is solved along with the conservation equations. This is known as a dynamic slip model [M-2]. The NAIADQ code assumes homogeneous flow with equal phasic velocities but allows the two phases to have different temperatures. A slip model is used with a homogeneous non-equilibrium model in the RAMONA 3B code.

The ANTI code utilizes the drift flux model, which accounts for the fact that the concentration and velocity profiles across the flow channel can vary independently of each other [C-11]. This is a flow regime-dependent model which assumes thermodyanmic equilibrium between the phases. These models are all improvements over the HEM formulation and can give more accurate results for many two-phase situations. However, none of these models attempt to describe rigorously the complex nature of two-phase flows. Real fluid flow in reactors is multidimensional and may exhibit important non-equilibrium and phase separation effects during transients. The sensitivity of

coupled codes to inadequacies in the two-phase flow model is probably enhanced, since phenomena such as the relative motion of phases and subcooled boiling affect the neutronic feedback.

When departures from homogeneous equilibrium flow are important, a model that treats each phase as a separate fluid and provides a detailed treatment of interphase transfer phenomena is called for. These multi-fluid codes (such as THERMIT) are, in principle, extremely powerful because of the generality of the model and the flexibility to adopt constitutive relations for distinct physical situations. A two-fluid model requires three conservation equations for each phase and is therefore also known as a six equation model. It has been suggested that even a two-fluid, six equation model may not be adequate for the treatment of dispersed and non-equilibrium flows and that as many as three fluids/nine field equations may be required [A-3]. However, to our knowledge no coupled code with more than six field equations has ever been developed.

The limitations of the state-of-the-art two-phase flow methods are mainly found in the constitutive relations. Constitutive relations are required for the exchange of mass, momentum and energy between the phases as well as the exchange of momentum and energy between the phases and solid surfaces. These models have the virtue of describing basic physical processes rather than the more artificial empiricism of constitutive relations for simpler methods. However, the basic physical processes which must be modeled are not well understood and are quite challenging to investigate experimentally. Nevertheless, the multi-fluid models are the best two-phase flow models available today.

2.3.6 Other Limitations in Fluid Dynamics Models

The ability to model multidimensional flow and the treatment of two-phase flow are two important characteristics of the fluid dynamics capability of a coupled code. As has been seen, limitations in these models restrict the accuracy and applicability of many codes. Many other limitations exist in the fluid dynamics models found in the available coupled codes. Some codes do not allow the system pressure, inlet flow rate and/or temperature of the coolant to vary during a transient. Such codes are obviously restricted to neutronically-driven transients. Furthermore, it has been shown that the flow rate and pressure may change significantly during neutronically-driven transients and that it can be non-conservative to neglect these changes [C-10]. Some codes do not solve a fluid momentum equation, thereby assuming a single pressure for the entire reactor. This means that any pressure change is transmitted instantaneously throughout the core. As a result, void distribution and, hence, the moderator density feedback are in error.

Other fluid dynamics model limitations in coupled codes include the inability to allow pressure boundary conditions at the core inlet and/or outlet, the assumption of incompressible flow, the inability to allow flow reversal and the restriction of fluid velocities to subsonic values. Some of these limitations are inherent in the models, others are related to the numerical techniques used. All of these limitations can be relaxed by state-of-the-art techniques.

2.3.7 Fuel Rod Heat Transfer Models

The final component of coupled code thermal-hydraulics to be considered is the fuel rod heat transfer package. This includes the

fuel rod model and the models for heat transfer between the fuel and the coolant. The fuel rod model is important because it provides one of the primary feedback parameters, the average fuel temperature, as well as two of the important safety parameters, the peak fuel centerline and peak cladding temperatures. The fuel-coolant heat transfer package directly affects essentially all the feedback and safety parameters. Several coupled codes used a simple lumped heat capacity model for the fuel. This type of model ignores the fuel-cladding gap and only calculates an approximate average temperature for the feedback calculation. A more sophisticated model calculates a radial distribution of temperatures in the fuel and cladding and accounts for the gap between them. Many of the models assume that the thermal properties of the fuel and cladding are not dependent on temperature and that the gap can be represented by a space- and time-independent heat transfer coefficient. A more rigorous fuel rod model includes the temperature-dependence of the fuel and cladding thermal properties and models the gap heat transfer coefficient as a function of space and time.

The results of transient calculations can be very sensitive to these two refinements [C-5,L-6,R-5]. The most sophisticated fuel rod models allow for the restructuring of fuel pellets, model fuel behavior beyond the melting point, allow for expansion of cladding and calculate stresses and strains. Such very detailed models are found only in LMFBR codes.

The fuel-coolant heat transfer packages of the coupled codes also vary in capability. Of course, many do not model boiling heat transfer since they are limited to single-phase conditions. The most

sophisticated codes include correlations which can span the entire range of heat transfer regimes and provide selection logic to determine which regime is appropriate. Among the important capabilities not present in many codes are CHF/DNB correlations, subcooled boiling capability, and post-CHF heat transfer correlations. A model for the zirconium-water reaction is absent from most of the codes. Nevertheless, there are state-of-the-art codes such as THERMIT and RETRAN 02 which contain most of the important fuel rod heat transfer capabilities needed for accurate transient analysis.

2.4 The Need for TITAN

The review of existing coupled neutronics/thermal-hydraulics codes indicates that a wide variety of models are used. An assessment of the neutronics and thermal-hydraulics models used in coupled codes shows that many assumptions, simplifications and approximations limit their accuracy and applicability. Among the codes reviewed, only eight contain three-dimensional neutronics models. Only five of these codes can model three-dimensional fluid flow. Of these, HERMITE and BWKIN are proprietary and thus not generally available. The remaining codes, MEKIN, MEKIN-B and ANTI, all provide significant capability for analyzing LWR transients. However, even these advanced codes are limited in certain specific models. MEKIN and MEKIN-B suffer from the following shortcomings [D-4,R-5].

1) The codes use an oversimplified heat transfer logic, which has resulted in large discrepancies in clad temperatures during severe power transients,

2) The fluid dynamics solution cannot allow flow reversal,

3) The fluid dynamics solution has a single simplified transverse momentum equation which makes crossflow results quite sensitive to axial mesh size,

4) They use a homogeneous equilibrium model with slip for two-phase flow,

5) A single space- and time-independent fuel/cladding gap heat transfer coefficient is employed.

In addition to these concerns, the cost of calculations with MEKIN is an almost insurmountable limiting factor. The finite difference method used to solve the three-dimensional neutron diffusion equations requires a tight neutronic mesh spacing, on the order of 2 cm, to achieve full convergence [L-7]. The tight spatial mesh also restricts the maximum time-step size, causing calculations to be quite expensive.

The ANTI code also has certain shortcomings. The most important is that the reactor model is limited to ten thermal-hydraulic channels. The neutronics model assumes one neutron energy group and requires user-specified parameters to calculate the nodal leakages. The fuel rod model assumes constant thermal properties.

The conclusion of this investigation is that none of the existing coupled neutronics/thermal-hydraulics codes combines the best available models for both neutronics and thermal-hydraulics. Some of the codes have been designed for specific applications, and all contain approximations and compromises in their models which limit their applicability and accuracy. QUANDRY and THERMIT represent state-of-the-art methods for LWR neutronics and thermal-hydraulics, respectively. Hence, the coupling of QUANDRY and THERMIT to yield TITAN represents an increased level of generality, sophistication, and physical rigor over the existing codes. Figure 2.8 compares the fundamental neutronics and thermal-hydraulics capability of TITAN and the existing coupling codes.

3-D kinetics	l			m						n
2-D kinetics	i	j	k							
1-D kinetics	g		h							
point kinetics	a	b	c	d		e				f
	1	2	3	4	5	6	7	8	9	10

total number of scalar field equations for fluid dynamics model

Key: a - NOWIG, FORE

b - FORE-II, "FORE-III"

c - CHIC-KIN, PARET, FREADM-1, SAS1A, SAS2A, SAS3A

d - NAIADQ

e - THIOD-K

f - THERMIT-3

g - WIGL, WIGL3, COSTANZA-CYLINDRICAL

h - ALMOS, RETRANO2

i - TWIGL, ADEP, COSTANZA(R,Z), RADYVAR

j - FX2-TH

k - COTRAN, BNL-TWIGL

l - QUANDRY

m - MEKIN, MEKIN-B, BWKIN, HERMITE, CRONOS, ANTI, RAMONA-3B

n - TITAN

Figure 2.8: Summary Grid of Coupled Neutronics/ Thermal-hydraulics Codes

Chapter 3 QUANDRY and THERMIT

3.1 Introduction

3.1.1 Objectives

This chapter addresses three separate, but related, objectives. The first objective is to provide a survey of the M.I.T. research efforts which directly benefited the current work. The previous chapters provide a broad overview of the technical background for coupled neutronics/thermal-hydraulics codes and offer motivation for the development of an advanced code like TITAN. The intent of the survey in this chapter is to provide a narrower historical and technical context for the development of TITAN at M.I.T. Specifically, the survey indicates the relationship of the current work to earlier (in some cases concurrent) research efforts.

The second objective is to provide sufficient background information to permit the current work to be understood. Hence, the QUANDRY and THERMIT codes are discussed herein, with emphasis on the physical models, solution strategies, numerical methods, operational characteristics, etc., which are important in the development of TITAN. Of course, this discussion is by necessity incomplete and the reader will find the primary references useful for detailed information (QUANDRY: S-1, G-2; THERMIT: K-1, R-6). Nevertheless, the intent here is to provide sufficient detail to understand the current work without referring to other references.

The third objective of this chapter is to review the relevant experience with QUANDRY and THERMIT, particularly any calculations which

demonstrate the capability and accuracy of the codes. Both codes have been subjected to significant testing and validation as part of their development. The results give a basis for confidence in the reliability of the two major components of TITAN as well as indicating potential weaknesses or problem areas. In addition, some relevant analyses performed with the coupled THERMIT-3 and THIOD-K codes are discussed.

3.1.2 History

The development of TITAN is a natural outgrowth of two separate research efforts at M.I.T. The original QUANDRY [S-1] and THERMIT [R-6] codes were developed essentially simultaneously and were completed and tested before the current work began in 1980. Indeed, second generation versions of QUANDRY [S-5] and THERMIT [K-1] were available at that time. The current work uses the original version of QUANDRY [S-1] and the second generation version of THERMIT (designated THERMIT-2) [K-1].

Even though QUANDRY and THERMIT evolved independently, their developers anticipated and recommended further development along the lines of the current work. Indeed, THERMIT was developed primarily to provide an advanced thermal-hydraulics code which could be linked to a neutronics model [R-7]. Dubé [D-4] subsequently produced a one-dimensional, fully implicit version of THERMIT called THIOD, while Kelley [K-1] developed a version with subchannel analysis capability, THERMIT-2, which was used in the current work. Dubé linked a point kinetics model to THIOD and THERMIT, resulting in versions designated THIOD-K and THERMIT-3, respectively. This effort was reasonably successful and demonstrated that

THERMIT was amenable to coupled analysis. Nevertheless, Dubé recommended that THERMIT be linked to a space-time neutronics model. Similarly, Smith [S-1] included a simple thermal-hydraulics model in QUANDRY and then recommended that a better reactor model be installed in the future. Hence, the need for an advanced coupled neutronics/thermal-hydraulics code and the concurrent development of QUANDRY and THERMIT at M.I.T. led naturally to the development of TITAN.

3.2 QUANDRY

3.2.1 Code Description

3.2.1.1 Overview

QUANDRY is an analytical tool for determining the space- and time-dependent neutron flux/power distribution within a nuclear reactor core. QUANDRY solves the steady-state and transient two-group nodal neutron diffusion equations in two-dimensional (planar) or three-dimensional Cartesian geometry. The highly efficient and accurate Quadratic Analytic Nodal Method is the basis for the QUANDRY code. In addition, QUANDRY contains models for control rod motion and simple thermal-hydraulic feedback. These features are discussed in greater details in subsequent sections.

Two fundamental approximations are inherent in QUANDRY:

1. the rigorous neutron transport equation is approximated by the two energy group neutron diffusion equation, and
2. appropriate auxiliary calculations determine equivalent "homogenized" neutron diffusion theory parameters so that

a heterogeneous reactor may be represented as a collection of homogenized regions (nodes).

These approximations are reasonable and are, in fact, typical for comparable neutronics codes. Indeed, the three-dimensional analysis of a modern commercial LWR would be practically impossible without these assumptions.

The procedure for performing a QUANDRY analysis actually consists of two parts. First, "equivalent homogenized diffusion theory parameters" for various regions in the core must be determined [S-6]. The spatial detail and material content of each core region is accounted for through auxiliary calculations which produce spatially constant (i.e., homogenized) macroscopic nuclear cross sections and diffusion constants. A typical region consists of one or more adjacent fuel assemblies. If the QUANDRY model is three-dimensional, these regions will subsequently be divided axially into nodes of length comparable to their width. If thermal-hydraulic feedback is to be included in the QUANDRY analysis, the auxiliary calculations must also provide partial derivatives of the homogenized nuclear parameters with respect to the feedback quantities. The proper calculation of equivalent diffusion theory parameters and feedback coefficients is a very important and difficult part of the process of reactor analysis with QUANDRY.

The second task involves using QUANDRY to determine the spatial flux/power distributions for a core model consisting of many homogenized rectangular parallelepipeds (hereafter called nodes). QUANDRY allows considerable flexibility in defining and arranging these nodes to model

a reactor. An arbitrary spatial mesh can be specified for each direction. The top and bottom boundaries must be planar, but the sides can be irregular, as in the jagged periphery of a nuclear reactor core. The boundaries are defined neutronically, at user option, as zero flux, zero current, or albedo surfaces. An albedo boundary condition is one for which the relationship between flux and current is specified. QUANDRY also allows for planes of radial symmetry which cut diagonally through nodes. Thus, any Cartesian reactor geometry for which equivalent homogenzied (two energy group) parameters are provided can be analyzed. QUANDRY solves for the static (steady-state) nodal flux/power distributions and the reactor criticality (eigenvalue), then, if desired, calculates the transient nodal flux/power distributions. Transients may be initiated by simulated control rod movement or by a simple thermal-hydraulic feedback model. Hence, QUANDRY is capable of analyzing many reactor transients of interest.

3.2.1.2 The Quadratic Analytic Nodal Method

A model which approximates a highly heterogeneous reactor core as many regions containing "equivalent" homogeneous nuclear properties naturally lends itself to the calculation of node-averaged fluxes. However, the traditional approach has been to solve the diffusion equations by finite difference methods. These methods require a very fine spatial mesh to obtain accurate results in regions where large spatial flux gradients occur. The fine mesh fluxes are expensive to calculate and are then averaged to give the desired node-averaged fluxes. Another

approach is to solve directly for the node-averaged fluxes, thereby saving much unnecessary computational effort. The nodal methods for solving the neutron diffusion equation are based upon this idea. Several different nodal methods have been developed [A-4, D-9, R-8, L-8, S-7], including the Quadratic Analytic Nodal Method upon which QUANDRY is based. The derivation of the nodal equations usually begins with the integration of the group diffusion equation over an arbitrary rectangular node. This produces a nodal balance equation which states that the sum of the net leakage rates across the faces of the node for a given neutron energy group is equal to the difference between the node-average neutron production and removal rates. The nodal balance equation is a rigorous statement of the neutron balance for any node. Indeed, the same nodal balance equation can be obtained directly in a formally exact fashion from the neutron transport equation. However, the nodal balance equations cannot be solved without obtaining additional equations specifying the relationships between the node-averaged fluxes and the face-averaged currents. Older nodal methods rely on adjustable parameters or albedoes which must be determined by auxiliary calculations. Systematically derived nodal methods, on the other hand, include nodal coupling equations which relate the nodal fluxes and currents and permit the nodal balance equation to be solved. The resulting set of equations can be arranged to have a structure similar to finite difference equations.

The nodal coupling equations are the distinguishing feature among different nodal methods. They typically relate the average net current across a nodal interface to the average fluxes in the two contiguous nodes

and, to a lesser extent, to other average currents. QUANDRY is based upon the analytic nodal method of Shober and Henry [S-7]. In this method, a differential equation specifying the nodal coupling for each direction in each node is obtained by integrating the basic space-time group diffusion equation over the two directions transverse to the direction of interest. The resultant coupling equation for direction "u" for a given node has the following (steady-state, one energy group) form:

$$- D \frac{\partial^2}{\partial u^2} \phi_u(u) + (\Sigma_A - \nu\Sigma_f) \phi_u(u) = - S_u(u); \quad u = x, y, z \qquad 3.1$$

where

ϕ_u = "one-dimensional" one-group flux for direction "u"

D = diffusion constant

Σ_A = macroscopic absorption cross section

$\nu\Sigma_f$ = number of neutrons per fission times macroscopic fission cross section

$S_u(u)$ = sum of the two net leakages transverse to the direction u, per unit u, divided by the area of the node in the u direction.

This equation, when multiplied by the volume of a slab of thickness du and cross sectional area of the "u" face, is a statement of the neutron balance in the differential slab. The desired nodal flux-current relationship could be obtained by solving Eq. 3.1 for the "one-dimensional" flux and then integrating this across the node in the "u" direction. However, the "u" dependence of the transverse leakage term must be known or approximated in order to solve Eq. 3.1. At this point, the

only approximation of the Analytic Nodal Method must be made. In Shober's original formulation the transverse leakages were assumed to be spatially flat with a node. The approach used in QUANDRY is a refinement of this method in which the shape of the transverse leakages is approximated by quadratic polynomial expansion functions and the average transverse leakages in three adjacent nodes [B-6]. The functional form of this approximation is as follows:

$$S_u(u) \cong \bar{S}_u^{\ell-1} \rho_u^{\ell-1}(u) + \bar{S}_u^{\ell} \rho_u^{\ell}(u) + \bar{S}^{\ell+1} \rho_u^{\ell+1}(u);$$

$$u = x, y, z \qquad 3.2$$

where

$\bar{S}_u^{\ell}$ = the sum of the nodal face-averaged transverse leakages for node ℓ and direction u

$\rho_u^{\ell}(u)$ = quadratic expansion function in u

The quadratic expansion functions are chosen such that the integral of the transverse leakage approximation over any of the three adjacent nodes preserves the average transverse leakage of that node. With this requirement imposed, the coefficients of the quadratic expansion functions are uniquely determined by the mesh spacing in the direction "u." The expansion functions for each node are unique, even though the coefficients for a given node also preserve the average transverse leakages of its adjoining nodes.

The specification of the transverse leakage approximation makes possible the application of the Analytic Nodal Method. The form of the

transverse leakage approximation is quite convenient since the nodal face-averaged transverse leakages are also unknowns in the nodal neutron balance equation. This method, called the Quadratic Analytic Nodal Method, was found to improve the accuracy of the original analytic nodal method.

3.2.1.3 Solution Method

QUANDRY solves two different forms of the nodal diffusion equations, static and time-dependent. In the static solution, the time derivatives are set to zero and a criticality calculation is performed. The reactor power is specified by the user and the calculated flux distribution is normalized to match the given power level. For transient applications, the time-dependent form of the nodal diffusion equations and the nodal delayed neutron precursor equations are solved. The methods that are used to solve both forms of the nodal diffusion equations are similar, but are discussed separately.

The equations for the static neutron balance and analytic solution of the spatial coupling equations with quadratic leakage terms can be written in super-matrix form as:

$$\begin{bmatrix} [\Sigma_t] & h_y^j h_z^k [I] & h_x^i h_z^k [I] & h_x^i h_y^i [I] \\ [F_x] & -[I] & \frac{1}{h_y^j}[G_x] & \frac{1}{h_z^k}[G_x] \\ [F_y] & \frac{1}{h_x^i}[G_y] & -[I] & \frac{1}{h_z^k}[G_y] \\ [F_z] & \frac{1}{h_x^i}[G_z] & \frac{1}{h_y^j}[G_z] & -[I] \end{bmatrix} \begin{bmatrix} [\bar{\phi}] \\ [\bar{L}_x] \\ [\bar{L}_y] \\ [\bar{L}_z] \end{bmatrix} =$$

$$= \frac{1}{\gamma} \begin{bmatrix} [M] & [0] & [0] & [0] \\ [0] & [0] & [0] & [0] \\ [0] & [0] & [0] & [0] \\ [0] & [0] & [0] & [0] \end{bmatrix} \cdot \begin{bmatrix} [\bar{\phi}] \\ [\bar{L}_x] \\ [\bar{L}_y] \\ [\bar{L}_z] \end{bmatrix} \qquad (3.3)$$

where

$[\bar{\phi}]$ ≡ a column vector containing the node-averaged fluxes

$[\bar{L}_u]$ ≡ a column vector containing the u-direction net leakages; u = x, y, z

$[F_u]$ ≡ a matrix containing elements coupling the u-directed net leakages to the node-averaged fluxes

$[G_u]$ ≡ a matrix containing elements coupling the u-directed net leakages to the average transverse leakages

$[\Sigma_T]$ ≡ a matrix containing elements which are the products of nodal volumes and nodal total-minus-in-scattering cross sections

[M] ≡ a matrix containing elements which are the products of nodal volumes and nodal $[\chi \cdot \nu \Sigma_f]$ terms.

h_u^{ℓ} ≡ the mesh spacing in direction u for location ℓ $\quad u = x,y,z \quad \ell = i,j,k$

The precise definitions of the matrix elements are given in Ref. S-1. The top row of matrices in Eq. 3.3 are simply the two-group nodal neutron balance equations. The remaining three rows of matrices are the result of the analytic coupling equations for each direction. This super-matrix equation is a set of linear equations in the four vector unknowns. The global reactor eigenvalue is also an unknown. These equations also require appropriate boundary conditions to be applied at the reactor surface. QUANDRY actually uses a different form of Eq. 3.3 obtained by substituting the last three blocks of equations into the first block of equations. The resulting equation is of the form:

$$[H]\ [\Psi] = \frac{1}{\gamma}\ [P]\ [\Psi] \tag{3.4}$$

This global reactor equation has the form of a classical eigenvalue problem, except that some of the elements of [H] depend on the eigenvalue, γ. These are the elements arising from the analytic solution of the one-dimensional diffusion equation, as previously discussed. Because of the complicated structure of Eq. 3.4, iterative methods are used to solve for the eigenvalue and the eigenvector ($[\Psi]$, a column vector of node-averaged fluxes and face-averaged leakages).

The solution of Eq. 3.4 involves three levels of iterations. The first level of iteration is the outer, or fission source, iteration. The outer iteration is applied to determine the maximum eigenvalue and the corresponding eigenvector. If p is used as the index of the outer iterations, Eq. 3.4 is written as:

$$[\Psi]_{p+1} = \frac{1}{\gamma_{p+1}} [H]_p^{-1} [P] [\Psi]_p; \; p = 0,1,\ldots,\infty \tag{3.8}$$

where γ_{p+1} is an estimate of the global static eigenvalue.

The outer iteration consists of calculating the new eigenvector by performing the indicated multiplication. The convergence rate of the fission source iteration is increased by "eigenvalue shifting" or Wielandt's fractional iteration [W-2]. The outer iterations are monitored for convergence of the eigenvalue as well as for convergence of the nodal powers. Periodically, the elements of the matrix [H] must be recalculated with the latest value of the eigenvalue.

In order to perform the outer iteration (Eq. 3.5), the matrix $[H]_p$ must be inverted. This is accomplished in an iterative fashion by means of a "modified" block Gauss-Seidel inner iteration. The inner iteration is a two step process. The first step consists of determining new node-averaged fluxes using the old leakages and fission source. This step is itself iterative, requiring the third level of iteration, the flux iteration. The flux iteration performs a matrix iteration by the Cyclic Chebyshev Semi-Iterative method [V-3]. This method is like a block successive overrelaxation method in which the relaxation parameter is varied from iteration to iteration in such a way as to increase the

average rate of convergence. The convergence of the flux iteration is attained when the reduction in the error of the nodal fluxes reaches a specified small value.

The second step of the inner iteration follows the completion of the flux iterations. The newly calculated fluxes are used to calculate new leakages. This step is not iterative, but requires many matrix multiplications. The number of inner iterations performed is determined by an input parameter. When the specified number of inner iterations has been completed, the value of the new eigenvalue is estimated and a new outer iteration is begun (if needed).

The solution procedure for the static nodal equation is efficient and reliable. The use of eigenvalue shifting increases the rate of convergence of the outer iterations, and the flux iteration technique maximizes its average convergence rate. Generally, one inner iteration per outer iteration is satisfactory. The static nodal equations and the methods used to solve them can be shown to have one important property. In the limit of infinitely fine mesh spacing, convergence to the exact solution of the two-group diffusion equations is guaranteed.

The solution of the time-dependent nodal equations is very similar to that of the static equations. The time-dependent equations contain additional terms consisting of the temporal derivative of the nodal flux multiplied by neutron speed and the delayed neutron source. A nodal delayed neutron precursor equation set also must be solved. These additonal terms are also present in the nodal coupling equations. The coupling equations (including delayed neutron precursor equation) can be solved analytically, as in the static case, by expanding the transverse

leakages in quadratic polynomials. To accomplish this, the time derivatives are approximated as follows:

$$\frac{\partial}{\partial t}\,\phi_u\,(u,t) = \omega_p(t)\,\phi_u\,(u,t)$$
$$\frac{\partial}{\partial t}\,C_d\,(u,t) = \omega_d(t)\,C_d\,(u,t) \qquad (3.6)$$

The space-dependent flux frequencies ($\omega_p(t)$) and delayed precursor frequencies ($\omega_d(t)$) are estimated from the latest and previous values of the nodal fluxes and precursor concentrations, respectively. (An option to estimate the frequencies with a simple point kinetics extrapolation model is also available.)

The analytic solution of the nodal coupling equations produces a system of spatially-discretized, time-dependent ordinary differential equations. These can be written in a super-matrix form similar to that of the static equations:

$$\begin{bmatrix} [V]^{-1}[0][0][0] \\ [0]\ \ [0][0][0] \\ [0]\ \ [0][0][0] \\ [0]\ \ [0][0][0] \end{bmatrix} \cdot \frac{d}{dt} \begin{bmatrix} [\bar{\phi}(t) \\ [\bar{L}_x(t)] \\ [\bar{L}_y(t)] \\ [\bar{L}_z(t)] \end{bmatrix} = \begin{bmatrix} [M][0][0][0] \\ [0][0][0][0] \\ [0][0][0][0] \\ [0][0][0][0] \end{bmatrix} \cdot \begin{bmatrix} [\bar{\phi}(t)] \\ [\bar{L}_x(t)] \\ [\bar{L}_y(t)] \\ [\bar{L}_z(t)] \end{bmatrix}$$
$$+ \begin{bmatrix} [F(t)] & [G_x] & [G_y] & [G_z] \\ [F_x(t)] & -[I] & [G_{xy}(t)] & [G_{xz}(t)] \\ [F_y(t)] & [G_{yx}(t)] & -[I] & [G_{yz}(t)] \\ [F_z(t)] & [G_{zx}(t)] & [G_{zy}(t)] & -[I] \end{bmatrix} \cdot \begin{bmatrix} [\bar{\phi}(t)] \\ [\bar{L}_x(t)] \\ [\bar{L}_y(t)] \\ [\bar{L}_z(t)] \end{bmatrix} + \sum_{d=1}^{D} \begin{bmatrix} [\chi_d \lambda_d \bar{C}_d(t)] \\ [0] \\ [0] \\ [0] \end{bmatrix} \qquad (3.7)$$

The details of the matrix elements are given in Ref. [S-1].

Equation 3.7, along with the nodal space- and time-dependent delayed neutron precursor concentration equations, represents the global system of equations which must be solved to obtain the space- and time-dependent flux/power distributions. Notice that only the equations represented by the first row of blocks in the matrices contain temperal operators. The solution method applies a time integration scheme to this portion of Eq. 3.7 as well as to the delayed precursor equations. The time integration scheme is the theta method [V-1], in which the temporal derivatives are approximated by finite difference and the other terms in the equations are evaluated at both the advanced and current time and weighted by $(1-\theta)$ and θ, respectively. The specification of separate thetas for the prompt and delayed equations allows the user to vary the time integration from fully explicit ($\theta = 0.0$) to a Crank-Nicholson ($\theta = 0.5$) to a fully implicit ($\theta = 1.0$) method.

This temporal integration scheme requires an iterative solution method. The resulting super matrix equation has the following form:

$$\begin{bmatrix} [P]^{N+1} & \theta_f[G_x]^{N+1} & \theta_f[G_y]^{N+1} & \theta_f[G_z]^{N+1} \\ [F_x]^{N+1} & -[I] & [G_{xy}]^{N+1} & [G_{xz}]^{N+1} \\ [F_y]^{N+1} & [G_{yx}]^{N+1} & -[I] & [G_{yz}]^{N+1} \\ [F_z]^{N+1} & [G_{zx}]^{N+1} & [G_{zy}]^{N+1} & -[I] \end{bmatrix} \cdot \begin{bmatrix} [\bar{\phi}]^{N+1} \\ [\bar{L}_x]^{N+1} \\ [\bar{L}_y]^{N+1} \\ [\bar{L}_z]^{N+1} \end{bmatrix}$$

$$+ \begin{bmatrix} [Q]^N & (1-\theta_f)[G_x]^N & (1-\theta_f)[G_y]^N & (1-\theta_f)[G_z]^N \\ [0] & [0] & [0] & [0] \\ [0] & [0] & [0] & [0] \\ [0] & [0] & [0] & [0] \end{bmatrix} \cdot \begin{bmatrix} [\bar{\phi}]^N \\ [\bar{L}_x]^N \\ [\bar{L}_y]^N \\ [\bar{L}_z]^N \end{bmatrix} +$$

$$+ \begin{bmatrix} \sum_{d=1}^{D} \frac{\lambda_d}{1 + \lambda_d \Delta t \cdot \theta_p} [\bar{C}_d]^N \\ [0] \\ [0] \\ [0] \end{bmatrix} \tag{3.8}$$

In order to advance from one time step to the next, the block matrix on the left hand side of Eq. 3.8 must be inverted. The structure of this matrix is similar to that of the matrix which is inverted for each outer iteration of the static solution. Hence, the same strategy is used to solve Eq. 3.8.

The transient solution method therefore consists of an inner iteration and a number of flux iterations. The flux iterations are also identical to those of the static solution. The convergence criterion for the flux iteration is based upon the average fractional change in nodal power decreasing to a value below a specified limit. The fluxes and leakages are extrapolated to new time levels by using estimates of the appropriate space- and time-dependent frequencies:

$$\begin{aligned} [\bar{L}_u]^{N+1} &= [\bar{L}_u]^N \, e^{[\omega_p]^N \Delta t} \\ [\bar{\phi}]^{N+1} &= [\bar{\phi}]^N \, e^{[\omega_p]^N \Delta t} \end{aligned} \tag{3.9}$$

These extrapolations improve the convergence of the solution method.

3.2.1.4 Control Rod Model

QUANDRY allows the motion of control rods to be modeled during the transient calculation. The motion of a control rod is modeled as spatially-uniform changes in macroscopic cross sections within individual nodes. These changes in cross sections can be applied

instantaneously or linearly over a given time interval. For the latter case, the cross sections in the node are modeled as the volume weighted average of the fully-rodded and fully-unrodded nodal cross sections. This method of obtaining a spatially uniform set of cross sections is not correct unless the flux is spatially flat within the node. The resulting error manifests itself in the phenomenon called cusping. Cusping is the over- and under-prediction of the differential control rod "worth" as the rod is moved across the node. An optional correction is available in QUANDRY which reduces the control rod cusping errors by approximately 50% [S-6]. The cusping correction is only valid for a uniform axial mesh spacing.

3.2.1.5 Simple Feedback Model

QUANDRY has a built-in thermal-hydraulic feedback capability, based on a simple lumped heat capacity model with a linear cross section model. The thermal-hydraulic model does not allow boiling or reverse flow, does not calculate a pressure drop, and uses constant thermal properties for the fuel, clad, and coolant. The neutronics and thermal-hydraulics equations are solved in tandem, with all cross sections treated as linear functions of fuel temperature, moderator temperature, and moderator density. A steady-state version of the simple thermal-hydraulics model is used during the static convergence and a separate transient version is used for time-dependent calculations. A thermal-hydraulically induced transient may be analyzed by specifying the time-dependent inlet flow rate or inlet coolant temperature.

The macroscopic cross section of type α for node (i,j,k) is determined by an equation of the form:

$$\Sigma_{\alpha(i,j,k)} = \Sigma^{*}_{\alpha\,(i,j,k)} + \left(\frac{\partial\Sigma_{\alpha}}{\partial T^{c}}\right)\left(T^{c}_{(i,j,k)} - T^{c*}\right)$$

$$+ \left(\frac{\partial\Sigma_{\alpha}}{\partial T^{f}}\right)\left(T^{f}_{(i,j,k)} - T^{f*}\right) + \left(\frac{\partial\Sigma_{\alpha}}{\partial \rho^{c}}\right)\left(\rho^{c}_{(i,j,k)} - \rho^{c*}\right) \qquad (3.10)$$

where T^{c} and T^{f} are node-averaged coolant and fuel temperatures, respectively, and ρ^{c} is the node-averaged coolant density. Quantities marked with * indicate user-supplied reference values. This type of relation describes cross sections accurately over only limited ranges of temperatures and densities. However, the model assumes that the linear functional form is valid over the entire range of thermal-hydraulic variables so that, if the reference cross sections and partial derivatives are known, the thermal-hydraulic feedback model can be completely specified.

3.2.2 QUANDRY Validation

3.2.2.1 Static Benchmark Calculations

QUANDRY has been applied successfully to a number of steady-state and transient benchmark problems. The static problems include two-dimensional BWR and PWR problems and a three-dimensional PWR problem. The purpose of these calculations was to test the accuracy and computational efficiency of the quadratic analytic nodal method. Table 3.1 summarizes the static benchmark problems.

QUANDRY was applied to the two-dimensional LRA BWR two-group benchmark problem. The QUANDRY model consisted of a 1/8 core symmetric section with a 15 cm spatial mesh. The benchmark problem includes several control rods in fully withdrawn positions, causing severe local

Table 3.1

QUANDRY Benchmark Calculations

Title	Type of Analysis	Number of Dimensions	Description
LRA BWR two-group	static	2	1/8 core with several withdrawn control rods
IAEA PWR two-group	static	2	1/8 core, two zone, reflectors, inserted control rods
BIBLIS PWR two-group	static	2	1/8 core, checkerboard board pattern, reflector, control rods
LMW LWR two-group	static	3	simplified two zone core, axial and radial reflectors
IAEA PWR two-group	static	3	1/8 core, two zone, reflectors, inserted control rods
TWIGL Seed-Blanket	transient	2	1/8 core, ramp and step positive reactivity insertions
LMW LWR Rod Withdrawal	transient	3	rod bank withdrawal and insertion
LRA BWR Rod Withdrawal	transient	2	ramp control rod removal with Doppler feedback

flux perturbations. The QUANDRY solution had maximum and average errors in nodal power of 0.19% and 0.07%, respectively. The error in eigenvalue was only $+5x10^{-5}$. The agreement between QUANDRY and the reference solution was obviously excellent. The finite difference code MEKIN requires a 2.5 cm spatial mesh and two orders of magnitude more computer time than QUANDRY to achieve a maximum assembly power error of 5% [H-6].

QUANDRY was also applied to the two-dimensional IAEA PWR two-group benchmark problem. The reactor consists of a two zone core with a radial and axial water reflector and nine fully inserted control rods. This configuration results in severe local flux perturbations which make accurate analysis quite challenging. QUANDRY solutions were obtained for an 1/8 core symmetric section and both 10 cm and 20 cm mesh spacings. For the 20 cm (assembly-size) mesh, the maximum and average errors in nodal power were 0.94% and 0.27%, respectively. For the 10 cm mesh (four nodes per assembly), the maximum and average errors in nodal power were 0.32% and 0.11%, respectively. The errors in eigenvalue for the 10 cm mesh and 20 cm mesh cases were $+1x10^{-5}$ and $+3x10^{-5}$, respectively. The agreement between QUANDRY and the reference solution was again excellent. It has been reported that finite difference methods require a spatial mesh of less than 1.25 cm to achieve similar accuracy [W-3].

The two-dimensional BIBLIS PWR static benchmark problem was the most difficult reported. The reactor has a checkerboard loading pattern with nine different compositions, control rods and a water reflector. This benchmark problem differs from the previous two in that it represents an actual operating reactor. A QUANDRY analysis of a 1/8 core symmetric section, rods withdrawn configuration, with assembly-width mesh

size (23 cm) produced a maximum and average error in nodal power of 1.91% and 0.56%, respectively. The error in eigenvalue was -1.8×10^{-4}. A QUANDRY analysis with an 11.5 cm mesh spacing had a maximum error in nodal power of less than 0.20%. Hence, the QUANDRY analysis showed good agreement with the reference solution. QUANDRY also compared very favorably with three other nodal methods.

QUANDRY has been applied to a three-dimensional problem known as the LMW (Langenbuch-Maurer-Werner) test problem. The reactor is a highly simplified LWR with a two zone core and axial and radial water reflectors. Though the LMW test problem is a slow rod withdrawal transient, the results of the pre-transient static calculation are also of interest. The QUANDRY solution had a maximum error in nodal power of 0.98%, and a maximum and average error in assembly power of 0.28% and 0.12%, respectively. The error in eigenvalue was $+8 \times 10^{-5}$. These results are quite good. The transient results are discussed in Sec. 3.2.2.2.

The final static benchmark problem analyzed was the three-dimensional IAEA PWR two-group test. This is a three-dimensional version of the previously described IAEA benchmark problem. In the three-dimensional problem, four partially inserted control rods and nine fully inserted control rods are present in the two zone core. The combination of inserted control rods and a water reflector results in severe local flux perturbations which make the problem challenging. The QUANDRY solution had maximum and average nodal power errors of 0.7% and 0.24%, respectively. The QUANDRY error in eigenvalue was +.001%, which is excellent agreement for this difficult test problem. A comparison of the QUANDRY results to those obtained with three other methods (nodal,

finite element, finite difference) showed that the accuracy and computational efficiency of QUANDRY were very good.

3.2.2.2 Transient Benchmark Calculations

QUANDRY has also been successfully applied to several two- and three-dimensional, two-group, transient reactor benchmark problems. These are summarized in Table 3.1. The first of these was a series of reactivity transients in a square unreflected seed-blanket reactor. The test problems were ramp or step positive reactivity insertions modeled in two-dimensional, eighth-core symmetry with one delayed precursor group. Table 3.2 shows the results obtained with QUANDRY and two other codes for a typical ramp perturbation calculation. For this case, the results indicate that the QUANDRY solution was consistently the most accurate. The maximum error in perturbed region power at t = 0.5s was less than 0.1% for QUANDRY. The computational efficiency of QUANDRY was as good or, in most cases, substantially better than that of other neutronics codes.

The second transient benchmark problem was the three-dimensional LMW (Langenbuch-Maurer-Werner) test problem. This problem consists of an operational transient in a highly simplified LWR with a two zone core and axial and radial water reflectors. The static results are discussed in Sec. 3.2.2.1. The transient consists of the relatively slow (3 cm/s) withdrawal of a bank of four partially inserted control rods followed by the insertion of a bank of five control rods at the same speed. This problem is a challenge for QUANDRY because of the problem of control rod representation and cusping (see Section 3.2.1). Table 3.3 shows

Table 3.2 [G-2]

Total Power Versus Time for 2-D TWIGL Seed-Blanket Reactor Problem (Coarse Mesh Ramp Perturbation, Δt = 5 ms)

	Code			
Time, s	2DTD[S-7]	CUBBOX[L-9]	QUANDRY	Ref.
0.0	1.0	1.0	1.0	1.0
0.1	1.305	1.321	1.305	1.307
0.2	1.951	1.985	1.953	1.957
0.3	2.064	2.074	2.074	2.074
0.4	2.081	2.092	2.092	2.092
0.5	2.098	2.109	2.109	2.109

Table 3.3 [G-2]

QUANDRY: Power Versus Time for the 3-D LMW Test Problem

(20 cm Axial Mesh)

	Mean Power Density (% Error)			
Time, s	$\Delta t = 5.0$	$\Delta t = 2.5$	$\Delta t = 1.0$	$\Delta t = 0.5$
0.0	150.0	150.0	150.0	150.0
5.0	168.8 (-.4)	167.6 (-1.1)	167.3 (-1.4)	167.3 (-1.3)
10.0	198.0 (-2.0)	197.9 (-2.1)	198.1 (-2.0)	198.2 (-1.9)
20.0	250.8 (-3.9)	253.0 (-3.0)	254.0 (-2.6)	254.4 (-2.4)
30.0	200.9 (-4.5)	203.7 (-3.0)	204.2 (-2.8)	204.8 (-2.5)
40.0	121.1 (-2.3)	121.2 (-2.2)	120.9 (-2.5)	121.1 (-2.3)
50.0	75.9 (-.8)	75.4 (-1.5)	75.1 (-1.9)	75.1 (-1.9)
60.0	57.9 (-1.2)	57.7 (-1.6)	57.6 (-1.7)	57.7 (-1.6)
Execution time, s (IBM 370/168)	33.0	48.6	80.4	111.0

the time-dependent power density calculated by QUANDRY for various time step sizes. A control rod cusping correction(see Sec. 3.2.1) was included in these calculations. The mean power densities were consistently under-predicted by one to five percent. These errors are due, in part, to residual control rod cusping effects. This was demonstrated by reducing the spatial mesh from 20 cm to 10 cm and analyzing the test problem for various time-step sizes. Table 3.4 shows that the errors in mean power density were significantly reduced, indicating that QUANDRY can predict the time-dependent mean power density with a maximum error of less than 2.0%. These results (and their sensitivity to control rod cusping effects) are particularly important to the current work, since several control rod removal transients have been analyzed with TITAN.

The final transient benchmark problem was the two-group two-dimensional LRA BWR problem with feedback. This problem consists of the ramp removal of four control rods from a two zone core with a water reflector. The control rods are positioned such that a quarter core symmetric section can be modeled, but the control rod is asymmetrically located within the quarter-core. The removal of the control rod results in a super-prompt critical excursion which is limited by Doppler feedback. For this problem the thermal group absorption cross section was modeled as linearly proportional to the square root of the average fuel temperature. A comparison of results obtained with several different nodal codes is presented in Table 3.5. These results indicate that QUANDRY is capable of producing very good results with high computational efficiency.

Table 3.4 [G-2]

QUANDRY: Power Versus Time for the 3-D LMW Test Problem

(10 cm Axial Mesh)

Mean Power Density (% Error)

Time, s	$\Delta t = 5.0$	$\Delta t = 2.5$	$\Delta t = 1.0$
0.0	150.0	150.0	150.0
5.0	169.9 (+0.3)	168.4 (-0.6)	167.6 (-1.1)
10.0	200.4 (-0.8)	199.8 (-1.1)	199.0 (-1.5)
20.0	254.5 (-2.4)	256.3 (-1.6)	256.8 (-1.4)
30.0	204.2 (-2.8)	206.4 (-1.7)	207.5 (-1.2)
40.0	122.3 (-1.3)	122.4 (-1.2)	122.4 (-1.2)
50.0	76.6 (+0.1)	76.0 (-0.7)	75.8 (-0.9)
60.0	58.4 (-0.3)	58.1 (-0.9)	58.1 (-0.9)
Execution time, s (IBM 370/168)	63.0	108.0	168.1

Table 3.5

QUANDRY Results for the 2-D LRA BWR Transient Benchmark Problem [G-2]

Computer Code:	2DTD [S-8]	CUBBOX [A-5]	NGFM [L-10]	IQSBOX [A-5]	QUANDRY	Reference Solution [S-8]
Number of Spatial Mesh Points:	121	121	121	121	121	484
Number of Time-steps:	1000	1200	500	522	329	2600
Time to First Peak, s:	1.426	1.421	1.434	1.445	1.429	1.436
Power at First Peak, MW:	5552.	5734.	5469.	5451.	5538.	5411.
Power at Second Peak, MW:	815.	≈830.	810.	≈800.	796.	784.
Power at Time = 3.0 s:	97.	≈60.	—	≈100.	96.2	96.
Computer Time, cpu-s:	210	180	150	255	118	1661
Type of Computer:	IBM 370/168	IBM 360/91	CYBER 175	CYBER 175	IBM 370/168	IBM 370/195

3.3 THERMIT

3.3.1 Code Description

3.3.1.1 Overview

THERMIT [R-6] is an advanced two-fluid thermal-hydraulics code capable of performing steady-state and transient analyses of water-cooled nuclear reactors in three dimensions. The reactor is modeled as a collection of calculational volumes (or nodes) in a Cartesian grid for which fluid dynamics and convective heat transfer calculations are performed. The fluid dynamics model is a distributed resistance (or porous body) formulation incorporating separate partial differential equations expressing conservation of mass, momentum, and energy for the vapor and liquid phases. Models for the exchange of mass, momentum, and energy between the phases are also included. As a result, both thermal and mechanical non-equilibrium in two-phase flow can be realistically modeled. The fluid dynamics equaitons are solved by a flexible and reliable method which is not limited by the speed or direction of the flow and is thus well suited for severe transients. THERMIT can model complex fluid dynamics conditions, such as natural circulation, blow-down, flow reversal, and phase separation.

The convective heat transfer model provides fuel temperatures and heat fluxes to the coolant. A complete boiling curve is used to determine the appropriate heat transfer regime. Appropriate heat transfer and DNB/CHF correlations are included which span the range of expected conditions. The fuel rod model solves the radial heat conduction equation for fuel temperatures, using (optional) temperature-dependent fuel and clad properties as well as a variable gap heat transfer coefficient model.

THERMIT provides considerable flexibility in modeling reactors. The original version [R-6] was designed for a reactor model consisting of volumes (nodes) no smaller than the width of a fuel assembly. A single average fuel rod is associated with each node. These nodes are defined by arbitrary mesh spacings for each coordinate direction. The reactor model can have irregular radial boundaries to account for the "zig-zag" design of most reactor cores.

The version used in the current work, THERMIT-2 [K-1], has the additional capability of modeling coolant-centered subchannels having widths comparable to the fuel rod pitch. Each subchannel is associated with four fuel rods. This permits the detailed thermal-hydraulic analysis of an individual fuel assembly. These two modeling options cannot be combined in the same reactor nodel. Hence, the subchannel modeling capability of THERMIT-2 is not utilized in the current work.

THERMIT permits flexible boundary condition specification. Either coolant velocity or pressure distributions can be specified for the core inlet and exit. The distribution of the coolant inlet temperature is also required. If desired, the heat transfer calculation can be replaced by a constant heat flux or omitted entirely. When a heat transfer calculation is performed, the spatial distribution is specified by an axial and a transverse profile. The heat generation profile within the fuel pellets must also be specified.

The method used to solve the fluid dynamics equations does not permit the direct solution of the steady-state hydraulics. Therefore, THERMIT uses a transient approach to steady-state in which an unperturbed transient is run until a solution is obtained which changes little from

time-step to time-step. The steady-state solution can then form the basis for a transient analysis. Transients may be produced by applying tabular forcing functions to the inlet and outlet velocity/pressure distribution boundary conditions and to the coolant inlet temperature distribution. These forcing functions are simple multipliers specified for discrete times. Hence, the spatial distributions of these boundary conditions are not changed by the forcing functions. The code interpolates linearly for transient times between the specified multipliers. The total reactor power can also be perturbed, either by tabular time-dependent multiplier or by an exponential model with specified reactor period.

THERMIT is designed to be operated interactively, with the user monitoring calculations at an on-line terminal. The code can be operated in two modes. In the direct mode, the transient approach to steady-state goes directly into the actual transient calculation when adequate convergence has been obtained. In the restart mode, the converged steady-state solution is saved on a disk file and the transient is begun from this file in a separate restart calculation. The restart approach allows the steady-state solution to be examined in detail before the transient perturbations are applied. In addition, a single steady-state dump file can be used for many transient restart calculations.

3.3.1.2 Models

The fluid dynamics model of THERMIT is distinguished by two features: a distributed resistance approach and a two-fluid representation. A distributed resistance model (or porous body model) is one in which time- and space-averaged conservation equations are solved for large control volumes. This approach has much in common with the nodal neutronics

methods. The control volumes usually have dimensions of the order of the width of a fuel assembly. The geometrical detail within the control volume is not modeled and, hence, the structure of the flow cannot be determined. Indeed, the term "distributed resistance" refers to the distribution of equivalent frictional resistances within the control volumes. Average fluid conditions are calculated for each control volume. The derivation of the THERMIT equations can be found in reference [K-1]. The distributed resistance formulation has been extended to subchannel-type control volumes in THERMIT-2.

THERMIT uses the two-fluid conservation equations, in which vapor and liquid phases are represented as separate fluids for which the equations of mass, momentum, and energy are solved. The two fluids (when present) are in direct contact with each other and are assumed to occupy the available volume. In the porous body formulation, the size and structure of the liquid-vapor interface cannot be determined. Only the vapor and liquid volume fractions can be determined for each control volume. The volume fractions of vapor and liquid are represented by the void fraction, α, which is actually the vapor volume fraction. Hence, the vapor volume fraction is α and the liquid volume fraction is $1-\alpha$.

The two-fluid model allows thermal and mechanical non-equilibrium between liquid and vapor phases. The conservation equations contain terms for the density, velocity, internal energy, etc. for each fluid. The assumptions of equal temperatures, velocities, etc. found in simpler two-phase flow models are not needed. However, the two-fluid equations contain terms representing the interactions of the liquid and vapor with the solid materials in the control volume and with each other. It is a

unique feature of the two-fluid models that the transport of mass, energy and momentum across liquid-vapor interfaces must be modeled explicitly. In addition, the fluid-solid interactions such as heat transfer and friction must be apportioned into liquid and vapor components. The gross assumptions of simpler two-phase models have been replaced by the addition of these interaction terms. Therefore, the two-fluid model is very general, yet dependent on the treatment of the interaction terms.

Two major assumptions and several minor assumptions are made in the process of deriving the THERMIT equations. The first major assumption is that the liquid and vapor pressures are assumed to be equal and uniform within a control volume. The second major assumption is that viscous stress and energy dissipation terms can be neglected. In the original version of THERMIT, the small scale turbulent effects were also neglected. However, these were added to THERMIT-2 and are therefore included in TITAN. Several secondary assumptions are also made. In the energy equations, the volume conduction terms are neglected, assuming that heat conduction between volumes is small compared to convection. In the momentum equations, velocities at the fluid-solid boundaries are assumed to be zero and the momentum exchange due to turbulence is only considered for the axial direction. The momentum equation is also transformed into a non-conservative form by using the mass equation to eliminate one of the derivative terms. The remaining assumptions all deal with equating the various integral terms with the exchange interactions. Semi-empirical models called constitutive relations must be supplied to provide values corresponding to these terms.

The time- and space-averaged two-fluid conservation equations, with appropriate definitions and assumptions applied, are as follows:

Conservation of Vapor Mass

$$\frac{\partial}{\partial t}(\alpha\rho_v) + \nabla\cdot(\alpha\rho_v \vec{V}_v) = \Gamma - W_{tv} \tag{3.11}$$

Conservation of Liquid Mass

$$\frac{\partial}{\partial t}[(1-\alpha)\rho_\ell] + \nabla\cdot[(1-\alpha)\rho_\ell \vec{V}_\ell] = -\Gamma - W_{t\ell} \tag{3.12}$$

Conservation of Vapor Energy

$$\frac{\partial}{\partial t}(\alpha\rho_v e_v) + \nabla\cdot(\alpha\rho_v e_v \vec{V}_v) + P\,\nabla\cdot(\alpha\vec{V}_v) + P\frac{\partial\alpha}{\partial t} = Q_{wv} + Q_{iv} - Q_{tv} \tag{3.13}$$

Conservation of Liquid Energy

$$\frac{\partial}{\partial t}((1-\alpha)\rho_\ell e_\ell) + \nabla\cdot((1-\alpha)\rho_\ell e_\ell \vec{V}_\ell) + P\,\nabla\cdot(1-\alpha)\vec{V}_\ell - P\frac{\partial\alpha}{\partial t} = Q_{w\ell} + Q_{i\ell} - Q_{t\ell} \tag{3.14}$$

Conservation of Vapor Momentum

$$\alpha\rho_v\frac{\partial\vec{V}_v}{\partial t} + \alpha_v\rho_v\vec{V}_v\cdot\nabla\vec{V}_v + \alpha\vec{\nabla}P - \alpha\rho_v\vec{g} = -\vec{F}_{wv} - \vec{F}_{iv} - \vec{F}_{tv} \tag{3.15}$$

Conservation of Liquid Momentum

$$(1-\alpha)\rho_\ell \frac{\partial \vec{V}_\ell}{\partial t} + (1-\alpha)\rho_\ell \vec{V}_\ell \cdot \nabla \vec{V}_\ell + (1-\alpha)\vec{\nabla}P - (1-\alpha)\rho_\ell \vec{g}$$

$$= -\vec{F}_{w\ell} - \vec{F}_{i\ell} - \vec{F}_{t\ell} \qquad (3.16)$$

where

α = vapor volume fraction (void fraction)

ρ = fluid density

e = fluid internal energy

$\vec{V}$ = fluid velocity vector

P = volume pressure

$\vec{g}$ = acceleration of gravity.

The subscripts ℓ and v denote liquid and vapor, respectively. All of the terms in these equations can be given physical meaning. The first term on the left side of each equation represents the time rate of change of mass, momentum, or energy in the control volume. The second term represents the convection of mass, momentum, or energy into and out of the control volume. The third term in each energy equation represents the rate at which internal energy is lost or gained because of the effects of expansion or compression of the fluids. In the momentum equations, the third term accounts for pressure forces acting to accelerate the fluids. The fourth term in each energy equation accounts for the work done on one phase when the other phase expands. In the momentum equations, the fourth term represents the force of gravity. Finally, the non-derivative terms on the right hand side of all the equations represent mechanisms for the

exchange of mass, momentum, or energy between the phases or the exchange of momentum or energy between fluid and solid materials. These exchange terms are very important to the two-fluid model and must be specified in order to solve the equations. The meaning of each term and its corresponding constitutive relation is discussed later in this section.

Equations 3.11 through 3.16 represent ten scalar conservation equations (in three dimensions, each vector momentum equation yields three scalar equations) with fourteen unknowns which must be found for each node. The fourteen unknowns (assuming that the exchange terms are knowns) are: void fraction, α; pressure, P; densities, ρ_v and ρ_ℓ; internal energies, e_v and e_ℓ; temperatures, T_v and T_ℓ; and the three components of the velocity vectors, $\vec{V}_v$ and $\vec{V}_\ell$. The additional relations needed are supplied by four equations of state:

$$\begin{aligned} \rho_v &= \rho_v\,(P,\, T_v) \\ \rho_\ell &= \rho_\ell(P,\, T_v) \\ e_v &= e_v\,(P, T_v) \\ e_\ell &= e_\ell\,(P, T_v) \end{aligned} \tag{3.17}$$

These equations are provided by empirical correlations for the state dynamic properties of water. The numerical techniques used to solve Eqs. 3.1 through 3.17 are discussed in Sec. 3.3.1.3.

The exchange terms in the two-fluid conservation equations are of three types: vapor-liquid interaction terms, fluid-solid interaction terms and turbulent interaction terms. The vapor-liquid interaction terms represent transport processes across the phase boundaries. They are as follows:

mass exchange rate (vapor production rate) $\equiv \Gamma$

interfacial momentum exchange rate (vector) $\equiv \vec{F}_{i\ell}, \vec{F}_{iv}$

interfacial heat transfer rate $\equiv Q_{i\ell}, Q_{iv}$

The fluid-solid interaction terms represent the exchange of energy and momentum between the solid materials and the two fluids. They are as follows:

fluid-solid (or "wall") heat transfer rate $\equiv Q_{w\ell}, Q_{w_v}$

fluid-solid frictional force (vector) $\equiv \vec{F}_{w\ell}, \vec{F}_{w_v}$

Only the above two types of exchange terms were included in the original version of THERMIT. The turbulent exchange processes were neglected because the large control volumes were assumed. However, the addition of subchannel analysis capability in THERMIT-2 necessitated the addition of terms accounting for these fine-scale turbulent effects. These terms represent the transfer of mass, energy and momentum across the interfaces between subchannels due to turbulent eddy transport. Though these turbulent mixing terms are not used in TITAN, they are present in the code and are presented for the sake of completeness. They are as follows:

turbulent mass exchange rates $\equiv W_{tv}, W_{t\ell}$

turbulent energy exchange rates $\equiv Q_{tv}, Q_{t\ell}$

turbulent momentum exchange rates (vector) $\equiv \vec{F}_{tv}, \vec{F}_{t\ell}$

The THERMIT two-fluid conservation equations include all of the important transport mechanisms for either large volumes or subchannels. Since the exchange terms all have rather precise physical interpretations,

it is theoretically possible to model two-phase flow accurately over a wide range of thermal-hydraulic conditions. However, many of these basic interactions are not well understood and empirical or semi-empirical models must suffice in most cases.

The model used to determine Γ, the rate of mass exchange between the two phases, must determine the vapor generation rate under equilibrium conditions (saturated boiling) and non-equilibrium conditions (subcooled boiling or liquid droplet vaporization). Two models are available in THERMIT-2. The original model in THERMIT cannot predict the generation of vapor when the bulk liquid temperature is subcooled. It can, however, model the generation of vapor when a reduction in pressure results in flashing. A second model was added to provide better results for the two-phase flow conditions usually encountered in LWRs. Here, the vapor generation rate is dependent on the heat transfer regime. The pre-CHF heat transfer regimes are represented by one model and the post-CHF heat transfer regimes are represented by a second model. The pre-CHF vapor generation rate model covers both subcooled and saturated boiling. The vapor generation rate for saturated boiling can be determined by an energy balance, since the two fluids are at thermal equilibrium. The model uses a correlation to determine the initiation of subcooled boiling. The model apportions the heat flux among the liquid and vapor components. The vapor component of the heat flux creates vapor, while the liquid component raises the liquid temperature. The model also accounts for the condensation of the vapor bubbles in the subcooled bulk liquid. A separate model is used to determine the vapor generation rate in the post-CHF suspended droplet vaporization regime. That second mass exchange

model is not appropriate for depressurization flashing. The first model is discussed in Ref. [R-6], while the second model is discussed in Ref. [K-5].

The interfacial energy exchange terms, $Q_{i\ell}$ and Q_{iv}, directly affect the vapor and liquid temperatures and, hence, control the thermal non-equilibrium. The model must address two rather different non-equilibrium situations, subcooled boiling and liquid droplet vaporization. In THERMIT-2, the model accounts for two energy exchange mechanisms, conduction and mass transfer. The energy exchange arising from mass transfer is equal to the mass transfer rate times the appropriate saturation enthalpy. Hence, this portion of the interfacial energy exchange model depends on the value of Γ (interfacial mass transfer rate) and on the pressure. The conduction portion is more difficult to model, since it must (ideally) account for the transfer of energy from superheated liquid to saturated vapor and then from saturated vapor to subcooled liquid (both present in subcooled boiling) as well as from superheated vapor to saturated liquid (droplet vaporization). The conduction energy exchange is modeled as a constant heat transfer coefficient multiplied by an appropriate temperature difference. The coefficient was chosen to force the vapor bubbles or suspended droplets to remain at the saturation temperature. A detailed explanation of this model is found in Ref. [K-1].

The interfacial momentum exchange terms, $\vec{F}_{i\ell}$ and $\vec{F}_{iv}$, represent the transfer of momentum from one phase to the other and thus control the relative velocity of the phases. The ability to calculate the velocity of each phase is an important advantage of the two-fluid method because

it makes possible accurate void fraction predictions. This is particularly important for TITAN, since the void fraction is (indirectly) one of the feedback mechanisms. Hence, the modeling of interfacial momentum exchange is quite important. The momentum exchange is strongly dependent on the flow conditions, because the flow conditions affect the structure of the flow. The area of the liquid-vapor interface depends on the flow structure and the momentum exchange is directly proportional to the interfacial area. The development of a model which includes all these effects is clearly a challenge. One approach is to incorporate a flow regime map which indicates the appropriate flow structure for the given (gross) flow conditions. Unfortunately, it is difficult to construct a map which will span all the flow conditions and two-phase regimes expected in LWRs. Hence, the THERMIT interfacial momentum exchange model has been formulated to be continuous for all flow regimes and no flow regime map is required. The coefficients of the vapor-liquid forces have been approximated by simple functions of the void fraction. At least five different forces can be postulated to exist between the phases. Of these, only two have been included in the THERMIT model, viscous and inertial forces. Viscous forces are due to shear stresses, while inertial (or drag) forces represent the loss of momentum because of the relative motions of the fluids. The forces associated with buoyancy effects and virtual mass effects and the Basset force [B-7] are neglected. The model does account for the momentum exchange associated with interfacial mass exchange. An alternative interfacial momentum exchange model developed at Los Alamos Scientific Laboratory [R-9] is also available on option.

The fluid-solid friction terms, $\vec{F}_{w\ell}$ and $\vec{F}_{wv}$, represent the loss of momentum experienced by the phases as a result of contact with fuel rods, spacer grids or any other solid components present in the control volume. Three types of friction are modeled: axial, transverse and spacer grid form loss. Single-phase axial friction is modeled with the standard expression and correlations for the laminar or turbulent friction factors. For two-phase flow, the single-phase expression is multiplied by a correction factor. Three correlations are provided for the two-phase multiplier. Since THERMIT is a two-fluid model, the friction must be apportioned between the liquid and the vapor. This is accomplished by means of a heat transfer regime-dependent liquid contact fraction. Transverse friction is treated the same way as axial friction except that one friction factor correlation is used for all single-phase flows. There is also a correlation for the two-phase multiplier for transverse friction. The axial friction can be augmented by a form loss expression to account for the presence of spacer grids. The two-phase form loss is based on the homogeneous flow model and requires user-supplied loss coefficients. The friction models and correlations are fully discussed in Ref. [R-7].

The remaining exchange terms are the fluid-solid heat transfer rates, $Q_{w\ell}$, Q_{wv}, and the turbulent mixing terms. The fluid-solid heat transfer rates are the fuel rod surface heat fluxes, apportioned to the liquid vapor phases. The basis for determining the heat flux to each phase is described later in this section. The models for the turbulent mixing terms are important for subchannel analysis, but not for the large control volume problems of interest in the current work.

Accordingly, these models are not discussed. A full discussion is available in Ref. [K-1].

The second major THERMIT calculational segment is the convective heat transfer package. This includes the fuel rod model and the clad-coolant heat transfer models. The main coupling between the fluid dynamics and the heat transfer segment is the heat flux at the fuel rod surface. The surface heat flux provides the energy exchange needed in the fluid energy equations as well as serving as a boundary condition for the fuel rod calculation. The heat transfer calculation also determines the heat flux fraction deposited in liquid and vapor, the liquid contact fraction for the friction calculation, and the onset of subcooled boiling. The heat transer package provides fuel and cladding temperatures and critical heat flux ratios.

The basic approach in THERMIT is to model the heat flux as the product of a heat transfer coefficient and the temperature difference between the cladding surface temperature and the bulk fluid temperature. Radiation heat transfer to the coolant is neglected. The heat transfer is strongly dependent upon the local flow conditions and on the temperature of the fuel surface. The relationship is so complicated that an appropriate heat transfer coefficient must be determined from an empirical correlation. Indeed, no single heat transfer correlation could be accurate over the entire range of conditions encountered in LWR transients. Therefore, the heat transfer package consists of a number of heat transfer correlations and a logic system for choosing the appropriate correlation in a given control volume at a given time.

The determination of heat transfer coefficients and heat fluxes is a two step process. The first step is to select the appropriate correlation by identifying the heat transfer regime. The correlation can then be applied to determine the heat transfer coefficient and the heat flux can be calculated. THERMIT uses a boiling curve as the basis for this process. Figure 3.1 shows a typical curve for pool boiling, in which the relationship between heat flux and cladding surface temperature is plotted. The boiling curve indicates five basic heat transfer regimes:

1) convection to single phase liquid
2) nucleate boiling
3) transition boiling
4) stable film boiling
5) convection to single phase vapor.

The heat transfer correlations in THERMIT are a modification of the BEEST (best estimate) heat transfer package [B-8]. Table 3.6 summarizes the correlations and the heat transfer regimes for which they are used. This table indicates that a distinction is made between forced convection and natural convection heat transfer to single phase coolant. A second important point is that there is no correlation given for the transition boiling regime. In this regime, an increase in the clad surface temperature results in a decrease in the heat flux (see Fig. 3.1). This type of behavior cannot be modeled as proportional to the temperature difference between the clad surface and bulk liquid temperatures. Hence, the heat flux in this regime is calculated directly as a combination of the highest heat flux in the nucleate boiling regime and the lowest heat flux in the film boiling regime (see Table 3.6, Note 1). Experiments

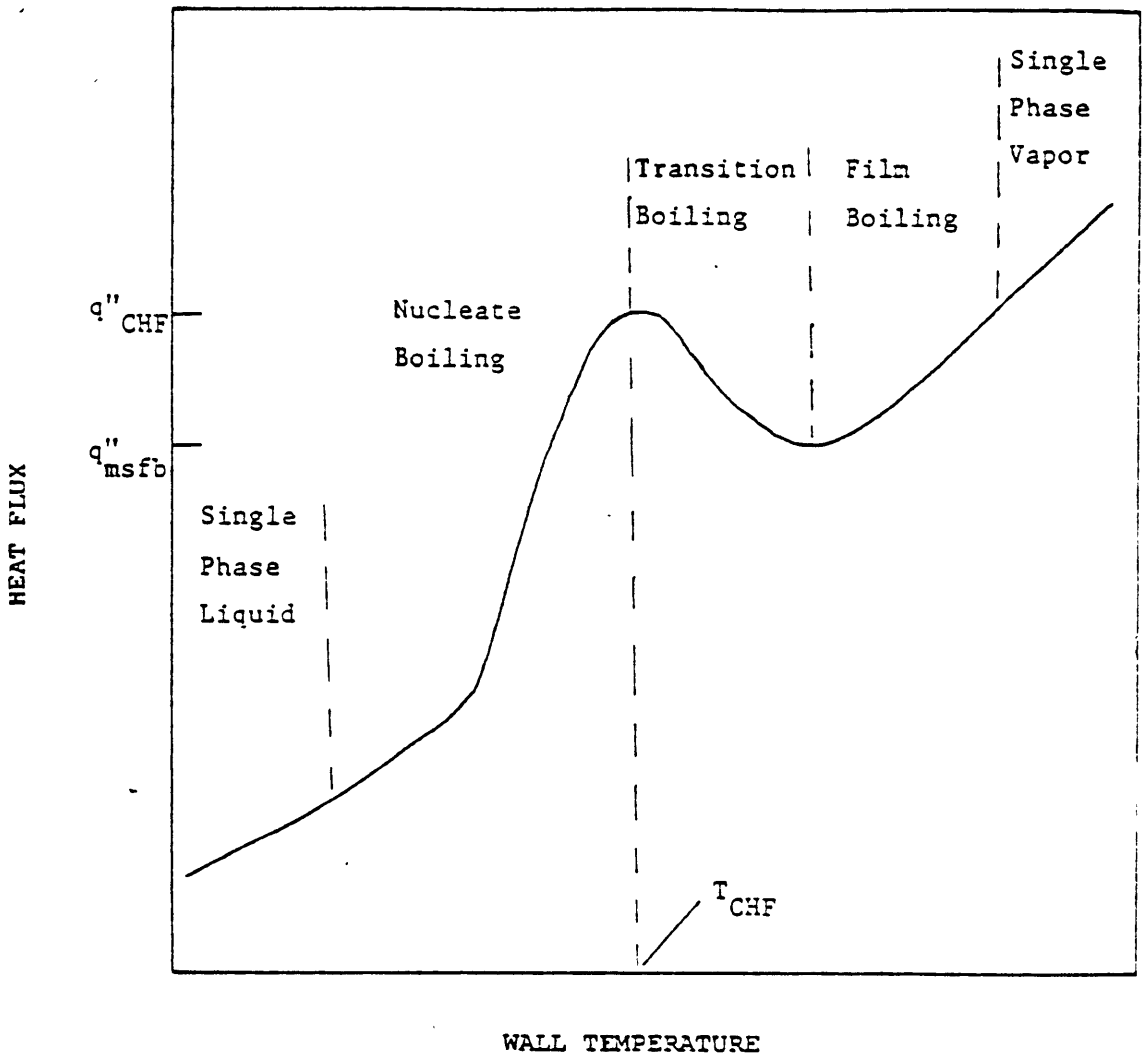

Figure 3.1 Typical Boiling Curve K-1

Table 3.6

Summary of THERMIT-2 Heat Transfer Correlations

	Regime	Correlation
1a.	Single-phase liquid, forced convection	Sieder-Tate
1b.	Single-phase liquid, natural convection	McAdams
2.	Subcooled and nucleate boiling	Chen
3.	Transition boiling	Interpolation[1] between q_{CHF} and q_{msfb}
4.	Low x film boiling	Combination of Sieder-Tate and Bromley[2]
5a.	Single-phase vapor, forced convection[3]	Sieder-Tate
5b.	Single-phase vapor, natural convection	McAdams

Notes:

1. $q_{TB} = \varepsilon q_{CHF} + (1-\varepsilon)\, q_{msfb}$

   $\varepsilon = [(T_w - T_{msfb})/(T_{CHF} - T_{msfb})]^2$

2. $h_{FB} = (1-\alpha)h_{Bromley} + \alpha\, h_{Sieder\text{-}Tate}$; Sieder-Tate for vapor

3. Sieder-Tate correlation also used for heat transfer to vapor in the dispersed flow convection regime per assumption of the non-equilibrium vapor generation model.

indicate that the duration of transition boiling is usually quite short for a heat flux controlled surface. Therefore, this regime is omitted for steady-state calculations.

The heat transfer regime selection process also involves several correlations, as indicated in Table 3.7. These regime checkpoints rely on local, instantaneous values of flow quantities and/or clad temperatures in their assessment. The actual structure of the heat transfer selection logic is discussed in Ref. [K-1]. The apportionment of the heat flux between vapor and liquid is also based on the heat transfer regimes. The heat flux is modeled to go entirely into the liquid phase for subcooled and saturated nucleate boiling and entirely to the vapor for film boiling and dispersed flow boiling. In the transition region, the heat flux is apportioned between liquid and vapor in a continuous manner. The combination of heat transfer correlations and heat transfer regime selection logic to "build" a complete boiling curve provides a reasonably realistic coupling between the fuel rods and the coolant.

The fuel rod conduction model completes the convective heat transfer package. In the original formulation of THERMIT (and in TITAN applications), the use of large control volumes for which average fluid conditions are calculated permits the modeling of a single average fuel rod per volume. THERMIT-2 models four fuel rods per subchannel volume, each having one-fourth the power output of a full rod. For each fuel rod modeled, the one-dimensional radial conduction equation is solved, subject to the power generated and the boundary conditions imposed by the clad-coolant heat transfer model. The time-dependent power produced in each volume is determined by input parameters. A radial power production

Table 3.7

THERMIT Heat Transfer Regime Selection Methodology

Checkpoint	Criterion	Correlation
Subcooled Boiling Inception	$T_w > T_s$	—
	$T_b > T_d$	Ahmad
Saturated Nucleate Boiling Inception	$T_b > T_s$	
Transition Boiling Inception	$T_w > T_{CHF}$	Biasi, W-3, CISE-4, Bowring, Barnett, Hench-Levy
DNB or dryout-CHF	$x > x_m$	Wallis
Film Boiling Inception	$T_w > T_{msfb}$	Henrv
Film Boiling/Vapor Convection Transition	$x > 0.99$	

T_w = cladding surface temperature

T_s = coolant saturation temperature

T_d = vapor bubble departure temperature

T_{CHF} = cladding surface temperature for critical heat flux

T_{msfb} = minimum stable film boiling cladding temperature

x = flow quality

profile with the fuel rod is also given in the input. The fuel pellet, cladding, and pellet-cladding gap are explicitly modeled in THERMIT. The fuel pellet is assumed to be solid and the geometrical characteristics of the fuel are time-independent. The steady-state form of the conduction equation can be solved, on option, resulting in fuel temperatures which are always computed to be in equilibrium with the fluid temperatures and heat transfer coefficients. The time-dependent conduction equation is solved for transient calculations.

The fuel rod model allows three levels of options for the thermal properties of the fuel. In the most basic option, the fuel and cladding are assumed to have temperature-independent specific heats and thermal conductivities and the gap is modeled by a constant heat transfer coefficient. The constant fuel properties are internally supplied, but the gap coefficient is an input parameter. A second option allows for temperature-dependent fuel properties with a constant gap coefficient. The temperature-dependent fuel and cladding heat capacities and conductivities are provided by internal correlations based upon the MATPRO model [M-5]. Several of the original MATPRO correlations were modified for use in THERMIT. The third fuel model option combines temperature-dependent fuel properties with a gap heat transfer model. A modified version of the MATPRO cracked-pellet gap model provides space- and time-dependent gap coefficients based upon four components:

1) Conduction through gas, or gases,
2) Partial pellet-cladding contact,
3) Radiation, and
4) Enhanced heat transfer because of a closed gap.

The gas conduction component assumes a mixture of the four noble gases helium, argon, krypton and xenon. The relative fractions of each are user-supplied. The partial contact component is a function of the user-supplied fuel burnup. Standard formulas depending on the fuel and clad emissivities are used for the radiation heat transfer component. A constant is added to the gap coefficient to account for a closed gap.

These three options provide considerable flexibility in modeling the fuel rods. In addition, the fuel rod calculation can be bypassed altogether for steady-state calculations if fuel temperatures are not of interest. This is possible because the specification of total reactor power and steady-state power profiles uniquely determines the heat flux in each volume.

3.3.1.3 Solution Methods

The equations for fluid dynamics, fuel rod conduction and the various models for heat transfer have been discussed. The utility of these carefully derived equations and state of the art constitutive relations is dependent upon the methods employed to solve them. The methods used in THERMIT to solve the two-fluid equations and the fuel rod conduction equations have been carefully selected to provide reliable and economical results for a wide range of transient conditions.

The fluid dynamics solution relies upon a spatial and temporal finite difference approximation to the conservation equations. The time derivatives are approximated by first-order finite differences, while the other terms are evaluated at either the old time-step (i.e., explicitly) or at the new time-step (i.e., implicitly). All terms except those related

to liquid and vapor convection are treated implicitly. This results in a stability limit on the time-step size given by

$$\max \left| \frac{\Delta x}{V \Delta t} \right| > 1 \qquad (3.18)$$

This combination of implicit and explicit terms is a compromise between the time-step limitations associated with explicit formulations and the difficulty of solving fully implicit formulations. The exchange terms and the sonic propagation terms are characterized by short response times and are therefore treated implicitly. The convection of mass, momentum and energy by the motion of the fluid has a longer response time and is treated explicitly. This formulation has one other very important ramification. There is no convenient way to solve the steady-state form of these finite difference equations. As a result, THERMIT generates a steady-state solution by solving the transient equations with constant boundary conditions and power until a steady solution is converged.

The application of finite difference approximations to the conservation equations results in a set of nonlinear equations for all the unknowns. These equations are solved for a staggered mesh consisting of large control volumes and the boundaries between them. All of the fluid quantities except the velocities are associated with the centers of the control volumes. The fluid velocities are associated with the control volume boundaries and the donor cell convention is used. Fictitious control volumes are added at the core inlet and outlet to provide for the boundary conditions.

The solution technique for the fluid dynamics equations was originally developed for the TRAC code [J-2]. A two level iterative procedure is used

to advance to a new time-step. An initial guess for the fluid parameters is required for the first time-step. The procedure is as follows:

1. The equations of state are used to eliminate the densities and internal energies from a linearized form of the finite difference equations.

2. The momentum equations are manipulated to yield an expression for the velocities in terms of the pressures. This is used to eliminate the velocities from the mass and energy equations. The result is a set of four equations for each volume having the form:

$$\begin{bmatrix} x & x & x & x \\ x & x & x & x \\ x & x & x & x \\ x & x & x & x \end{bmatrix} \begin{bmatrix} P_i \\ \alpha \\ T_v \\ T_\ell \end{bmatrix} + \begin{bmatrix} x & x & x & x & x & x \\ x & x & x & x & x & x \\ x & x & x & x & x & x \\ x & x & x & x & x & x \end{bmatrix} \begin{bmatrix} P_{i+1} \\ P_{i-1} \\ P_{j+1} \\ P_{j-1} \\ P_{k+1} \\ P_{k-1} \end{bmatrix} = \begin{bmatrix} x \\ x \\ x \\ x \end{bmatrix} \qquad (3.19)$$

   where each "x" represents a known coefficient. These equations are the basis for the iterative solution method.

3. The Newton, or outer, iteration has two parts. The first part consists of inverting the 4x4 matrix of known coefficients and multiplying through by the inverse. The result is a set of four equations for each volume which express the pressure, void fraction, vapor temperature and liquid temperature, respectively, in terms of the pressures in the six adjacent volumes. This leads to the pressure, or inner, iteration.

4. One of the four equations produced by the previous step relates the pressure in a given node to the pressures in the six adjacent notes. The pressure iteration consists of taking all such equations and solving them by a block Gauss-Seidel iteration to yield the pressure field. The code sweeps systematically

through all the channels, solving for all pressures in a given channel simultaneously with a forward elimination-back substitution logic. The newest values of pressure in the four adjacent channels are used. This reduces to a direct solution for single channel models or one-dimensional flow models.

5. The Newton iteration is completed by solving the remaining linear relations for α, T_v and T_ℓ using the new pressures. The new pressures and temperatures and the full, non-linear equations of state are then used to calculate the densities and internal energies. Finally, the velocities are calculated along with fluid properties such as enthalpies, viscosities, etc.

This procedure can handle flow reversal, sonic velocity propagation, blowdown and natural circulation flow. The Newton procedure also will converge to the true solution from any reasonable initial guess, provided the time-step size is small enough and sufficient iterations are performed.

The isolated channel method is an important feature added to THERMIT by Kelley [K-5]. The purpose of this method is to improve the computational efficiency of steady-state calculations. This method, given as an input option, allows a three-dimensional problem to be solved initially with no cross-flow between the channels. After several steps, the isolated channels are "opened up" and the full three-dimensional solution is obtained. This approach is based upon the assumption that the transverse flow between channels is small. The one-dimensional fluid dynamics solution is much faster than the three-dimensional solution and provides a good initial guess for the full calculation. Kelly reported savings in computing time of 25-90% with this method.

The remaining solution method to be described is that of the fuel rod heat conduction equation. The equation is approximated by a first-order

finite difference equation and solved by a two-step fully implicit forward elimination-back substitution technique. The fuel and cladding are divided into several annular cells of equal thickness, as specified by input parameters. (The inner-most cell of the fuel is a solid cylinder.) The finite difference equations are solved for the temperatures at the boundaries between these cells, including the fuel centerline, the fuel surface, the cladding inside surface and the cladding outside surface. The heat transfer coupling to the coolant is also handled in a fully implicit manner, as shown in Table 3.8 (adapted from Kelly, Kao, and Kazimi, [K-1]).

Table 3.8 [K-1]

THERMIT: Implicit Heat Transfer Algorithm

1. Calculate H^n using previous time-step wall and fluid conditions.

2. Set up fuel rod conduction equation using the boundary condition

$$q'' = H^n \, (T_w^{n+1} - T_f^{n+1})$$

at this stage the assumption $T_f^{n+1} = T_f^n$ is made.

3. Forward Elimination of the rod conduction problem yields both an initial guess for new wall temperature,

$$T_w^{n+1,0} \text{ and } \partial T_w^{n+1} / \partial T_f^{n+1}.$$

4. Solve the fluid dynamics equations using

$$q'' = H^n \, (T_w^{n+1,(0)} - T_f^{n+1}) + H^n \, (\partial T_w^{n+1} / \partial T_f^{n+1})(T_f^{n+1} - T_f^n)$$

5. Once T_f^{n+1} is found, T_w^{n+1} is calculated using

$$T_w^{n+1} = T_w^{n+1,(0)} + (\partial T_w / \partial T_f)^{n+1} \, (T_f^{n+1} - T_f^n)$$

6. Complete the backward substitution step of the rod conduction equation.

3.3.2 THERMIT Validation

THERMIT has been subjected to extensive assessments in order to demonstrate the validity of the various models. The assessments include comparisons with both measured data and analytical results. The number and scope of these assessments are too large to be effectively discussed here, so the intent of this section is to summarize the assessment program and provide explicit references where detailed information may be obtained. This discussion is further limited to the assessment of models used in core-wide analyses.

The THERMIT fluid dynamics models were assessed through comparisons with both measured data and analytical results, as shown in Table 3.9. These comparisons included steady-state and transient, one- and three-dimensional flow fields. The THERMIT method of calculating interbundle cross-flow was assessed by comparison with measured reactor data and also with experimental rod bundle data. The correct treatment of the transient mass and energy balance equations was demonstrated by comparison to the exact analytical solution of a simplified one-dimensional two-phase flow transient. This comparison also demonstrated the versatility of the two-fluid formulation in accepting the very large interfacial exchange rates needed to produce homogeneous equilibrium two-phase flow. Finally, the blowdown experiment simulation showed THERMIT's capability in handling very rapid depressurization transients.

Table 3.9

Assessment of THERMIT Hydraulics Model

Primary Capability Tested	Reference Data Source	Parameters Compared	Notes	References
Steady-state three-dimensional flow	Maine Yankee Core Exit Temperature Distribution	Coolant Temperatures	Agreement within 3°K for most channels	[K-5]
Transient three-dimensional flow, interbundle cross-flow	Babcock and Wilcox isothermal two channel simulated rod bundle experiment	Pressure Distribution, inferred fluid velocities	Cross-flow created by inlet flow mismatch	[R-7]
Transient mass and energy balance in one dimension	Homogeneous equilibrium two-phase transient, exact analytic solution	time-dependent quality and flow rate	also demonstrates capability of two-fluid model to simulate homogeneous equilibrium model	[R-7]
Transient one-dimensional fluid flow: rapid depressurization	Edward's Pipe blowdown experiment	Pressure history	THERMIT analysis used flashing-type vapor generation model	[K-5]

A fundamental aspect of THERMIT which sets it apart from most other thermal-hydraulics codes is the two-fluid formulation. The two-fluid model involves interfacial exchange terms which have a controlling influence on the phases. Several authors, including Agee [A-3], Ishii [I-2] and Jones [5-3], have discussed the significance of the interfacial terms as well as the difficulty in obtaining appropriate expressions for them. Table 3.10 summarizes the assessment effort for the THERMIT interfacial exchange relations. The THERMIT models for the exchange of mass, momentum, and energy between vapor and liquid have been assessed by comparison to a number of boiling experiments. The interfacial momentum exchange relations were assessed by comparison to high quality data from void fraction experiments. In these cases the vapor and liquid were (at least on the average) in thermal equilibrium, so no interfacial energy exchange was involved and the vaporization rate can be determined from an energy balance. The effect of the interfacial momentum exchange rate is to determine the relative speeds of the liquid and vapor. Thus, a void fraction comparison indicates the appropriateness of the interfacial momentum exchange model.

The assessment of the interfacial mass and energy exchange models was somewhat more difficult because their effects cannot be measured or interpreted independently. These models are both important in the subcooled boiling and droplet vaporization regimes. Together they determine how much of the power goes into sensible heat addition and how much into phase change under non-equilibrium conditions. In the subcooled boiling regime, the interfacial mass exchange model was assessed by comparison to low quality void fraction data. The

Table 3.10

Assessment of THERMIT Two-Fluid Interfacial Exchange Relations

Vapor-Liquid Exchange Mechanism	Reference Data Source	Parameters Compared	Notes	References
Interfacial Mass Exchange:				
pre-CHF (subcooled and nucleate boiling)	one-dimensional void fraction experiments, low quality data	void fraction	wide range of pressure, flow rate and inlet subcooling	K-1, K-5, K-6, K-7
post-CHF (droplet vaporization)	one-dimensional heated tube experiments	tube surface temperature	tube surface temperature and known heat flux indicate amount of vapor superheat and, indirectly, the vapor generation rate	
Interfacial Momentum Exchange:	one-dimensional void fraction experiments, high quality data	void fraction	thermal equilibrium of nucleate boiling allows independent momentum exchange rate assessment	K-1, K-5, K-6, K-7
Interfacial Energy Exchange:				
pre-CHF (subcooled boiling)	one-dimensional void fraction experiments, low quality data	vapor and liquid temperatures	assessment by qualitative inference	K-1, K-5, K-6, K-7
post-CHF (droplet vaporization)	one-dimensional heated tube experiments	vapor and liquid temperatures	assessment by qualitative inference	

interfacial energy exchange model was assessed qualitatively by inference from the same data (liquid temperatures were not available). In other words, agreement or disagreement on void fraction for the low quality data was the measure of performance for the mass exchange relations and the prediction of qualitatively correct thermal non-equilibrium between vapor and liquid was the measure of performance for the energy exchange relations. In the droplet vaporization regime, the mass exchange relations were assessed indirectly from tube temperature data, relying on the existence of tight coupling between the amount of vapor superheat and the vaporization rate. Of course, the interfacial energy exchange relations also play an important role in determining the amount of superheat produced. As in the subcooled boiling regime, only the qualitative correctness of the thermal non-equilibrium between the phases was taken as a measure of the energy exchange relations. These assessments can be done in greater detail only if techniques are developed to measure the vapor-liquid exchange rates more directly. Even so, the models in THERMIT were tested over the full range of fluid conditions for which the code was designed (depressurization events were excluded from the assessment).

The THERMIT validation program included some assessment of the heat transfer model, as shown in Table 3.11. The heat transfer correlations for both pre- and post-CHF regimes and the steady-state and transient critical heat flux predictive capability were investigated by comparing THERMIT to appropriate experimental data. The imposed heat fluxes were known in each case, so the fuel rod model was not used and was not assessed.

Table 3.11

Assessment of THERMIT Heat Transfer Models

Primary Capability Tested	Reference Data Source	Parameters	Notes	References
Heat Transfer Correlations:				
pre-CHF (subcooled boilng)	one-dimensional void fraction experiments, low quality data	location of inception of subcooled boiling	correlation dependent on coolant temperature and pressure	K-1, K-5, K-6, K-7
(saturated boiling)	one-dimensional heated tube experiments	tube surface temperatures	tube temperature typically overpredicted by 10°K	K-5, K-6
post-CHF (film boiling or single-phase vapor)	one-dimensional heated tube experiments	tube surface temperatures	results strongly dependent on interfacial energy and mass exchange models	K-5, K-6
Steady-State Critical Heat Flux	one-dimensional heated tube experiments	steady-state critical heat flux ratio or critical power ratio	results strongly dependent on correlation used	K-1, K-5, K-6, K-7
	nine-rod BWR-type rod bundle experiments			K-8
	sixteen-rod PWR-type rod bundle experiments			R-10
	twenty-rod PWR-type rod bundle experiments			K-1
Transient Critical Heat Flux Prediction	nine-rod BWR-type rod bundle experiments	time to critical heat flux	flow decay transients	K-8
	heated tube experiments	time to critical heat flux	power jump and flow decay transients	K-1

The final analyses in the validation of THERMIT are the transient integral assessments, shown in Table 3.12. These analyses are characterized as integral because they test the combined contributions of the convective heat transfer models and the two-phase fluid dynamics solution. The first three assessments involve comparisons to experimental data performed by Tsai [T-3]. These experiments consisted of the heatup, level swell and boil-off of water in an electrically heated rod bundle. These phenomena are important for the reflood portion of post-LOCA analyses and for transients resulting in core uncovery. The THERMIT analyses tested both heat transfer and fluid flow models in calculating fuel rod surface temperatures, bundle pressure drops, and froth level and collapsed liquid mass histories.

THERMIT was also applied to two PWR control rod ejection analyses and the results were compared to those obtained with the COBRA-IV code [S-8]. The analyses were three-dimensional with different initial reactor conditions. Both transients involved boiling and the second produced flow reversal and coolant expulsion. These tests therefore showed the versatility of the fluid dynamics model under such conditions.

The THERMIT validation effort involved many calculations and comparisons. The nature of thermal-hydraulic modeling is such that the validity of a code cannot be expressed in terms of a few parameters which are poorly or well-predicted. The detailed comparisons are far too voluminous to be discussed here, particularly when they are available in the various references cited in Tables 3.9 - 3.12. However, the overall conclusion of the validation program is that

Table 3.12

Transient Integral Assessments of THERMIT

Transient Description	Experiment/Code	Parameters Compared	Notes	References
rod bundle boil-off	FLECHT SEASET experiments	fuel rod surface temperatures; pressure drop, dryout time, froth level history	1-D simulation; uniform radial power shape	T-3
rod bundle boil-off	Westinghouse 336-rod heated bundle experiments	fuel rod surface temperatures; collapsed liquid mass history	1-D simulation: uniform radial power shape	T-3
core uncovery	Semiscale TMI-2 experiments	fuel rod surface temperatures: collapsed water level history, void fraction distribution history	1-D (lumped channel) and 3-D (subchannel simulations: non-uniform radial power shape	T-3
control rod ejection, hot zero power, full flow	COBRA IV - implicit	time-dependent maximum cladding temperatures: time-dependent void fraction	no flow reversal; three-dimensional	K-5
control rod ejection, low power, low flow	COBRA IV - explicit	time-dependent maximum cladding temperatures: time-dependent void fraction: mass flow rates	flow reversal and coolant expulsion: three-dimensional	K-5

THERMIT is reliable and well tested for the reactor applications of interest in this work. No substantial problems were found: indeed, THERMIT generally performed very well with difficult problems such as post-CHF heat transfer and subcooled boiling. Thus, THERMIT has been suitably assessed to be included in TITAN.

3.4 THIOD-K and THERMIT-3

3.4.1 Code Descriptions

Two coupled codes strongly related to the current work were recently developed at M.I.T. by Dubé [D-4]. THIOD, a version of THERMIT having a fully implicit, one-dimensional fluid dynamics model, was coupled to a point kinetics model via a reactivity feedback loop and designated THIOD-K. In addition, the identical point kinetics model was coupled to THERMIT, resulting in a new version that is designated THERMIT-3. These two codes are significant for the current work in that they represent the first attempt at combining reactivity feedback with two-fluid thermal-hydraulics. Furthermore, THERMIT-3 is used directly in the current work in Chapter 7.

The neutronics model coupled to both THIOD and THERMIT was GAPOTKIN [H-7], which solves the space-independent kinetics equations for a very general form of the reactivity function. The code operates rapidly, allows varying time-steps, and is numerically unconditionally stable for all values of the reactivity or time-step. The reactivity is specified as functions of time to simulate control rod motion, as well as functions of thermal-hydraulics parameters such as void fraction, coolant temperature, and fuel temperature. The coupling between neutronics and thermal-hydraulics is by a reactivity feedback loop,

requiring the calculation of reactivity feedback coefficients.

The point kinetics model is only used for transient calculations. No feedback is modeled for steady-state calculations. As in all point kinetics codes, it is assumed that the static power and power shape are known and that the reactor is initially critical. Since the point kinetics model was coupled to THERMIT and THIOD in a tandem fashion, the reactor power is held constant during each thermal-hydraulic time-step. At the completion of each thermal-hydraulic time-step, a new reactor power is calculated by the point kinetics model by including fuel temperature, coolant temperature and coolant density reactivity feedback as well as external reactivity contributions. As mentioned, with THIOD it is desirable to use large time-steps because of the great computational effort per time-step. However, it is necessary to update the reactivity values often enough to keep step changes in reactor power from being too dramatic, resulting in unrealistic results. To reconcile these conflicting imperatives, a linear reactivity extrapolation technique was programmed into the THIOD feedback loop. This model calculates an initial reactivity for the feedback calculation based on a linear extrapolation of the reactivity calculated prior to the previous thermal-hydraulic calculation. This method generally works well, but it was found that when time-step sizes are too large, extrapolation of the reactivity can actually render the solution procedure unstable.

3.4.2 Reactivity Feedback Calculations with THIOD-K and THERMIT-3

Dubé used THIOD-K and THERMIT-3 to perform two groups of reactivity feedback analyses. The first group consisted of four simulated BWR transients. The second group consisted of two "benchmark" calculations.

Most of these calculations involved THIOD-K rather than THERMIT-3. The first group began with a simulated BWR flow transient in which an exponential decrease in core inlet flow was modeled with THIOD-K. It was found that the maximum calculated errors in reactor power (compared to reference case with smallest time-step) could be as large as 18% if the time-steps were large and/or the transient time constants were small. However, it was found that even relatively large deviations in power did not cause large discrepancies in void fraction or fuel temperature. Hence, although smaller time-steps may be necessary to calculate the transient reactor power accurately, the important thermal-hydraulic variables of interest such as maximum fuel and clad temperatures and minimum CHFR can be calculated quite accurately with relatively large time-step sizes. A second set of transient analyses with THIOD-K resulted in an operational map of core power as a function of rated core flow for a BWR plant. The values were determined by performing several flow transients until the neutral void reactivity effect reestablished a steady-state condition. These calculations matched the reference power versus flow curve very well. THIOD-K was then used to analyze a simulated BWR feed-water heater transient. In this accident, decreased inlet temperature results in decreased boiling and a very gradual power rise because of the negative void coefficient of reactivity. The final power increase calculated was in very good agreement with the reference value. However, some difficulties were experienced when large time-steps (3 and 4 seconds) were used. The solution became unstable, apparently because the thermal-hydraulic updates were too infrequent.

The final calculation in the first group was that of a BWR rod drop accident. For this problem, THERMIT-3 was used with a single assembly modeling the core. The reactor was assumed to be at full power when a high worth control rod dropped out of the core. The reactivity insertion was assumed to occur at a constant rate. The reactor was scrammed at 0.2 seconds after core power reached 120% of the rated value. The negative reactivity insertion was also assumed to occur at a constant rate. Temperature-dependent fuel properties were used in the calculation. The reactor power was calculated to increase to 2.6 times the steady-state value before being turned around by the scram. It was found that changes in fuel temperature and void fraction were negligible contributors to the transient behavior between time of the rod drop and the scram. About 2% of the total energy produced was deposited directly into the coolant, contributing somewhat to the void reactivity feedback. The magnitude of the void reactivity feedback was found to be about twice as great as that due to the Doppler effect. No verification of the accuracy of these results was given.

The first of the benchmark cases was an analysis of a reactivity insertion transient experiment performed with the SPERT III E-Core reactor. This reactor was essentially a small PWR in which the fuel was enclosed in cans. Because of the severity of the transient, small time-steps were deemed necessary and hence THERMIT-3 was used. The calculated results were in excellent agreement with the experimental measurements. The calculated peak power was within the uncertainty of the experimentally measured value and occurred only 0.005 seconds later than the measured peak. The second benchmark case was a calculation of

the first Peach Bottom-2 turbine trip experiments. Three pressurization transients were performed at the BWR plant in April 1977 in which the turbine was manually tripped at different power levels and near rated core flow. An intentional delay in the scram circuit logic permitted limited neutron flux increases as a result of the void collapse caused by the core pressurization. The signal to scram was eventually initiated by a high neutron flux level. The reactor was modeled by a single average-powered assembly and THIOD-K was used for the analysis. A major problem in specifying the problem was the unavailability of the core average coefficients of reactivity needed for the feedback calculation. Published reactivity coefficients which appeared to be the best available were used, but it was found that the results were extremely sensitive to the value of the void reactivity coefficient. It was assumed that 1.86% of the total power was directly deposited in the moderator. Core inlet flow and outlet pressure boundary conditions were used as calculated by RETRAN and adjusted for use in MEKIN. After the turbine trip, the pressure remained constant for approximately 0.35 seconds and rose thereafter. The transient was analyzed using several different time-steps. A time-step of 0.05 seconds was found to be too large; so calculations with time-steps of 0.02 and 0.01 seconds were performed. These small time-steps were not required by stability considerations, but rather by the accuracy of the calculated results. One result of this was that THERMIT-3 would have been more appropriate than THIOD-K for this analysis. The measured peak power and time to peak power could not be matched with the reference reactivity coefficients, so the void reactivity coefficient was "fine-tuned" until

the calculated results agreed well with the measurements. This emphasizes a major problem with reactivity feedback loops. The feedback calculation is only as good as the reactivity coefficients used in the model. Core average reactivity coefficients are limited in their accuracy and are difficult to calculate. Even when the calculation matched the experimental peak power and time of peak power fairly well, the total energy deposited during the transient was significantly less than the experiment indicated. This was largely due to a more gradual power increase calculated by THIOD-K. Dubé explained this discrepancy as a combination of the two problems· an inadequate reactor model and the existence of multidimensional effects which could not be accounted for.

3.5 Summary

The neutronics code QUANDRY and the thermal-hydraulics code THERMIT have been discussed and the relevant testing of each has been presented. These codes represent the state-of-the-art in their respective areas. They use advanced models and methods to analyze steady-state and transient reactor conditions. The analytic nodal method in QUANDRY is a significant advance over finite difference methods, both in efficiency and accuracy. QUANDRY uses a systematically derived nodal method which, unlike more primitive nodal codes, does not require special problem-dependent coupling parameters to be specified. A simple feedback capability is included. QUANDRY has been shown to give excellent results when compared to several benchmark problems, including a three-dimensional reactivity transient with feedback. All

of these features make QUANDRY a very good choice for the neutronics portion of an advanced core dynamics code.

THERMIT-2 is among the most advanced and rigorous codes for core thermal-hydraulics available. It has a full three-dimensional Cartesian fluid dynamics model which is not limited by the speed or direction of the flow. The two-fluid model with advanced constitutive relations provides the best treatment of two-phase flow in any code of its type. The accurate calculation of fluid conditions, particularly two-phase flow, is very important for a coupled neutronics/thermal-hydraulics, code. Similarly, the fuel rod model and heat transfer package are very important in determining the correct Doppler feedback. The THERMIT-2 heat transfer package provides appropriate heat transfer coefficients for the entire range of expected reactor conditions. The fuel rod model includes temperature-dependent material properties and a gap heat transfer model. THERMIT-2 has been tested against many experimental measurements and several analytical results, producing very good results in many cases and satisfactory results for even the most demanding tests. The development and application of THERMIT-3 and THIOD-K indicate that THERMIT is amenable to being coupled with a neutronics code. Hence, THERMIT has many important features which make it a good choice for the thermal-hydraulics portion of an advanced core dynamics code.

CHAPTER 4: CODE DEVELOPMENT

4.1 Introduction

The need for codes combining neutronics, thermal-hydraulics and feedback has been established and the capabilities of many of the existing codes of this type have been reviewed. It was found that none of these codes contain state-of-the-art models for both neutronics and thermal-hydraulics. A code containing rigorous and widely applicable models for both neutronics and thermal-hydraulics is highly desirable both as a safety analysis tool and as standard for assessing simpler methods. This is the motivation for the development of TITAN. The purpose of this chapter is to describe how this was accomplished.

4.2 Preliminary Considerations

The development of TITAN began with the nodal neutronics code QUANDRY and the two-fluid thermal-hydraulics code THERMIT. The models, features, capabilities and validation of these codes are discussed in Chapter 3. QUANDRY and THERMIT represent the state-of-the-art among codes of their respective types. They offered, therefore, the basic components required for the development of a code like TITAN. However, the efficacy of selecting QUANDRY and THERMIT was dependent not only upon their individual merits but also upon issues of suitability and compatibility. "Suitability" means the absence of any characteristics, either in the basic physics, numerical solutions or computer implementation of QUANDRY or THERMIT which preclude their use as part of a core dynamics code. Similarly, "compatibility" means the absence of any

characteristics which preclude combining QUANDRY and THERMIT in a core dynamics code.

QUANDRY and THERMIT were found to be suitable for inclusion in a core dynamics code. The suitability of the models of QUANDRY was demonstrated during its original development. Smith incorporated a simple thermal-hydraulics model and a linear cross section model in QUANDRY and successfully analyzed steady-state and transient benchmark problems with feedback. In addition, Langenbuch, et al [L-8] concluded that coarse mesh neutronics methods were accurate for kinetics calculations, even in the presence of strong space-dependent feedback. Similarly, Dubé [D-4] coupled a point kinetics model to THERMIT and performed several analyses with feedback. This indicates that THERMIT can provide adequate global feedback in response to changes in global reactor power. Furthermore, experience with MEKIN [L-6] and QUABOX/CUBBOX [L-8] indicates that control volumes like those used by THERMIT are adequate for calculations with space-dependent feedback. Hence, THERMIT also is suitable to be included in a core dynamics code.

Given that THERMIT and QUANDRY are individually suitable for inclusion in a core dynamics code, their mutual compatibility was still required for the successful development of TITAN. Fortunately, the codes proved to be sufficiently compatible to eliminate any major barriers to their use. Specifically, the codes are applicable to the same types of reactors and use very similar geometrical representations. It is particularly important that QUANDRY and THERMIT both rely upon three-dimensional Cartesian coordinates and model a core as a collection of rectangular parallelepiped control volumes. The typical dimension of the control volumes for each code is the same; namely, the width of a

single fuel assembly. Both codes allow irregular circumferential boundaries like those found in commercial reactor cores. Both codes are appropriate for the steady-state and transient analysis of reactors which use light water coolant and moderator. Finally, both codes are written in the FORTRAN IV computer language and are therefore basically compatible in their implementation. In summary, QUANDRY and THERMIT are compatible with each other and are appropriate choices for the development of TITAN.

Although QUANDRY and THERMIT were found to be compatible in all substantive areas, there was one area of incompatibility which had to be resolved before the development of TITAN could begin. QUANDRY was developed, made operational, and tested on an IBM 370/168 computer, while all of the THERMIT work was done on the Multics (Honeywell) computer. Obviously, it was necessary to have both codes available on the same computer in order to couple them together. Therefore, the first task in the development of TITAN was the development of a MULTICS version of QUANDRY. This approach was chosen for two reasons:

1. The interactive mode of operation of the MULTICS system is used significantly in THERMIT, and it was desirable to retain this capability.
2. The cost of computing on the MULTICS system was less than on the IBM system.

The development of a MULTICS version of QUANDRY involved some significant changes to the source code. These changes are described in Appendix B. After making the computer system conversion, several QUANDRY benchmark problems were performed to demonstrate the correct operation of the new QUANDRY version. The results were essentially identical to the original IBM version results, given that there are

slight differences in the accuracies of the computers.

4.3 TITAN Methodology

4.3.1 The Basic Approach

The actual development of TITAN followed the development of the MULTICS version of QUANDRY. The main objective of this task was to develop a core dynamics code that is accurate, efficient, and applicable to a variety of PWR and BWR transients. This was to be accomplished starting with two complete and independent codes, each with its own input and output procedures, data management logic, timing routines and initialization procedures.

The first step in the development of TITAN was the development of a methodology for combining the neutronics and thermal-hydraulics models. On the theoretical level, the methodology had to provide for the temperature and density dependence of the nuclear parameters and the local variation of the power generation. The methodology had also to incorporate the numerical methods and structural characteristics of the neutronics and thermal-hydraulics models. The TITAN methodology was devised after review of other core dynamics codes and consideration of QUANDRY and THERMIT characteristics. Two general approaches were considered. The first approach involved a fully integrated solution of the neutronics, thermal-hydraulics and feedback equations. The second approach was the tandem method, in which the thermal-hydraulics and neutronics equations are solved separately with feedback information exchanged between each segment.

The integral solution method provides the best analogy to a reactor core, in that all the processes are assumed to occur simultaneously and all the unknown parameters are solved for simultaneously. However, the simultaneous solution of the complicated set of differential and algebraic equations is a difficult proposition. Indeed, none of the core dynamics codes reviewed use an integral solution method. It is also unclear whether an integral solution is of real benefit even if one could be developed. First, the neutron diffusion equations and fluid dynamics/heat transfer equations do not have any common primary unknowns. They interact only through the nuclear parameters and the reactor power distribution, all of which are derived quantitites. Second, the disparity between the neutronic and thermal-hydraulic response times is large, so that the need for simultaneous solutions is reduced. Third, the differential equations are not solved continuously in either space or time (except for very simple problems): rather, numerical solutions at discrete points in time and space are obtained. The numerical integration which advances the solution in time involves discrete perturbations in both the specified and calculated parameters. A simultaneous solution of neutronics and thermal-hydraulics equations would require an iterative solution for all parameters in order to advance the time integration. This would lead to a considerable amount of computational effort and would not take advantage of the differences in response time inherent in the system. Furthermore, the development of an integral solution would require starting with the basic equations and devising a dedicated numerical method to solve them. However, in the current work, the existing numerical methods are of great complexity in theory as well as in implementation and are specific

to the particular equations of nodal diffusion theory and two-fluid thermal-hydraulics. Furthermore, the utility of both QUANDRY and THERMIT is strongly dependent on their numerical methods. Thus, it was deemed prudent to devise a methodology which left the basic computational components intact while unifying them into a self-contained program. Accordingly, the integral solution methodology was not pursued.

The second methodology considered was the tandem approach. This approach leaves the neutronic and thermal-hydraulic solutions in distinct computational segments coupled by the exchange of feedback information. The feedback information is the set of results provided by one calculational segment and used by the other. Thus, the results of the thermal-hydraulic calculation are used to determine the reactivity or neutron cross sections used in the neutronics calculation and the power distribution calculated by the neutronics segment is used, in turn, in the thermal-hydraulics calculation. The neutronics and thermal-hydraulics solution methods do not interact with each other, but cooperate in supplying values for some of the needed variables. The tandem coupling methodology organizes the neutronics and thermal-hydraulics segments into feedback loops which are used to obtain the desired solution.

The major assumption of the tandem method is that feedback effects can be neglected <u>within</u> each calculational segment. The feedback parameters are calculated after each half of a feedback loop is completed. As a result, the feedback is introduced at discrete points in the calculation and takes the form of step changes. This can produce oscillatory behavior [C-5] or even lead to numerical instabilities [D-4]. Therefore,

a successful tandem coupling methodology must be carefully designed.

A review of most of the existing core dynamics codes showed that all of them used a tandem methodology. Experience with these codes indicates that tandem codes can be successfully developed and generally perform well. For example, the tandem method was successfully employed to combine existing neutronics and thermal-hydraulics codes in the development of MEKIN and HERMITE, among others. When all the factors were considered, it was decided that the tandem methodology provided the best framework for the development of TITAN.

4.3.2 Overview of Tandem Coupling

The primary task of the TITAN coupling methodology is to provide the necessary structure and logic to incorporate the neutronics models of QUANDRY, the thermal-hydraulics models of THERMIT and appropriate feedback models in a unified LWR core dynamics code. The coupling must provide for two modes of operation: steady-state and transient. In the steady-state mode, the coupling methodology must provide a mechanism for generating a consistent set of neutronic and thermal-hydraulic parameters corresponding to a steady-state, critical condition for the reactor modeled. In the transient mode, the coupling methodology must provide a framework for the analysis of a variety of transients. Transients of interest may involve one or more of the following types of perturbations: control rod motion or other applied reactivity change, changes in core flow, core inlet temperature, inlet or outlet pressure. The coupling methodology must also provide for the transition between steady-state and transient modes.

The elements of a tandem coupling methodology can be divided into two categories:

1. Procedures for the organization and control of the neutronics and thermal-hydraulics calculational segments, and
2. Logic and models for the calculation and transfer of feedback parameters.

The feedback logic and models provide the coupling between neutronics and thermal-hydraulics segments. The same elements in this category are generally appropriate for both the steady-state and transient modes. The tandem procedures define and control the feedback loops and thus dictate the use of the feedback logic and models. The procedures are highly dependent on the solution methods of the neutronics and thermal-hydraulics segments. Moreover, the procedures needed to generate a steady-state solution may be quite different from those used in a transient analysis. The discussion of the TITAN methodology is organized with these functional perspectives in mind, beginning with the steady-state procedures, followed by the transient procedures and ending with the feedback models and logic.

4.3.3 Tandem Procedures

4.3.3.1 Steady-State Mode

The steady-state procedures have a very specific reactor state to achieve within the context of many constraints. The steady-state reactor power and the core boundary conditions (all thermal-hydraulic and neutronic) are given as part of the problem specification. The space- and feedback-dependent macroscopic neutron cross sections are also specified. The tandem procedures must produce a set of reactor parameters representing balances in the production and destruction of neutrons and in the production and removal of energy consistent with the known power, boundary

conditions, and feedback. The most important results of the steady-state procedures are the determination of the spatial dependence of the reactor power and the reactor criticality. Indeed, codes using point kinetics do not require a coupled steady-state calculation because the power shape is assumed to be known and the reactor is assumed to be critical. A multi-dimensional code such as TITAN does not make such assumptions and therefore must include procedures to calculate these unspecified elements of the steady-state condition. The purpose of this section, therefore, is to describe the development of the steady-state mode of the TITAN tandem coupling methodology.

Though the tandem method is conceptually straightforward, the development of steady-state procedures for TITAN was complicated by the dissimilar solution methods of QUANDRY and THERMIT. The QUANDRY solution method provides for the direct calculation of the static (steady-state) nodal neutron diffusion equations. This procedure involves an iterative scheme to determine the nodal neutron balance and the reactor criticality (eigenvalue). The details of the QUANDRY static solution method are discussed in Chapter 3.

THERMIT, on the other hand, does not have a direct solution of the steady-state fluid conservation equations. The semi-implicit Newton-Raphson numerical method used in THERMIT solves the time-dependent form of the conservation equations. Steady-state solutions are obtained by running an unperturbed transient from an initial guess of thermal-hydraulic conditions. This somewhat cumbersome transient approach to steady-state eventually results in a solution which changes little from time-step to time-step. The details of this method are also given in Chapter 3.

The steady-state solution methods of QUANDRY and THERMIT suggested three possible approaches to generating a coupled steady-state solution:

1) Develop a direct steady-state solution for THERMIT and combine this with the QUANDRY steady-state solution,

2) Develop procedures for a coupled transient approach to steady-state, or

3) Develop procedures to couple the QUANDRY steady-state solution to the THERMIT transient procedure.

Only one of these approaches was actually feasible. The first approach requires the development of a direct solution for the steady-state two-fluid conservation equations. The current semi-implicit formulation in THERMIT includes convective terms evaluated at the "old" time-step. However, for a direct solution of the steady-state equations, all the terms must be evaluated implicitly. Although techniques have been developed to solve a fully implicit formulation of the one-dimensional two-fluid conservation equations, including a version of THERMIT called THIOD [D-4], an attempt to extend the THIOD technique to the three-dimensional two-fluid equations was unsuccessful. Thus, since the development of a fully implicit version of THERMIT is a difficult task beyond the scope of the current work, the first approach to generating a coupled steady-state solution was impractical.

The second possible approach involved developing procedures for using the transient solution methods of both QUANDRY and THERMIT in a coupled transient approach to steady-state. Like the first approach, the second involves using one of the calculational segments in a manner different from its original design (i.e., using the QUANDRY transient solution method to generate a steady-state solution), and again, this fact renders the second approach impractical.

An important part of the steady-state neutronics calculation is the determination of the reactor criticality, in the form of the effective multiplication factor or eigenvalue. In general, a non-trivial solution to the steady-state neutron diffusion equations exists only if the reactor is exactly critical. The eigenvalue is a parameter which makes it possible to solve the steady-state equations for a non-critical reactor by artificially adjusting the average number of neutrons produced per fission. The determination of the critical eigenvalue is part of the QUANDRY static solution. On the other hand, the transient solution in QUANDRY assumes that the critical eigenvalue is known and corresponds to a precise steady-state neutron balance, thus avoiding an unphysical reactivity perturbation.

The eigenvalue search in the QUANDRY static solution is only one of a number of different approaches to the criticality determination. Other approaches assume an eigenvalue of unity and make adjustments in control rod positions, soluble boron concentration, coolant inlet temperature or flow rate in order to produce a critical reactor. This type of criticality determination is attractive for a coupled transient approach to steady-state because the eigenvalue search is eliminated. However, the usual approach in safety analysis is to define the initial reactor configuration, including control rod positions, coolant inlet conditions and soluble boron concentration rather than leave one to be a free parameter in the criticality determination. Therefore, it was desirable to retain the eigenvalue search in the TITAN steady-state procedures.

The procedures for a coupled transient approach to steady-state had to provide the calculation of the critical eigenvalue, therefore. This could be provided by performing a static QUANDRY calculation prior to the

coupled transient approach to steady-state. However, the critical eigenvalue is dependent on the thermal-hydraulic feedback and thus cannot be calculated accurately without the feedback contribution. A successful coupling procedure therefore requires not only a preliminary static neutronics calculation but also periodic recalculations of the eigenvalue as the thermal-hydraulic solution is converged. This would require switching back and forth between the static and transient solution methods of QUANDRY. Though this procedure could work, there is no apparent benefit derived for the considerable complexity of using both the static and transient neutronic solution methods to generate a steady-state solution. Since the static neutronics solution is obviously required, an approach combining the THERMIT transient approach to a steady-state with the QUANDRY static solution alone seems to be more straightforward.

The remaining approach involves developing procedures to combine the existing dissimilar steady-state solution methods of QUANDRY and THERMIT. The advantage of this approach is that it does not require substantial changes to the existing solution methods. The disadvantage is that the procedures must be carefully formulated to generate a consistent coupled steady-state using a hybrid steady-state/transient solution method. This type of steady-state solution is unique among the coupled codes previously reviewed. Nevertheless, there was no apparent reason why this type of solution could not be developed, since the capability to calculate the fundamental parameters such as the spatial fluxes, the critical eigenvalue, the fuel temperatures, the moderator temperatures and densities, etc. is present in the two methods. Therefore, this was the approach that was chosen for the steady-state mode of TITAN.

The steady-state solution methods of QUANDRY and TITAN are discussed in some detail in Chapter 3. Certain of these details bear a brief review at this point. The THERMIT transient approach to steady-state begins with an initial guess for the thermal-hydraulic parameters and integrates forward in time with no perturbations of the boundary conditions or power shape. At each time-step, a two level iteration is performed to determine the parameter at the next time-step. The inner iteration involves a solution of the pressure field and the outer iteration determines the velocities, temperatures, etc. from the pressures. The fuel rod heat conduction solution is fully implicit, so the time derivatives can be (on option) set to zero, forcing equilibrium with the current heat transfer and fluid flow conditions. After several unperturbed time-steps, a solution is attained which changes little from time-step to time-step. This convergence is measured by global energy and mass balances.

The QUANDRY static solution involves two principal levels of iteration, the first for the nodal fluxes and leakages and the second for the critical eigenvalue. An optional feedback capability is included as part of this procedure. A very simple non-boiling lumped capacity thermal-hydraulic model and a linear cross section model provide periodic updates of the nodal cross sections. The feedback calculations are performed during the outer iterations. A converged steady-state is obtained when the reactor criticality is close enough to unity (according to a user-supplied error bound) and when the maximum change in nodal powers between iterations has been reduced below a specified value. This solution procedure is very accurate and fast running.

The most basic application of the tandem method for generating a coupled steady-state solution involves alternating steady-state critical neutronics and steady-state thermal-hydraulics solutions. The thermal-hydraulics segment performs a steady-state calculation using the power shape generated in a previous critical neutronic calculation. The resulting fuel and coolant temperatures and coolant densities are used to produce new cross sections for a subsequent static neutronic calculation. After a number of such feedback loops, a converged coupled steady-state solution would be obtained.

An important feature of this most basic tandem procedure is that no feedback occurs during the neutronics or thermal-hydraulics calculations. Indeed, a crude version of this procedure could be done manually with separate neutronics and thermal-hydraulics codes. Therefore, the basic tandem method has the advantages of being conceptually uncomplicated and likely to produce a satisfactory result. However, it is very inefficient to use procedures which require a complete steady-state neutronic and thermal-hydraulic convergence for each feedback loop when the methods are as complicated as those of THERMIT and QUANDRY. In particular, the THERMIT transient approach to steady-state requires too much computational effort to converge to a new steady-state solution after each static neutronics calculations. Many feedback loops might be required, with each loop involving many thermal-hydraulic time-steps. Furthermore, a considerable amount of computational effort would be wasted during the latter feedback loops when the changes in the power shape and cross sections are small. Thus, this type of tandem coupling was clearly inappropriate for the current work, and a more sophisticated tandem coupling methodology was needed for TITAN.

The solution methods of QUANDRY and THERMIT provide several ways to improve upon the basic tandem coupling approach. Since both codes use iterative solutions, it is possible to calculate and exchange feedback information at selected points during the steady-state convergence procedures. Tandem procedures which couple the two solution methods at the level of their iterative procedures should require less computational effort than the basic approach. However, such procedures are more complicated because the solution methods are dissimilar and require some modification to produce a coupled steady-state. Discussions of three different approaches follow.

The first approach considered is a straightforward modification of the QUANDRY static calculation with feedback. It consists (conceptually) of replacing the simple thermal-hydraulics model with the THERMIT models. The THERMIT models would be used during the static neutronics convergence to provide updated cross sections corresponding to the power shape obtained during the most recent flux iteration. This procedure is illustrated in Fig. 4.1. Convergence of the eigenvalue and nodal powers would guarantee a coupled solution because the cross sections used are obtained from a converged steady-state thermal-hydraulics solution. The procedure therefore consists of a number of steady-state thermal-hydraulics solutions within a single static neutronics solution, the convergence of the latter involving continual updates of the thermal-hydraulics conditions. Since the logic for this coupling is already present in QUANDRY, the development of the TITAN steady-state procedures along these lines would have been relatively easy. Furthermore, this approach should produce a satisfactory coupled solution. It is also an

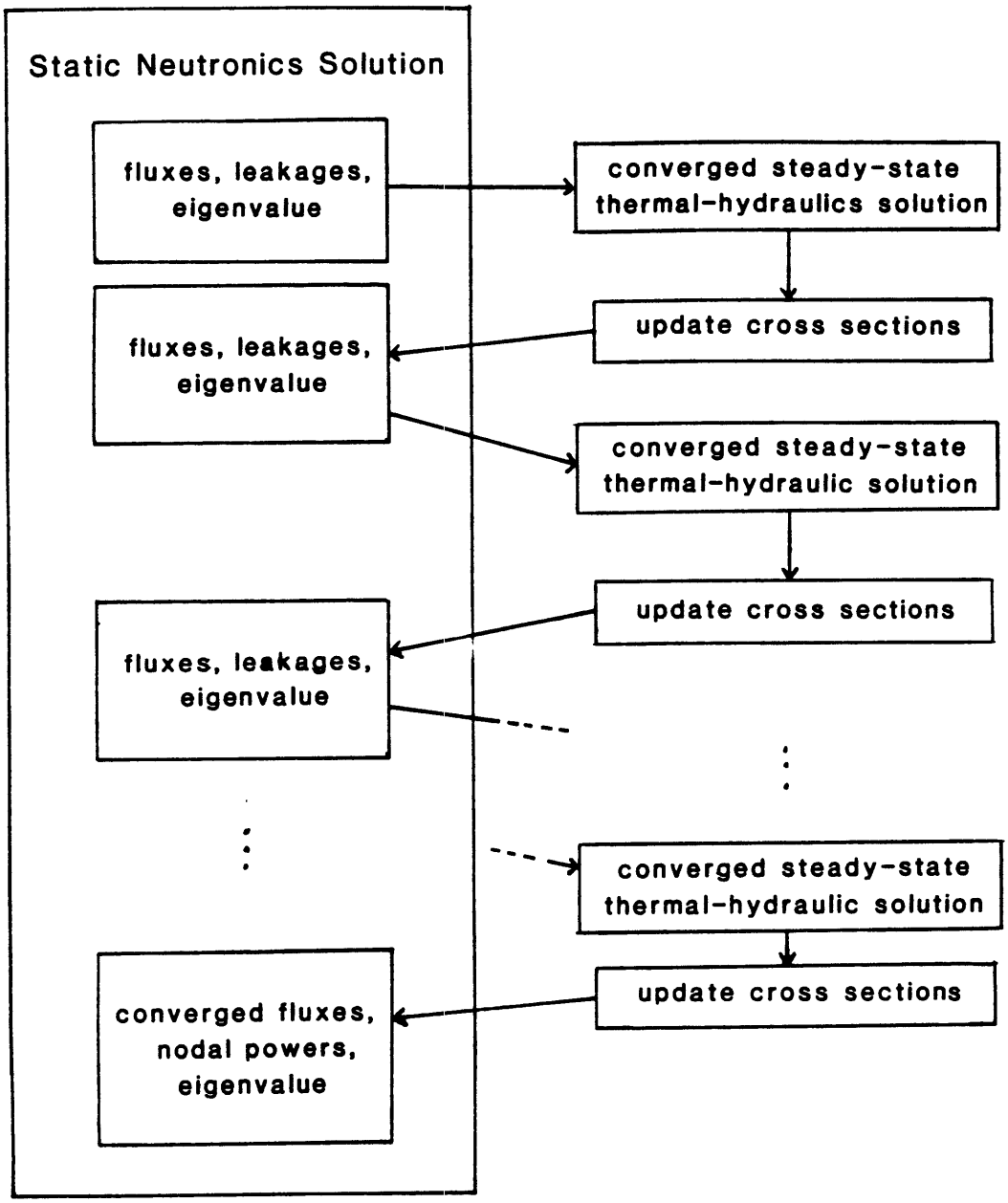

Figure 4.1 QUANDRY Approach to Steady-state

Coupling Procedures

improvement over the basic tandem approach in that only one converged static neutronic calculation is required. However, the cost of performing a number of steady-state thermal-hydraulic calculations remains too high for this approach to be practical. Therefore, an approach which only requires one steady-state thermal-hydraulic calculation was sought.

The second approach considered involved a concurrent static neutronics and steady-state thermal-hydraulics convergence. This is illustrated in Fig. 4.2. The code alternates between neutronic outer iterations and thermal-hydraulic time-steps, exchanging feedback information each time. The feedback information is based on the latest iteration or time-step and thus reflects the "error" associated with the converging solutions. The effect of these feedback errors on the steady-state convergence is not clear. This approach also modifies a fundamental feature of the THERMIT transient approach to steady-state; namely, a steady-state is to be produced with a time-varying power shape. The power shape should approach a constant as the solution converges, but prior to that the feedback will essentially provide a regular perturbation to the fluid dynamics calculation. The convergence of the thermal-hydraulics cannot take place until these perturbations are reduced to very small levels. Therefore, the thermal-hydraulic convergence would require more time-steps than if no feedback were involved. It is also not clear how to ensure that both the neutronics and thermal-hydraulics will reach a state of mutual convergence using these procedures. It is quite possible that the neutronic convergence criteria could be satisfied while the thermal-hydraulics is still unconverged. Therefore,

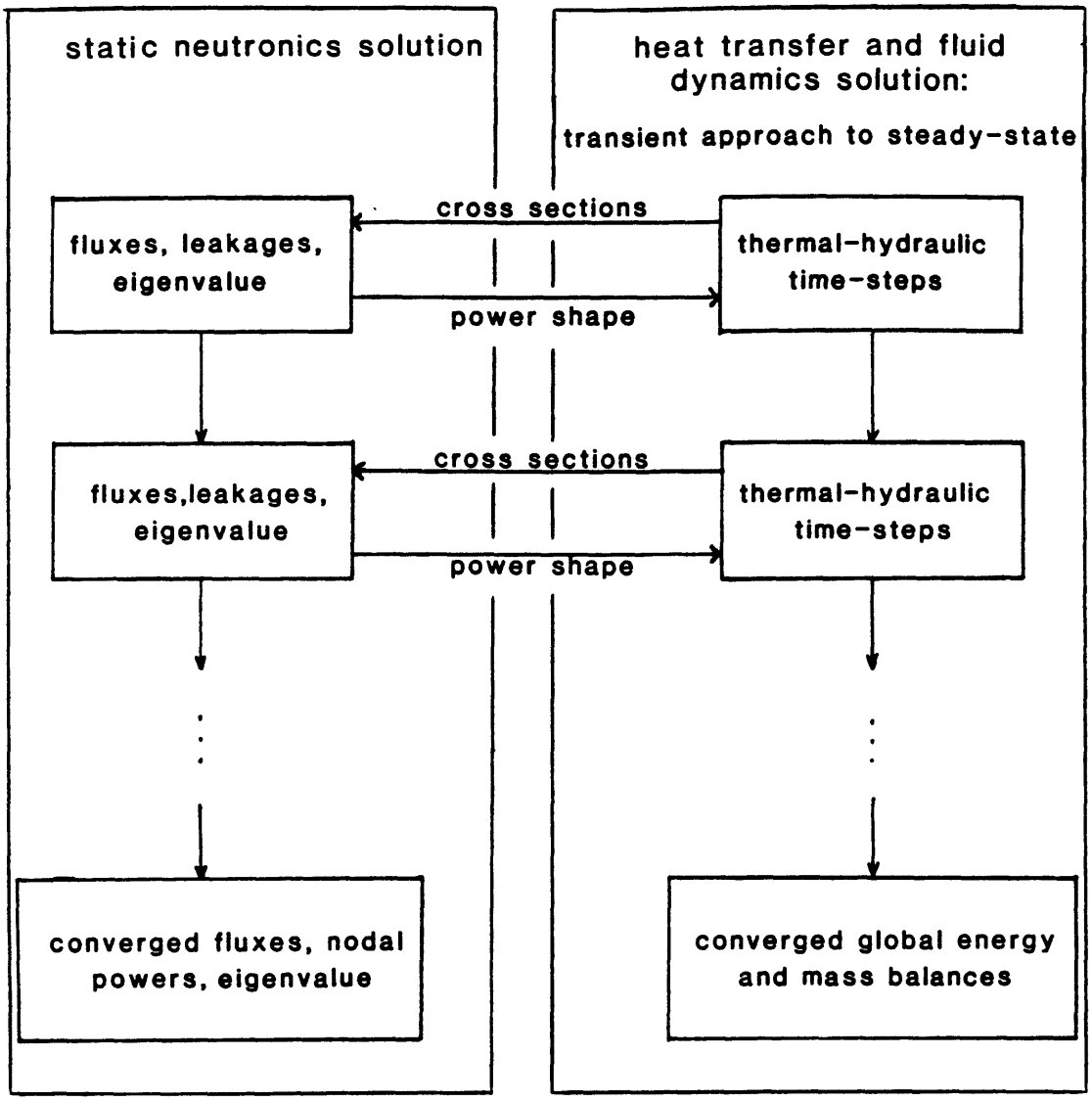

Figure 4.2 Concurrent Single Convergence

Steady-state Coupling Procedures

this approach suffers from uncertainties about attaining a converged coupled steady-state solution. Nevertheless, it is likely that this approach could be made to work and that it would be more computationally efficient than the approaches previously considered. However, the potential problems associated with this approach motivated consideration of one additional method.

The final approach considered is the "opposite" of the QUANDRY method. It is motivated by the fact that more computational effort is required to produce a THERMIT steady-state than to produce a QUANDRY steady-state (for the same geometry and the type of nodes that are pertinent to the current work). The method consists of a single steady-state thermal-hydraulics convergence within which a number of static neutronic calculations are performed. This is illustrated in Fig. 4.3. A steady-state solution is obtained with alternating thermal-hydraulic time-steps and static neutronic calculations. Each neutronics calculation uses cross sections based upon the latest fuel temperatures, coolant temperatures and coolant densities. A converged static solution with no feedback is obtained and the new power shape is used in one or more thermal-hydraulic time-steps. As in the previous approach, the time-varying power shape will affect the convergence of the thermal-hydraulic solutions, probably inhibiting convergence until after an essentially constant power shape is achieved. However, the fact that a fully converged neutronics calculation is performed each time ensures that convergence of the thermal-hydraulics portion results in a converged coupled solution. This approach takes advantage of the computational efficiency of QUANDRY yet does not have many of the potential problems of

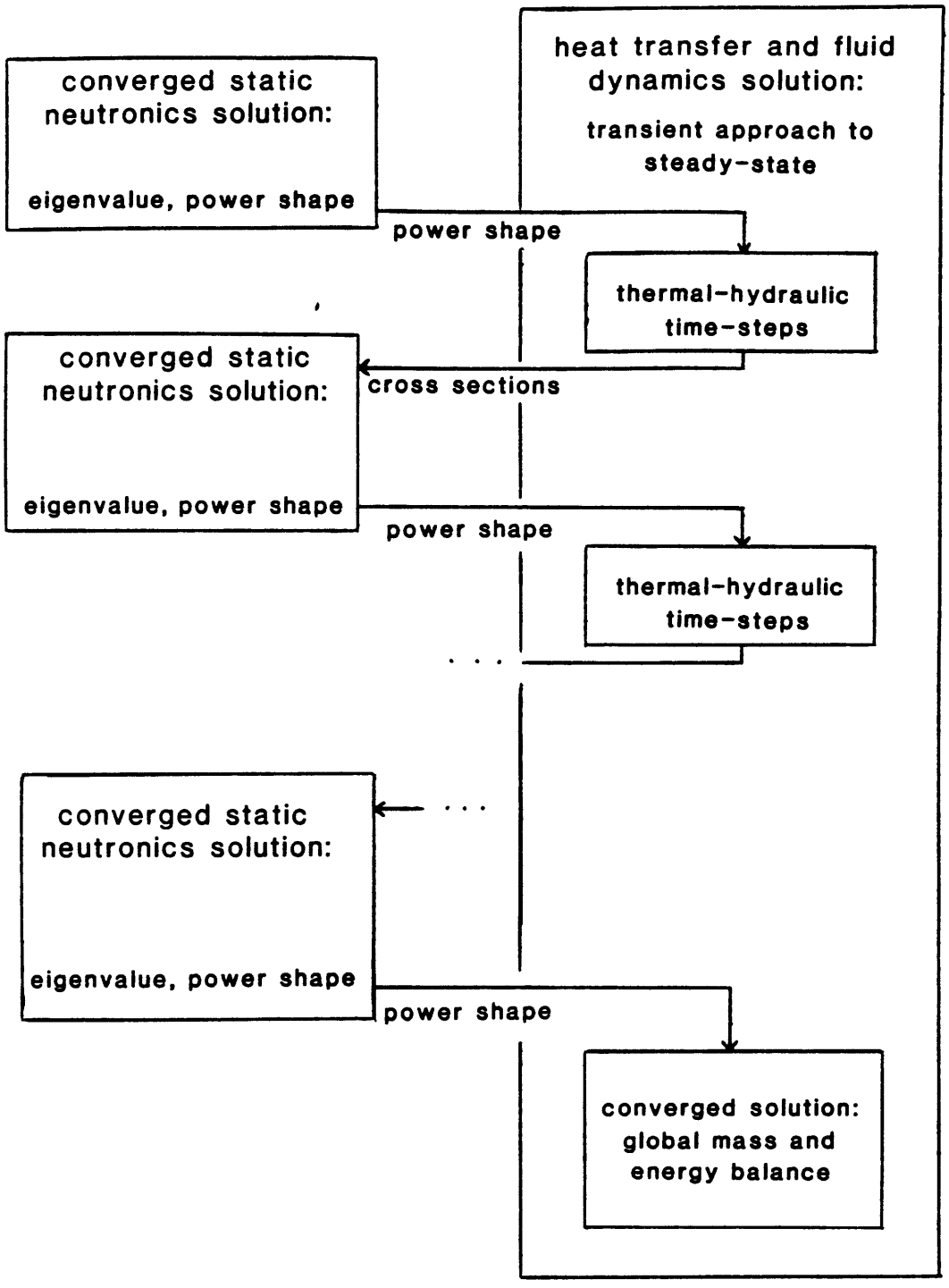

Figure 4.3 TITAN Steady-state Coupling Procedures

the previous method. Accordingly, this final approach was selected for the steady-state mode of TITAN.

The TITAN procedures for generating a steady-state solution are thus based upon repeated hybrid feedback loops, consisting of a static neutronic calculation and one or more thermal-hydraulic time-steps. The feedback models and logic use the latest thermal-hydraulic data to generate nodal cross sections. These cross sections are used to converge a neutronics solution. This produces a new flux distribution and critical eigenvalue corresponding to the current thermal-hydraulic conditions. The flux distribution is used to produce a new power distribution for the thermal-hydraulic calculation. One or more unperturbed thermal-hydraulics time-steps are then performed. The number of thermal-hydraulic time-steps per static neutronics calculation is selected by the user and can be varied as the convergence progresses. The utility of this feature is that the frequency of neutronic calculations can be matched to the rate at which the feedback parameters are changing. Hence, it may be quite appropriate to use one thermal-hydraulic time-step per static neutronic calculation initially and increase to ten thermal-hydraulic time-steps per static neutronic calculation during the latter stages of convergence. This can save a significant amount of computer time with no impact on the results obtained. The feedback loop is completed when the specified number of thermal-hydraulic time-steps have been completed. The next feedback loop begins with the calculation of new cross sections using the new thermal-hydraulic data. A number of these feedback loops are required to obtain a satisfactory converged coupled solution. Convergence is attained when the errors in the flow and energy balances have been reduced to the order of 10^{-3} to 10^{-5}.

An additional feature of the steady-state procedures increases the efficiency of the calculation by reducing the number of neutronic outer iterations required. Each static neutronic calculation (after the first one) uses the converged critical eigenvalue from the previous feedback loop as the first guess for the current eigenvalue.

4.3.3.2 Transient Mode

As has been stated previously, the primary task of the transient coupling procedures is to provide the necessary structure to permit the neutronic and thermal-hydraulic analysis of a variety of transients. The transients of interest may be initiated by changes in reactivity, core flow rate, inlet temperature, reactor pressure or combinations of these. The transient procedures of TITAN must combine the transient neutronics solution of QUANDRY with the transient thermal-hydraulics solution of THERMIT. The procedures assume that a consistent set of neutronic and thermal-hydraulics conditions corresponding to a steady-state, critical reactor are available. As in the development of the steady-state procedures, the particular characteristics of the two solution methods were important factors affecting the transient procedures. Unlike the steady-state case, both codes have solution methods for the transient form of their respective equations. As a result, the transient procedures were much more straightforward than their steady-state counterparts.

The transient procedures perform two main functions:

1. Define the structure of the tandem coupling
2. Control and coordination of time-steps.

In the tandem method, the neutronic and thermal-hydraulics segments integrate forward in time independently, using the latest feedback

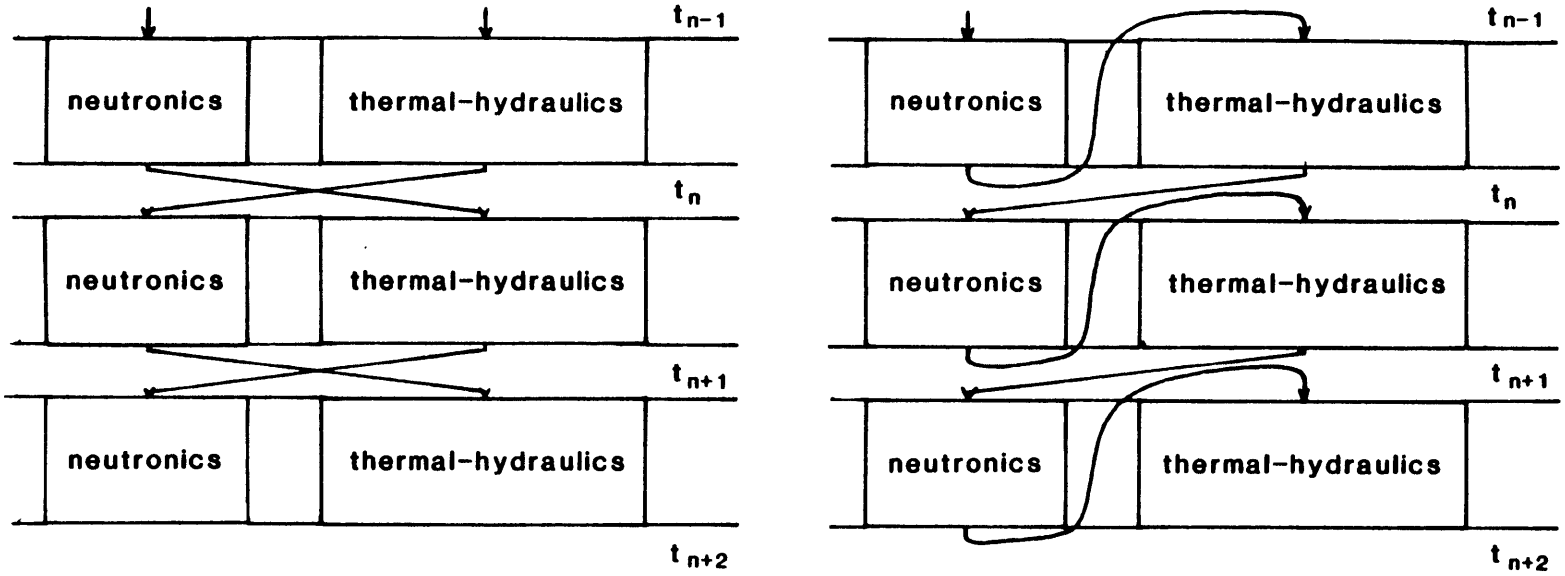

Figure 4.4 Tandem Code Structures for Transient Calculations

information and any applied perturbations to determine the parameters at the advanced time level. The procedures must coordinate these calculations so as to exchange the feedback information correctly and keep the calculational segments "in step" with each other.

The major assumption of the tandem method is that the feedback can be neglected during each time integration and then applied at the beginning of the subsequent time-step. As a result, the feedback is introduced at discrete time intervals and takes the form of step changes in the cross sections and local power. The transient procedures coordinate the neutronic and thermal-hydraulic calculations and the exchange of feedback information.

Two different tandem procedures were considered for TITAN, as illustrated in Fig. 4.4. The "parallel" procedure and the "staggered" procedure differ in the exchange of feedback and in the logic needed for the first time-step. In the parallel procedure, feedback is exchanged only when both calculational segments have completed the time integrations required to reach the new time level. Thus, each neutronic calculation is performed using the cross sections corresponding to the previous thermal-hydraulics calculation and including any applied perturbations as specified by the user. Similarly, each thermal-hydraulic calculation is performed using the power distribution corresponding to the previous neutronic calculation and including any applied perturbations. One ramification of this approach is that the effects of any perturbation in one calculational segment are not transmitted to the other calculational segment until the following time interval. Thus, the feedback lags behind the true response, as illustrated in the following example. Suppose a

control rod motion provides the impetus for the transient to be analyzed. At the beginning of the first time interval the steady-state cross sections are perturbed by the control rod motion and a neutronic calculation is performed to advance to the end of the time interval. A thermal-hydraulic calculation is also performed, advancing to the new time using the unperturbed steady-state power shape. The order of the two calculations does not matter, since they are both completed before any exchange of information is performed. As a result, all transients can be handled with the same structure and the choice of whether to perform neutronics or thermal-hydraulics calculations first is of no concern. Procedures based upon a parallel structure are therefore rather simple to devise. However, the merit of this simplicity is probably not sufficient enough to compensate for the problem of time lag inherent in this approach. Continuing with the example, the power distribution and feedback-modified adjusted cross sections from the end of the first time interval are exchanged between the neutronics and thermal-hydraulics segments prior to the calculation of the second time interval. The power distribution being used corresponds to the control rod motion of the first time interval without any feedback contribuiton. Similarly, the cross sections being used correspond to the steady-state condition, since no perturbation was applied to the thermal-hydraulics calculation during the first time interval. The results of the neutronics calculation for the second time interval will therefore not reflect any feedback contribution. Indeed, the thermal-hydraulic feedback will not be felt until the beginning of the third time interval, at which time thermal-hydraulic conditions corresponding to the control rod motion of the first

time interval will be used. Hence, the parallel structure compounds the time lag inherent in the tandem method with an additional time lag caused by the controlling logic. Therefore, parallel procedures were not used in TITAN.

The transient procedures in TITAN are based upon a staggered structure, in which feedback information is exchanged within a given time interval. The staggered procedures reflect three basic premises:

1. There is a natural order to tandem calculations which is determined by the transient initiator;

2. Within a given time interval, one or the other of the neutronics or thermal-hydraulics time integrations is performed first;

3. Calculations should always use the latest feedback information available.

The staggered procedures begin by identifying whether the transient is initiated by thermal-hydraulics or by neutronics. The first time integration is performed with the initiating segment, subject to the initial (steady-state) conditions and the applied perturbation. The results of this calculation include either a new power distribution or new thermal-hydraulic parameters at the new time level. The new feedback parameters are then used in the time integration which advances the other segment to the new time level. The next time integration proceeds as the first, with the initiating segment going first and using the latest feedback information from the other segment. This continues until the transient is finished. The staggered approach has the advantage of removing part of the time delay associated with the parallel approach. It has the disadvantage of requiring procedures which are dependent on the type of transient analyzed and therefore involve somewhat more

complicated logic. However, the benefits of the staggered approach were of greater value than the slight "cost" of increased complexity.

The remaining issue in the development of tandem procedures was the control of time-steps. Both the neutronics and thermal-hydraulics segments require the specification of time-steps for transient calculations. The time-steps specify the discrete points in time for which the solutions are obtained. Obviously, it is necessary to have the neutronics and thermal-hydraulics solutions coincide at frequent time intervals so that feedback information can be exchanged. However, there can be a large difference in time scales between the transient behavior of thermal-hydraulics and neutronics. Therefore, it is likely that the appropriate neutronic and thermal-hydraulic time-steps will be different during a transient calculation. Furthermore, the numerical methods of QUANDRY and THERMIT have different requirements regarding time-step selection. The QUANDRY method allows a fully implicit solution of the transient nodal diffusion equations. Thus, no restrictions are placed upon the time-step size for the neutronic portion of TITAN. However, the semi-implicit fluid dynamics solution has a numerical stability limit in the form of the "Courant" condition:

$$\Delta t < \left| \frac{\Delta x}{V_{max}} \right| \tag{4.1}$$

where Δx is the axial mesh spacing and V_{max} is the largest fluid velocity. The maximum time-step size for most LWR applications is of the order of tens of milliseconds, but can be smaller under severe boiling conditions.

The control of time-steps for the thermal-hydraulics portion of TITAN poses several problems. Since the maximum allowable time-step will

often change during a transient, it is impossible to know the time-step limit prior to a given analysis. Yet, there is an economic incentive to use the largest time-step possible in order to reduce the calculational effort required to analyze practical transients. As a result, the THERMIT code was written to determine the appropriate size of each time-step as the transient analysis progresses. This was done by calculating the maximum time-step for stability, as given in Eq. 4.1, and comparing it to user-supplied maximum and minimum time-step values. If the Courant limit time-step size falls between the specified maximum and minimum values, the Courant time-step is used. If the calculated time-step size limit is greater than the specified maximum time-step size, the specified value is used. Under certain circumstances, the time-step size is reduced internally during a calculation. A time-step size less than the specified minimum will cause the calculation to stop. Thus, the only way to control the thermal-hydraulic time-step size is to set the maximum size to a relatively small value. This is impractical for problems containing many nodes and involving more than a few seconds of transient time. It was therefore important for TITAN to retain the logic which selects the maximum thermal-hydraulic time-step during the transient analysis.

The TITAN coupling methodology links a calculational segment which remains stable with any time-step size (the neutronics) to a second segment which has a stability limit and internally calculates the maximum stable time-step. In addition, the coupling together of neutronics and thermal-hydraulics imposes certain restrictions on time-step size. Dube [D-4] found that time-step sizes which may be adequate

for the neutronic and thermal-hydraulic components separately can result in unstable coupled solutions. The tandem coupling method requires that feedback information be exchanged frequently because of the possibility of such problems.

A number of different time-step control approaches are conceivable. One possible approach would allow each segment to have independent time-step sizes and use interpolation or extrapolation to produce cross sections and nodal powers at the appropriate times for exchange. This is a complicated and dubious scheme. A more plausible approach is to include additional logic to the thermal-hydraulic time-step logic to generate the neutronic time-steps. This was the approach taken, in its simplest form. Since the transients of interest in the current work were primarily very rapid, requiring frequent feedback calculations, it was assumed that very short time-step sizes would be appropriate for both segments. Thus, both segments could use the same time-step sizes for transient calculations. The actual time-step size used is controlled by the existing THERMIT logic, thereby satisfying the Courant stability condition while utilizing the flexibility of the fully implicit solution of QUANDRY. This type of time-step logic is not appropriate for all transients, nor does it produce an optimum relationship between the neutronic and thermal-hydraulic calculations. However, the development of a comprehensive time-step control was not required for the initial development and testing of TITAN and has been left for future investigators.

4.3.4 Feedback Logic and Models

The feedback logic and models provide the coupling between the neutronics and thermal-hydraulics segments. The steady-state and transient procedures control the feedback calculations, which produce the power distribution for the thermal-hydraulics segment and cross sections for the neutronics segment. The feedback logic and models are essentially the same for both the steady-state and transient modes.

The feedback logic controls the production and transfer of information between the neutronics and thermal-hydraulics segments. Part of this logic is the association of neutronic and thermal-hydraulic control volumes. As has been mentioned, one of the areas of compatibility between THERMIT and QUANDRY is in the use of large rectangular parallelepiped control volumes. THERMIT also has the capability to perform rod bundle analyses using coolant-centered subchannels. This type of analysis gives much more detailed thermal-hydraulic information than the large rod-centered control volumes. However, THERMIT does not allow both types of control volumes in the same model. Since one fuel assembly contains many subchannels, it is impractical to analyze problems containing multiple fuel assemblies with coolant-centered control volumes. Therefore, only the rod-centered control volumes are used in TITAN.

The QUANDRY and THERMIT codes allow considerable flexibility in specifying the dimensions of control volumes. The codes allow irregular mesh spacings for all three coordinate directions. Thus, TITAN could also allow flexible geometric models.

It would be possible to devise logic in TITAN to permit a significantly different arrangement of thermal-hydraulic and neutronic control volumes. However, an important element in the specification of the geometry within TITAN is the scheme for numbering the control volumes. Unfortunately, THERMIT and QUANDRY use numbering schemes which are different and, equally important, deeply imbedded in the codes. This makes the logic required for a very general, flexible correspondence between neutronic and thermal-hydraulic control volumes very complicated. Furthermore, the benefit of ths flexibility in the initial development and testing of TITAN is limited. Therefore, it was decided that the logic would assume both segments would use the same dimensions and arrangement of control volumes. This simplified the logic and was thought to provide adequate capability for the current work.

The feedback logic also includes the means for taking the results of the neutronics calculation and providing an appropriate power distribution for the thermal-hydraulics calculation. In THERMIT, the power distribution is specified by the product of the total reactor power, an axial power shape, and a transverse power shape. The total power can vary during a transient, but the power shapes remain constant. This was not appropriate for a three-dimensional coupled code like TITAN. Even though the two power shapes could be calculated from the nodal fluxes for each feedback loop, they do not allow the representation of an arbitrary power shape. Therefore, the THERMIT power distribution specification was abandoned in favor of a straightforward nodal power array. At the end of each neutronic calculation, the nodal fluxes are

multiplied by the macroscopic fission cross section and a factor converting fission rate to power output. In steady-state calculations, the nodal powers are normalized to maintain the total power at the specified level. The nodal powers are then used in the thermal-hydraulics segment to calculate the necessary heat fluxes and power densities.

The final contribution of the feedback logic is the generation of cross sections which reflect the thermal-hydraulic conditions present in the core. This is done by means of models which represent the dependence of the cross sections on parameters such as the fuel temperatures, moderator temperatures and moderator densities. Two such models are present in TITAN, either of which may be selected by the user. The first model is the original model in QUANDRY and the second was adapted from the MEKIN-B code [A-1].

i) The Linear (QUANDRY) Feedback Model

The QUANDRY cross section model is based upon the assumption that the nodal cross sections have a linear dependenceon the node average fuel temperature, moderator temperature, and moderator density. The macroscopic cross section of type α for node (i,j,k) is calculated by an equation of the form:

$$\Sigma_\alpha^{(i,j,k)} = \Sigma_\alpha^{*(i,j,k)} + \left[\frac{\partial \Sigma_\alpha}{\partial T_c}\right]_{\rho_c} \left[T_c^{(i,j,k)} - T_c^*\right]$$

$$+ \left[\frac{\partial \Sigma_\alpha}{\partial T_f}\right] \left[T_f^{(i,j,k)} - T_f^*\right] + \left[\frac{\partial \Sigma_\alpha}{\partial \rho_c}\right]_{T_c} \left[\rho_c^{(i,j,k)} - \rho_c^*\right], \quad (4.2)$$

while the fast and thermal group diffusion constants are calculated by an equation of the form:

$$D_{1,2}^{(i,j,k)} = \{\frac{1}{D_{1,2}^{*(i,j,k)}} + [\frac{\partial(\frac{1}{D_{1,2}})}{\partial T_c}]_{\rho_c} [T_c^{(i,j,k)} - T_c^*]$$

$$+ [\frac{\partial(\frac{1}{D_{1,2}})}{\partial T_f}] [T_f^{(i,j,k)} - T_f^*]$$

$$+ [\frac{\partial(\frac{1}{D_{1,2}})}{\partial \rho_c}]_{T_c} [\rho_c^{(i,j,k)} - \rho_c^*]\}^{-1} \qquad (4.3)$$

In these equations, T_c and T_f are node average coolant and fuel temperatures, respectively, and ρ_c is the node average coolant density. Quantities marked with * indicate user-supplied reference values. The reference cross sections and feedback coefficients are supplied for each unique neutronic composition. A linear relationship of this type can describe cross sections accurately over only limited ranges of temperatures and densities, particularly when a change of phase occurs in the coolant. Cook [C-5] concluded that the moderator density term may require a higher order representation in order to give accurate results.

ii) The Linear/Quadratic Feedback Model

The second cross section model in TITAN assumes a linear dependence on node average coolant temperature and on the square root of node average fuel temperature, with a quadratic dependence on node average moderator density. This formulation is an improvement over the original QUANDRY model in several respects. Cheng [C-12] has shown that the cross section dependence on moderator density is well represented by a quadratic expression. Dresner [D-10] has shown that the resonance integral for heterogeneous fuel varies with the square root of the fuel temperature. Furthermore, the model contains a correction for the effect of moderator density on control rod worth (see 1.3.3). The macroscopic cross section of type α and the diffusion constants for node (i,j,k) are calculated by an equation of the form:

$$\Sigma_\alpha^{(i,j,k)} = \Sigma_\alpha^{*(i,j,k)} + [1 - f^{(i,j,k)}] \cdot [(\frac{\partial \Sigma_\alpha^u}{\partial \rho_c})_{T_c} (\rho_c^{(i,j,k)} - \rho_c^*)$$

$$+ 1/2(\frac{\partial^2 \Sigma_\alpha^u}{\partial \rho_c^2})_{T_c} (\rho_c^{(i,j,k)} - \rho_c^*)^2] + [f^{(i,j,k)}] \cdot [(\frac{\partial \Sigma_\alpha^p}{\partial \rho_c})_{T_c} (\rho_c^{(i,j,k)} - \rho_c^*)$$

$$+ 1/2(\frac{\partial^2 \Sigma_\alpha^p}{\partial \rho_c^2})_{T_c} (\rho_c^{(i,j,k)} - \rho_c^*)^2] + (\frac{\partial \Sigma_\alpha}{\partial \sqrt{T_f}}) (\sqrt{T_f}^{(i,j,k)} - \sqrt{T_f}^*)$$

$$+ (\frac{\partial \Sigma_\alpha}{\partial T_c})_{\rho_c} (T_c^{(i,j,k)} - T_c^*). \qquad (4.4)$$

where T_c, T_f and ρ_c are as previously defined. The superscripts u and p indicate unperturbed and perturbed, respectively, and the factor $f^{(i,j,k)}$ is the fraction of the node (i,j,k) which is perturbed. All nodes are "unperturbed" during a steady-state calculation, so the factor f is set to zero for all nodes. During a transient, the factor f is determined for each node involved in control rod motion. This is illustrated in Figure 4.5.

Both of the cross section models require the calculation of the average fuel temperature and the average moderator temperature and density for each node. Since TITAN contains two-fluid thermal-hydraulics, temperatures and densities are calculated for the fluid and the vapor in each node. This requires averaging logic to produce the necessary coolant parameters. The fact that the coolant is moving through the control volume raises questions about the proper type of averaging. Rodack and Wolf [R-5] considered the appropriate type of averaging schemes for neutronic feedback calculations and concluded that volume weighting is more appropriate than volumetric flow weighting for determining the average coolant density. The neutronic time scale is so much shorter than the hydraulic time scale that the coolant is effectively stationary relative to the neutrons. Accordingly, the node average coolant density in TITAN is calculated as follows:

$$\bar{\rho}_c = \alpha\rho_v + (1 - \alpha)\rho_\ell \tag{4.5}$$

where

$\bar{\rho}_c$ = node-averaged coolant density

α = node void fraction

ρ_v = vapor density

ρ_ℓ = liquid density.

NODE INITIALLY CONTAINING A CONTROL ROD:

CONTROL ROD WITHDRAWAL

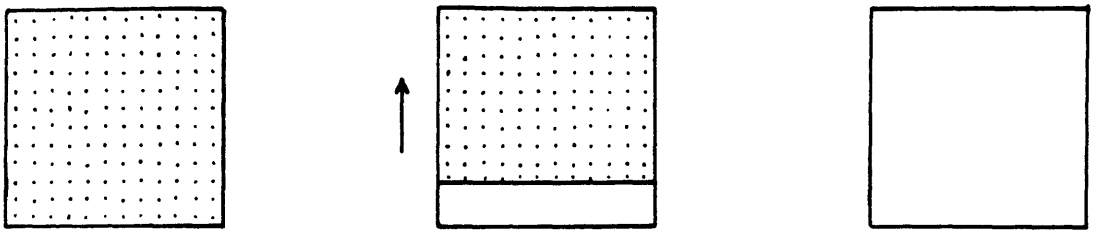

NODE INITIALLY WITHOUT A CONTROL ROD:

CONTROL ROD INSERTION

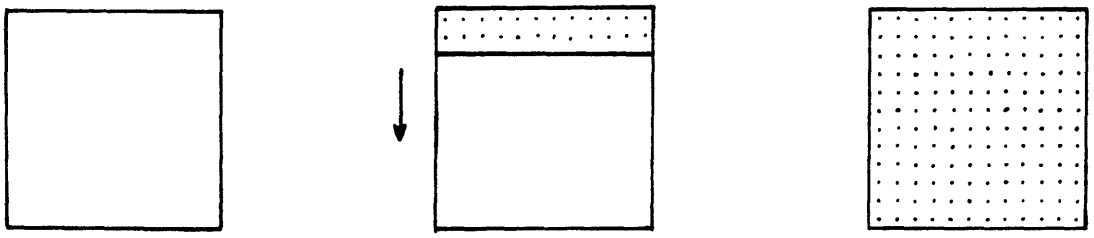

Figure 4.5 Control Rod Movement and Feedback:

"f" Factor Illustration

The node average coolant temperature calculation also requires an appropriate averaging scheme. The moderator temperature feedback effect involves the energy distribution of thermal neutrons as determined by the temperature of the slowing down medium (see Sec. 1.3.3). The appropriate average coolant temperature is, then, one that is weighted by the number of molecules (equivalently, the mass) having a given temperature. Accordingly, the node average coolant temperature in TITAN is calculated as follows:

$$\bar{T}_c = \frac{\alpha\rho_v T_v + (1-\alpha)\rho_\ell T_\ell}{\bar{\rho}_c} \tag{4.6}$$

where

$\bar{T}_c$ = node-averaged coolant temperature,

T_v = vapor temperature, and

T_ℓ = liquid temperature.

All other parameters have been previously defined.

The final averaging scheme required was for the fuel temperature calculation. The heat transfer package allows for the calculation of a radial temperature distribution for an average fuel rod in each node. The fuel is divided radially into regions, or cells, and the temperatures at the cell interfaces are calculated. The number of cells in the fuel is specified by the user, including one cell for the gap and one or more cells for the cladding. Since the gap and cladding do not contribute to the feedback effect, the temperature is volume-averaged over the fuel itself, as follows:

$$\bar{T}_f = \frac{\sum_{i=1}^{N} \pi (0.5) (T_{i+1} + T_i) (r_{i+1}^2 - r_i^2)}{\pi r_{n+1}^2} \qquad (4.7)$$

where

$\bar{T}_f$ = node-averaged fuel temperature

T_i = calculated temperature at point "i" in the fuel

r_i = radial location of point "i" in the fuel, and

N = number of calculational cells in the fuel.

4.4 Implementation

4.4.1 Introduction

The steady-state and transient procedures and the feedback logic and models constitute a methodology for coupling QUANDRY and THERMIT. The development of TITAN required that this methodology be implemented correctly and augmented by such additional logic as needed to produce a working coupled code. This effort began with two complete and separate computer codes, each with its own input and output routines, data management logic, timing routines, initialization routines, and overall structure. The original THERMIT and QUANDRY source codes each contained around 5,000 lines of FORTRAN.

The objective of the implementation was to produce a fully integrated code which is efficient and convenient to use. In accordance with the tandem coupling approach, the implementation strategy was to integrate the common support functions (input, output, data management, etc.) as fully as possible while linking the dissimilar computational elements together

in the manner described previously. This required numerous changes to both of the original source codes. The details of these changes are too lengthy to be presented in this report. Three general topics regarding implementation are discussed in this section, as follows: code structure; input and data management; and the initialization function, In addition, a number of code enhancements are discussed in Section 4.5.

4.4.2 Code Structure

The first implementation task was to merge the two source codes and install the coupling methodology. This required fundamental changes in the structure of both codes as well as a new mode of operation for one of the codes. QUANDRY was written to perform a steady-state and transient analysis in one continuous calculation. This allows either batch or interactive operation, but requires that each transient calculation be preceded by a steady-state calculation. THERMIT, on the other hand, was written to be operated in an interactive fashion. The most common usage of THERMIT involves a two step procedure with separate steady-state and transient calculations. The steady-state calculation is performed (with the convergence monitored from an on-line data terminal) and the results are stored in disk files following successful convergence. One file contains the output requested by the user and a second file contains the necessary data to enable a restart of the calculation. The transient analysis is a separate problem, beginning with the initial conditions obtained from the restart file. This two step method allows the user to monitor the steady-state convergence and to ensure that an appropriate set of initial conditions are used in the transient calculation. In addition,

a number of transient calculations can be performed using the same steady-state solution. THERMIT can also be operated in a one step mode in which the user triggers the beginning of the transient calculation from the data terminal. Unlike QUANDRY, THERMIT cannot be operated in a batch mode without changes to the code.

The selection of a code structure for TITAN was dependent upon the choice of either the one or two step mode of operation. Since the steady-state convergence of TITAN was expected to be more difficult than that of THERMIT, the utility of the two step approach appeared to be even greater for a coupled code. The efficiency of using a single steady-state solution for a number of transient calculations was also very attractive. Furthermore, the two step process does not limit TITAN to computer systems which are amenable to interactive processing. A batch version would require some additional programming to control the end of the calculation. This, however, was not necessary nor desirable for the initial development of TITAN. The structure of TITAN was therefore based upon a two step, interactive mode of operation like that of THERMIT.

The decision to abandon the one step procedure of QUANDRY in favor of the two step procedure of THERMIT led naturally to the designation of THERMIT as the "host" code. This means that the basic structure of THERMIT was used and the essential QUANDRY routines were installed within that structure. The steady-state procedures involving static neutronics calculations performed periodically during the thermal-hydraulic transient approach to steady-state were well suited to this choice of structure. Both QUANDRY and THERMIT were written in a modular form with the major computational functions and the logic controlling them segregated into

individual subroutines. The implementation of the coupling methodology involved consolidation of the controlling subroutines with few changes to the computational subroutines. The steady-state procedures were installed, debugged and tested first, followed by the transient procedures. The code structure proved to be expedient for both development and application.

4.4.3 Input and Data Management

The consolidation of input and data management functions was a major task in the implementation of the TITAN coupling methodology. The input data consists of alpha-numeric variables, real and integer constants, and real and integer arrays. Both QUANDRY and THERMIT had internal logic for the management of input and internally generated data. In QUANDRY, all input data are read using standard specified formats. Most of the array data are handled by a routine which places them in a single container array and calculates pointers to determine the address of specific values within the array. The routine also determines the length of the container array and defines the arrays' dimensions uniquely and exactly each time QUANDRY is executed. This object-time dimensioning saves core storage and prevents many of the errors associated with explicitly dimensioned arrays. However, the array management routines were not transferrable to the MULTICS computer, so they had to be abandoned in favor of explicit dimensioning.

THERMIT is somewhat more flexible than QUANDRY in the reading of input data. Integer and real constants are read in free format. Integer and real arrays are read by a free format processor which uses a logical analogue to the distributive law of multiplication to reduce the specification of

repeated fields. This can simplify the input considerably. As in QUANDRY, the integer and real array data are placed in a container array for which appropriate pointers are calculated. The container array is placed in the blank common, while the pointers are placed in a named common block. In consolidating the input of QUANDRY and THERMIT, the QUANDRY constants were read in free format and the array data were added to the container array and read via the free format array processor. Additional logic was added to calculate the new pointers, resulting in approximately 25 integer and 150 real arrays.

The consolidation of input data also resulted in the removal of redundant or irrelevant input requirements. Redundant input data included mesh spacings, reactor power specification, and time-step specification, among others. Irrelevant data included power shape specification, reactor period and reactor power forcing functions. All input data was programmed to be read from an on-line data file. The two step structure of TITAN required that some data be removed from the input disk file set and be read directly from the on-line data terminal. The details of the input requirements are discussed in Ref. [T-4].

The internal transfer of data in TITAN was a major problem in the implementation of the coupling methodology. All of the QUANDRY variables had to be passed through the new controlling subroutines, either via common blocks or argument lists. The details of this work are not given here, but suffice it to say that the proper handling of data was a constant concern throughout the development of TITAN.

The final data management issue involved the creation and retrieval of the restart file. The basic logic for this was already present in THERMIT, so only an expansion of the existing routines was required. The restart function in THERMIT is accomplished by "dumping" the contents of all the common blocks onto the disk file and then later reading the contents of this file back into the same common blocks. This simple method requires that all the necessary data be placed in a common block and does not discriminate between useful and irrelevant restart data. The necessary QUANDRY data was all placed in common blocks which were added to the routines responsible for creating and retrieving the restart.

4.4.4 Initialization Function

The final area of work in the implementation of the TITAN coupling methodology involved the initialization function. Initialization involves calculations and data manipulation required before the main computational routines are entered. An example is the processing of input data regarding reactor geometry to produce volumes, cross-sectional areas, flow areas, and expansion functions for the nodal leakages. In addition, iterative solution methods such as those used in QUANDRY and THERMIT require initial guesses for the primary unknowns. These initial guesses are also supplied, in part, via initialization routines. Both QUANDRY and THERMIT include logic appropriate to initialize themselves. Many of these initialization functions were not affected by the coupling of the two codes. Three major categories were affected, however, and the changes involved are discussed here. The three categories are geometry processing, neutron cross section initialization, and initial guess for thermal-hydraulic arrays.

The original QUANDRY and THERMIT codes have procedures for processing the input geometry specification. This allows the minimum input necessary to produce all the geometrical parameters needed in the analyses. The TITAN feedback logic called for a unified geometrical model with identical mesh spacings and a one-to-one nodal correspondence. In order to limit the TITAN input requirements to a single set of geometrical parameters, some additional initialization logic was required. The neutronics and thermal-hydraulics portions of TITAN use different mesh spacing arrays and node numbering schemes throughout their subroutines. Logic was added to produce the necessary redundant geometrical parameters internally. This could be dispensed with by modifying one of the segments to use the geometrical scheme of the other.

The second initialization task added to TITAN involved cross sections for the steady-state calculation. The steady-state procedures begin with a static neutronics calculation. The power distribution from the neutronics calculation is then used for one or more thermal-hydraulic time-steps. The user supplies reference cross sections and feedback coefficients for the various neutronic compositions and a nodal composition map. The reference cross sections could be used for the first calculation, but a better result would be obtained if thermal-hydraulic feedback were included in even the initial set of cross sections. Accordingly, a very simple thermal-hydraulics model [K-9] was included in TITAN for the purpose of calculating the cross sections prior to the first neutronics calculation. The model can calculate the average fuel temperature, average coolant temperature, and average coolant density at steady-state for each node, assuming no cross-flow between channels, no

pressure drop, and no reverse flow. The model is capable of handling both single- and two-phase flows under the assumption of homogeneous equilibrium conditions. The fuel rod model uses a simple lumped capacity approximation which neglects the existence of a fuel-cladding gap. A power shape is generated by assuming a spatially flat flux shape and using the reference fission cross sections to calculate the nodal powers. The simple thermal-hydraulic model requires some additional input information, but provides a good first guess of the feedback parameters needed to initialize the nodal cross sections. The feedback parameters are used in either of the cross section models to produce the nodal cross sections which are, in turn, used inthe first static neutronics calculation. The impact of this initialization procedure is to produce a better power distribution for the first thermal-hydraulic time-step, thereby improving the convergence of the coupled solution.

The third intialization function incorporated into TITAN involves the thermal-hydraulics calculation. The solution methods of THERMIT require that initial guesses for the pressure, void fraction, vapor temperature, vapor axial velocity, and cladding surface temperature in each node be supplied. The user must therefore determine appropriate initial conditions from some auxiliary calculation or simply make a reasonable guess. Even though experience with THERMIT has not indicated that there is much sensitivity of running time or steady-state solution to these initial conditions, it was suggested that the convergence of TITAN might be more sensitive because of the feedback [S-10]. Accordingly, a procedure was developed to use the simple thermal-hydraulics model to provide an initial guess for some of the parameters. In particular, the vapor and liquid

temperature in each node are set equal to the node average coolant temperature calculated by the simple model and the average fuel temperatures are used to initialize the fuel rod temperature distributions. The simple model also calculates average coolant densities for each node, but these cannot be converted to void fractions accurately, since no pressure drop is calculated. Therefore, the initial guesses for nodal pressure, void fraction and axial vapor velocity remain a part of the required input information.

4.5 Code Enhancements

4.5.1 Direct Moderator Heating

The energy released by nuclear fission occurs in several forms. The largest part is contained in the kinetic energy of the fission products, which is converted to heat energy within the fuel. A portion of the energy is contained in the gamma rays, beta particles and neutrons produced in the fission reaction. Some of this energy escapes the fuel and is deposited directly into the coolant by gamma ray absorption and neutron moderation. This direct heating of the moderator has been shown to be an important contributor for some reactor transients of interest [C-8]. Accordingly, a model was added to TITAN to account for this effect. The model allows for the partitioning of the nodal powers into a portion which is deposited in the fuel and a portion which is deposited directly into the coolant. It is assumed that energy deposited directly in the coolant is dependent on the node average coolant density. The fraction of the fission energy which is deposited directly in the coolant is determined for each node (i,j,k) by the following relation:

$$E_d^{(i,j,k)} = \Theta \cdot \frac{\bar{\rho}_c^{(i,j,k)}}{\rho_c^*} \qquad (4.8)$$

where Θ is a user-supplied constant, $\bar{\rho}_c^{(i,j,k)}$ is the node averaged coolant density and ρ_c^* is a user-supplied reference coolant density. The "Θ" parameter is the fraction of the energy absorbed directly into the coolant when the coolant density is the reference value, ρ_c^*. These two constants are assumed to be the same for all neutronic compositions in a given problem. They must be determined by some auxiliary calculation. The energy not deposited directly into the coolant is assumed to be deposited in the fuel.

4.5.2 Equilibrium Xenon Model

Xenon (Xe-135) is one of the most important fission product poisons produced in a nuclear reactor. Xenon absorbs thermal neutrons very strongly, having a microscopic cross section of about 2.7×10^6 barns at 0.025 eV. Xenon is produced directly in fission and after the decay of another fission product isotope, iodine-135. This process occurs as follows:

$$\begin{array}{ccccccc} \text{fission} & & & & \text{fission} & & \\ \downarrow & & & & \downarrow & & \\ Te^{135} & \xrightarrow[(0.5\ \text{min.})]{\beta-} & I^{135} & \xrightarrow[(6.7\ \text{hr.})]{\beta-} & Xe^{135} & \xrightarrow[(9.2\ \text{hr.})]{\beta-} & Cs^{135} \end{array} \qquad (4.9)$$

The production of xenon is dependent on the local neutron flux. More xenon is produced in regions of high flux and less is producedin regions of low flux. Since the production of xenon tends to reduce the available thermal neutrons, it acts as a kind of feedback and should be included in

core analysis. The nature of the fission product chain is such that, for a given constant flux level, the concentration of xenon reaches an asymptotic equilibrium value. The xenon concentration can be assumed to have reached equilibrium for any power level when 30 hours have passed since startup [H-3].

An optional model was added to TITAN to calculate the nodal equilibrium xenon cross section during the steady-state convergence. The equilibrium concentration in a node is given by the following expression:

$$N_{Xe} = \frac{(\gamma_I + \gamma_{Xe})\ (\Sigma_{f2}\ \phi_2 + \Sigma_{f1}\ \phi_1)}{\lambda_{Xe} + \sigma_{2,Xe}\ \phi_2 + \sigma_{1,Xe}\ \phi_1} \tag{4.10}$$

where

γ_I = fission yield of I^{135}

γ_{Xe} = fission yield of Xe^{135}

$\Sigma_{f1 \text{ or } 2}$ = macroscopic fission cross sections

$\phi_{1 \text{ or } 2}$ = nodal neutron fluxes

λ_{Xe} = Xenon decay constant

$\sigma_{1 \text{ or } 2,Xe}$ = microscopic Xenon absorption cross sections.

The TITAN model makes the following assumption:

$$\sigma_{1,Xe}\ \phi_1 \ll \lambda_{Xe} + \sigma_{2,Xe}\ \phi_2. \tag{4.11}$$

With this assumption, the expression for the equilibrium xenon cross section becomes

$$\Sigma_{1,Xe} = 0$$

$$\Sigma_{2,Xe} = \frac{\sigma_{Xe}(\gamma_I + \gamma_{Xe})\ (\Sigma_{f1}\ \phi_1 + \Sigma_{f2}\ \phi_2)}{\lambda_{Xe} + \sigma_{Xe}\ \phi_2} \qquad (4.12)$$

Equation 4.12 is the basis for the equilibrium xenon model in TITAN. The model calculates the equilibrium xenon cross section for each node and adds it to the thermal absorption cross section for the node prior to every steady-state iteration. The xenon cross sections are considered to be constant during transient calculations.

4.5.3 Control Rod Cusping Correction Model Enhancement

The nodal neutronics model in TITAN requires spatially uniform cross sections within each node, even when a control rod is moving through the node. The usual approach is to volume-weight the cross sections of the rodded and unrodded compositions. This leads to an error in the reactivity contribution of the control rod, known as cusping. QUANDRY contains a simple model to correct for these cusping effects. This model approximates the axial flux shape within a node i,j,k as a function of the node average flux in the node i,j,k and the nodes above and below. The original QUANDRY implementation of this model assumed that all problems included a reflector above and below the core. In the current work, several applications do not have such reflectors. Thus, the original model could not be applied if a node at the top or bottom of the core experienced control movement. This limitation was removed by including an approximation for the missing fluxes. The flux in the missing node is linearly extrapolated from the boundary node and the existing adjacent node:

$$\begin{aligned} \phi_{i,j,k-1} &= 2\phi_{i,j,k} - \phi_{i,j,k+1} \quad \text{(bottom node)} \\ \phi_{i,j,k+1} &= 2\phi_{i,j,k} - \phi_{i,j,k-1} \quad \text{(top node)} \end{aligned} \qquad (4.13)$$

4.6 Operational Description

The coupling methodology and code enhancements described in this chapter have all been incorporated into TITAN. The purpose of this section is to describe how TITAN operates, and, in so doing, summarize the results of the code development.

The steady-state mode of TITAN involves most of the input and initialization functions required for the code. Most of the input data is read from an on-line data file, but certain data are entered directly by the user from an on-line terminal. The code is designed to be used interactively, with the user controlling the operation remotely at a terminal. The analysis of a transient requires two separate calculations. The first calculation generates the steady-state conditions and the second analyzes a transient, starting with those steady-state conditions. The two step method allows the user to monitor the steady-state convergence and ensure that an appropriate set of initial conditions are used in the transient calculation. The steady-state procedure is as follows:

1) Read in input data from an on-line data file. Free format is used; data arrays are placed in a large container array and a pointer system is used to locate individual subscripted variables. This permits object-time dimensioning, if desired.

2) Perform initializations. The initial thermal-hydraulic conditions are calculated with a simple model and the initial cross sections are calculated.

3) An entire static neutronics calculation is calculated with the current cross sections. No feedback updates are performed during the static convergence.

4) The nodal powers are calculated and these are passed to the thermal-hydraulics segment.

5) A thermal-hydraulics calculation is performed for one or more unperturbed time-steps (time-step size determined by the code). The average nodal thermal-hydraulic feedback parameters and the new cross sections are calculated.

6) The current transient time is checked to see if the end of the current time domain has been reached. If the time domain end has not been reached, return to 3) and continue until the end of the time domain. If the end of the last time domain has been reached, the code will do one of two things, depending on the input option selected. One option is for the calculation to end, writing the steady-state conditions on a disk file if desired. The other option is for the user to be prompted at the terminal for additional time domain information to continue the convergence procedure. If the energy and flow errors displayed at the terminal indicate satisfactory convergence, the user can end the calculation, saving the steady-state conditions on a disk file or a transient calculation. If not, the specification of new time domain information will continue the procedure, returning to 3).

As in the steady-state mode, transients are designed to be run interactively. Steady-state conditions must have been previously generated and stored on an on-line disk file in order to do a transient analysis. Additional input data required includes time-dependent pressure and flow boundary conditions and/or cross section perturbations. Cross section perturbations may be applied instantaneously or over a continuous time interval. Only one cross section perturbation per node is allowed during a transient. For the initial coupling, it was assumed that the neutronic and thermal-hydraulic time-steps were identical. The transient procedure is as follows:

1) Read common blocks and container array from steady-state disk file,

2) Read transient input from data file,

3) Perform any needed initializations,

4) Calculate the time-steps, subject to Courant numerical stability limitations and user-supplied upper and lower bounds,

5) Determine whether the transient is initiated in the neutronics segment or in the thermal-hydraulics segment. If neutronics, go to 6). If thermal-hydraulics, go to 7),

6) Perform one complete feedback loop, beginning with the transient neutronics calculation. Calculate the new nodal powers and update these in the thermal-hydraulics calculation for the same time period. Calculate the average feedback parameters and the new cross sections. Go to 8),

7) Perform one complete feedback loop, beginning with the thermal-hydraulics calculation. Calculate the average feedback parameters and the new cross sections. Perform the transient neutronics calculations for the same time period. Calculate the new nodal powers and update them in the thermal-hydraulics segment.

8) Check for the end of the current time domain. If the end has not been reached, return to step 4). If the time domain has ended, the calculation ends or the user is prompted for new time domain information.

The steady-state and transient operational strategies are shown in Fig. 4.6 and 4.7, respectively.

These procedures are now fully operational in TITAN and have been successfully demonstrated. This demonstration is presented in the following chapters. An input specification for TITAN is found in Ref. [T-4].

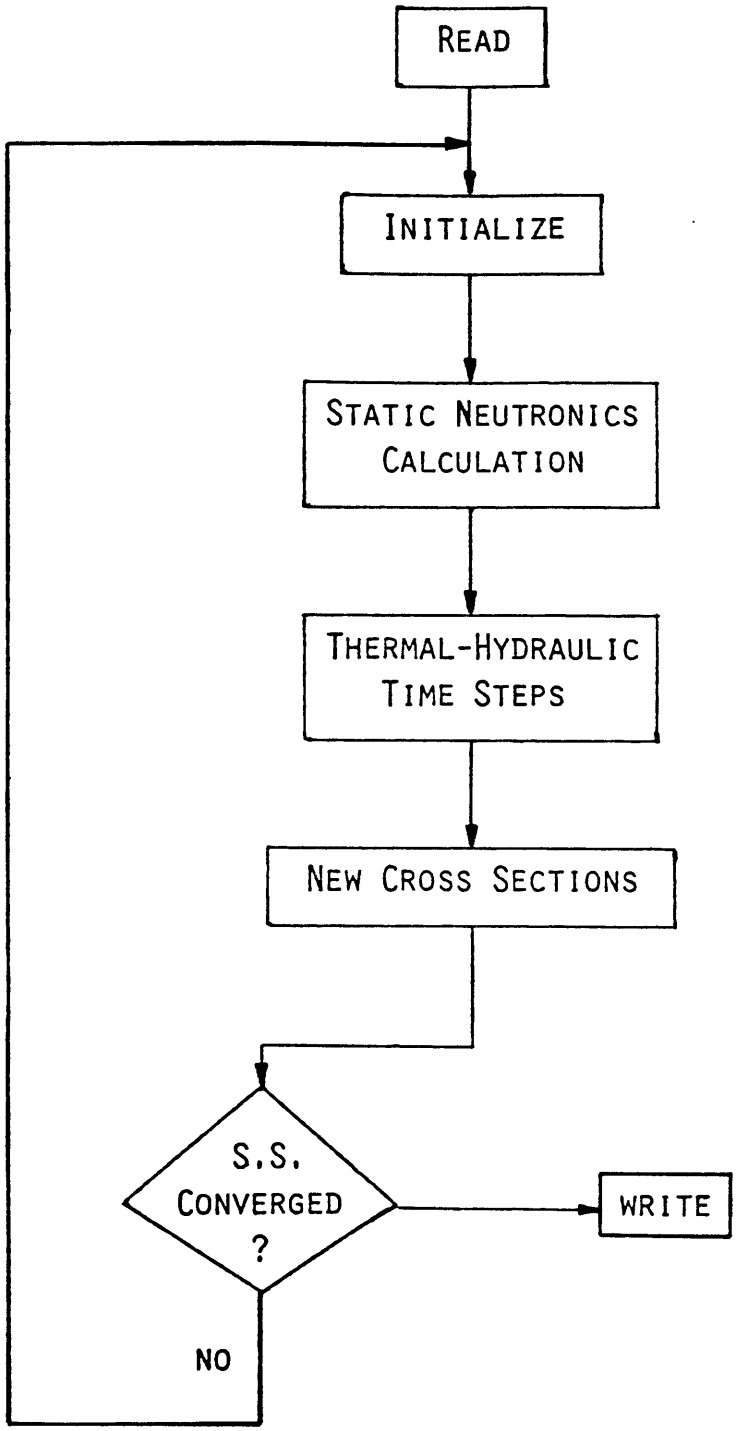

Figure 4.6 TITAN Steady-state Operational Strategy

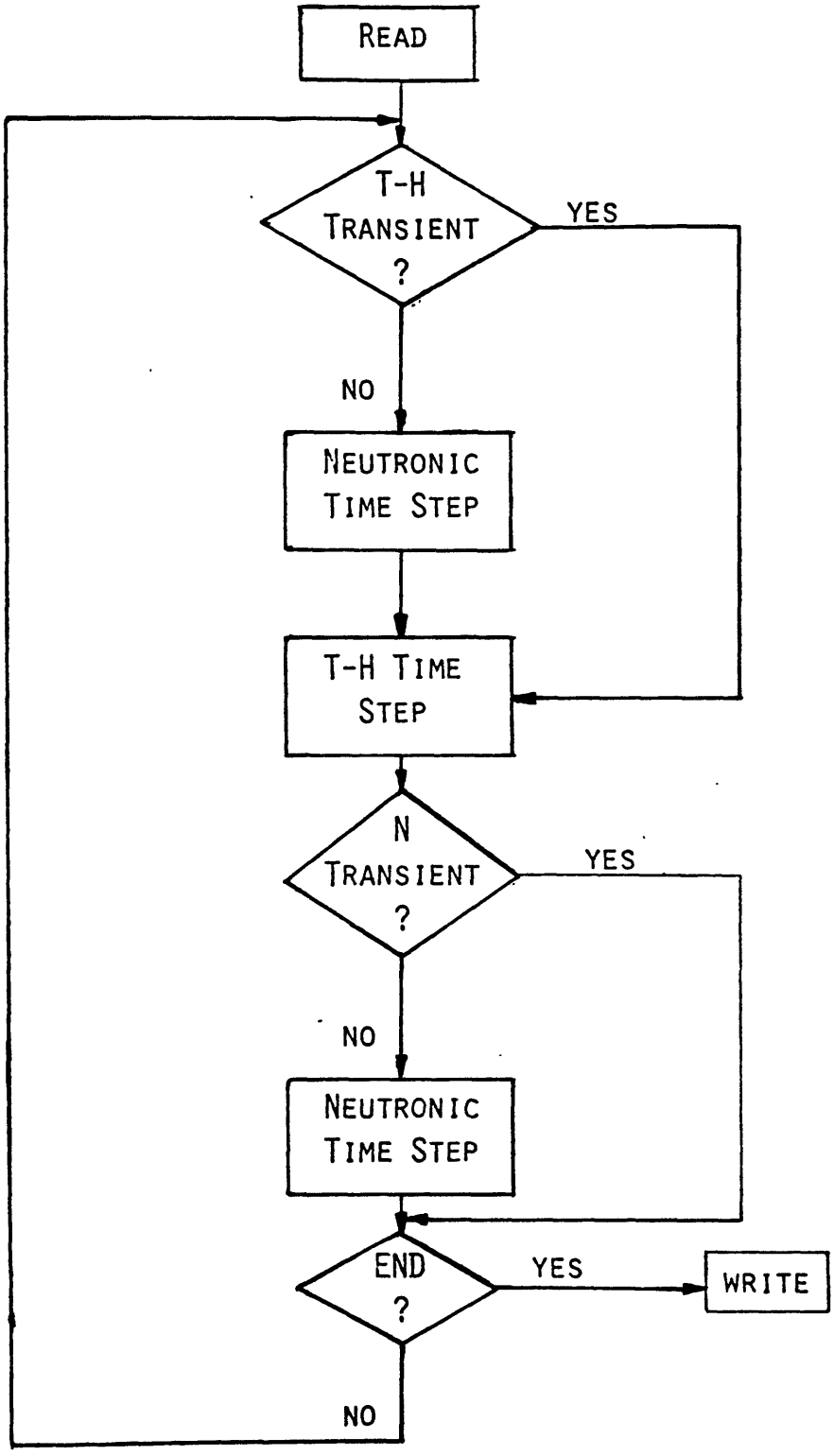

Figure 4.7 TITAN Transient Operational Strategy

CHAPTER 5:

APPLICATION OF TITAN TO A BOILING WATER TWO CHANNEL PROBLEM

5.1 Introduction

The previous chapters introduce coupled neutronic/thermal-hydraulic analysis of reactor cores, review the existing approaches to such analysis and the codes which perform the analysis, summarize the neutronics and thermal-hydraulics models used in TITAN, and present the details of the TITAN coupling methodology. This capter describes the application of TITAN to a Boiling Water Two Channel (BW2C) problem. Clearly, the production of results with TITAN was possible only after a considerable effort was expended in implementing the coupling methodology. The BW2C problem was used extensively in the debugging effort which followed the transformation of THERMIT and QUANDRY into TITAN. The details of this significant part of the TITAN development are not reported, however, because they contain little of general interest.

TITAN was applied to the BW2C problem in order to satisfy the following objectives:

1. To demonstrate the correct implementation of the TITAN methodology,
2. To demonstrate that the TITAN methodology can produce steady-state and transient coupled solutions,
3. To assess the accuracy and reliability of TITAN,
4. To determine the computational effort required for TITAN analyses,
5. To investigate modeling options and operational characteristics of TITAN, and
6. To discover fruitful areas for future work.

The BW2C problem was selected to provide a basis for satisfying these objectives. This problem is described in Section 5.2. A number of steady-state and transient analyses were performed with TITAN. These are reported in Sections 5.3 and 5.4, respectively. Table 5.1 presents an inventory of all the analyses performed. A summary of the BW2C problem results in Section 5.5 completes the chapter.

5.2 Boiling Water Two Channel Problem Description

A sample problem was selected for debugging, testing and verification of the TITAN code. The problem consists of two adjacent part-length boiling water reactor fuel assemblies, as shown in Figure 5.1. Each assembly has a partially inserted control rod. The problem was devised at M.I.T. [R-11] to serve as the basis for a transient benchmark problem to check the numerical accuracy of codes which model three-dimensional neutronics with feedback. The geometrical characteristics of the problem are typical of commercial BWRs (in particular, the Brown's Ferry plants). The model was limited to two part-length assemblies in order to keep computational costs low. However, the BW2C problem was designed to present a challenge to a coupled code by using neutronic boundary conditions and control rod positions to induce large horizontal power gradients and by having substantial boiling at steady-state to strengthen the feedback effects. Furthermore, a steady-state MEKIN solution with which TITAN results could be compared was available.

The neutronic parameters describing the BW2C problem were obtained informally from Science Applications, Inc. [G-3] and were based upon parameters supplied by Brookhaven National Laboratory and General Electric

Table 5.1

Summary of BW2C

Steady-State QUANDRY Analyses

BW2C-R: 10 axial nodes with and without feedback

BW2C-T: 10 axial nodes with and without feedback

Steady-State TITAN Analyses

BW2C-R: 10 axial nodes: simple fuel rod model

BW2C-T: 10 axial nodes: simple, intermediate and full fuel rod models

BW2C-T: 10 axial nodes; 1, 2, 4, 8 time-steps per static neutronic calculation

Transient QUANDRY Analyses

Rod Withdrawal: 10 axial nodes: no feedback: cusping: time-step: time-step = 0.025, 0.01, 0.005 s.

Transient TITAN Analyses

Null Transients, thermal-hydraulic and neutronic

Turbine Trip #1: 10 and 20 axial nodes

Turbine Trip #2: 10 axial nodes

Rod Withdrawal: 10 axial nodes: cusping: time-steps = 0.05, 0.01, 0.005 s.

Rod Withdrawal: 20 axial nodes: cusping: time-steps = 0.01, 0.005 s.

Rod Withdrawal: 30 axial nodes: cusping: time-steps = 0.01, 0.005 s.

Rod Withdrawal: 10 axial nodes: no cusping model: time-steps = 0.05, 0.01 s.

Rod Withdrawal: 10 and 20 axial nodes: no cusping model, time-step = 0.01 s.

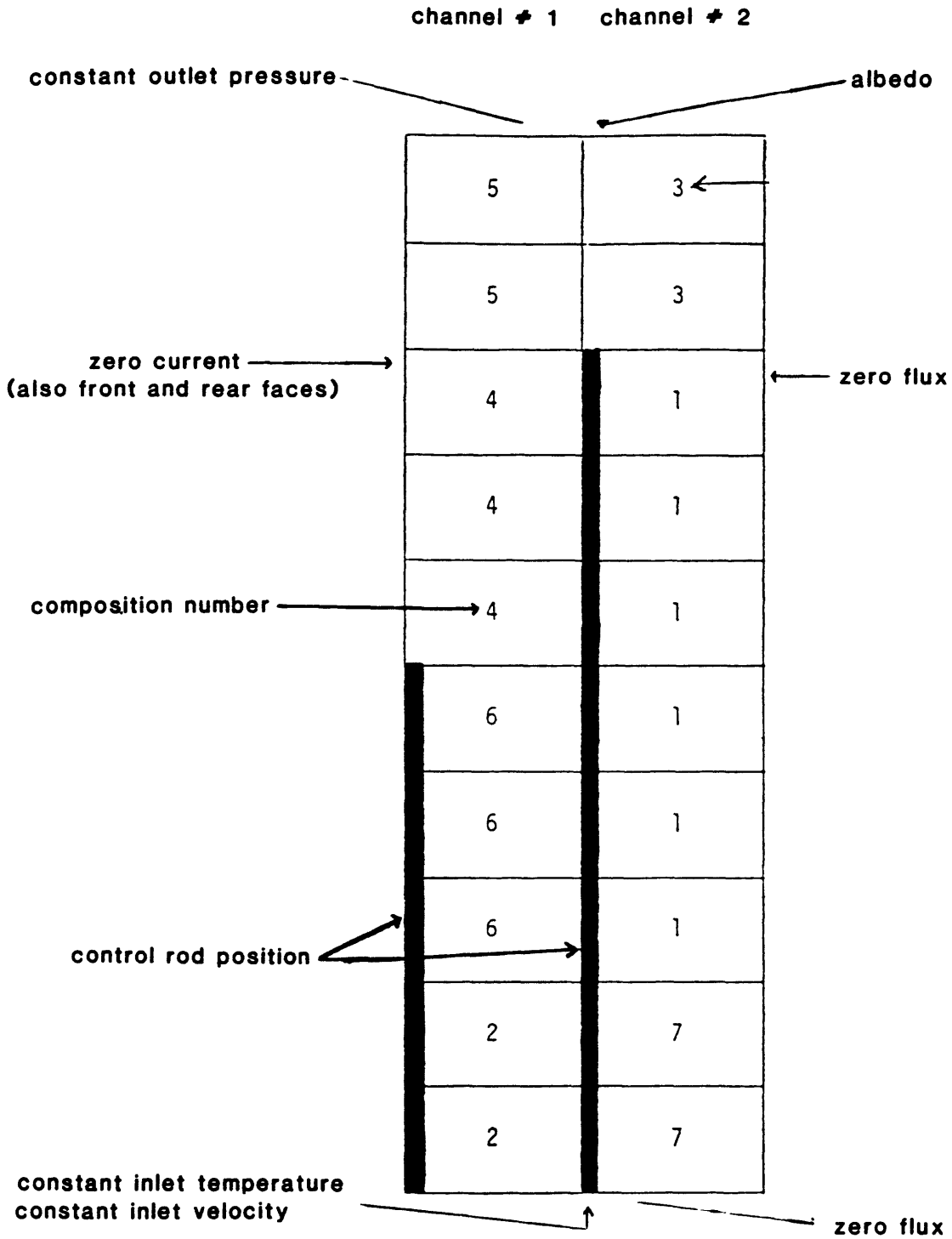

Figure 5.1 BW2C Geometry and Boundary Conditions

Company for the Brown's Ferry beginning-of-life core. Seven different neutronic compositions are present for the control rod configuration shown in Figure 5.1. The neutronic boundary conditions are zero current on three vertical sides, zero flux on the bottom and the fourth vertical side, and specified albedos on the top. Both channels have control rods modeled at steady-state as homogeneous absorbers. For channel 1, the control rod is inserted 76 cm, half-way up the channel. The control rod in channel 2 is inserted four-fifths of the length of the channel, a distance of 121.6 cm. The boundary conditions and control rod positions are not typical of commercial reactors. Rather, they produce the large horizontal flux tilts mentioned previously. The base case model divides the two channels into 10 axial nodes each. The thermal-hydraulic boundary conditions specified are inlet coolant velocity and temperature and exit pressure. Table 5.2 summarizes the important characteristics of the BW2C problem. The neutronic parameters are given in Appendix C.

Table 5.2 shows dual values for several of the BW2C problem parameters because two versions of the same problem were analyzed. The "reference" values are those used in the steady-state MEKIN analysis of Rodriques-Vera [R-11]. Steady-state solutions for this problem were obtained with QUANDRY and TITAN and are compared to the MEKIN results in Section 5.3.1. It was found that the average linear heat generation rate for this problem was rather high (9.496 kw/ft), leading to unusually high fuel temperatures at steady-state. Accordingly, a modified version of the reference conditions, denoted the "test" conditions, was obtained by reducing the total "reactor" power from 6077.6 kw to 4000.0 kw and adjusting the coolant inlet velocities to give approximately the same outlet

TABLE 5.2

SUMMARY OF BW2C PROBLEM CHARACTERISTICS

	Reference/Test
Total power, kw	6077.6/4000.0
Number of fuel assemblies	2
Assembly length, cm	152.4
Number of fuel rods per assembly	64
Average fuel power density, w/cm^3	366.38/241.13
Average linear heat generation rate, kw/ft	9.496/6.250
Fuel rod diameter, cm	1.226
Clad thickness, cm	0.0813
Gap thickness, cm	0.0114
Inlet temperature, °K	548
Total flow rate, kg/s	31.703/20.841
Channel 1 flow velocity, m/s	1.946/1.28
Channel 2 flow velocity, m/s	2.511/1.65
Outlet pressure, MPa	7.136
Channel flow area, cm^2	93.5
Channel 1 control rod insertion distance, cm	76.0
Channel 2 control rod insertion distance, cm	121.6
Direct moderator heating fraction	0.0164
Xenon	none

void fractions. The "test" conditions were used for steady-state modeling studies and all transient calculations. The reference and test conditions for the boiling water two channel problem are hereafter denoted BW2C-R and BW2C-T, respectively. Furthermore, the left assembly is called channel 1 and the right assembly is called channel 2 throughout this chapter.

5.3 Steady-State Results

5.3.1 BW2C Problem: Reference Conditions

5.3.1.1 Feedback Assessment

Steady-state analyses of the BW2C reference problem were performed with QUANDRY with and without feedback. These analyses show the significance of feedback for this case. Several important parameters are compared in Table 5.3 and the axial power shapes are shown in Figures 5.2 and 5.3. The effect of the feedback is clearly shown by a comparison of the eigenvalues and the power shapes. The inclusion of feedback reduces the eigenvalues, because the calculated average fuel temperature is higher than the reference values and the calculated average coolant density is lower than the reference values. Two of the three feedback effects therefore reduce the core reactivity. The spatial impact of the feedback is seen in both the axial and radial power shapes. The QUANDRY results show that the power in channel 1 is more than twice that of channel 2. This is because the channel 2 control rod is inserted farther than that of channel 1 and a zero flux boundary condition exists on the right boundary of channel 2. The inclusion of feedback reduces the disparity between the channel powers slightly. The axial power shapes for both channels show the effect of the control rods, in that the power is strongly peaked in the upper nodes. As Figure 5.2 shows, the inclusion of

TABLE 5.3

COMPARISON OF STEADY-STATE GLOBAL PARAMETERS FOR THE BW2C PROBLEM, REFERENCE CONDITIONS, WITH AND WITHOUT FEEDBACK (QUANDRY)

	No Feedback	Feedback
Eigenvalue	0.82067	0.73740
Normalized Assembly Powers		
Channel 1	1.4485	1.3733
Channel 2	0.5515	0.6267
Core average fuel temperature, °K	922.0	1339.9
Core average coolant temperature, °K	559.0	555.2
Core average coolant density, kg/m^3	739.9	625.2

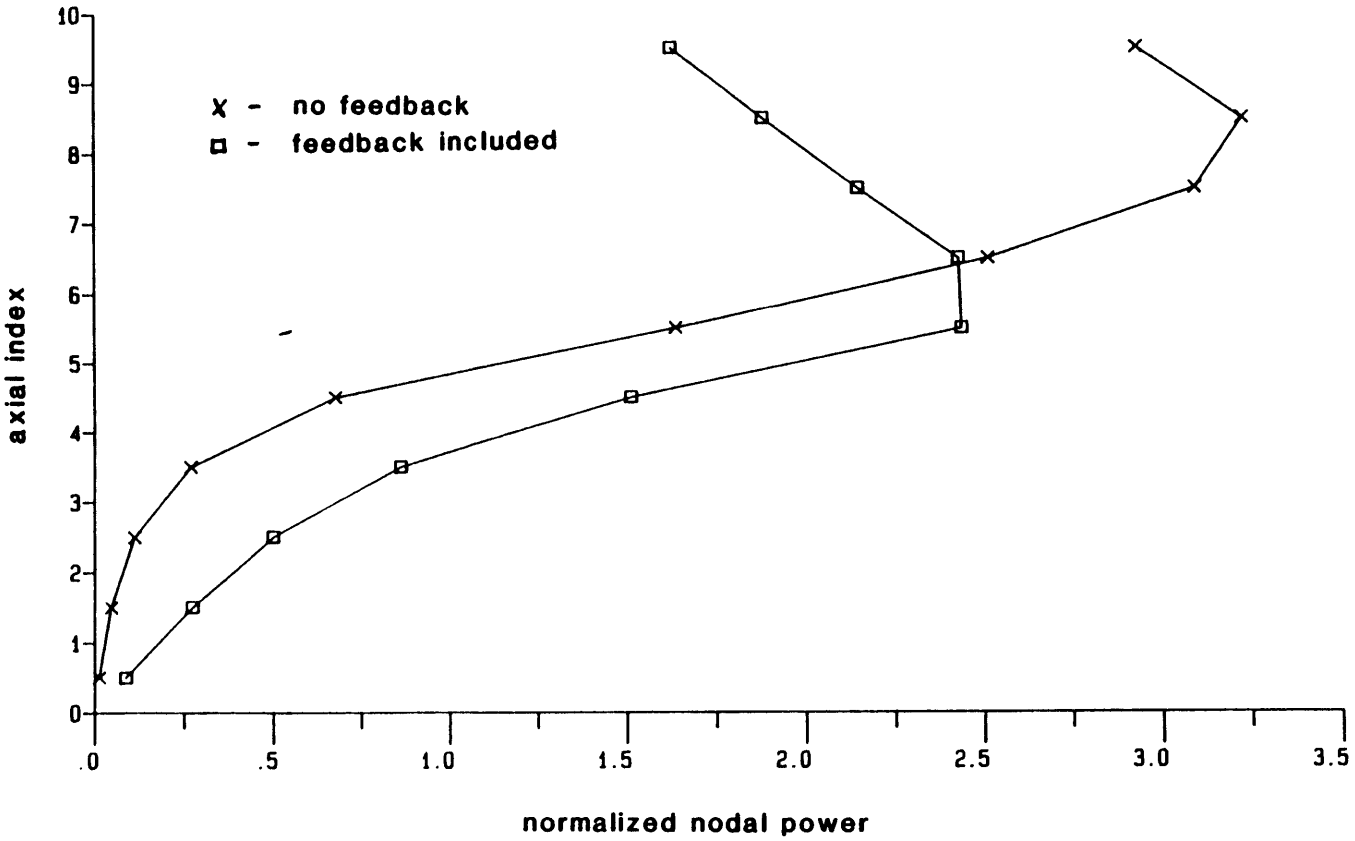

Figure 5.2 BW2C-R Axial Power Profile, Channel 1:

QUANDRY with and without feedback

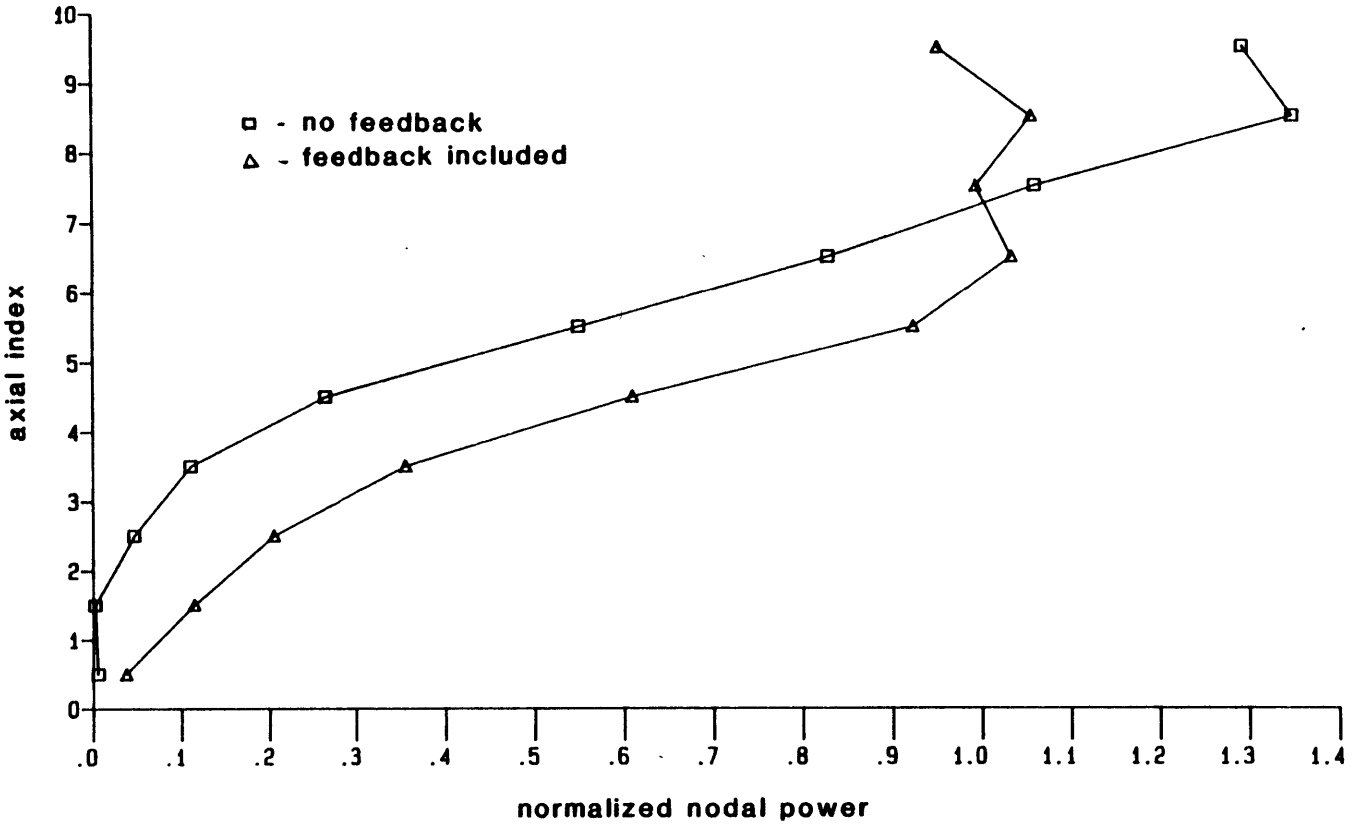

Figure 5.3 BW2C-R Axial Power Profile, Channel 2:

QUANDRY with and without feedback

feedback reduces the power peaking in the upper nodes, particularly in channel 1. The effect of the feedback is strongest in the top three nodes of channel 1 where boiling is most pronounced. This boiling effect may actually be exaggerated because the simple boiling model in QUANDRY assumes homogeneous equilibrium flow. In any case, the BW2C-R problem is strongly affected by the inclusion of feedback and is therefore a good test for TITAN.

5.3.1.2 Comparison of TITAN, QUANDRY and MEKIN Results

The steady-state BW2C-R problem was analyzed with TITAN in order to compare the results to those of MEKIN and QUANDRY with feedback. MEKIN is a three-dimensional coupled code based on a finite difference neutronics model (see Appendix A). On the other hand, QUANDRY uses the same nodal neutronics model as TITAN, but with a very simple thermal-hydraulics model. The purpose of this comparison is to demonstrate that the TITAN steady-state methodology has been implemented correctly and produces reasonable results. The TITAN analysis was set up to be as close as possible to the MEKIN analysis. For example, the simple fuel rod model with constant fuel properties and constant gap heat transfer coefficient was used for this particular comparison.

Comparisons of the normalized nodal powers as calculated by MEKIN, QUANDRY, and TITAN for channels 1 and 2 are presented in Figures 5.4 and 5.5, respectively. The nodal powers are normalized to the average nodal power. TITAN produced axial power profiles which are in good agreement with the MEKIN results, while the QUANDRY results do not agree as well. The TITAN nodal powers are somewhat lower in the upper nodes and higher in the lower nodes than those of MEKIN, particularly in channel 1. QUANDRY

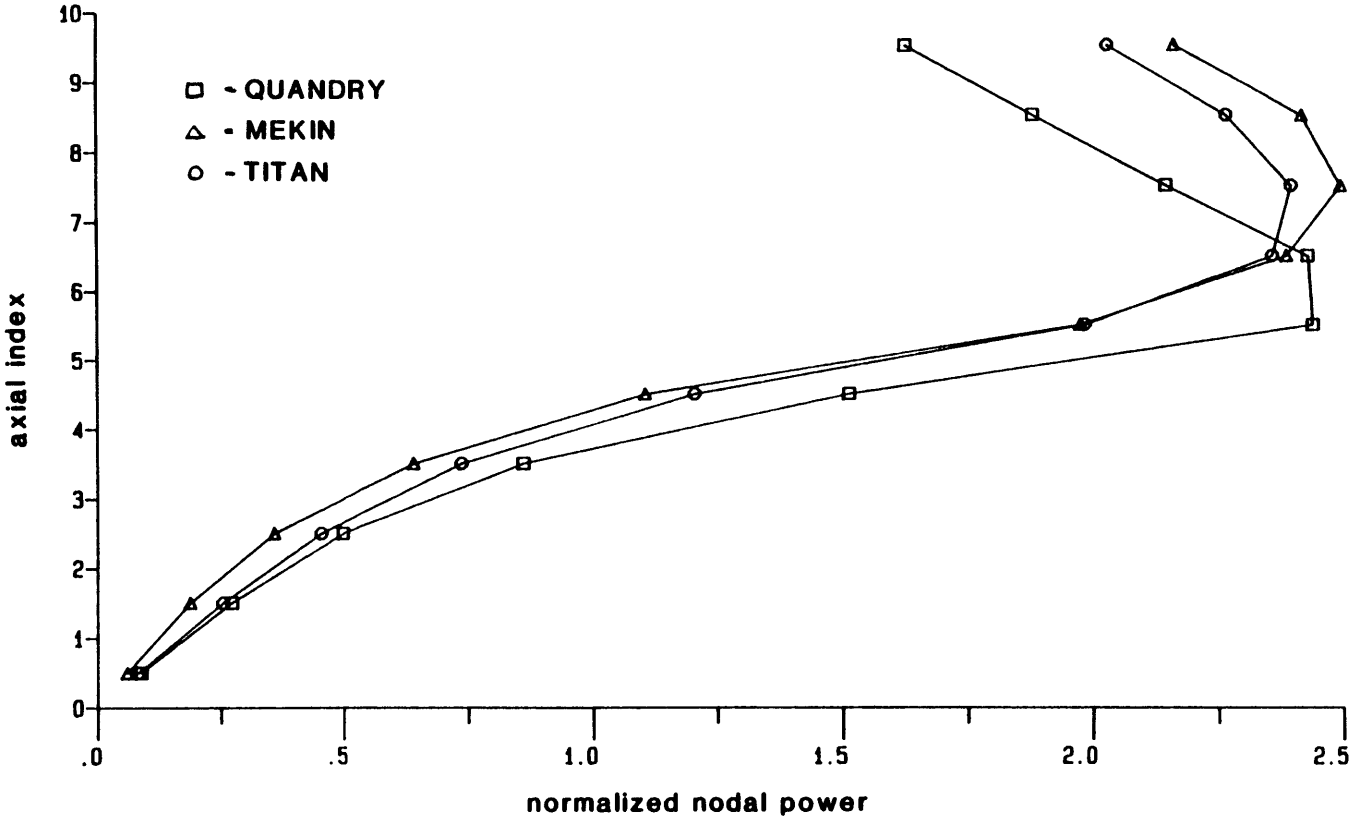

Figure 5.4 BW2C-R Axial Power Profile, Channel 1:

QUANDRY, MEKIN and TITAN

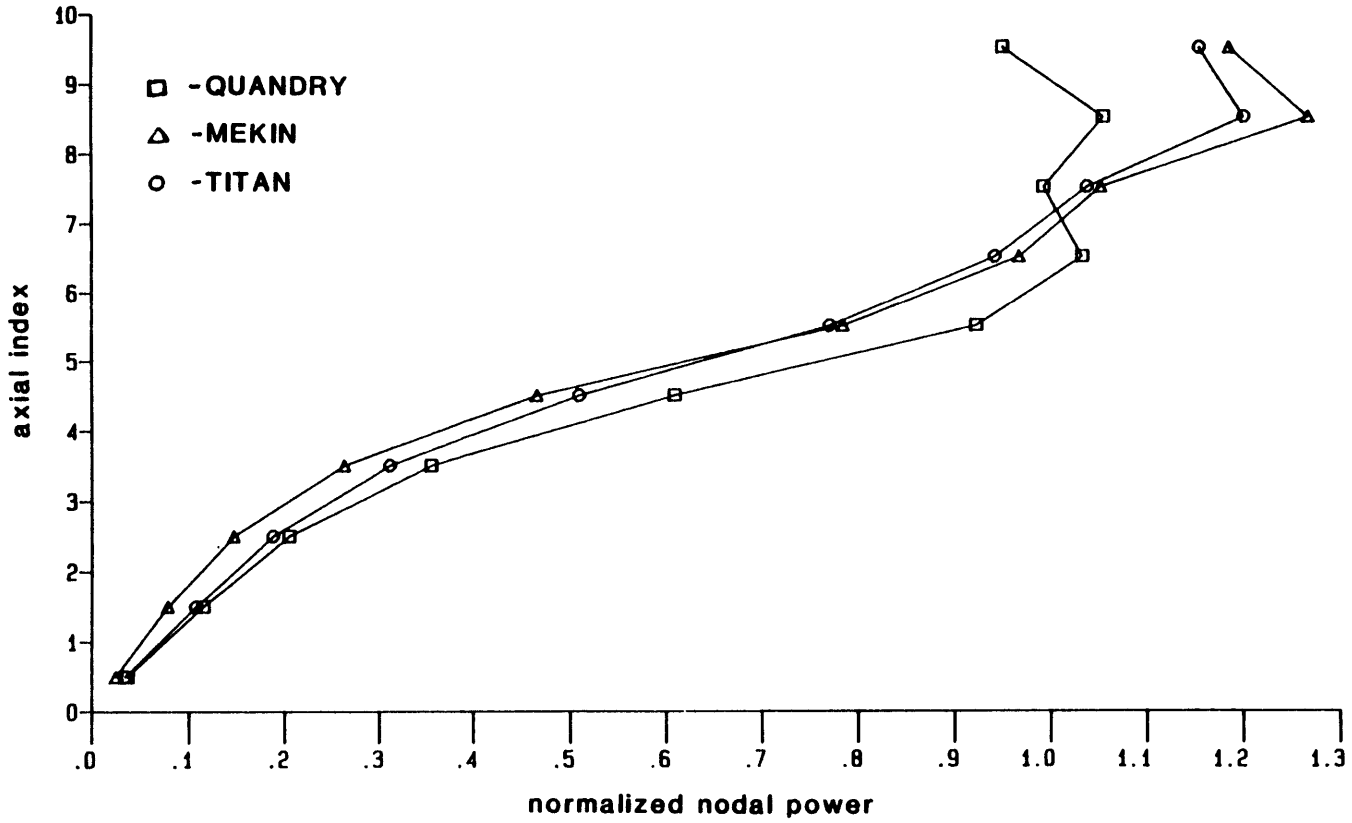

Figure 5.5 BW2C-R Axial Power Profile, Channel 2:

QUANDRY, MEKIN and TITAN

produced nodal powers which are higher than both MEKIN and TITAN in the middle nodes and lower than both MEKIN and TITAN in the top three nodes of both channels.

Table 5.4 presents a comparison of the values of the core eigenvalues, normalized assembly powers, and selected thermal-hydraulics parameters predicted by QUANDRY, MEKIN, and TITAN. The QUANDRY value for the reactor eigenvalue was less than that of TITAN by 6.3×10^{-3}, or 0.85%. However, the MEKIN eigenvalue was greater than that of TITAN by 7.3×10^{-3}, or 0.98%. The three codes were in excellent agreement on the normalized assembly powers, predicting that the power in channel 1 is approximately 2.2 times that in channel 2. These results indicate that the TITAN methodology has been implemented correctly and is capable of producing a coupled steady-state solution. Furthermore, the results obtained with TITAN are reasonable and compare well with results from the two other coupled codes.

Some of the observed differences in the QUANDRY, MEKIN and TITAN analyses of the BW2C-R problem can be explained by examining the thermal-hydraulic parameters in Table 5.4. Most of the TITAN and MEKIN thermal-hydraulics parameters agree well (less than 5% difference), though the maximum and core average fuel temperatures and channel 2 exit void fractions differ by 10-20%. Of particular concern are the discrepancies in fuel temperatures, because of the magnitude of the differences and the importance of the Doppler feedback mechanism. Table 5.4 indicates that the TITAN maximum and core average fuel temperatures exceed those of MEKIN by 692.5 °K and 145.7 °K, respectively. Figures 5.6 and 5.7 show the node average fuel temperatures for channels 1 and 2, respectively, as calculated

Table 5.4

Comparison of Parameters from TITAN, MEKIN and QUANDRY
Analyses of the Steady-State BW2C-R Problem

Parameter Description	TITAN	MEKIN	QUANDRY
Eigenvalue	0.7437	0.7510	0.7374
Normalized power, channel 1	1.375	1.377	1.373
Normalized power, channel 2	0.625	0.623	0.627
Maximum fuel temperature, °K*	3597.9	2905.4	2463.0
Core average fuel temperature, °K	1313.7	1168.0	1339.9
Maximum coolant temperature, °K	560.4	560.3	560.3
Core average coolant temperature, °K	554.6	554.6	555.2
Minimum coolant density, kg/m^3	284.6	286.7	222.0
Core average coolant density, kg/m^3	628.3	617.6	625.2
Exit quality, channel 1, %	15.76	15.30	13.40
Exit quality, channel 2, %	2.96	2.80	3.85
Exit void fraction, channel 1	0.65	0.65	0.70
Exit void fracton, channel 2	0.31	0.36	0.42
Maximum cladding temperature, °K	586.9	593.8	**

* TITAN and MEKIN: centerline temperatures; QUANDRY: fuel rod average temperature

**QUANDRY lumped fuel rod model does not yield separate cladding temperatures

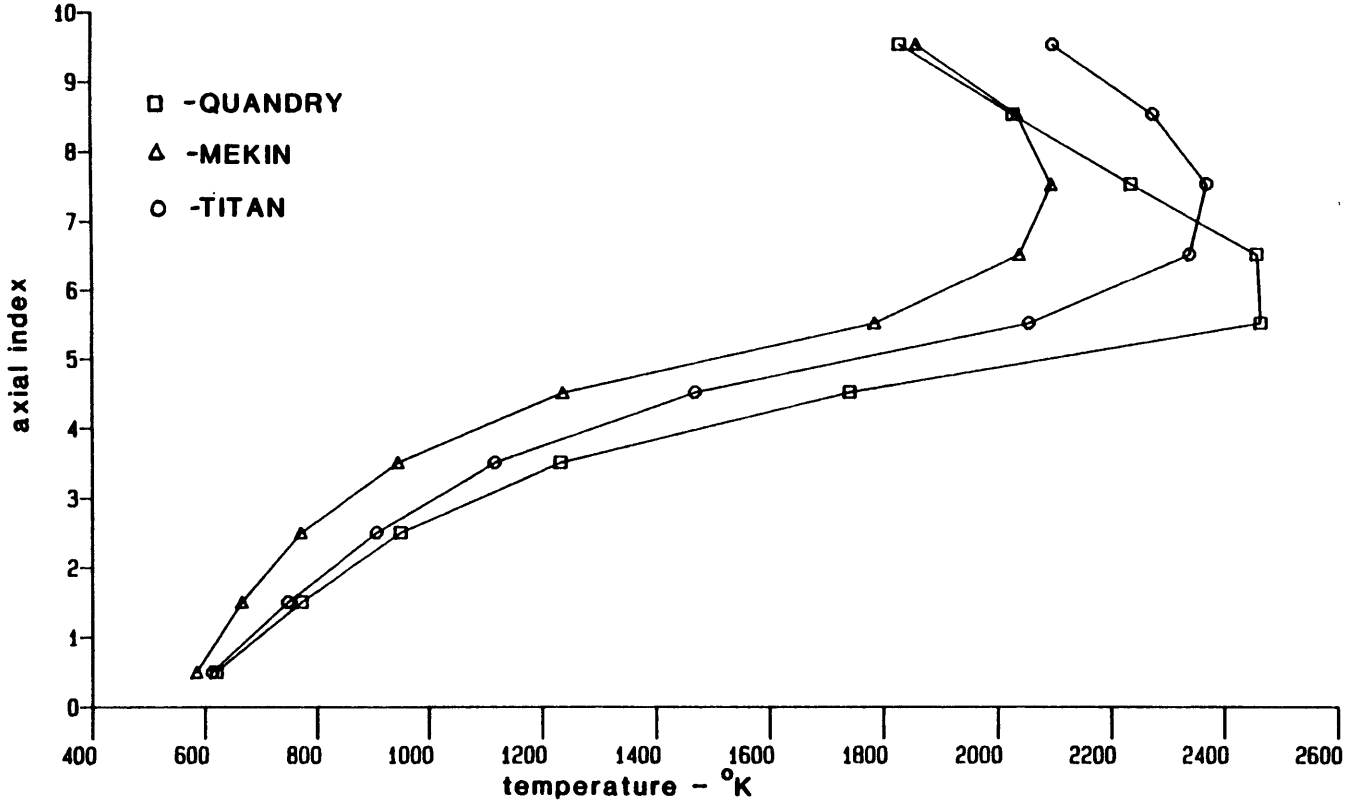

Figure 5.6 BW2C-R Nodal Fuel Temperatures, Channel 1:

QUANDRY, MEKIN and TITAN

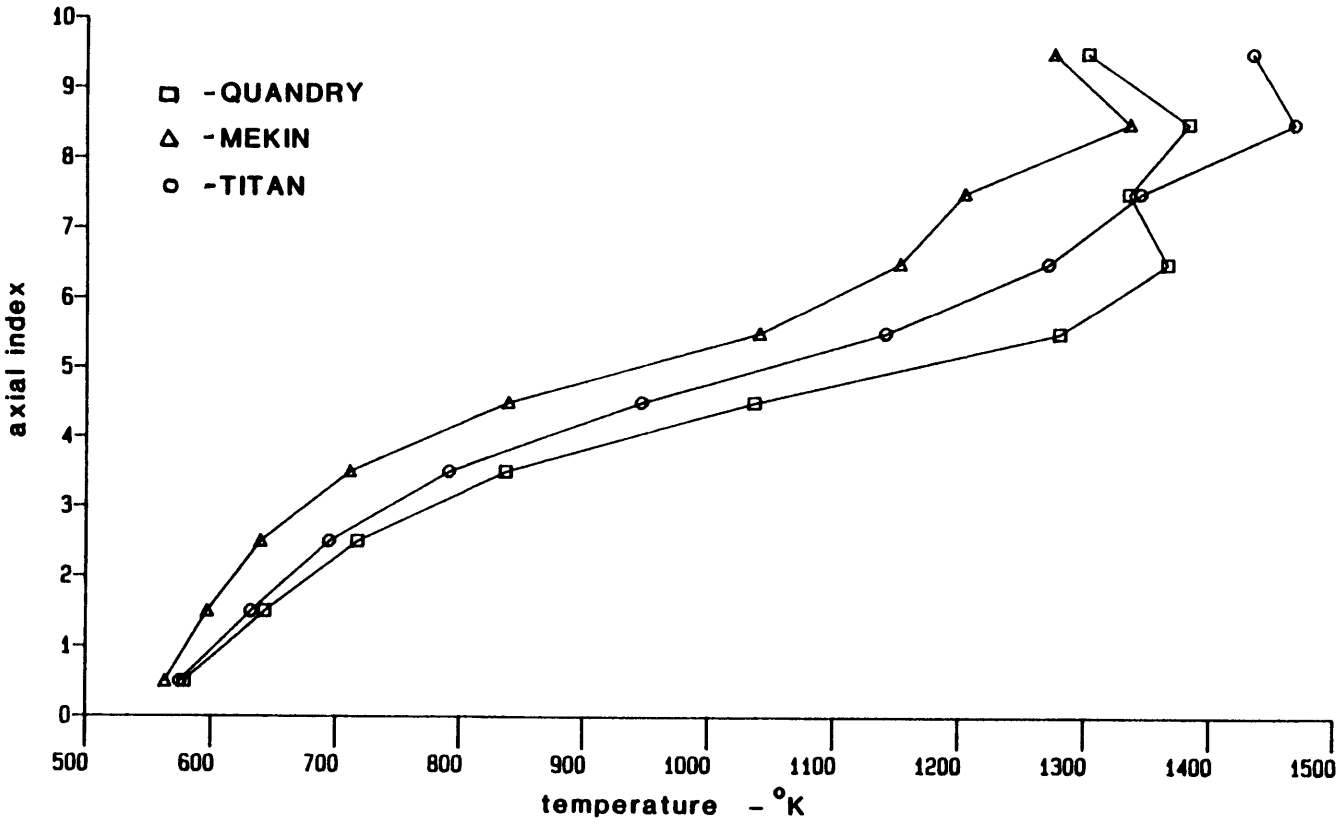

Figure 5.7 BW2C-R Nodal Fuel Temperatures, Channel 2:

QUANDRY, MEKIN and TITAN

by MEKIN, QUANDRY and TITAN. The TITAN node average fuel temperatures are consistently higher than the corresponding MEKIN fuel temperatures, even for the nine nodes in which the TITAN powers are lower than the MEKIN powers. The reason for this is that the two analyses used different fuel properties, leading to different fuel temperatures. The user-supplied fuel thermal conductivity used in MEKIN was 3.46 w/m-°K, while TITAN used the built-in value of 2.4 w/m-°K. TITAN therefore would have calculated higher fuel temperatures than MEKIN even if the power and heat transfer boundary conditions were identical. For TITAN, the higher temperatures in the top of the core produce a larger Doppler feedback, reducing the nodal power there and increasing the power in the other nodes. Neither the TITAN nor the MEKIN results can be claimed to be "correct," since fuel properties are in fact temperature-dependent. Recall, however, that TITAN is capable of accounting for the effect of temperature on fuel properties as well as the temperature dependence of the fuel-cladding gap heat transfer. The sensitivity of steady-state results to the choice of fuel rod models is discussed in Section 5.3.2.4.

The contributions of coolant temperature and coolant density feedback to the differences in the MEKIN and TITAN results are apparently less significant than that of the fuel temperature feedback. Table 5.4 indicates very close agreement in the core average and maximum coolant temperatures. This is not surprising, since much of the coolant is at the saturation temperature. Coolant temperature feedback effects do not help explain the differences between the results, therefore. A more important feedback effect is the coolant density. Table 5.4 shows that TITAN calculated a lower minimum nodal coolant density and a higher core average

coolant density than did MEKIN. The treatment of two-phase flows in MEKIN and TITAN is quite different, producing the axial coolant density profiles shown in Figures 5.8 and 5.9 for channels 1 and 2, respectively. These figures show that TITAN predicts a somewhat higher nodal coolant density in the saturated boiling regions. The two-fluid model of TITAN allows the liquid and vapor to have different speeds, but the homogeneous equilibrium model of MEKIN assumes both phases move at the same speed. In TITAN, the vapor will often have a higher velocity than the liquid, yielding a lower void fraction and, hence, a higher average coolant density than would be calculated with equal phase velocities. This is consistent with the results shown in Figures 5.8 and 5.9.

The impact of the different two-phase flow models of TITAN and MEKIN on the calculated power distributions is opposite to that of the different fuel rod models. The higher nodal coolant densities calculated by TITAN should have a positive reactivity effect, leading to higher power in the nodes having two-phase coolant. However, Figures 5.4 and 5.5 show that TITAN calculated lower nodal powers than did MEKIN in the nodes with substantial boiling. The differences in the fuel temperature calculations are largely responsible for the discrepancies in nodal powers, therefore, and the differences in coolant density mitigate the fuel temperature effect somewhat.

A similar conclusion about the relative importance of the differences in the TITAN and MEKIN calculations of fuel rod temperature and coolant density can be drawn for the global criticality of the reactor. As Table 5.4 shows, the MEKIN eigenvalue was somewhat greater than that of TITAN, while the core average fuel temperature and core average coolant

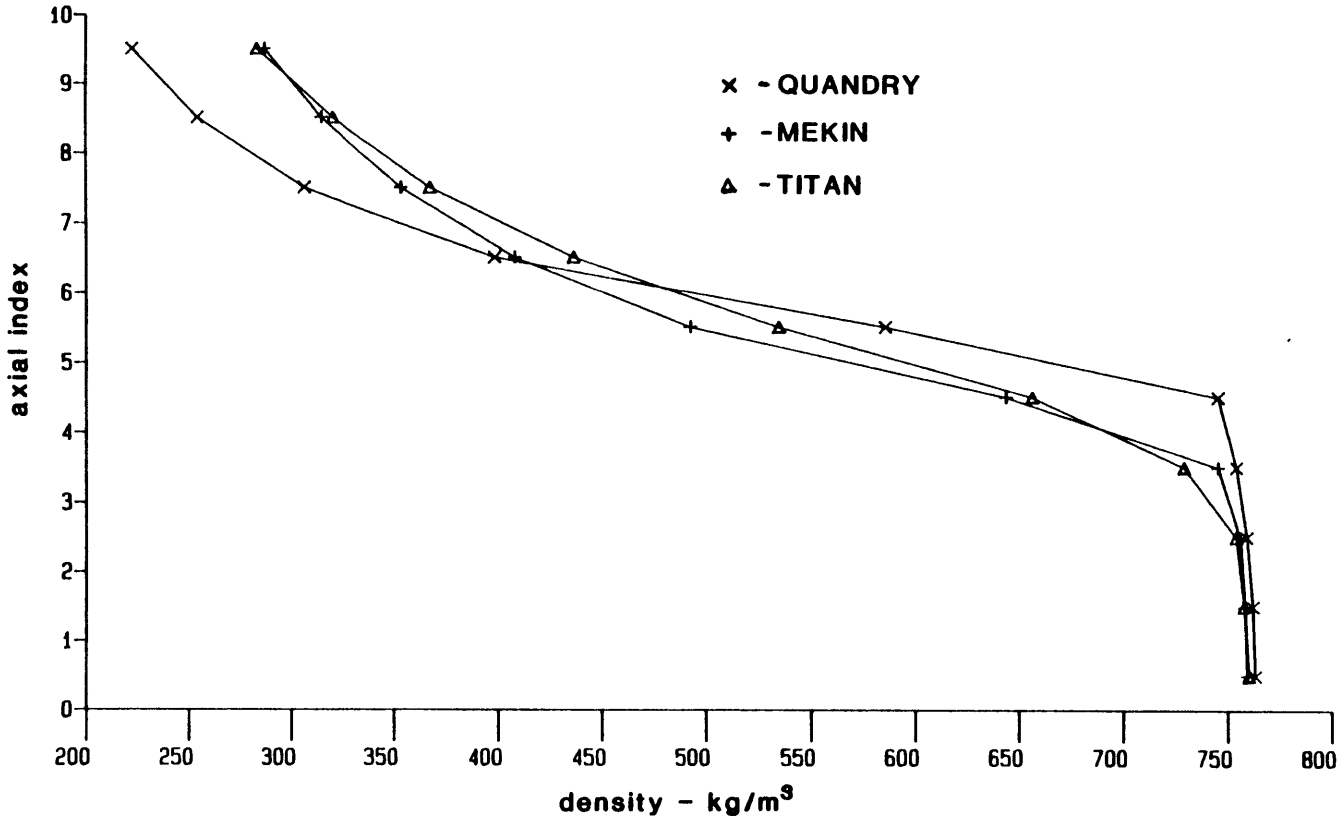

Figure 5.8 BW2C-R Nodal Coolant Densities, Channel 1:

QUANDRY, MEKIN and TITAN

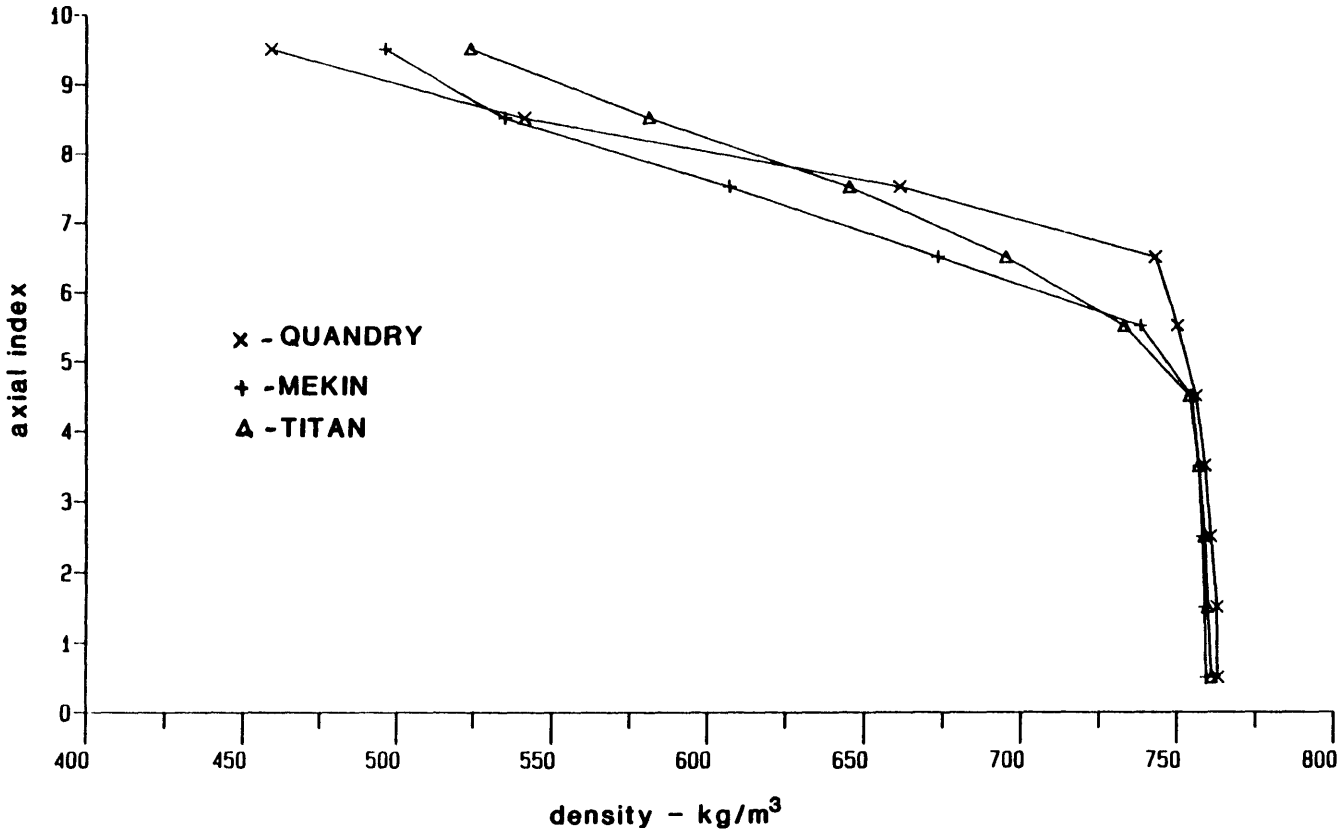

Figure 5.9 BW2C-R Nodal Coolant Densities, Channel 2:

QUANDRY, MEKIN and TITAN

density was less than calculated by TITAN. Since a lower average fuel temperature increases the eigenvalue and a lower average coolant density decreases the eigenvalue, we can infer that the differences in the MEKIN and TITAN fuel temperature calculations have a greater global feedback effect than do the differences in the two-phase flow calculation.

The simple QUANDRY thermal-hydraulics model yielded results which, while differing significantly in exit quality, void fraction and coolant density, and maximum fuel temperature, were in good agreement with TITAN for core average fuel temperature, maximum and core average moderator temperature, and core average coolant density. The observed differences are directly attributable to limitations in the simple QUANDRY thermal-hydraulics model. For example, the QUANDRY maximum fuel temperature is lower than either MEKIN or TITAN because it is the lumped average temperature at the hot spot rather than a true maximum (centerline) temperature. However, the QUANDRY core average fuel temperature is higher than TITAN and much higher than MEKIN. Figures 5.6 and 5.7 show that QUANDRY produced node-averaged fuel temperatures which were higher than MEKIN in all but two nodes and higher than TITAN in all but six nodes. A comparison of the QUANDRY axial power shapes for channels 1 and 2 (Fig. 5.4 and 5.5) to the QUANDRY node-averaged fuel temperatures reveals a strong correlation between the two shapes, as would be expected. Indeed, the differences in the TITAN and QUANDRY axial power profiles can be partially explained by the fuel temperature profiles. The heat transfer from fuel rod to coolant is modeled by a constant heat transfer coefficient in the QUANDRY model. In TITAN and MEKIN (and in reality), the heat transfer changes significantly along the channel,

particularly when boiling begins. Thus, the QUANDRY analysis, using an "average" heat transfer coefficient, overpredicts the heat transfer in the lower nodes and underpredicts the heat transfer in the upper nodes of each channel. This results in node-averaged fuel temperatures which are low relative to the nodal power in the top nodes. This, in turn, tends to depress the nodal power in the top nodes and increase the power in the bottom nodes, as seen in Figures 5.6 and 5.7.

The discrepancies in the fuel temperature calculations alone do not account for the observed QUANDRY power shapes. The spatial behavior of the coolant density, shown in Fig. 5.8 and 5.9 also is significant. The QUANDRY axial coolant density profiles are significantly different than those of TITAN and MEKIN. All three codes are essentially in agreement when the coolant is single-phase (nodes 1-3 of channel 1, nodes 1-5 of channel 2). However, the coolant density profiles of MEKIN and TITAN diverge from the QUANDRY profiles when boiling begins. A comparison of the QUANDRY axial coolant density profiles and the axial power profiles (Figures 5.4 and 5.5) shows a good correspondence between the nodes having higher coolant density and higher power, reflecting the impact of moderator density of feedback on the power shape. Similarly, correspondence is seen between nodes having lower coolant density and lower power. The QUANDRY assumption of a single uniform coolant pressure contributes to the discrepancies in the coolant density profiles. In addition, the coolant flow rates were different in the QUANDRY analysis because a uniform core inlet flow is assumed. In the MEKIN and TITAN analyses, the flow rate in channel 1 was less than that in channel 2 (see Table 5.2). This also explains the exit quality values in Table 5.4,

since the QUANDRY model assumed a higher flow rate in channel 1 and a lower flow rate in channel 2, resulting in the exit quality values seen in the table.

In summary, the TITAN results for the BW2C-R problem were in good agreement with the MEKIN reference solution. The main difference was in the fuel temperatures, for which TITAN consistently predicted higher values. The source of this disagreement was the fuel thermal properties used in the analyses. The QUANDRY results for this problem showed some significant differences with respect to MEKIN and TITAN. This reflects the impact of the very simple and approximate thermal-hydraulics model contained in QUANDRY.

5.3.2 BW2C Problem: Test Conditions

5.3.2.1 Comparisons of TITAN and QUANDRY

The BW2C test problem is a reduced power version of the BW2C problem with reference conditions (see Table 5.2). It is designed to preserve the large transverse power gradient and significant boiling of the reference problem, without the very high fuel temperatures. An average linear heat generation rate of 6.25 kw/ft is more representative of commercial BWR power plants than that of the reference problem, thereby resulting in peak nodal powers and centerline fuel temperatures which are within reasonable limits. The channel inlet coolant velocities have been reduced to produce an axial coolant density distribution similar to that of the reference problem. All of the geometric and neutronic characteristics of the test problem are identical to those of the reference problem.

As in the reference problem, QUANDRY was used to provide an assessment of the feedback impact of the test problem. The BW2C-T problem

was analyzed at steady-state with QUANDRY with and without feedback. A comparison of selected parameters is given in Table 5.5 and the axial power shapes for channels 1 and 2 are shown in Figs. 5.10 and 5.11, respectively. The results are very similar to those obtained for the reference problem. The inclusion of feedback reduces the eigenvalue, reduces the disparity beween the assembly powers slightly, and depresses the power sharply in the upper nodes.

The BW2C-T problem was analyzed with TITAN in order to compare the results to those obtained with QUANDRY and to provide a base case result for the modeling studies which follow. No MEKIN analysis of the BW2C-T problem exists. For this analysis, the full fuel rod model with temperature-dependent fuel properties and gap heat transfer model was used. A discussion of the fuel rod models and the related input parameters is given in Section 5.3.2.4.

Table 5.6 presents a comparison of selected results from the QUANDRY and TITAN analyses. These results are very similar to those obtained for the BW2C-R problem, except that the maximum and core average fuel temperatures are lower. In the case of QUANDRY, the reduction in maximum and core average fuel temperatures were 629.0°K and 267.6°K, respectively. The TITAN analysis showed a reduction in maximum and core average fuel temperatures of 1447.1°K and 224.9°K, respectively. Part of the reduction in the TITAN fuel temperatures may be the result of using the full fuel rod model in the test problem analysis. Figures 5.12 and 5.13 show the normalized nodal powers as a function of axial position for channels 1 and 2, respectively. The spatial distribution of the nodal powers is essentially the same as that which was calculated for the BW2C-R problem

TABLE 5.5

COMPARISON OF STEADY-STATE GLOBAL PARAMETERS FOR

THE BW2C-T PROBLEM WITH AND WITHOUT FEEDBACK (QUANDRY)

	no feedback	feedback
Eigenvalue	0.82067	0.74491
Normalized assembly power:		
Channel 1	1.4485	1.3761
Channel 2	0.5515	0.6239
Core average fuel temperature, ^{o}K	922.00	1072.26
Core average coolant temperature, ^{o}K	559.0	551.1
Core average coolant density, kg/m^3	739.87	626.40

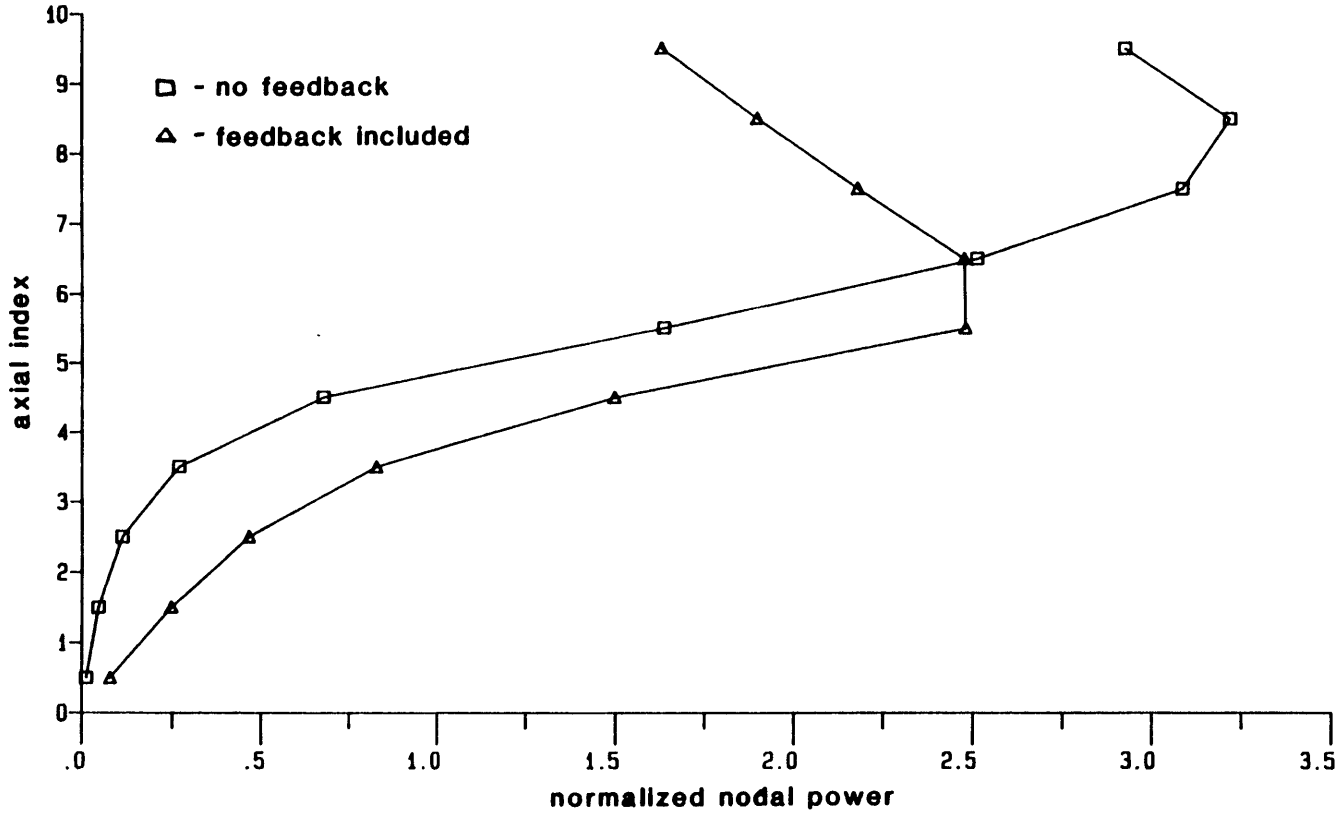

Figure 5.10 BW2C-T Axial Power Profile, Channel 1:

QUANDRY with and without feedback

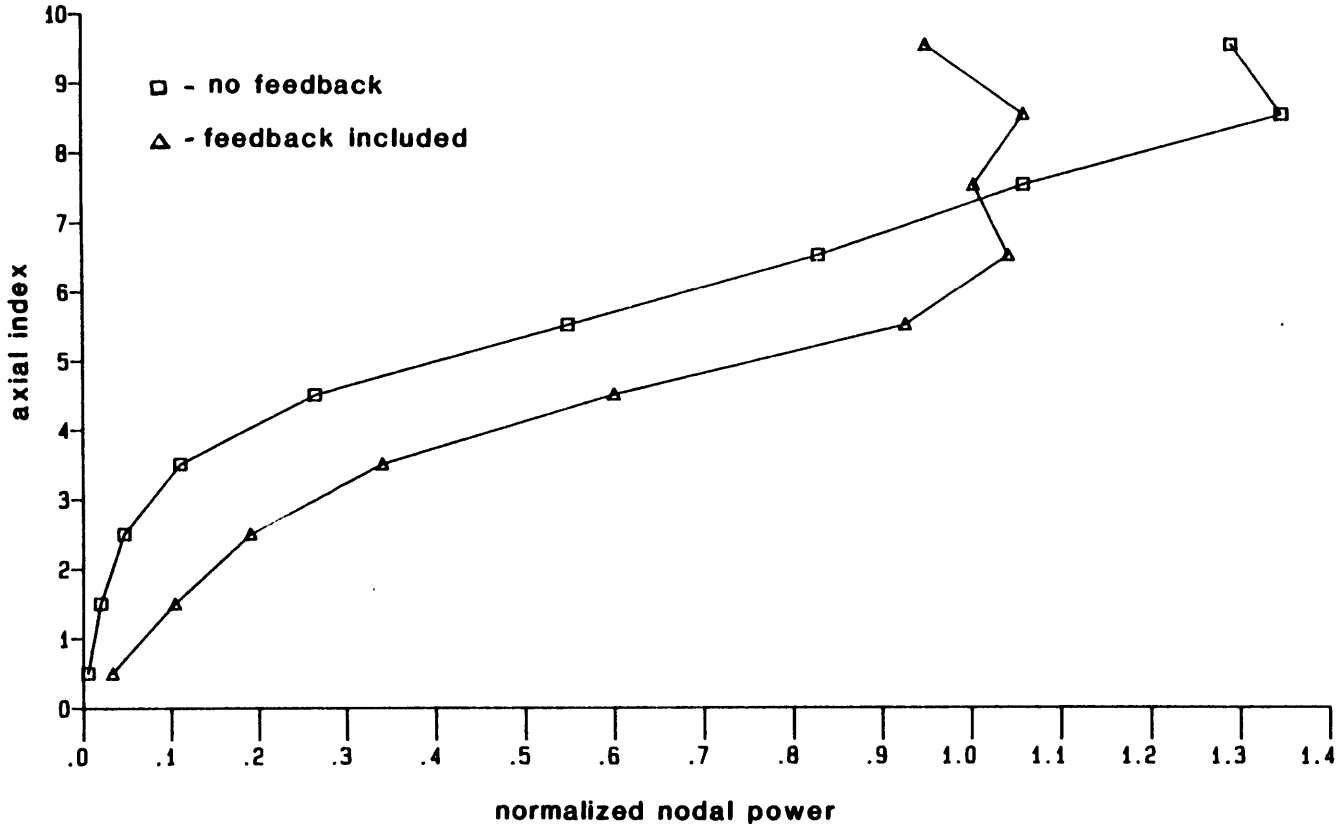

Figure 5.11 BW2C-T Axial Power Profile, Channel 2:
QUANDRY with and without feedback

Table 5.6

Comparison of Parameters from TITAN, MEKIN and QUANDRY
Analyses of the Steady-State BW2C-T Problem

Parameter Description	TITAN	QUANDRY
Eigenvalue	0.7586	0.7449
Normalized power, channel 1	1.380	1.376
Normalized power, channel 2	0.620	0.624
Maximum fuel temperature, °K*	2150.8	1834.0
Core average fuel temperature, °K	1088.8	1072.3
Maximum coolant temperature, °K	560.3	560.3
Core average coolant temperature, °K	554.6	555.1
Minimum coolant density, kg/m^3	288.9	221.0
Core average coolant density, kg/m^3	635.8	626.4
Exit quality, channel 1, %	15.86	13.45
Exit quality, channel 2, %	2.86	3.82
Exit void fraction, channel 1	0.64	0.70
Exit void fracton, channel 2	0.29	0.42

* TITAN and MEKIN: centerline temperatures; QUANDRY: fuel rod average temperature

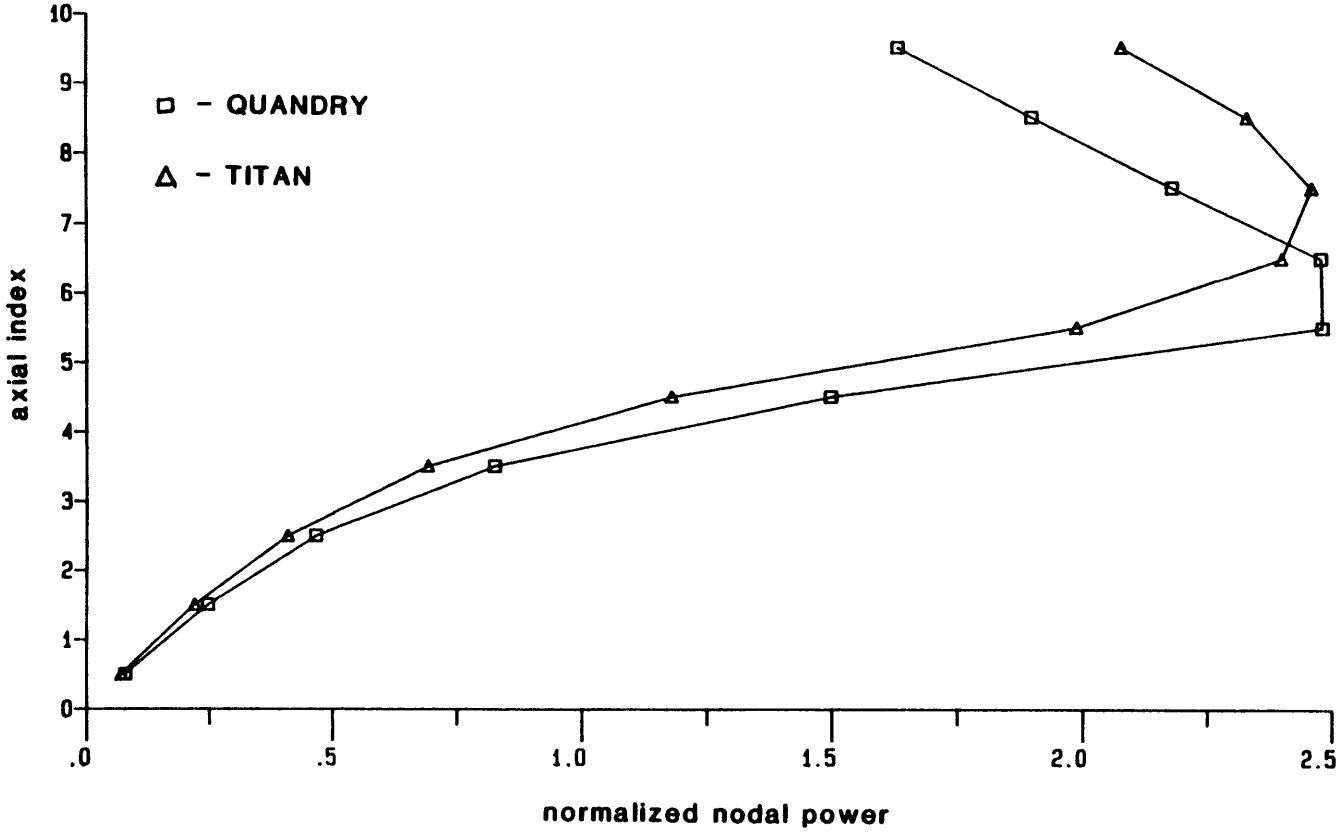

Figure 5.12 BW2C-T Axial Power Profile, Channel 1:

QUANDRY and TITAN

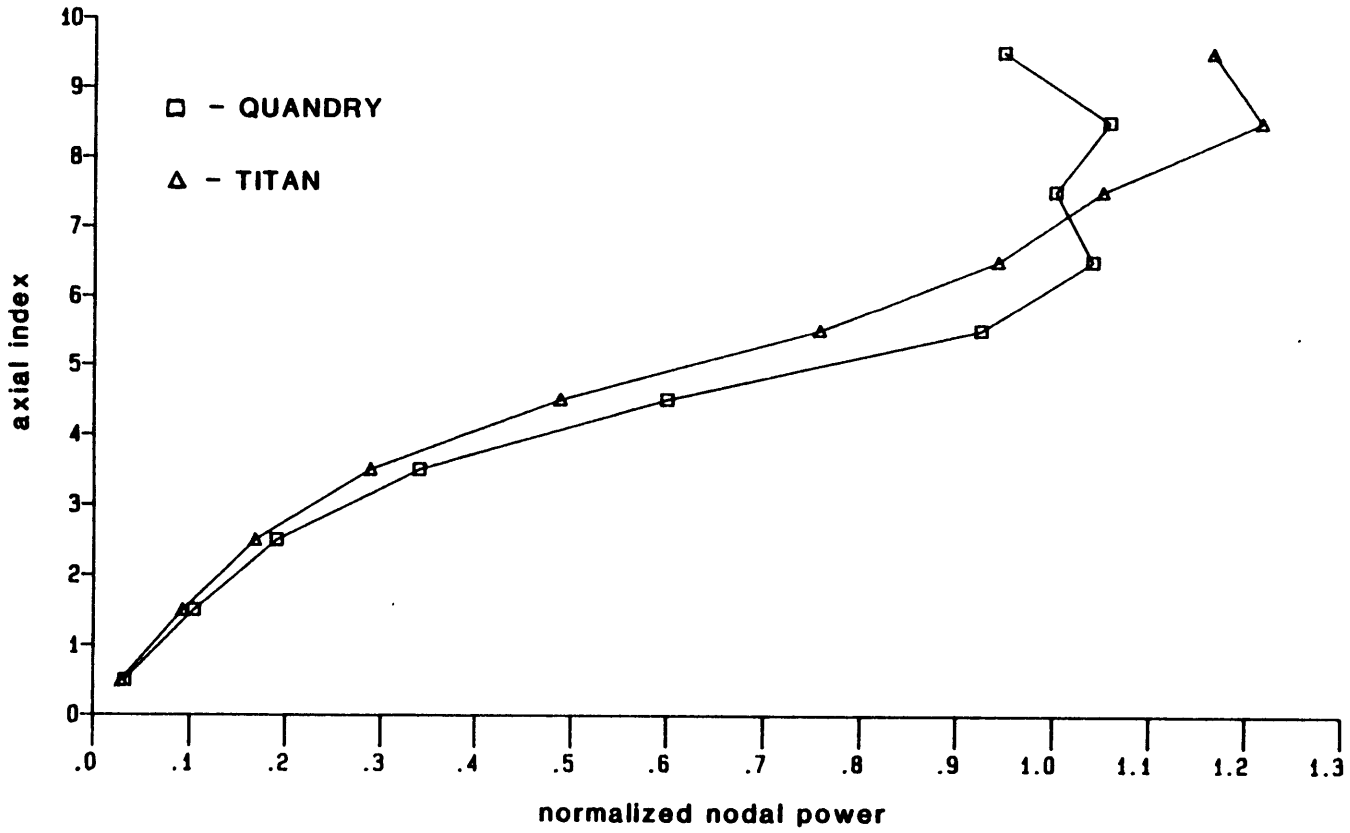

Figure 5.13 BW2C-T Axial Power Profile, Channel 2:

QUANDRY and TITAN

(see Figures 5.4 and 5.5). Thus, the objective of reducing the high fuel temperatures of the reference problem while retaining a power and void distribution approximately the same has been attained.

5.3.2.2 Nodalization Sensitivity Study

The TITAN analyses of the BW2C reference and test problems discussed heretofore used nodes with dimensions typical of the width of a fuel assembly. The constituent elements of TITAN (i.e., the QUANDRY nodal neutronics code and the THERMIT porous body two-fluid thermal-hydraulics code) were formulated for just this size of control volume. As was discussed in Chapter 3, QUANDRY and THERMIT have been shown to be accurate predictors of "coarse mesh" parameters such as neutron fluxes and void fractions as well as global parameters such as reactor eigenvalue and pressure drop. The steady-state TITAN analyses of the BW2C problem for both reference and test conditions suggest that control volumes of this size are adequate for coupled calculations. However, it is possible that TITAN results are strongly dependent on the dimensions of the control volumes. Accordingly, a pair of additional TITAN analyses of the test problem with finer axial meshes were performed. Table 5.7 presents selected results from the TITAN analyses of the test problem with ten, twenty and thirty axial nodes. In addition, the normalized nodal powers for channels 1 and 2 as calculated with ten, twenty and thirty axial nodes are shown in Figures 5.14 and 5.15, respectively. All of the results show that there was very little sensitivity to the reduction of the axial mesh spacing by as much as a factor of three. This brief study gives some confidence that the base case geometry with ten axial nodes is adequate for the steady-state analysis of either of the BW2C problems. Accordingly, all further steady-state calculations are performed with ten axial nodes.

TABLE 5.7

SENSITIVITY OF SELECTED STEADY-STATE TITAN RESULTS TO AXIAL MESH SPACING, BW2C-T PROBLEM

PARAMETER			
Number of axial nodes	10	20	30
Axial mesh spacing, cm	15.24	7.62	5.08
Reactor eigenvalue	0.75858	0.76071	0.76146
Normalized assembly powers:			
Channel 1	1.380	1.382	1.382
Channel 2	0.620	0.618	0.618
Maximum fuel temperature, °K	2150.8	2160.0	2149.3
Maximum cladding temperature, °K	581.6	582.5	582.9
Minimum critical heat flux ratio	1.8834	1.8409	1.6812
Coolant exit quality, %:			
Channel 1	15.86	15.89	15.90
Channel 2	2.86	2.79	2.71
Coolant exit void fraction:			
Channel 1	0.640	0.641	0.641
Channel 2	0.291	0.287	0.282

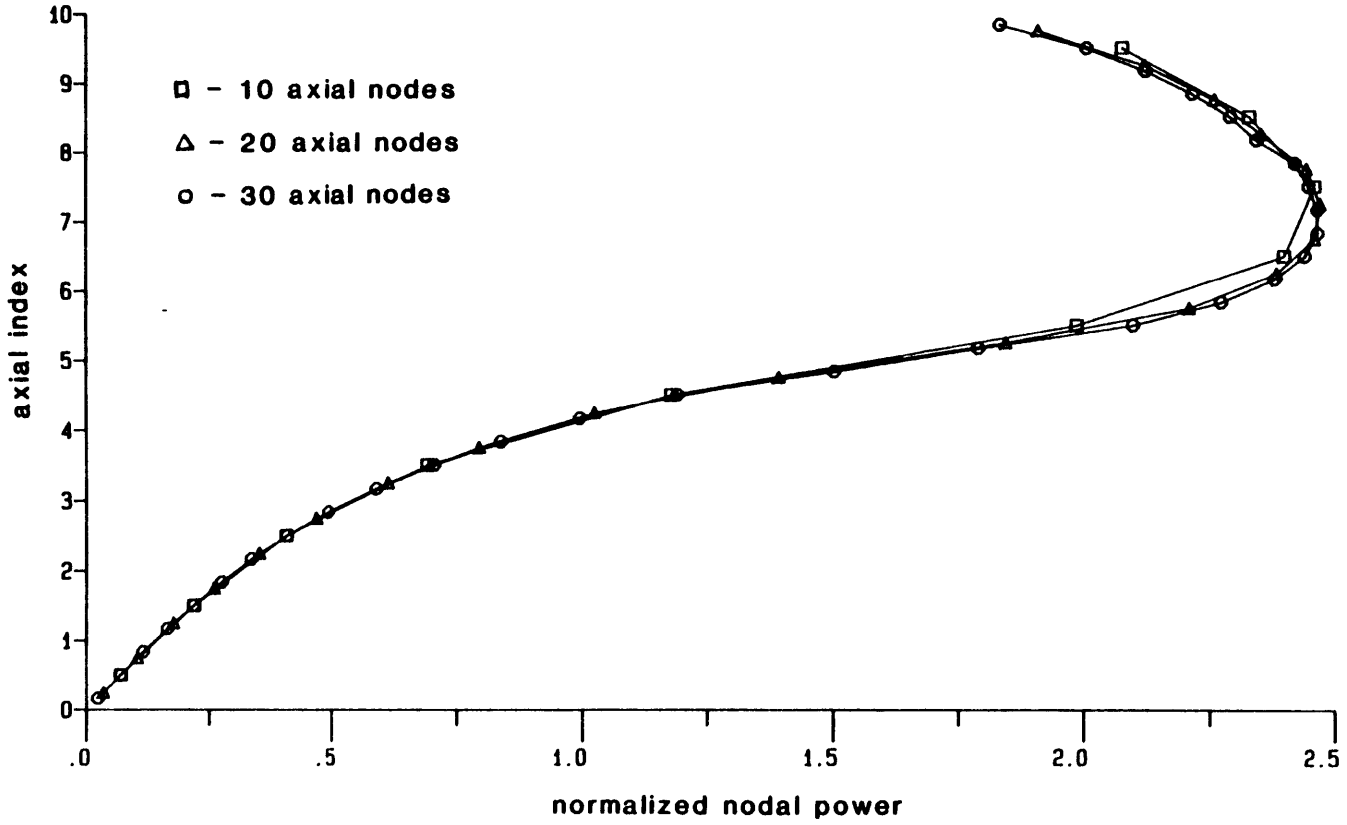

Figure 5.14 BW2C-T Axial Power Profile, Channel 1:

TITAN with 10, 20 and 30 axial nodes

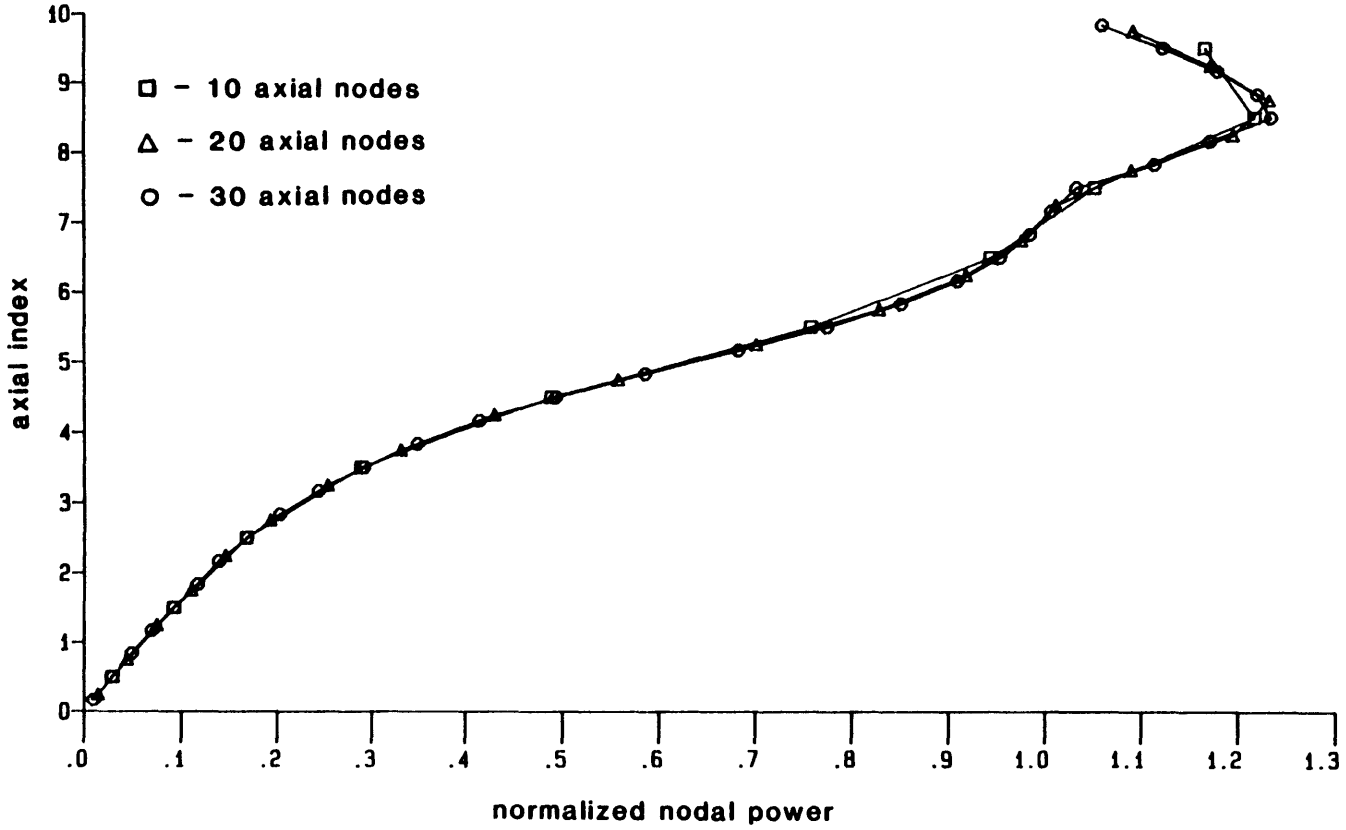

Figure 5.15 BW2C-T Axial Power Profile, Channel 2:

TITAN with 10, 20 and 30 axial nodes

5.3.2.3 Neutronic Calculational Frequency

The TITAN coupling methodology for steady-state calculations has been successfully demonstrated for the BW2C problem. The techniques described in Chapter 4 have been used to produce converged steady-state solutions and these have been described. However, the details of how the converged solution is obtained and the computational effort required remain to be discussed. One feature of the coupling logic is the capability of varying the ratio of thermal-hydraulic time-steps to static neutronic calculations. The purpose of this subsection is to investigate this coupling feature and its impact on computational effort and calculational results.

A group of four steady-state TITAN analyses of the BW2C-T problem were performed. Each case was identical, except that the number of thermal-hydraulic time-steps per static neutronic calculation was varied. An equal number of time-steps was calculated in each case, but with one, two, four or eight time-steps per neutronics calculation. These analyses, which are summarized in Table 5.8, showed that the computer time required is very sensitive to the frequency of neutronic calculations, but the results are not too sensitive. The calculation with eight thermal-hydraulic time-steps per neutronic calculation produced results nearly identical to those obtained with one thermal-hydraulic time-step per neutronic calculation and with a reduction in computing time by a factor of more than 4.7. This is a significant benefit to economy with no degradation of code performance. The limit to which the variation of thermal-hydraulic time-steps to neutronic calculations can be increased without degrading the results is not known. It is likely to be somewhat problem-dependent and could be affected by the various neutronic and thermal-hydraulic convergence criteria.

TABLE 5.8

SENSITIVITY OF TITAN STEADY-STATE RESULTS,

BW2C-T PROBLEM, TO THE STATIC NEUTRONIC CALCULATION FREQUENCY

Number of thermal-hydraulic time-steps per static neutronic calculation	1/1	2/1	4/1	8/1
Converged flow balance error	-2.68×10^{-5}	-2.20×10^{-5}	-2.50×10^{-5}	4.77×10^{-5}
Converged energy balance error	-3.03×10^{-4}	-2.66×10^{-4}	-2.90×10^{-4}	1.48×10^{-4}
"Reactor" eigenvalue	0.7586	0.7586	0.7586	0.7586
Maximum fuel temperature, °K	2150.8	2150.8	2150.8	2150.7
Maximum change in nodal power (w.r.t. 1/1 case), %	-	< 0.001	< 0.001	0.022
Running time, MULTICS cpu seconds*	655.91	356.72	215.25	138.64
Running time "density," cpu seconds per time step	8.63	4.69	2.83	1.82

The observation that the frequency of neutronic calculations during steady-state convergence can be reduced without affecting the final results fulfills one of the expectations of the TITAN coupling methodology. Since the thermal-hydraulic solution converges in a transient fashion over a number of time-steps, the feedback parameters often do not change significantly from one time-step to the next. This explains why it is not necessary to perform a recalculation of the static neutronics after every thermal-hydraulic time-step. This fact is illustrated by Figures 5.16 and 5.17, in which the convergence of the normalized power in two individual nodes with one and with eight time-steps per neutronic calculation is plotted. Indeed, these figures show that a reduction in the frequency of neutronic calculations can avoid some dramatic shifts in local power during the first few time-steps. Another observation is that the nature of the nodal power convergence is qualitatively different when intermittent neutronic calculations are performed. A convergence in which neutronic calculations follow each thermal-hydraulic time-step seems to produce (after a few time-steps) a smooth or even monotonic approach to the final power in a given node.

Conversely, a convergence with intermittent neutronic calculations produces an oscillation about the individual nodal powers which eventually damps out to give the final nodal power. This suggests that a more sophisticated method of controlling the feedback loops could optimize the convergence and produce good results with less computational effort.

5.3.2.4 Fuel Rod Model Sensitivity Study

The TITAN code allows three different options for modeling the fuel rods. Since the nodal average fuel temperature is one of the three

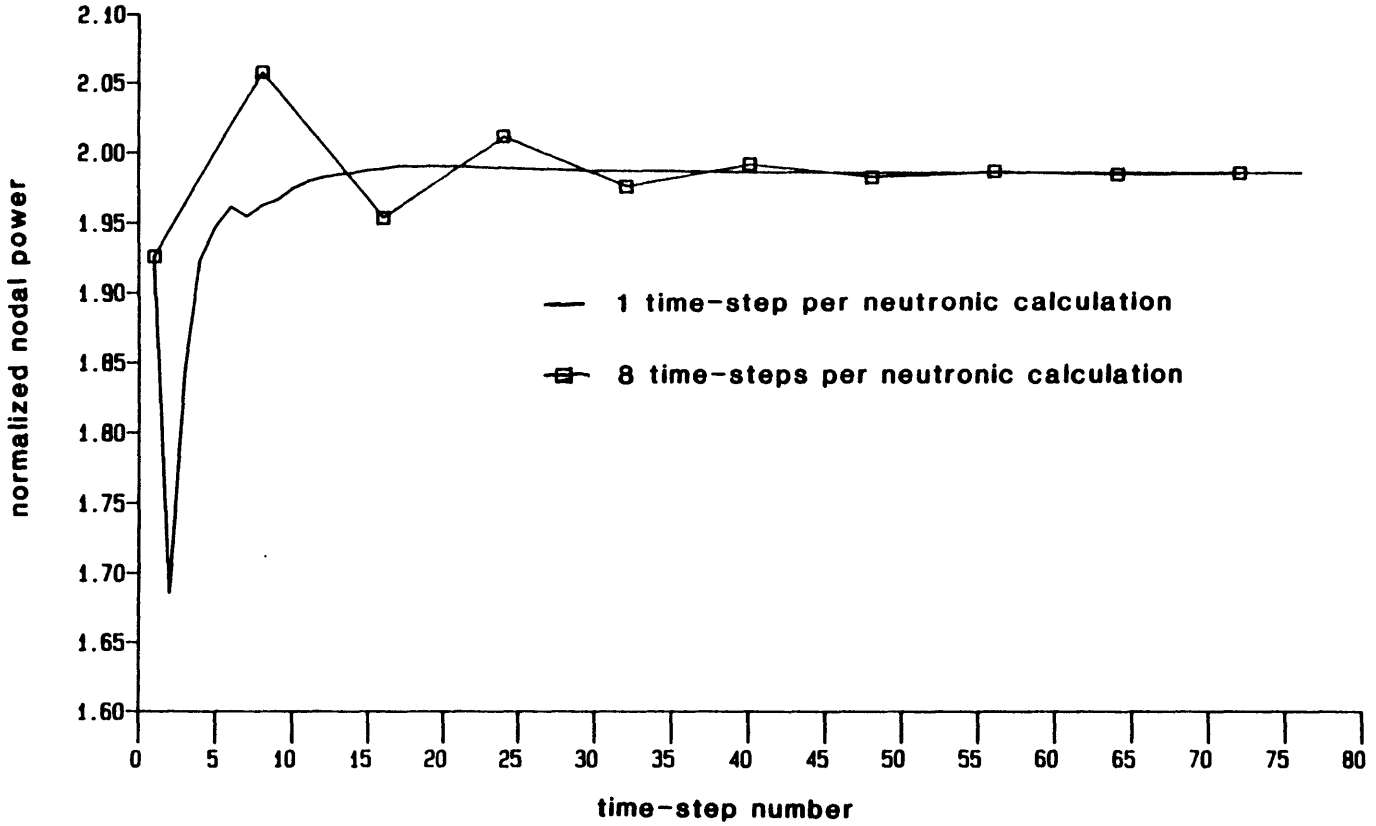

Figure 5.16 Comparison of Steady-state Nodal Power Convergence, BW2C-T, Node 1,6:

TITAN with 1 and 8 time-steps per neutronic calculation

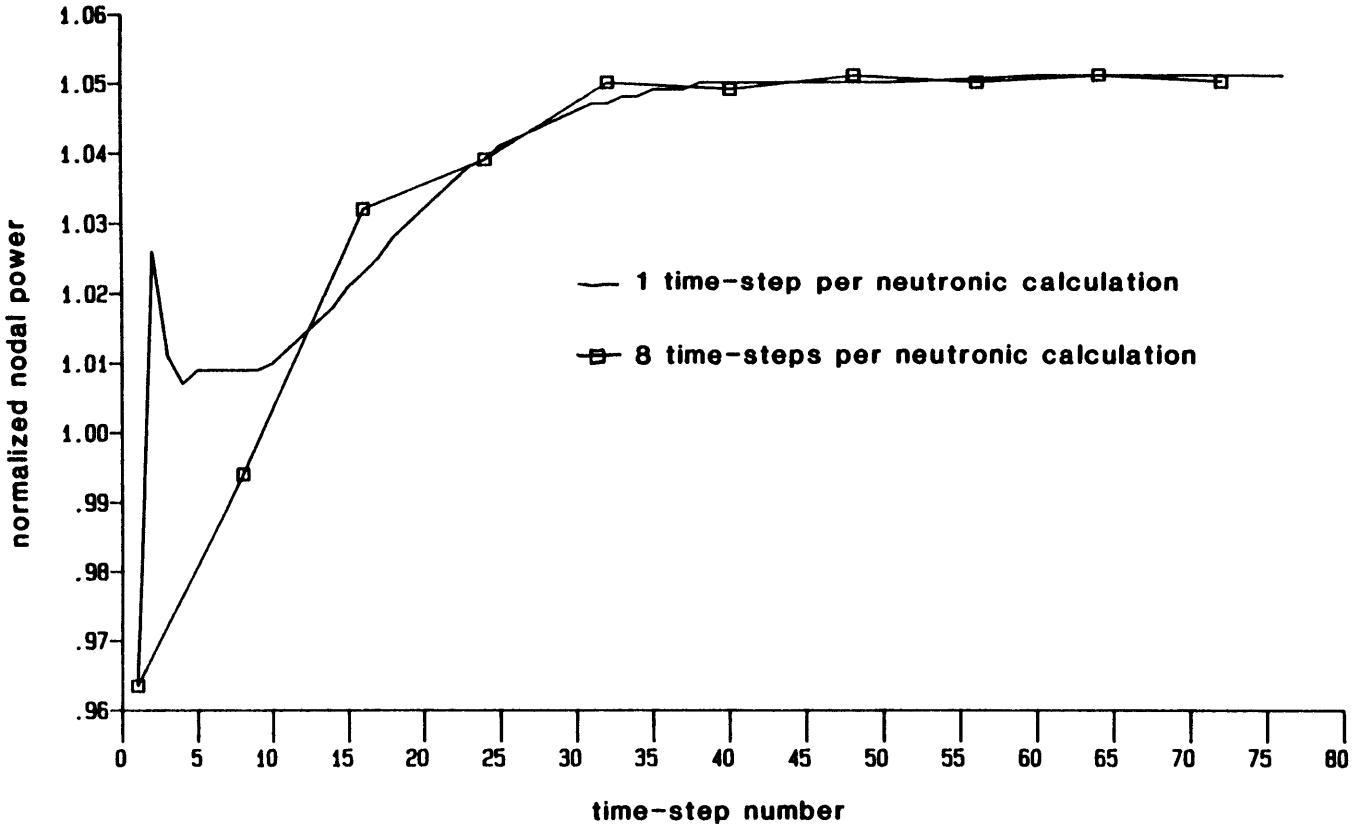

Figure 5.17 Comparison of Steady-state Nodal Power Convergence, BW2C-T, Node 2,8:

TITAN with 1 and 8 time-steps per neutronic calculation

feedback parameters, the sensitivity of the steady-state results to the choice of fuel rod options was assessed. This was done by performing three steady-state analyses of the BW2C test problem, each identical except for the fuel rod model selected. The analyses were converged to approximately the same flow and energy errors. In each case, the fuel rods were modeled with six regions in the fuel pellet, one gap region, and three clad regions.

The three fuel rod options are described in Section 3.3.1.2, as part of the THERMIT discussion. A brief review and definition of terms is appropriate here. In the first option, the fuel and clad are assumed to have temperature-independent thermal conductivities and heat capacities with a constant gap heat transfer coefficient. The fuel properties are built-in, while the gap coefficient is an input parameter. This option is referred to as the "simple" fuel rod calculation. The second fuel rod option uses temperature-dependent fuel properties with a user-supplied constant gap coefficient. The temperature-dependent fuel properties are supplied by TITAN subroutines containing correlations for the fuel and cladding materials. This option is referred to as the "intermediate" fuel rod calculation. The final fuel rod option combines temperature-dependent fuel properties with a model to calculate the local gap heat transfer coefficient. This option is referred to as the "full" fuel rod calculation. The parameters used in these models are given in Table 5.9.

Figures 5.18 and 5.19 show the fuel centerline temperatures as a function of axial position for channels 1 and 2, respectively. The three fuel rod options were used so that the impact of selecting a simple, intermediate or full fuel rod model could be assessed. The results indicate that the fuel centerline temperatures were rather sensitive to

Table 5.9

Parameters Used in TITAN Fuel Rod Model Options

Simple Fuel Model	
fuel thermal conductivity	2.4 w/m-°K
cladding thermal conductivity	10.7 w/m-°K
fuel volumetric heat capacity	3.4125×10^6 j/m^3-°K
cladding volumetric heat capacity	2.093×10^6 j/m^3-°K
fuel/cladding gap heat transfer coefficient	5678.3 j/m^2-s-°K
Intermediate Fuel Model	
fuel and cladding properties	temperature-dependent
fuel theoretical density fraction	0.95
fuel PuO_2 fraction	0.00
fuel/cladding gap heat transfer coefficient	5678.3 j/m^2-s-°K
Full Fuel Model	
fuel and cladding properties	temperature-dependent
fuel theoretical density fraction	0.95
fuel PuO_2 fraction	0.00
fuel/cladding gap heat transfer coefficient	temperature-dependent
fuel contact pressure	0.35 MPa
gap roughness	4.4×10^{-6} m (default)
gap gas pressure	7.136 MPa
helium fraction	1.00
fuel burnup	1000 MWd/MTU

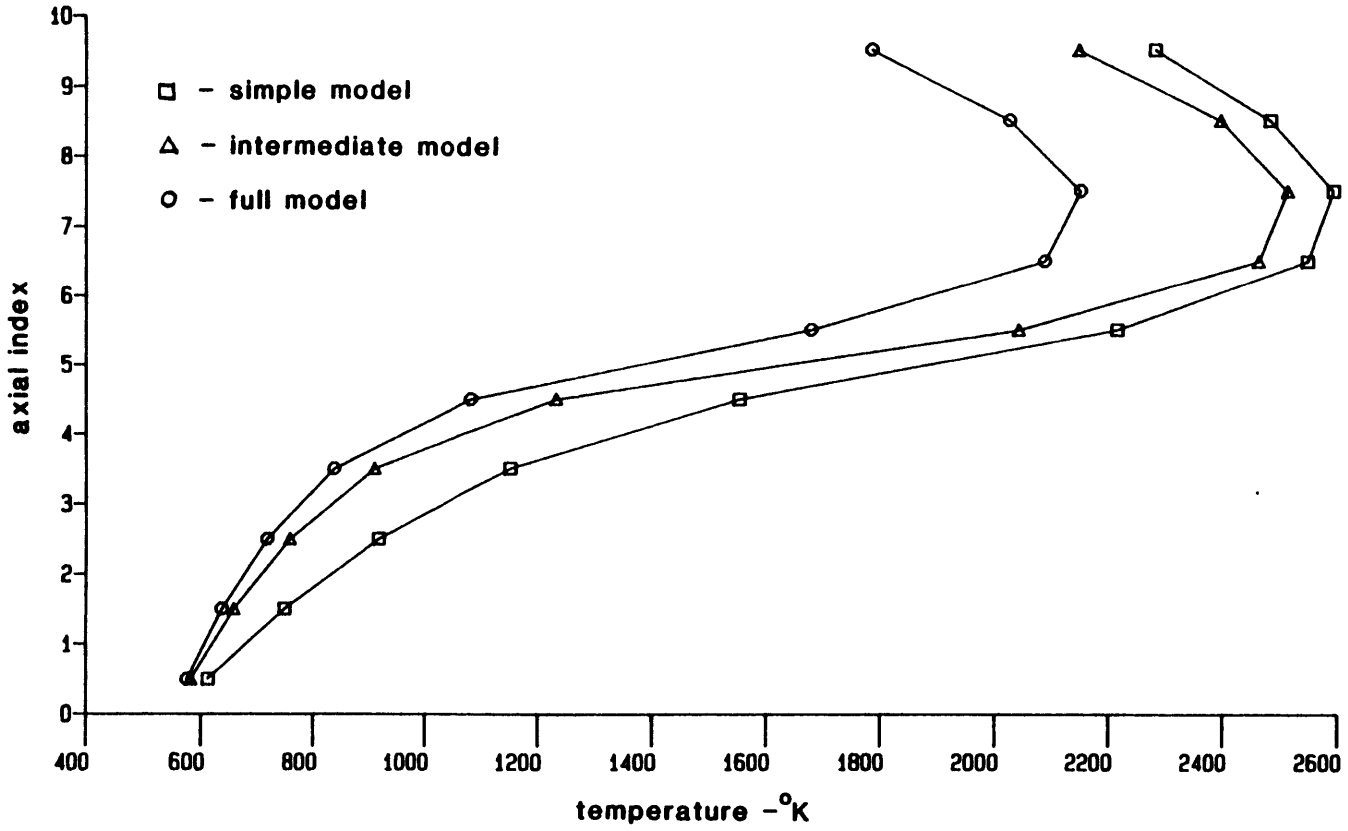

Figure 5.18 Comparison of Steady-state Fuel Centerline Temperatures, BW2C-T, Channel 1: TITAN with simple, intermediate and full fuel rod models

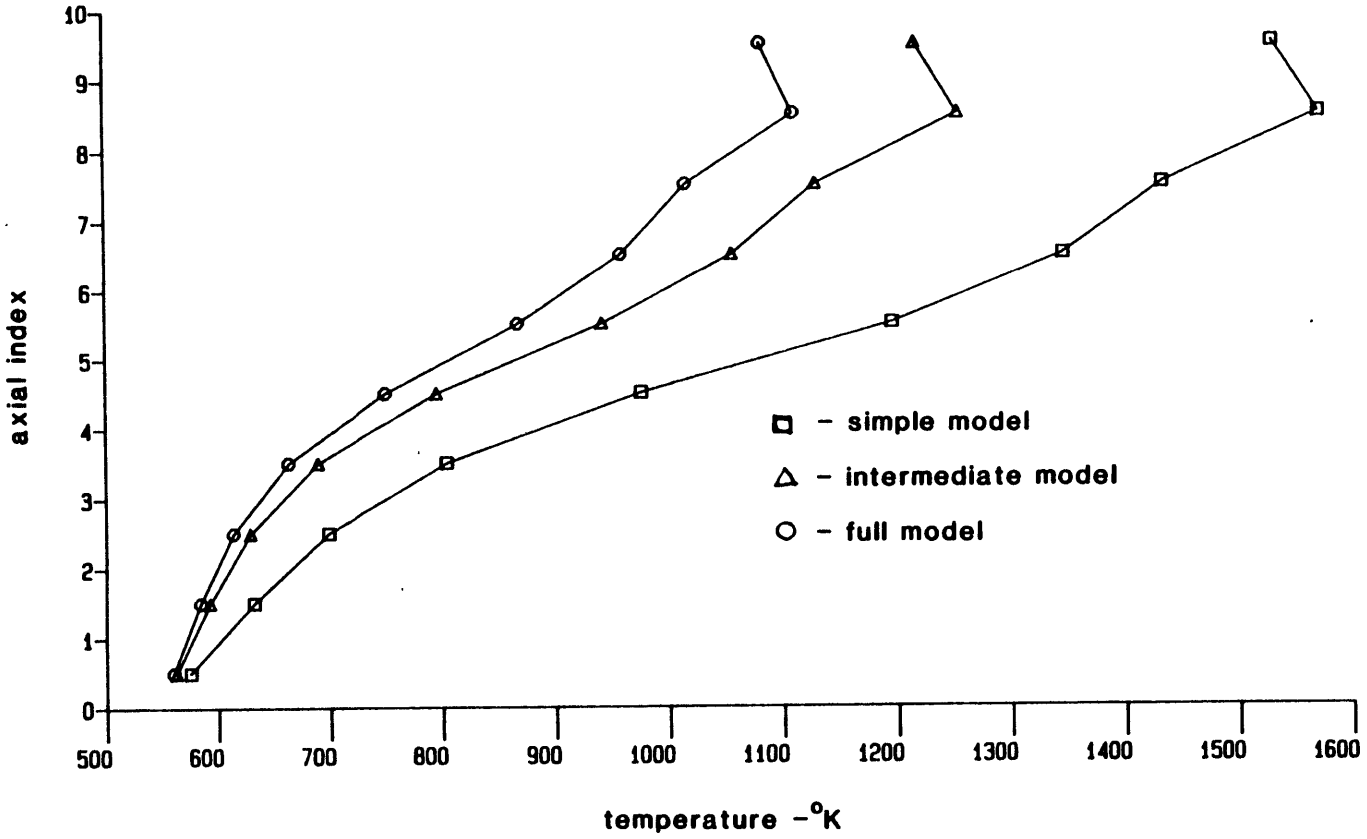

Figure 5.19 Comparison of Steady-state Fuel Centerline Temperatures, BW2C-T, Channel 2: TITAN with simple, intermediate and full fuel rod models

the model employed. The simple model consistently produced the highest centerline temperatures, while the full fuel rod model consistently produced the lowest centerline temperatures. The centerline temperatures calculated with the intermediate model always fell between those of the other two models.

When the fuel temperatures are relatively low (as in nodes 1-5, of channel 1 and all of channel 2), the intermediate model is closer to the full model than to the simple model. In the high temperature regions (such as nodes 6-10 in channel 1), the reverse is true. This indicates that the gap conductance model has a greater impact when the linear heat generation rate (and thus the fuel temperature) is high. In the peak power node, the centerline temperature calculated with the simple model exceeded that calculated with the intermediate and full fuel rod models by 78.9^{o}K and 442.1^{o}K, respectively.

The results indicate that the selection of a fuel rod model can be significant if fuel temperatures are expected to be limiting. However, few of the other key parameters were sensitive to the choice of fuel model. The eigenvalues, normalized assembly powers and computer times for the TITAN calculations with three different fuel models are given in Table 5.10. The difference in the eigenvalues is less than 1% and the effect on the transverse power distribution is insignificant. The intermediate model added about 0.33% to the computer time required for an analysis with the simple fuel model and the full fuel rod model added about 2.36%. The only potentially significant effect of the different

TABLE 5.10

SENSITIVITY OF SELECTED STEADY-STATE TITAN RESULTS

TO FUEL ROD MODEL, BW2C-T PROBLEM

PARAMETER	SIMPLE MODEL	INTERMEDIATE MODEL	FULL MODEL
"Reactor" eigenvalue	0.75262	0.75489	0.75858
Normalized power, channel 1	1.378	1.379	1.380
Normalized power, channel 2	0.622	0.621	0.620
Computer time, MULTICS cpu seconds	210.29	210.99	215.25

fuel rod models is in the axial power shapes. The change in power among the high power nodes in each channel (nodes 6-10) was around 1% (or less), but the power in the remaining nodes was changed by between 1% and 7%. The largest proportional changes were in the lowest power nodes, so the actual change in power was still quite low. Thus, the choice of fuel rod models does not seem to have much net impact on the Doppler feedback. However, it is not clear that this conclusion can be extended to transient calculations.

5.4 Transient Results

5.4.1 Null Transients

The first transient analyses performed with TITAN were null transients. A null transient is one in which no perturbations are applied to the steady-state solution. This type of analysis is very useful for testing a code because it is very simple and the correct "answer" is known. If the steady-state solution is properly converged and the transient solution method is operating correctly, the results of a null transient analysis should preserve the steady-state solution. A null transient analysis should reveal whether the transient solution method itself introduces any changes to the converged steady-state.

The TITAN transient solution method uses a staggered tandem coupling which involves a different calculational order for thermal-hydraulically and neutronically initiated transients. Therefore, two "different" null transients were performed, thereby testing both transient modes. Both null transients used the same steady-state solution of the BW2C-T problem with ten axial nodes and the full fuel rod model.

The thermal-hydraulic null transient was initiated by using a time-independent core outlet pressure forcing function of unity. The neutronic null transient was initiated by ejecting a "control rod" having a zero neutron cross section from channel 2. Both analyses used about 40 equal time-steps of 26.5 milliseconds, giving more than one second of transient time. The calculated reactor power as a function of time for the thermal-

hydraulic and the neutronic null transients are shown in Figures 5.20 and 5.21, respectively. The two analyses produced very similar results. In both cases the reactor power rose slightly during the first five or six time-steps, reaching a maximum value of 4001.2 kw, a rise of 0.03%. This is followed by a decrease in reactor power which lasts for about ten time-steps and results in a nearly constant power of 4000.3 kw, a net power rise of 0.0075%. Thus, the null transients do produce some drift in the steady-state power, though the magnitude is quite small. This power drift appears to be independent of the type of initiation. It should also be noted that in neither case was any change observed in the spatial distribution of the power.

The results of the null transient analyses indicate that the TITAN transient solution method can maintain a steady-state condition when no perturbations are applied. The small deviations in reactor power observed are not considered significant in comparison to the changes in power expected in most transients of interest. They are certainly well within the accuracy which could be expected for transient reactor core analysis.

5.4.2 Thermal-hydraulically Initiated Transients

5.4.2.1 Problem Descriptions

The TITAN code was applied to a pair of transients driven solely by changes in thermal-hydraulic boundary conditions. The purpose of these analyses was to verify that TITAN results for such transients are consistent with the expected response of the two channel boiling water "reactor." The BW2C-T problem with full fuel rod model was used as the basis for these analyses.

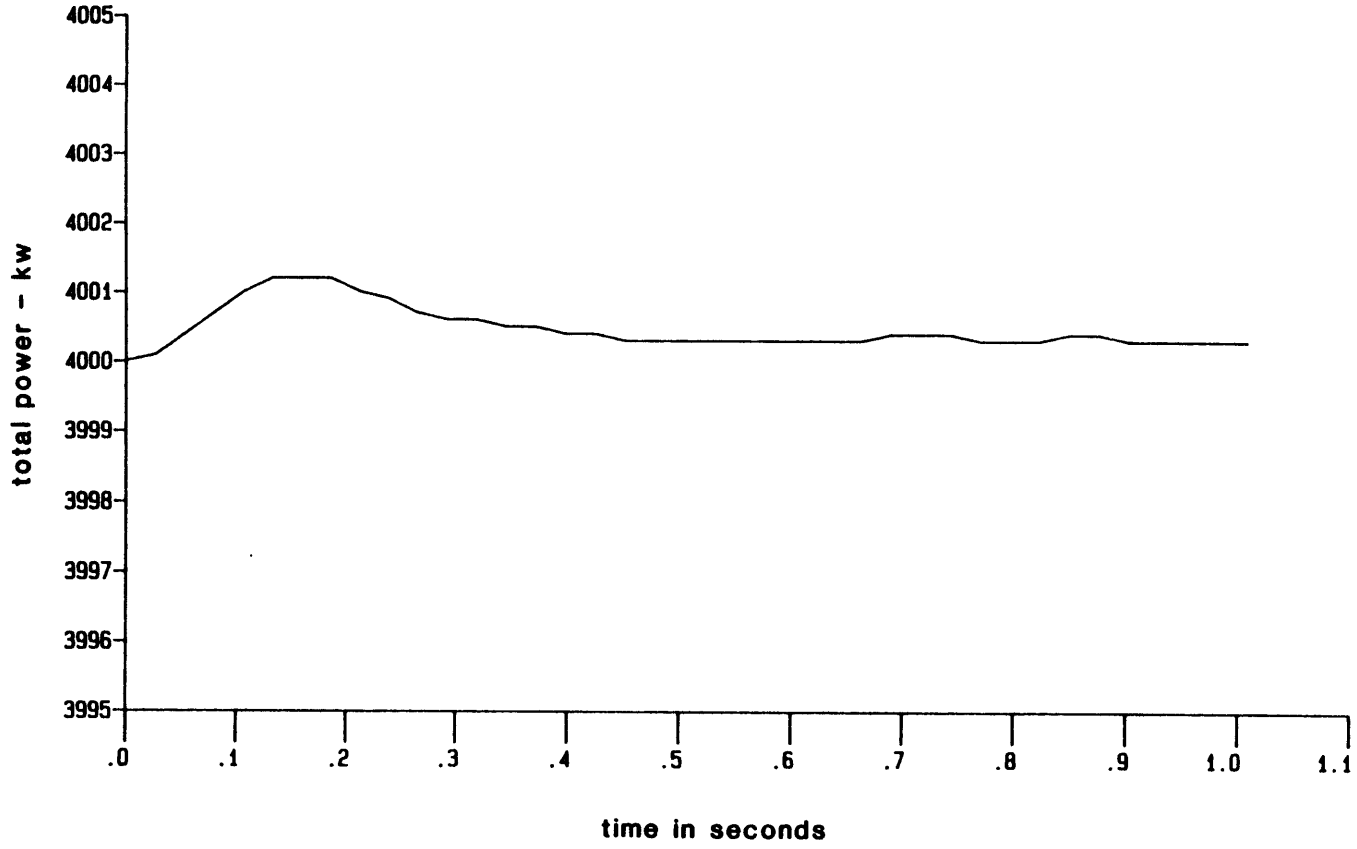

Figure 5.20 BW2C-T Null Transient, TITAN, Thermal-hydraulic Mode: Power versus Time

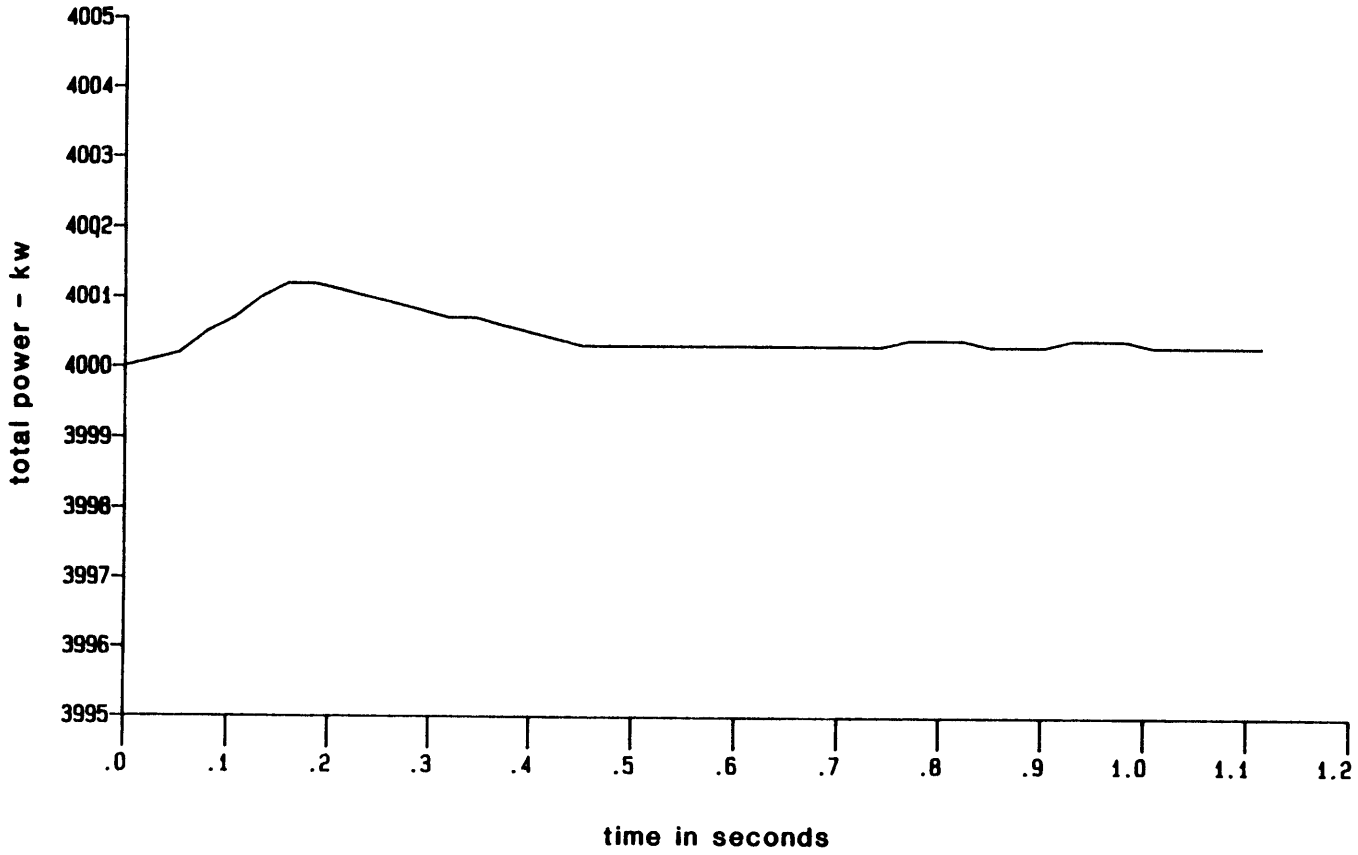

Figure 5.21 BW2C-T Null Transient, TITAN, Neutronic Mode:
Power versus Time

Two simulated turbine trip transients were analyzed with TITAN using time-dependent inlet flow rate and outlet pressure boundary conditions forcing functions. The first transient, designated Turbine Trip #1, was based on Test 1 of the Peach Bottom Station-Unit 2 experiments [B-9]. Figure 5.22 shows the actual forcing functions used in the TITAN analysis. The BW2C-T problem to which these forcing functions were applied does not match the actual operational conditions of the Peach Bottom reactor, so the TITAN results should not be compared to measurements taken during the actual turbine trip event. In particular, the actual turbine trip was initiated with the reactor at reduced power, while the initial conditions of the BW2C-T problem represent full power conditions. One consequence of this choice of initial conditions and forcing functions is that the measured reactor response cannot be used to verify the TITAN results except on a very broad qualitative basis. Furthermore, no other independent solution exists to which the TITAN results can be compared. Nevertheless, Turbine Trip #1 provides a meaningful test which exercises the thermal-hydraulic transient mode of TITAN and gives results which can be checked for qualitative correctness and consistency. In addition, the problem provided a basis for investigating the sensitivity of thermal-hydraulic transient results to axial mesh spacing.

A second turbine trip simulation was performed with TITAN in order to supplement the Peach Bottom problem. This transient, designated Turbine Trip #2, is somewhat more severe and of longer duration than the Peach Bottom transient. In addition, the flow and pressure forcing functions correspond to a representative turbine trip from full power without bypass and with 60% relief flow. The forcing functions were

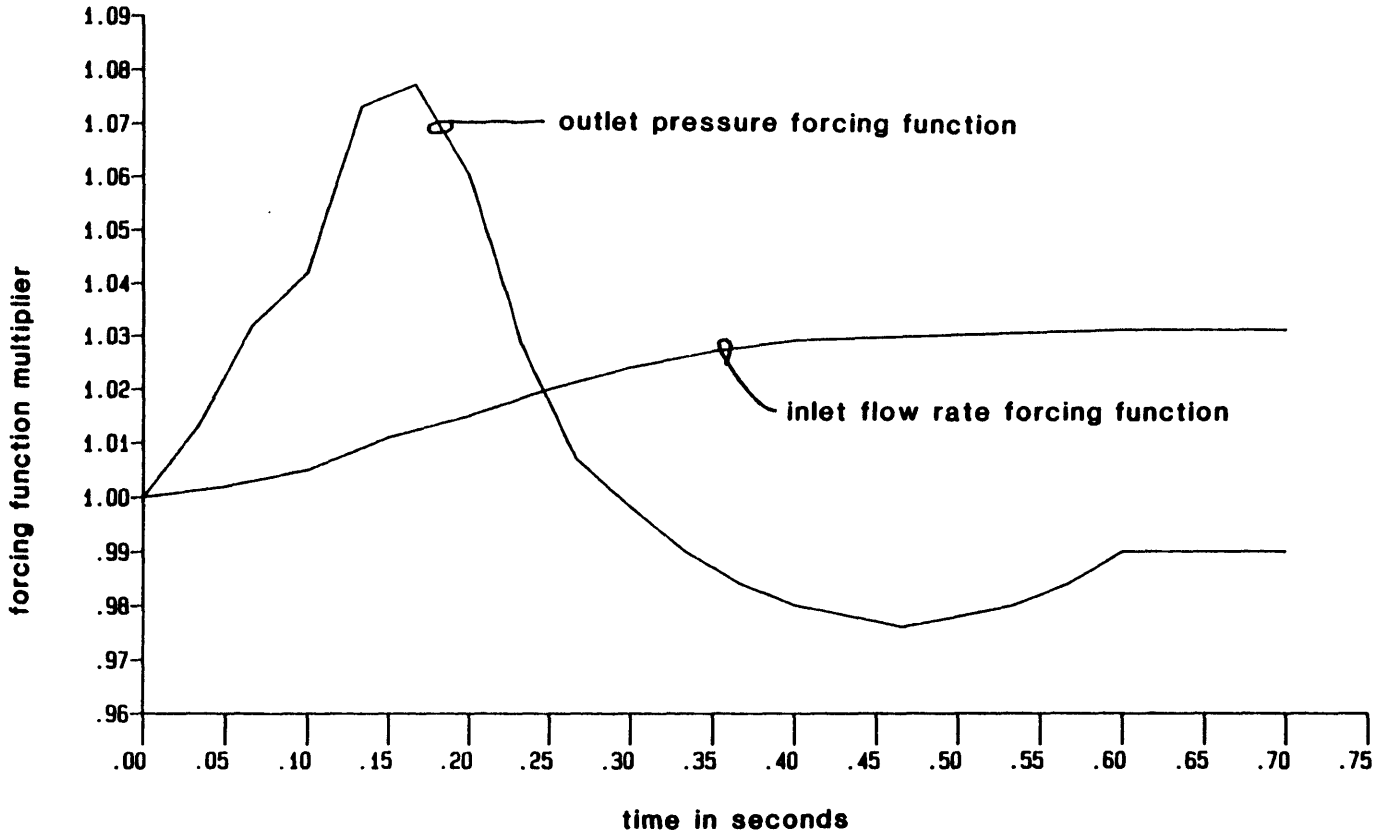

Figure 5.22 Forcing Functions for Turbine Trip #1

taken from the Preliminary Safety Analysis Report of the Duane Arnold Energy Center, as shown in Figure 5.23. This figure also contains some results from a licensing calculation of the event. Hence, Turbine Trip #2 provides realistic forcing functions, similar (i.e., full power) initial conditions, and a solution to which qualitative comparisons may be made. The actual forcing functions used in the TITAN analysis are depicted in Figure 5.24.

5.4.2.2. Turbine Trip #1

The TITAN results for the reactor power during the Turbine Trip #1 are given in Figure 5.25. The reactor power rises rapidly, attaining a maximum of 1.8 times the initial power at 0.265 seconds, and then decreases rapidly, eventually falling to only 90% of the initial power. The rise and fall in power is in response to the changes in the nodal feedback parameters caused by the applied time-dependent flow and pressure boundary conditions. No scram or other control rod motion was modeled. The increase in inlet flow and core pressure reduces the void fraction in the boiling nodes, thereby increasing the moderator density. An increase in moderator density has a positive effect on the core reactivity, resulting in the observed power rise. This is illustrated in Figure 5.26, which shows the time-dependent core average feedback parameters during the transient. The rise in core average moderator density shown in Figure 5.26b corresponds well to the observed rise in core power. The rapid decrease in core power which follows the peak power is explained by the behavior of the core average fuel temperature, shown in Figure 5.26a. The fuel temperature rises in response to the power rise, producing a negative contribution to the core reactivity

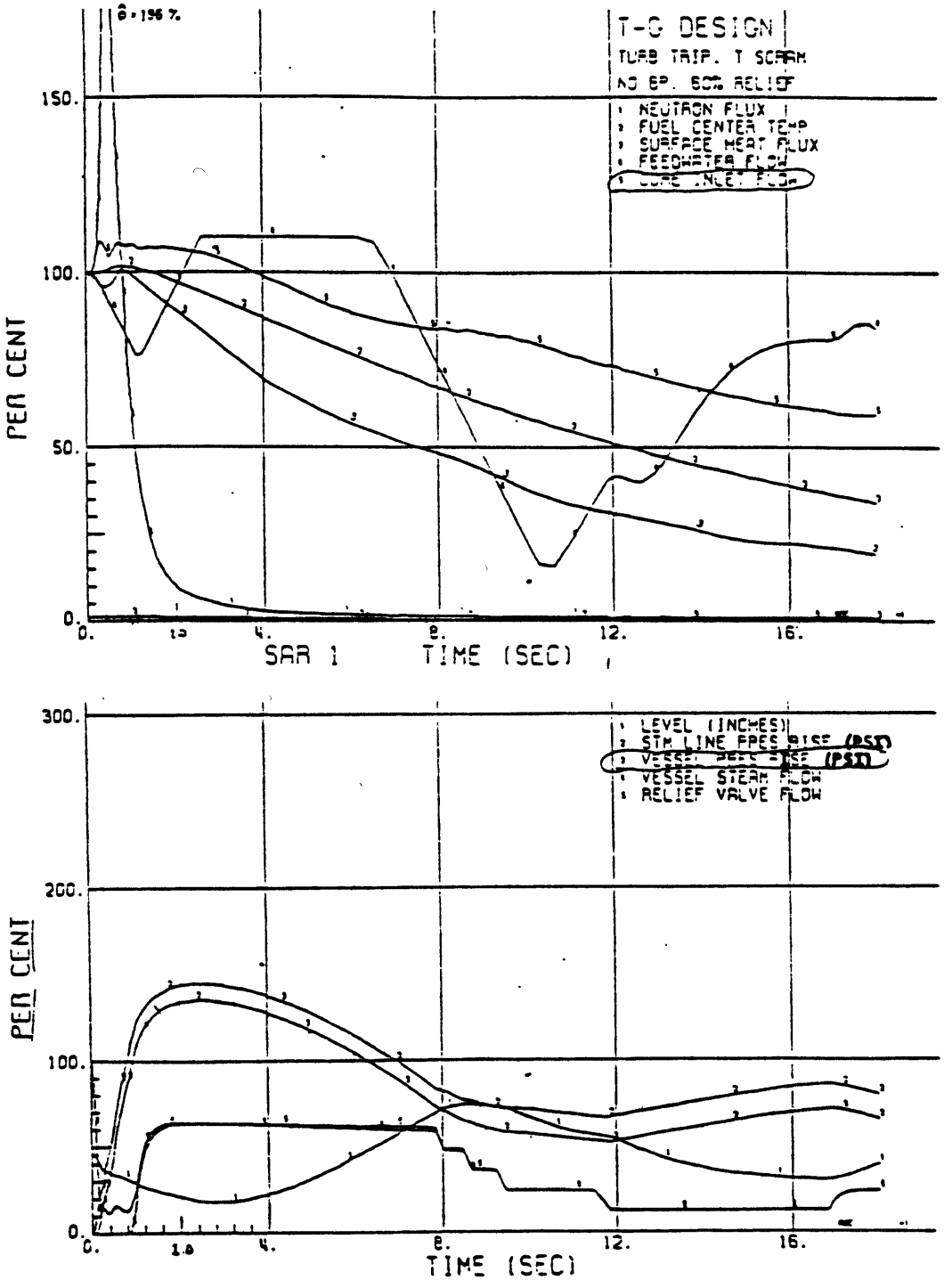

Figure 5.23 PSAR Licensing Calculation Results, Duane Arnold Plant Turbine Trip Event I-3

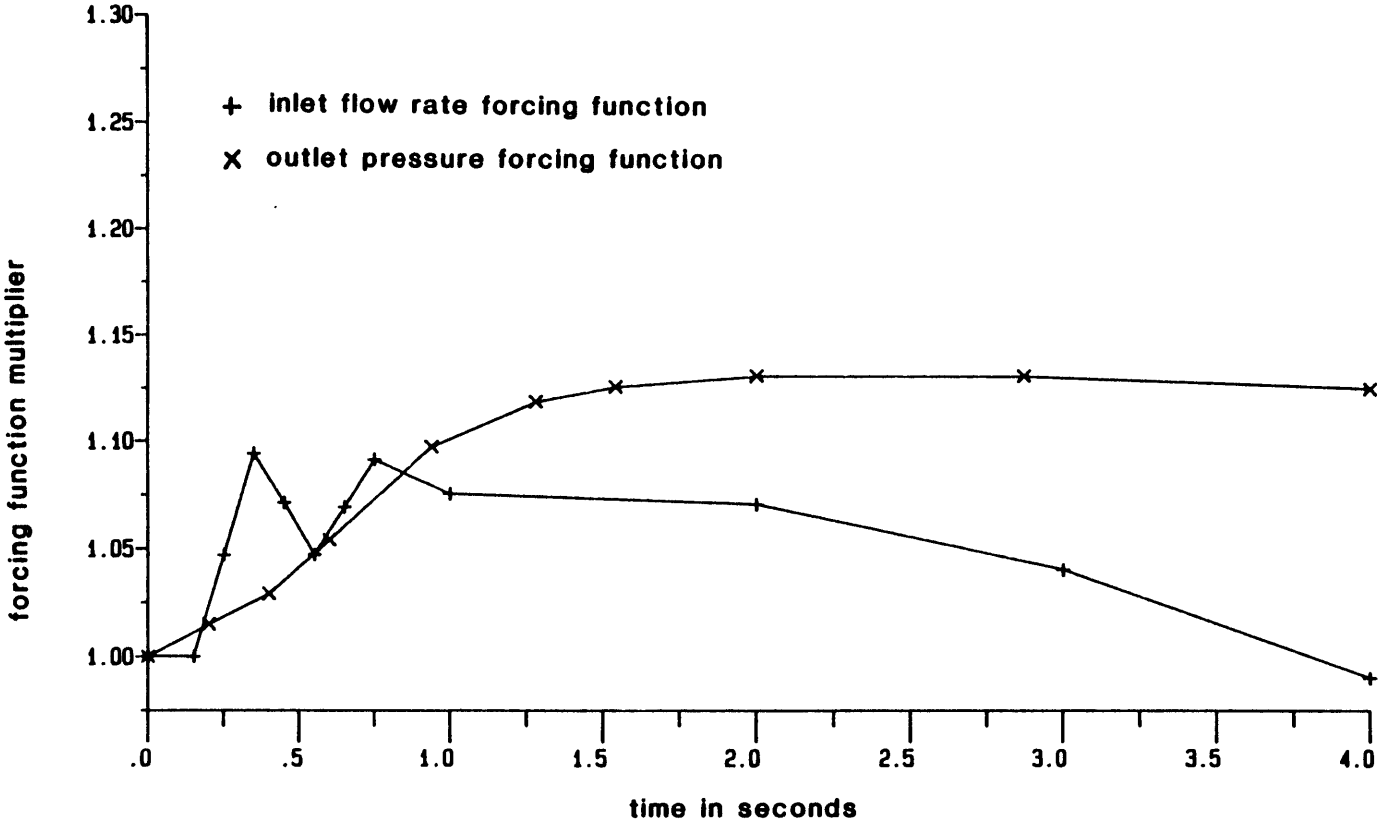

Figure 5.24 Forcing Functions for Turbine Trip #2

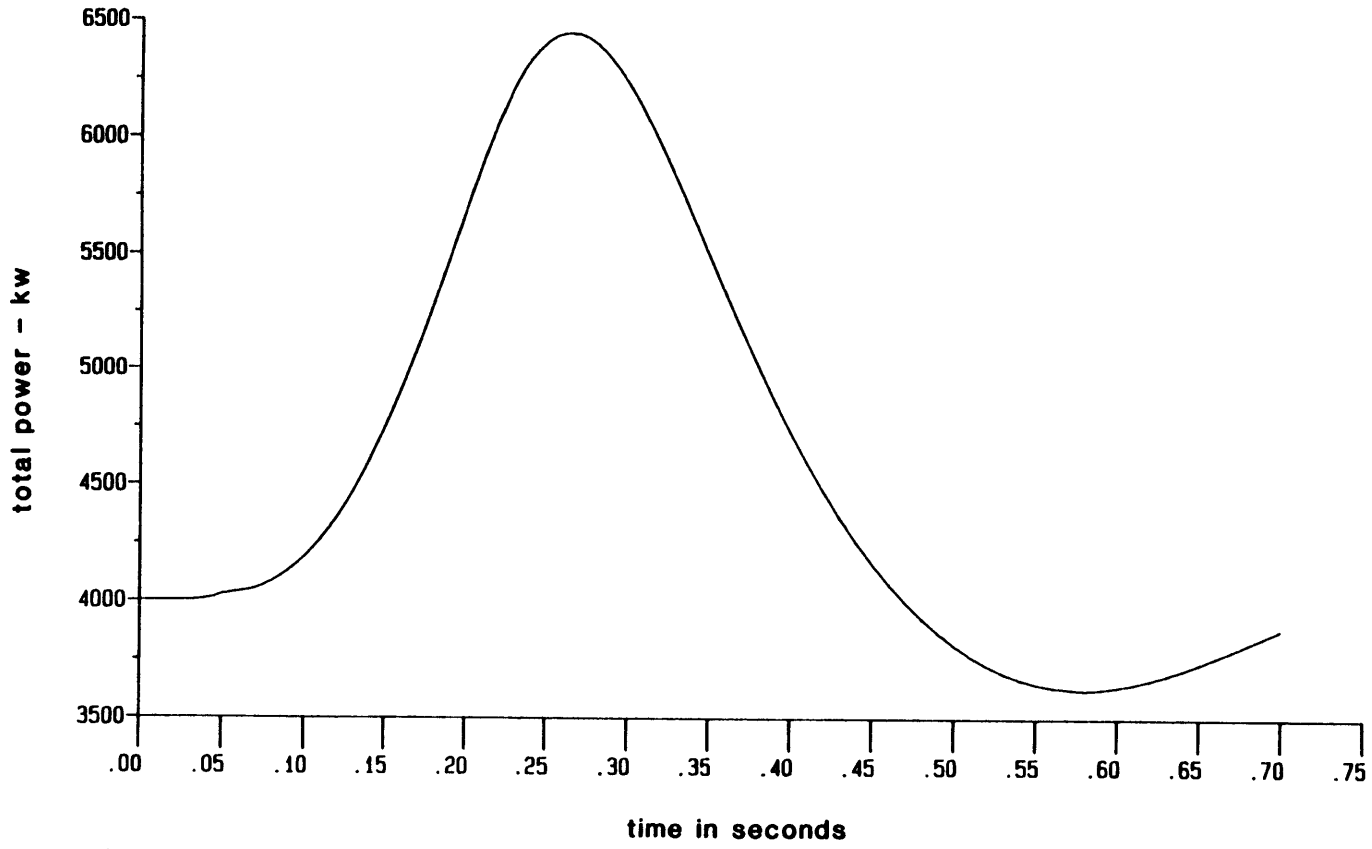

Figure 5.25 Turbine Trip #1, BW2C-T, TITAN: Power versus Time

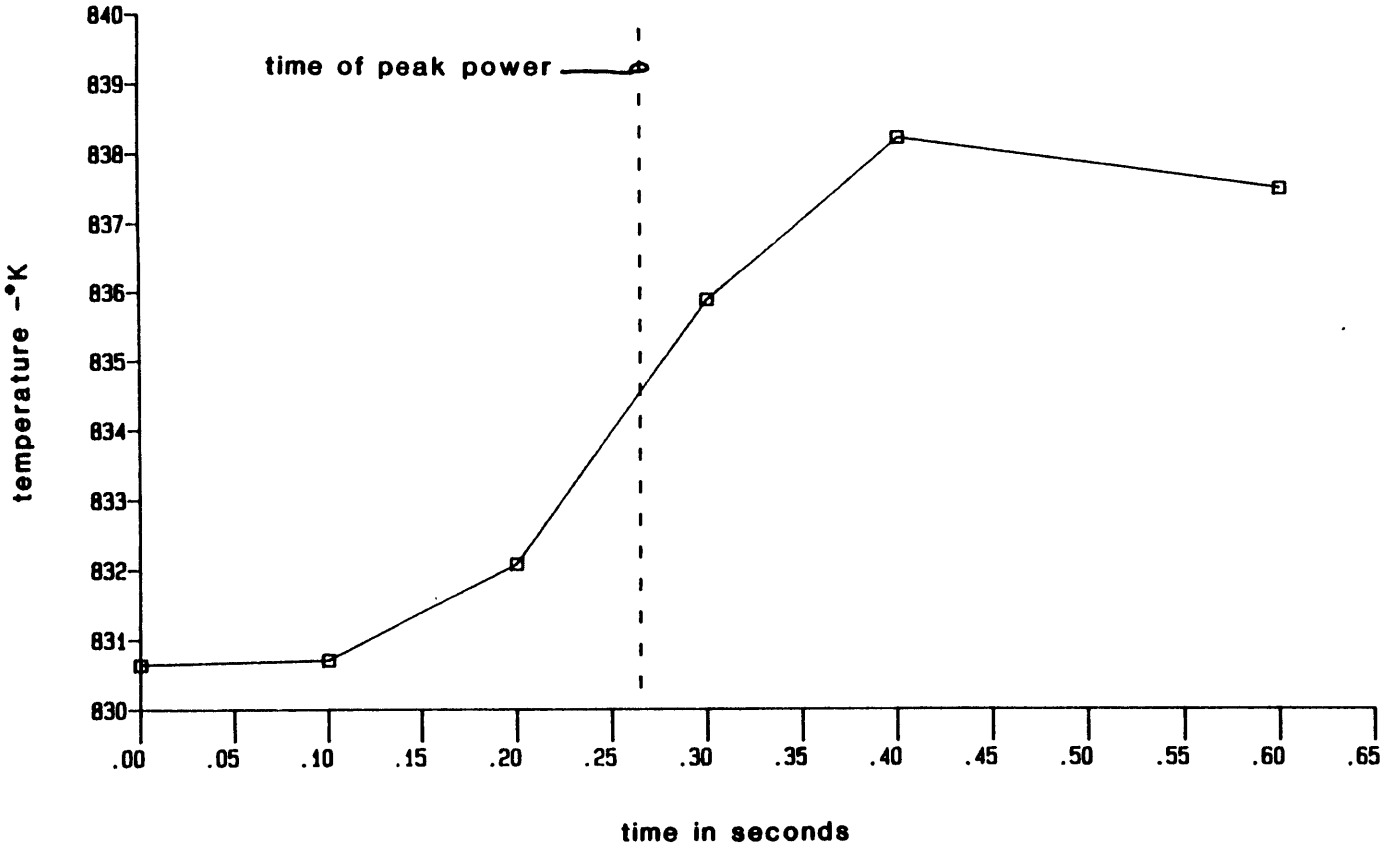

Figure 5.26a Turbine Trip #1, BW2C-T, TITAN:

Core-average Fuel Temperature versus Time

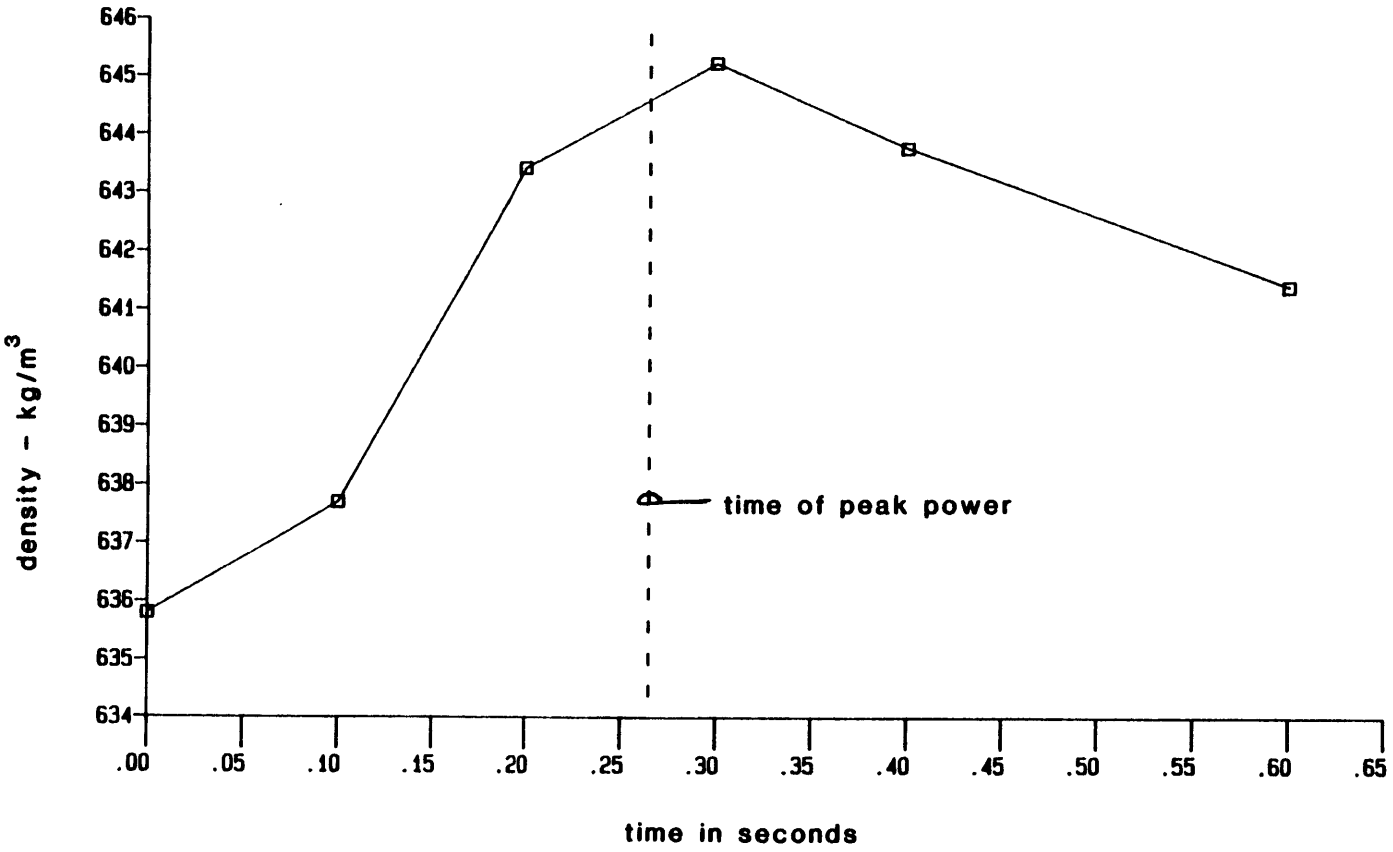

Figure 5.26b Turbine Trip #1, BW2C-T, TITAN:

Core -average Moderator Density versus Time

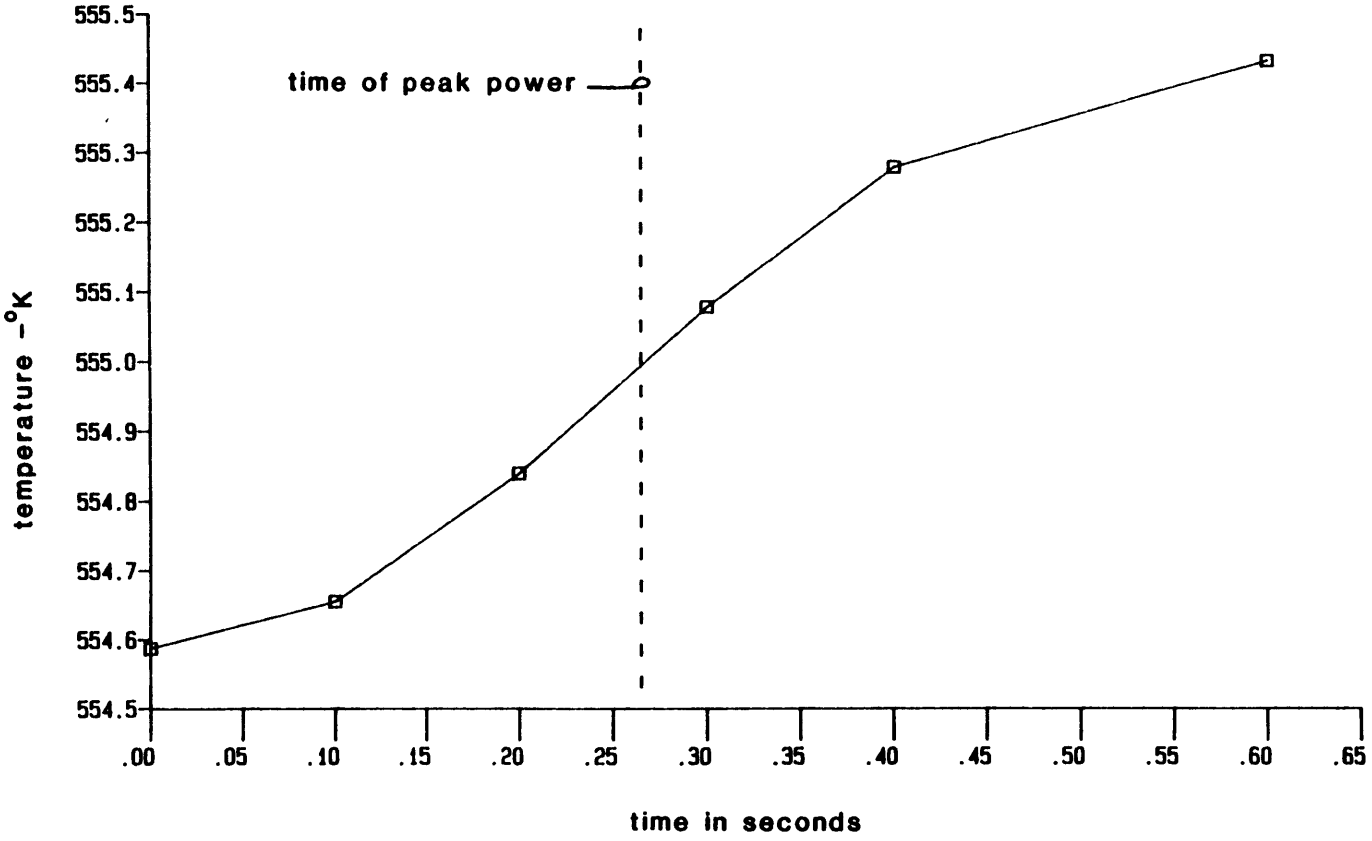

Figure 5.26c Turbine Trip #1, BW2C-T, TITAN:

Core-average Moderator Temperature versus Time

because of the Doppler feedback mechanism. Thus, the reactor power decreases when the fuel temperature increase overcomes the increase in moderator density. In addition, the moderator density eventually decreases as a result of increased heat transfer and decreased inlet flow rate.

The observed global reactor behavior is the sum of changes in the nodal powers. These local changes may not preserve the steady-state relative powers, resulting in spatial variations during the transient. One would expect that a turbine trip would produce spatial variations because the strongest positive feedback occurs in boiling regions of the core. As was discussed in Chapter 2, the spatial effects in a turbine trip are predominently in the axial direction. Indeed, turbine trip analyses are often performed with one-dimensional neutronics models. This general behavior was confirmed by the TITAN analysis of Turbine Trip #1. The normalized assembly powers remained nearly constant throughout the transient, with a maximum change of less than 0.3%. The axial power shapes were subject to somewhat larger variations during the transient. As would be expected, the changes in relative nodal power were greatest (and positive) in the center nodes where the collapse of voids and the neutron fluxes are large. Even so, the magnitude of the maximum change in relative nodal power was less than 2.8%. Thus, TITAN indicates that spatial effects are not large for this transient.

To summarize: The results of the TITAN analysis of Turbine Trip #1 are reasonable, through their accuracy has not been quantified. The calculated behavior of the global reactor power and its spatial distribution is in qualitative agreement with the expected behavior of a reactor following a turbine tip. In addition, the TITAN results were internally consistent. Finally, the analysis demonstrates the effective operation of the thermal-hydraulic initiation mode of the transient coupling methodology.

5.4.2.3 Turbine Trip #2

The TITAN results for the time-dependent reactor power during Turbine Trip #2 are shown in Figure 5.27. The analysis produced rather dramatic results characterized by two large power excursions followed by two smaller excursions. The excursions resulted in power peaks of 2.09, 2.19, 1.63 and 1.37 times the steady-state power occurring at 0.42, 0.88, 1.37 and 1.96 seconds, respectively. Following the last excursion, the reactor power decreases monotonically until the end of the analysis, at which time the power is only 2.75% above the steady-state value. The first two power peaks correspond to peaks in the forcing function for inlet flow. Figure 5.28 shows the time-dependent behavior of the core average feedback parameters during the transient. This figure shows the competing effects of increasing moderator density and increasing fuel temperature. Initially, the moderator density increases while the fuel temperature remains nearly constant. As a result, the reactor power rises rapidly. The rise in power produces a rise in fuel temperature which continues until 3.0

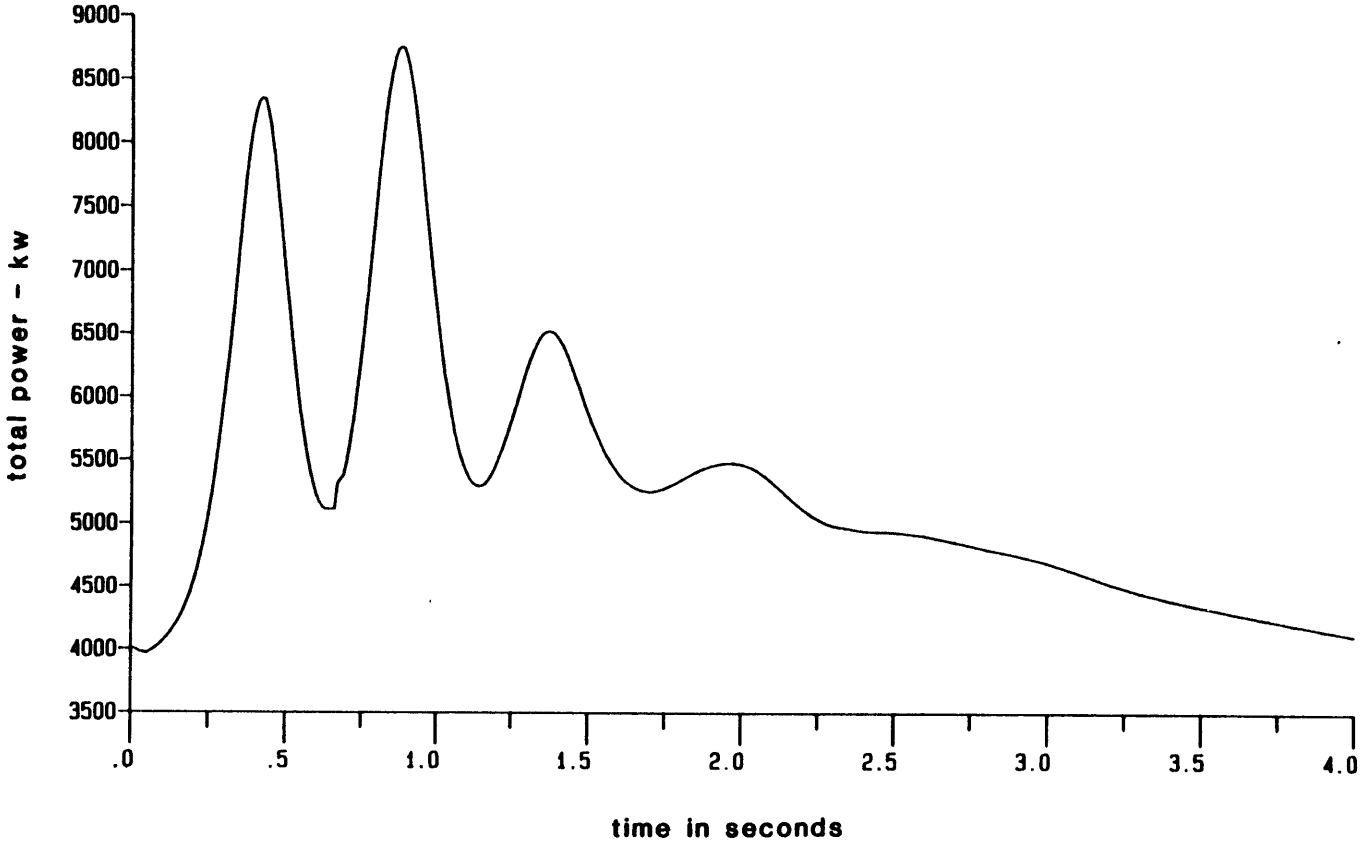

Figure 5.27 Turbine Trip #2, BW2C-T, TITAN: Power versus Time

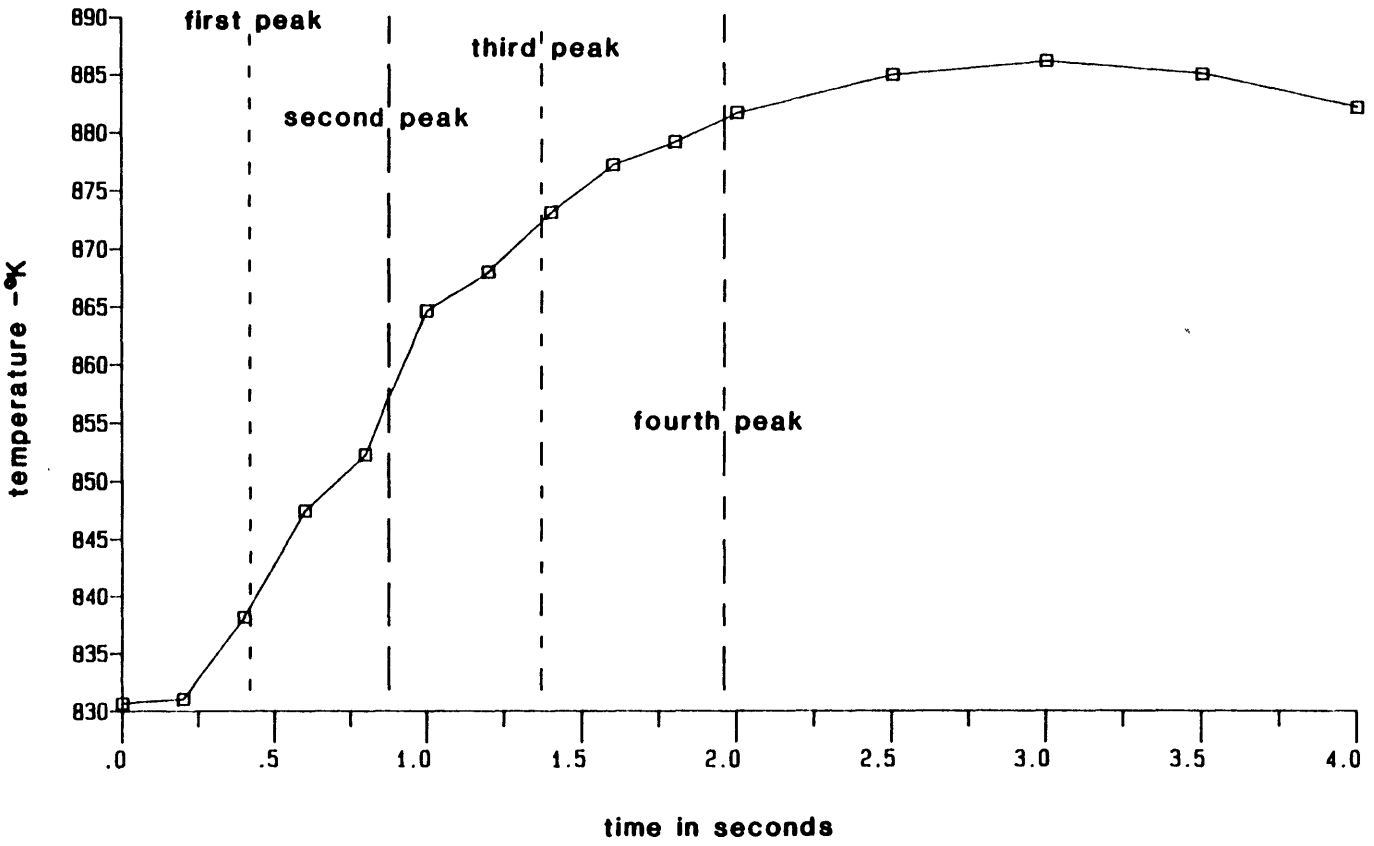

Figure 5.28a Turbine Trip #2, BW2C-T, TITAN:

Core-average Fuel Temperature versus Time

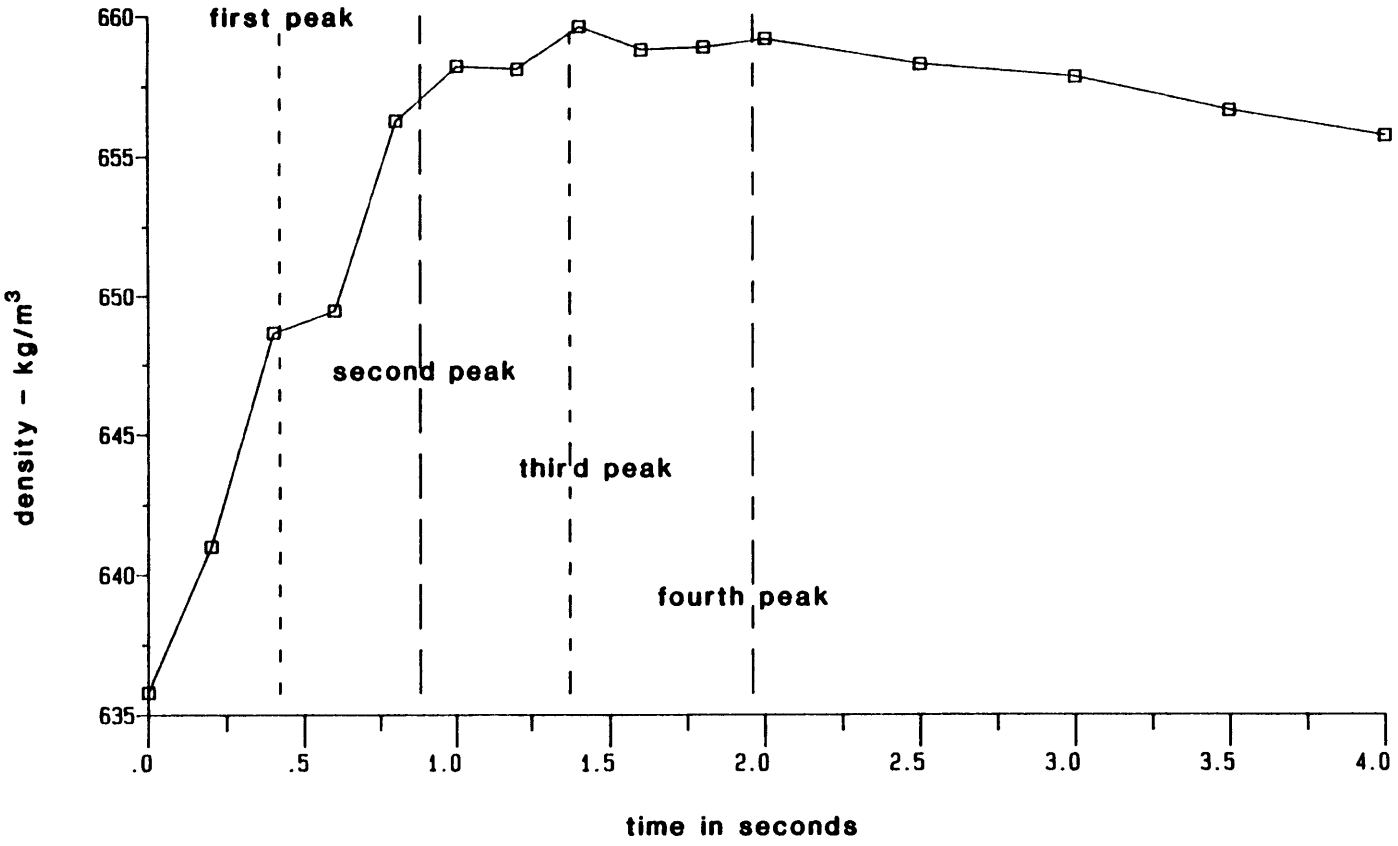

Figure 5.28b Turbine Trip #2, BW2C-T, TITAN:

Core-average Moderator Density versus Time

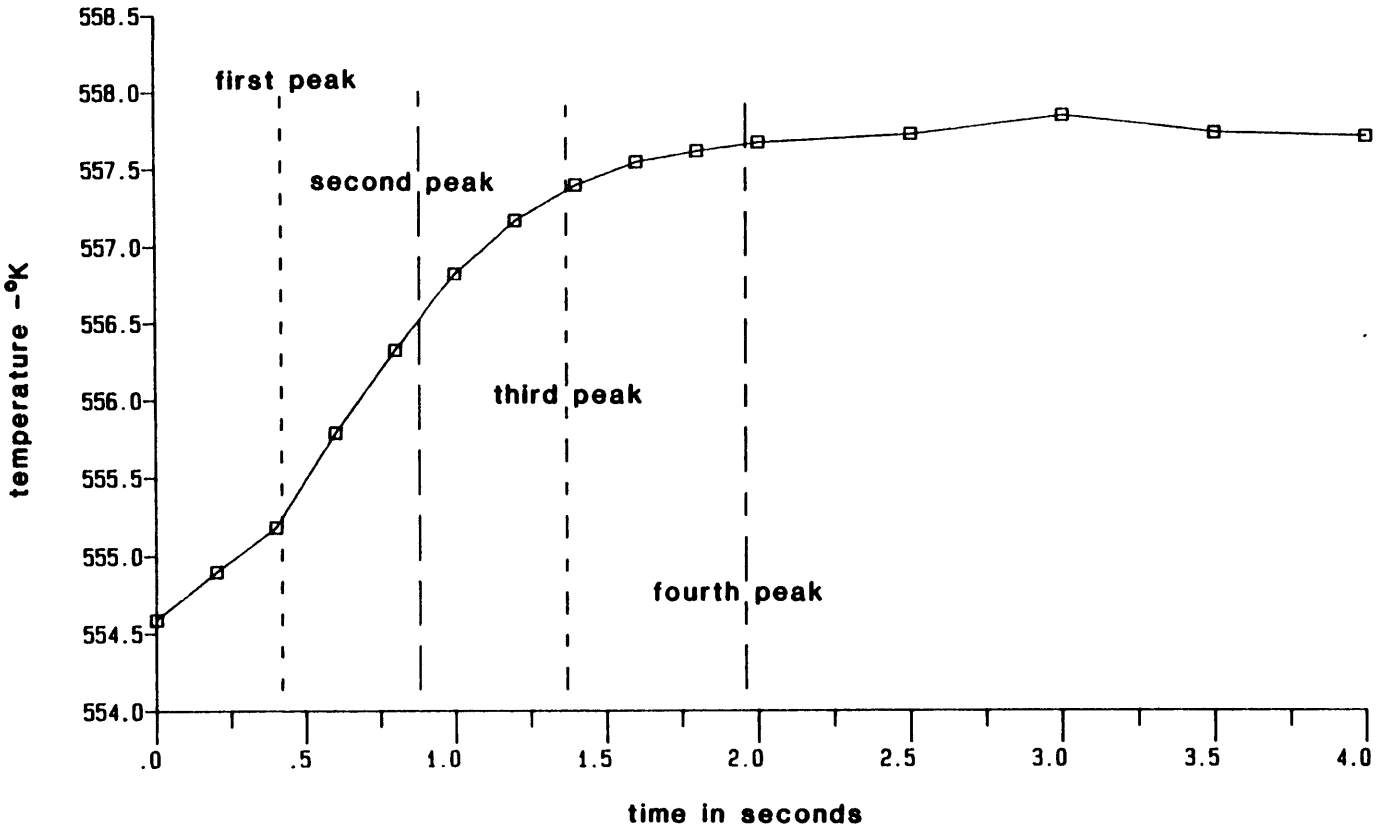

Figure 5.28c Turbine Trip #2, BW2C-T, TITAN:

Core-average Moderator Density versus Time

seconds into the transient. Similarly, the moderator temperature increases throughout the first 3.0 seconds of the transient. The first and subsequent three power excursions were terminated by a combination of the continuous increase in fuel and moderator temperatures and a lack of increase in the moderator density. As Figure 5.28b shows, each power peak is followed by a drop in the rate of increase of moderator density. The net effect of the three feedback mechanisms was to produce the global power behavior of Figure 5.27.

The TITAN results for Turbine Trip #2 seem to be qualitatively correct. Figure 5.23 shows the time-dependent neutron flux as calculated for the Duane Arnold PSAR. These results are similar to those obtained with TITAN, given that the PSAR calculation modeled a delayed scram which terminated the power excursion. The magnitude of the peak flux is the PSAR calculation was 1.96 times the steady-state value, as compared to the TITAN power peak of 2.09 times the steady-state power. However, the duration of the excursion and the time of the peak did not coincide in the two analyses. Nevertheless, the similarities between the PSAR results and the TITAN results gives creedence to the qualitative correctness of the TITAN analysis.

The TITAN analysis of Turbine Trip #2 involved 401 time-steps of 0.01 seconds each. The analysis required 522.56 seconds of Multics c.p.u. time (approximately equivalent to 130 seconds of IBM 370/168 c.p.u. time). Therefore, the "rate" of computer time usage was 0.065 Multics c.p.u. seconds per time-step per node.

5.4.2.4 Axial Mesh Sensitivity Study

The TITAN analysis of Turbine Trip #1 discussed in Section 5.4.2.2 was performed with 10 axial nodes and an axial mesh spacing of 0.152^4 m. As has been shown, the transient is driven by changes in the feedback parameters and results in both global and spatial power variations. These feedback parameters are averaged over the nodal volumes, so the choice of node size could effect the analytical results. Therefore, a second TITAN analysis with 20 axial nodes and an axial mesh spacing of 0.0762 m was performed. The results did show some sensitivity to the axial mesh size. Figure 5.29 shows a comparison of the time-dependent reactor power as calculated with both 10 and 20 nodes. In addition, a comparison of other selected parameters from the two analyses is presented in Table 5.11. The analysis with 20 axial nodes produced a peak power which was 4.53% higher that that of the 10 axial node case.

An increase in the peak fuel temperature of 10.5°K also resulted from the reduction in axial mesh spacing. Little or no difference in integrated power and the time of the power peak was observed. Only the difference in the peak power seems to be significant, particularly since the effect is non-conservative. However, the limiting parameter for this event is fuel enthalpy, not peak power. Since the peak fuel temperature was largely insensitive to the axial mesh spacing, the larger axial mesh spacing appears to be adequate. It should be noted that one very significant sensitivity was observed. The case with 20 axial nodes required approximately twice as much computer time as did the 10 axial node case.

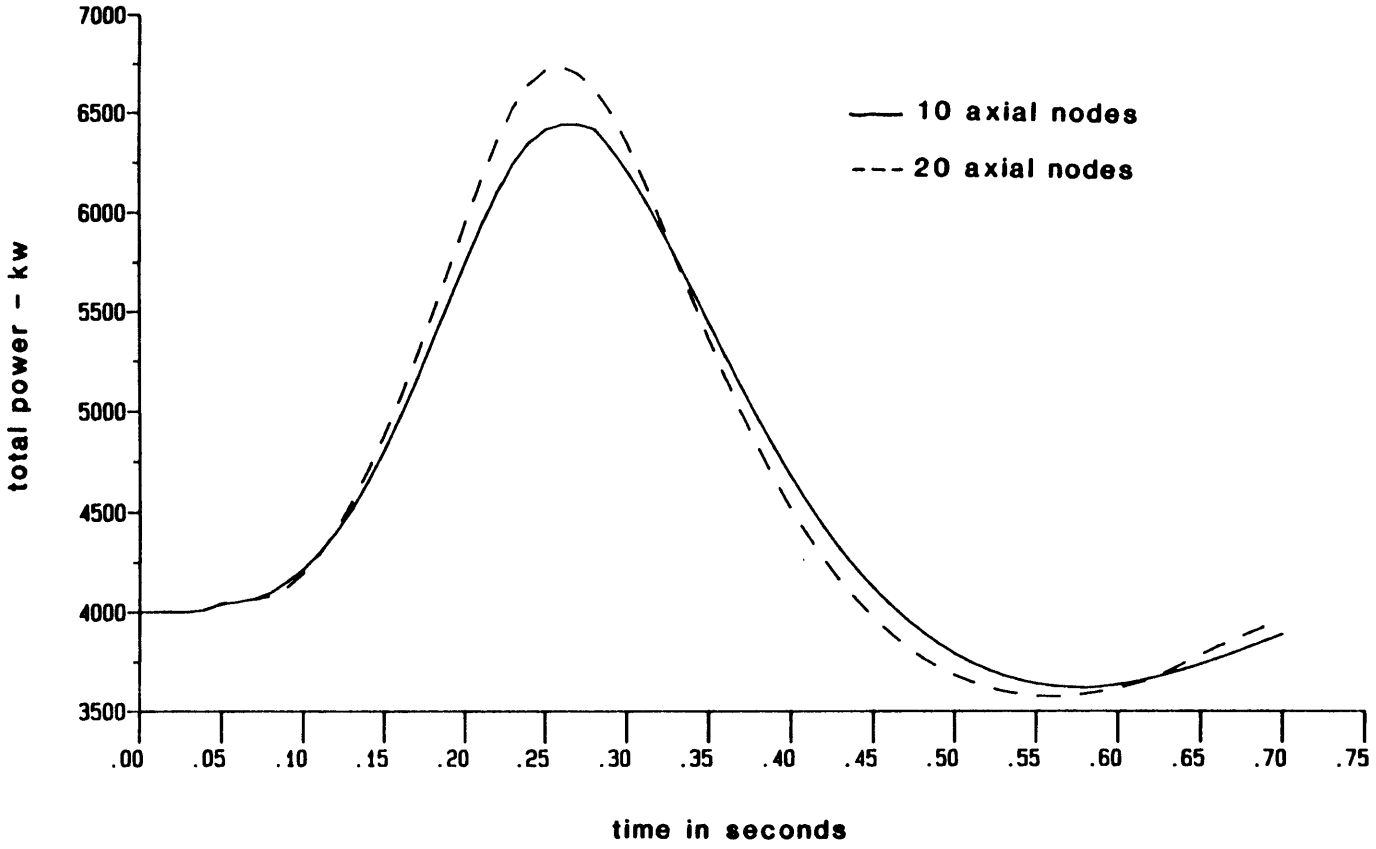

Figure 5.29 Turbine Trip #1, BW2C-T with 10 and 20 Axial Nodes, TITAN: Power versus Time

TABLE 5.11

SENSITIVITY OF TITAN RESULTS FOR TURBINE TRIP #1

(BW2C-T PROBLEM) TO AXIAL MESH SIZE

Number of axial nodes	10	20
Axial mesh size, m	0.1524	0.0762
Time-step size, s	0.01	0.01
Peak power, kw	6436.5	6728.1
Time of peak power, s	0.26	0.26
Integrated power, MW-s	3.219	3.229
Maximum fuel temperature, °K	2168.51	2179.01
Computer time, MULTICS cpu seconds	81.97	165.20
cpu seconds per time-step per node	0.068	0.069

5.4.3 Neutronically Initiated Transients

5.4.3.1 Problem Description

TITAN was applied to a neutronically initiated transient based upon the BW2C-T problem. The transient consisted of the continuous withdrawal of the channel #2 control rod. The control rod was withdrawn with a constant velocity of 1.276 m/s. At this rate, the control rod is completely withdrawn in 1.0 seconds.

The rod withdrawal problem was designed as a benchmark calculation for the MEKIN code to compare the results obtained with fine and coarse mesh thermal-hydraulic models [R-11]. The problem is intended to present a significant challenge for a coupled code. The reactivity insertion is large, estimated to be greater than $3.2 (based on static QUANDRY calculations by Rodriguez-Vera). In addition, significant spatial effects were expected because the control rod is withdrawn from the low power fuel assembly. For these reasons, the rod withdrawal transient was also a good test for TITAN. Furthermore, the opportunity of comparing TITAN and MEKIN results and computational requirements was quite important. Unfortunately, the MEKIN analyses were never completed and no other solutions exist. Nevertheless, the BW2C rod withdrawal problem provided a good basis for demonstrating the neutronic mode of the TITAN transient coupling methodology. The results have also been examined for qualitative plausibility and internal consistency, both from a global and a spatial perspective. Finally, investigations were undertaken to determine the effect of axial mesh spacing, time-step size and the cusping correction option on the results.

5.4.3.2 Rod Withdrawal Results

A TITAN analysis of the BW2C-T rod withdrawal transient was performed with a model having ten axial nodes and the full fuel rod model. The rod withdrawal begins at 0.0 and is concluded at 1.0 seconds with the cusping correction in effect. The transient calculation spanned the control rod withdrawal with 110 time-steps of 0.01 seconds each. Figure 5.30 shows the calculated reactor power as a function of time for the rod withdrawal. The transient produced a very large power excursion early in the rod withdrawal and a second peak of much smaller magnitude late in the withdrawal. The first peak reaches a maximum power of 80.75 times the initial power, P_0, after only 0.13 seconds of transient time. The excursion ends with a very rapid power decrease, returning to the original steady-state power at approximately 0.185 seconds and eventually reaching a minimum of 0.22 P_0 at 0.31 seconds. Note that the control rod is still being withdrawn throughout the period of decreasing reactor power. Thus, after reaching its minimum level, the power rises at a relatively moderate rate until a second peak of 3.02 P_0 is attained at 0.87 seconds. The reactor power decreases thereafter, falling to a final value of 1.35 P_0 at 1.1 seconds. The integral of the reactor power over the course of the analysis was 15.221 Mw-s.

In the absence of any reference solution, the TITAN results for the rod withdrawal problem must be assessed for qualitative correctness and self-consistency. Both the global and the spatial behavior merit examination in order to provide some confidence in the TITAN results. One approach was to perform a neutronics-only QUANDRY analysis of the rod withdrawal transient. A QUANDRY analysis with feedback is not possible because the simple thermal-hydraulics model cannot handle

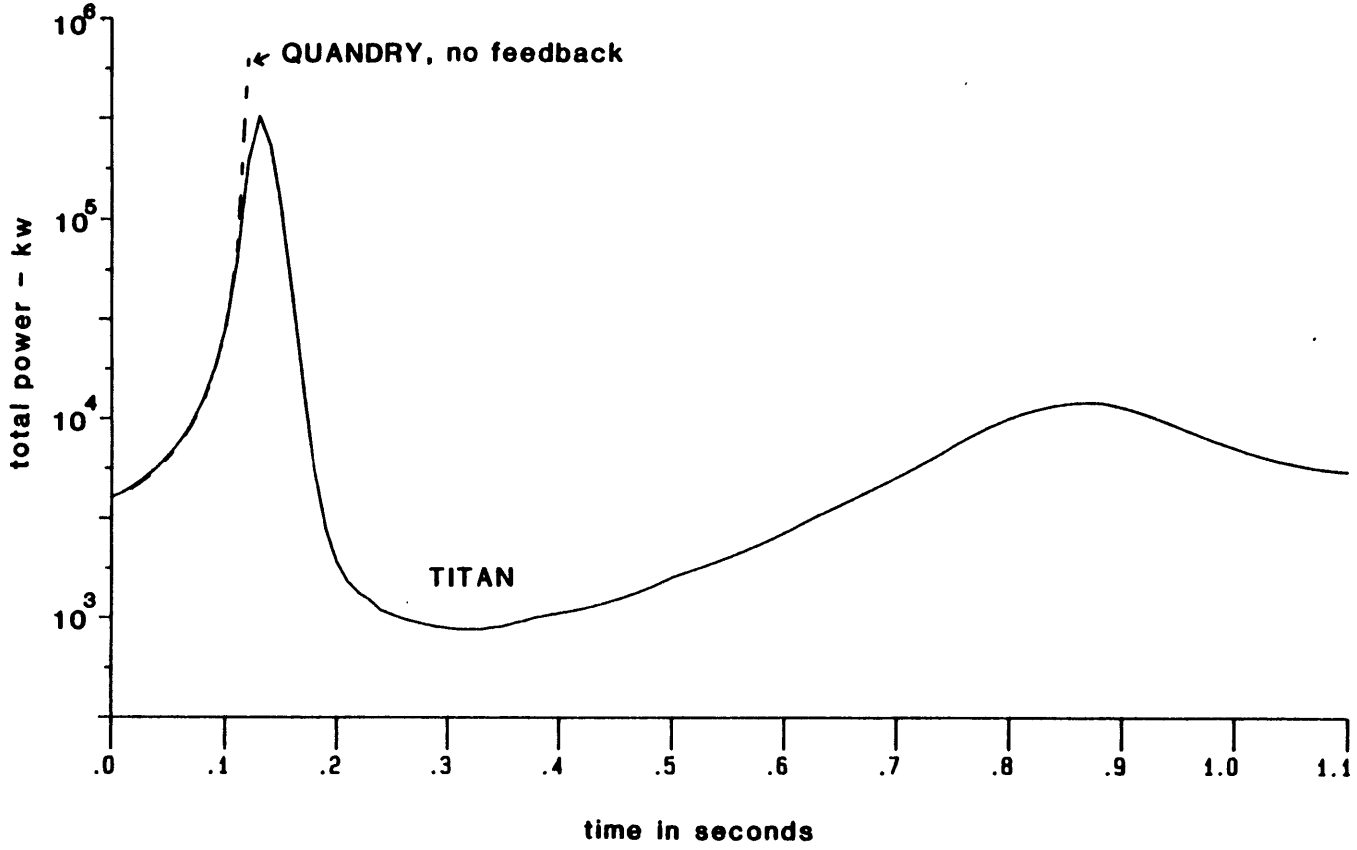

Figure 5.30 BW2C-T Rod Withdrawal, TITAN and QUANDRY (no feedback): Power versus Time

transient two-phase conditions. Nevertheless, an analysis without feedback is of value because it gives results which should show clearly the effect of feedback in the early part of the transient. The neutronics-only QUANDRY results for the reactor power are shown in the dashed line on Figure 5.30. The results only span 12 time-steps because overflow errors terminated the calculation beyond that point. For the first 10 time-steps, the QUANDRY results match the TITAN results very well. Clearly, the absence of feedback was of little consequence during the early part of the transient. However, the significant impact of feedback is evident for the remaining two time-steps. The reactor power calculated by QUANDRY continues to rise at a very high rate, exceeding the TITAN power by 9.8% at 0.11 seconds and by 217.3% at 0.12 seconds. The agreement of TITAN and QUANDRY in the early part of the rod withdrawal gives support to the TITAN results, and shows that the coupling has not degraded the performance of the analytic nodal method. The rapid increase in power is characteristic of a prompt-critical excursion and its early occurrence indicates the large reactivity impact of the initial rod motion. This can be explained, in part, by the steady-state power shapes (see Figures 5.12 and 5.13), which are significantly peaked in the upper nodes. Thus, the initial movement of the control rod perturbs a region of relatively high neutron flux, producing a large reactivity insertion. Conversely, the latter control rod motion occurs in regions of low (steady-state) neutron flux and the reactivity impact is low.

The neutronics-only QUANDRY calculation demonstrated that feedback was not significant during the first 0.10 seconds. It also gives

creedence to the TITAN results for the same period. However, the behavior of the reactor power from that point on was strongly effected by the response of the thermal-hydraulic model to the initial rapid increase in power. In order for the remaining TITAN results to be credible, there must be consistency between the neutronics and thermal-hydraulics calculations throughout the course of the rod withdrawal. Therefore, it is instructive to examine the time-dependent behavior of the three feedback parameters. This is shown in Fig. 5.31a-c, each parameter calculated on a core average basis. The figures show little change in the core average moderator density and temperature and only a 6.6°K increase in core average feedback during the first 0.10 seconds of the transient. This explains why essentially no difference was seen between the TITAN results and those of QUANDRY without feedback for this part of the transient. However, Figs. 5.31a and 5.31c show that both the fuel temperature and the moderator temperature begin to increase rapidly after 0.10 seconds, producing the feedback that stops the power excursion at 0.13 seconds. The moderator density decrease adds a small contribution at this point, but is more significant after the initial power peak.

The average fuel temperature continues to rise sharply for a time after the reactor power has started to decrease. The maximum temperature rise of ∿172°K occurs 0.05 seconds after the peak. A combination of the fall in power production and somewhat increased heat transfer from fuel to coolant allows the fuel temperature to decrease until 0.72 seconds into the transient. Thus, the fuel temperature provides negative feedback for a short time after the peak of the initial excursion which, combined with the other two mechanisms, serves to drive the power down

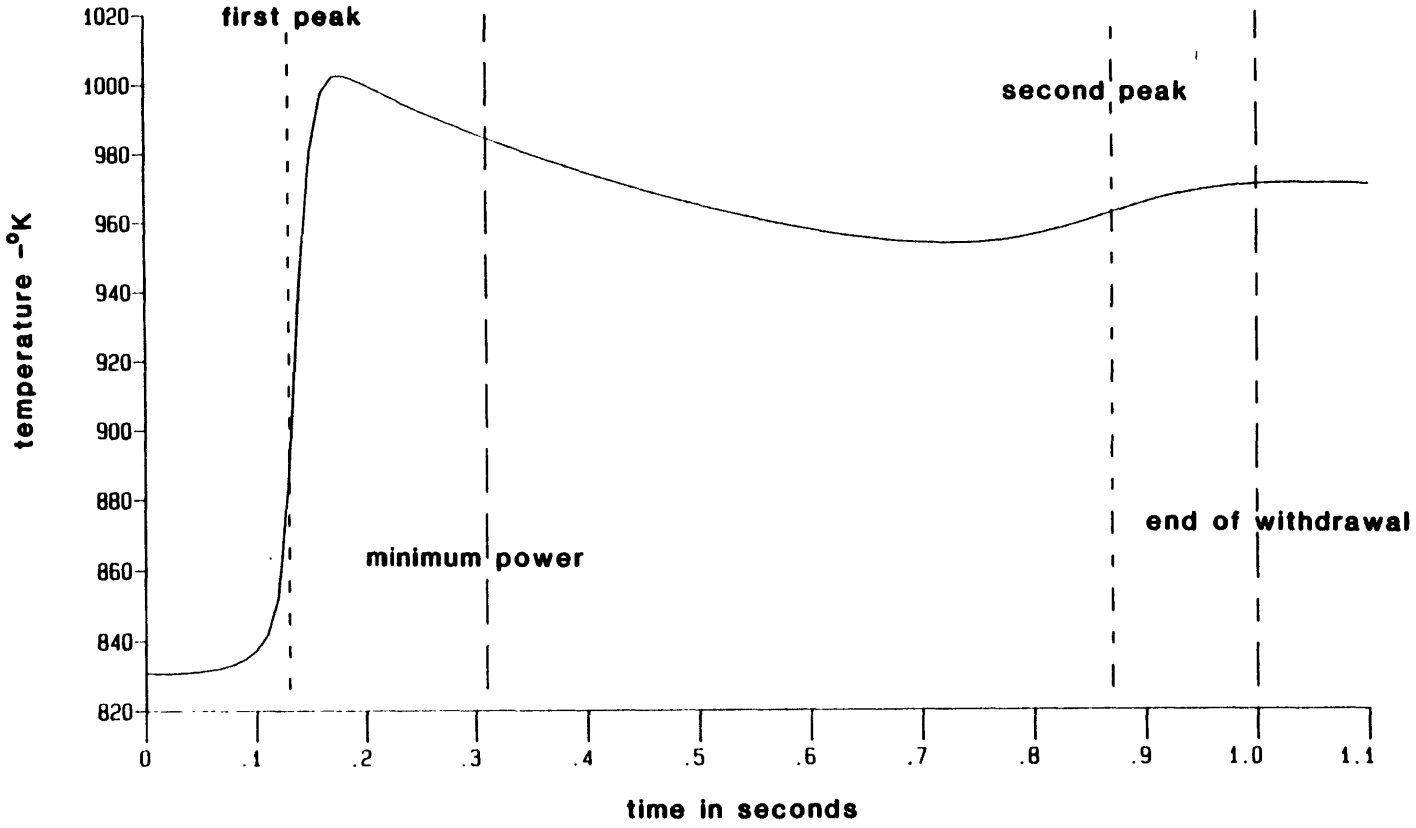

Figure 5.31a BW2C-T Rod Withdrawal,TITAN:

Core-average Fuel Temperature versus Time

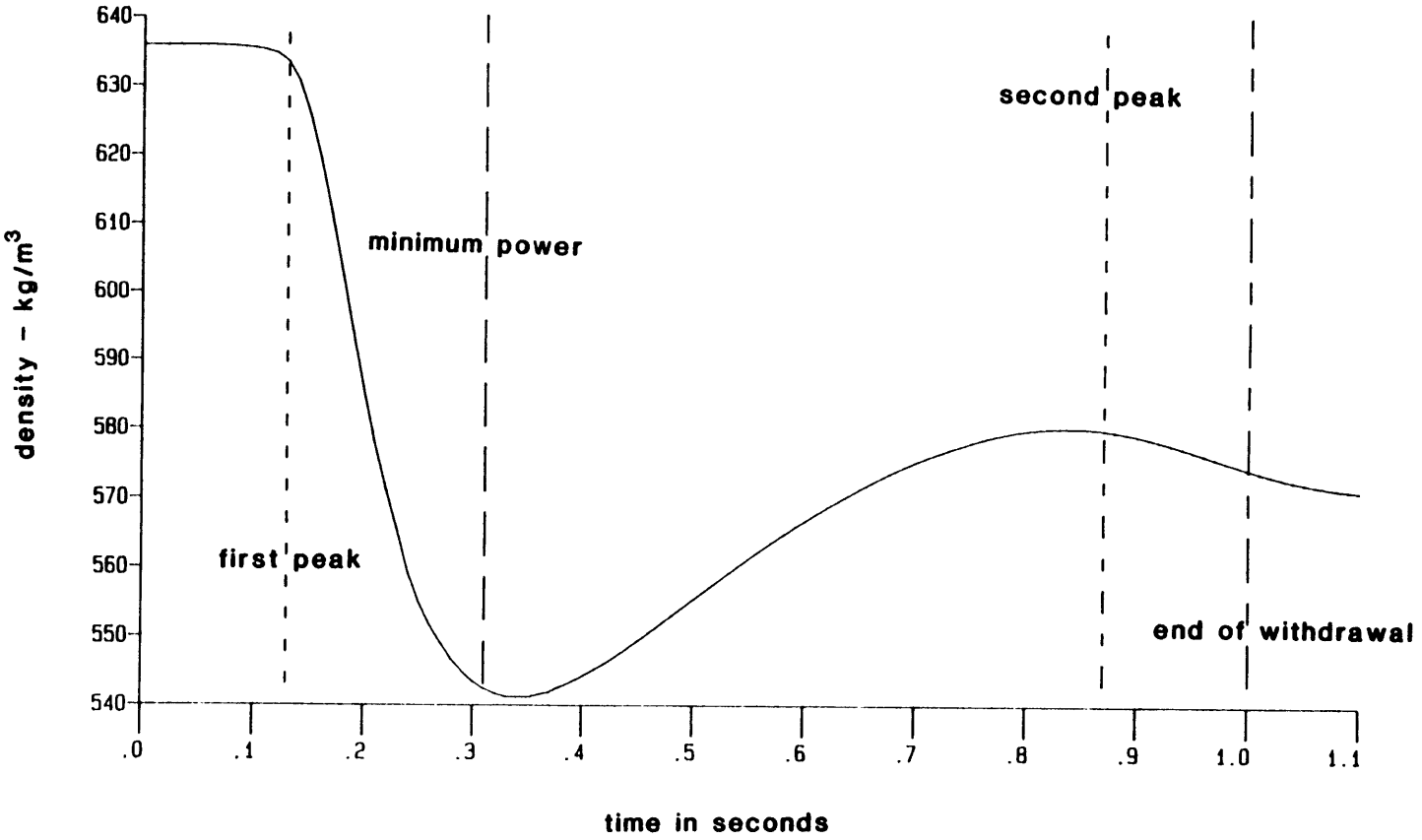

Figure 5.31b, BW2C-T Rod Withdrawal, TITAN:

Core-average Moderator Density versus Time

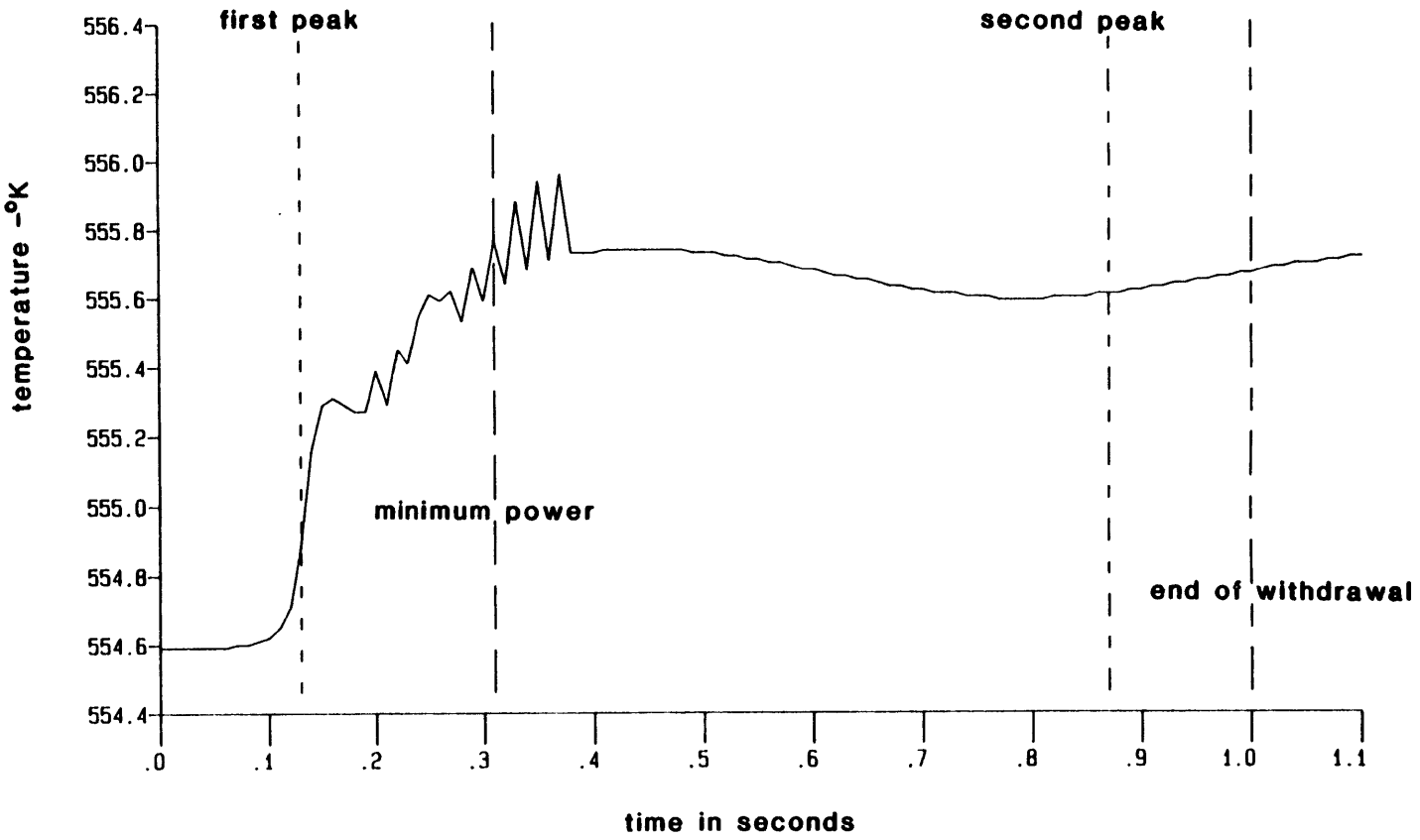

Figure 5.31c BW2C-T Rod Withdrawal, TITAN:

Core-average Moderator Temperature versus Time

strongly. The core average moderator density decreases significantly following the initial excursion, as the large additional energy deposited in the fuel is conducted through the fuel into the coolant. In addition, the direct deposition of energy on the coolant is an instantaneous, though much smaller ($\sim$1%), contributor to the decrease in moderator density. The minimum moderator density of 541.2 kg/m^3 occurs at 0.34 seconds, a decrease of 94.6 kg/m^3 from the steady-state value. The period during which the moderator density is decreasing correlates very closely with the drop in reactor power after the initial excursion is terminated. This adds another strong negative feedback to the fuel temperature in the first 0.05 seconds after the peak and acts to continue the drop in power after the fuel temperature feedback becomes positive. The moderator temperature is also generally increasing in the time period following the initial excursion, though its behavior is somewhat more complicated, as Figure 5.31c shows. The small oscillations in core average moderator temperature seen there are thought to be the result of numerical round-off.

The remainder of the rod withdrawal transient can be explained in a manner analogous to the explanation of the initial excursion. The reactor power begins to rise after 0.31 seconds because the control rod is continually being withdrawn and the feedback mechanisms are either weakly negative (moderator temperature and density) or positive (fuel temperature). Shortly after the second power rise begins, the moderator density begins to increase and the moderator temperature to decrease in response to the low power produced over the previous 0.1 seconds. At this point, and for more than 0.2 seconds thereafter, all three feedback mechanisms add to the reactivity insertion. Ultimately, the power rises

enough that the fuel temperature begins to increase, followed by an increase in the moderator temperature and a decrease in the moderator density. This terminates the second excursion in the same manner as the first, though the magnitudes of the feedback and the rate of the power changes are much smaller. In summary, the behavior of the core average feedback parameters and the reactor power during the rod withdrawal transient are quite consistent and explainable.

The spatial effects evidenced by the TITAN analysis of the rod withdrawal also merit examination and explanation. The removal of a partially inserted control rod from one of the two fuel assemblies would be expected to produce spatial changes in both the transverse and axial directions. Figures 5.32 and 5.33 show the normalized axial power shapes at the beginning and end of the TITAN analysis for channels 1 and 2, respectively. The figures show that the change in axial power shape was more pronounced in channel 2 than in channel 1. In channel 2, the normalized power increased in the lower eight nodes and decreased in the top two nodes. As a result, the peak power changes from node 9 to node 7. Nevertheless, the power still remains strongly peaked in the upper half of the channel. In channel 1, the normalized power increased in the lower six nodes and decreased in the upper four nodes. The peak power shifted from node 8 to node 7, but the axial power shape remained very strongly peaked in the top half of the channel. In summary, the withdrawal of the control rod does produce an increase in the power in the bottom half of the core relative to the top half. However, the most significant feature of the axial power shapes, i.e., the strong upper peaking, largely remains.

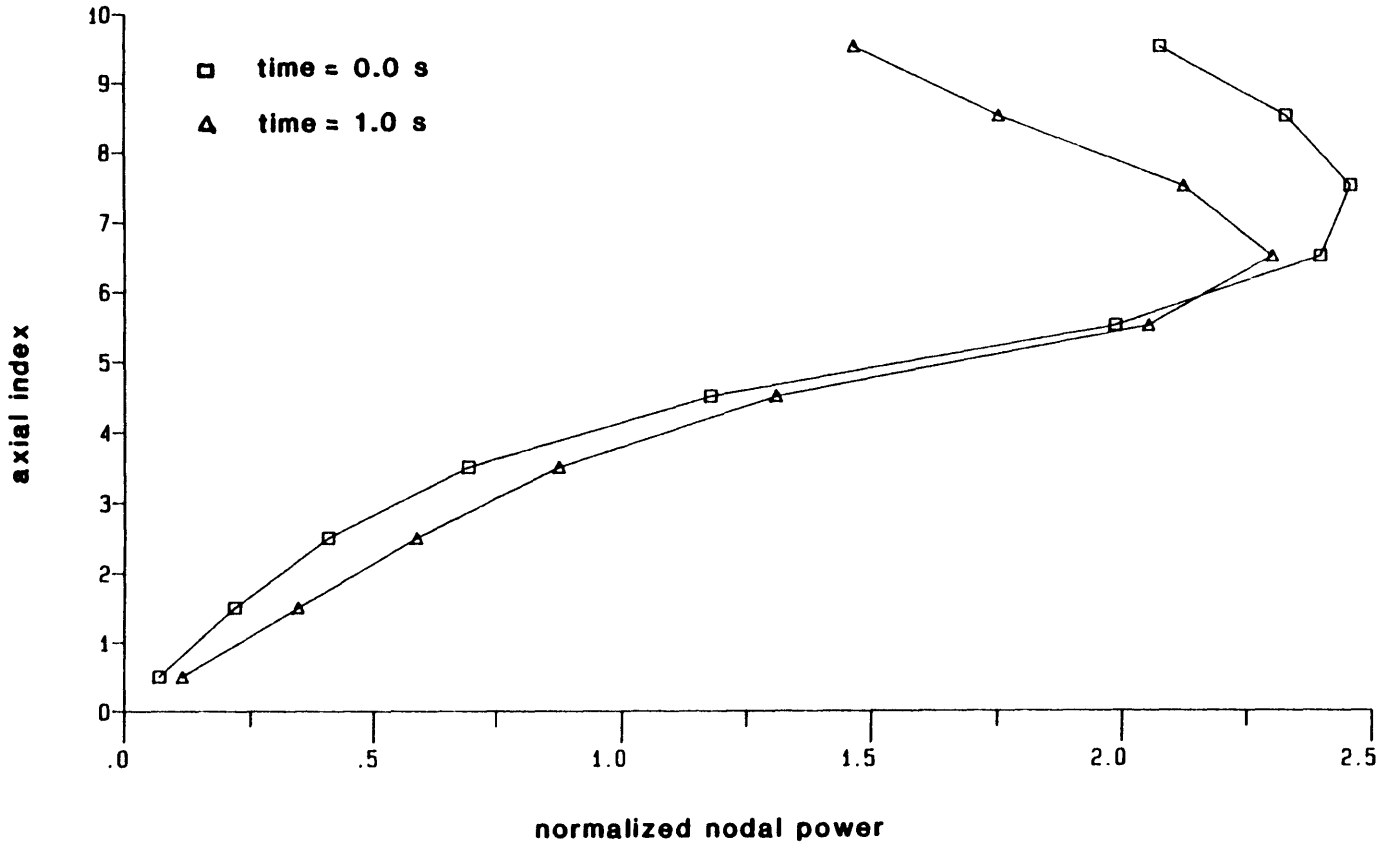

Figure 5.32 BW2C-T Rod Withdrawal, TITAN:

Change in Axial Power Profile, Channel 1

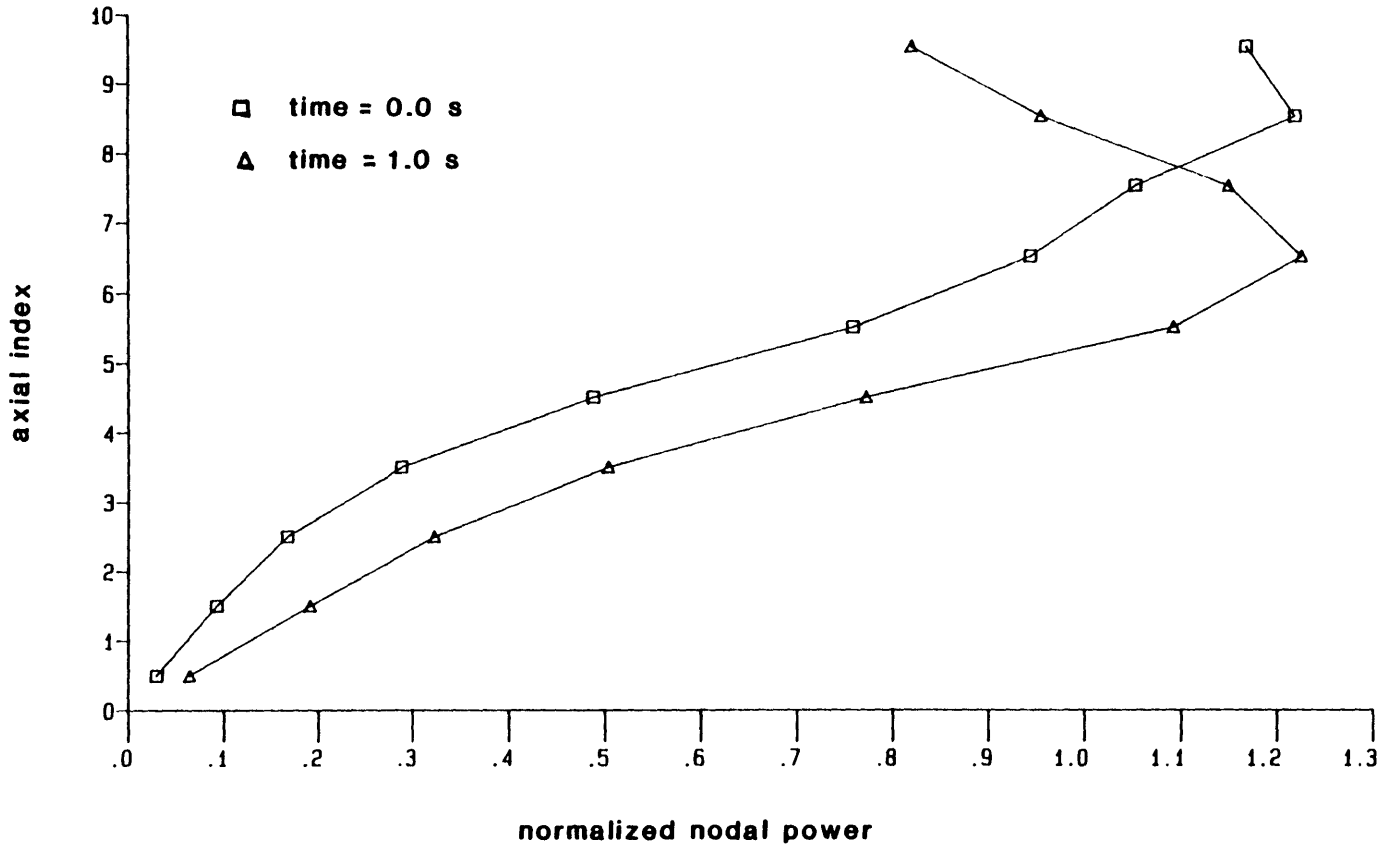

Figure 5.33 BW2C-T Rod Withdrawal, TITAN:

Change in Axial Power Profile, Channel 2

The transverse power shape was not significantly changed by the rod withdrawal. Figure 5.34 shows the variation of the assembly power split during the transient. The figure shows a small ($< 5\%$) shift in power at the end of the transient from channel 1 to channel 2. Thus, the total removal of the control rod from channel 2 does not cause the large tilt in the transverse power shape which might have been expected. Apparently the neutronic coupling between the two assemblies is significant and the zero flux boundary condition dominates the transverse power shape.

One final check for self-consistency of the TITAN rod withdrawal results was performed. A fundamental task of the coupling methodology is to link the neutronics and thermal-hydraulics segments by the nodal powers. The neutronics segment determines the nodal powers at each time-step and these are used to specify the rate of energy deposition in the fuel and moderator. Obviously, it is important that this nodal power coupling be done correctly so that safety and feedback parameters will be calculated correctly. One way to check this coupling is to perform an energy balance over the course of a transient. The objective of an energy balance is to show that all of the energy "produced" by the neutronics segment can be accounted for in the thermal-hydraulics results. The energy must appear in one of three categories:

1. Energy removed from the reactor by convection,
2. Energy stored in the coolant, and
3. Energy stored in the fuel.

The energy balance test of TITAN can therefore be stated as follows: The integral of the power production over the time of the transient should be equal to the sum of the integral of the power

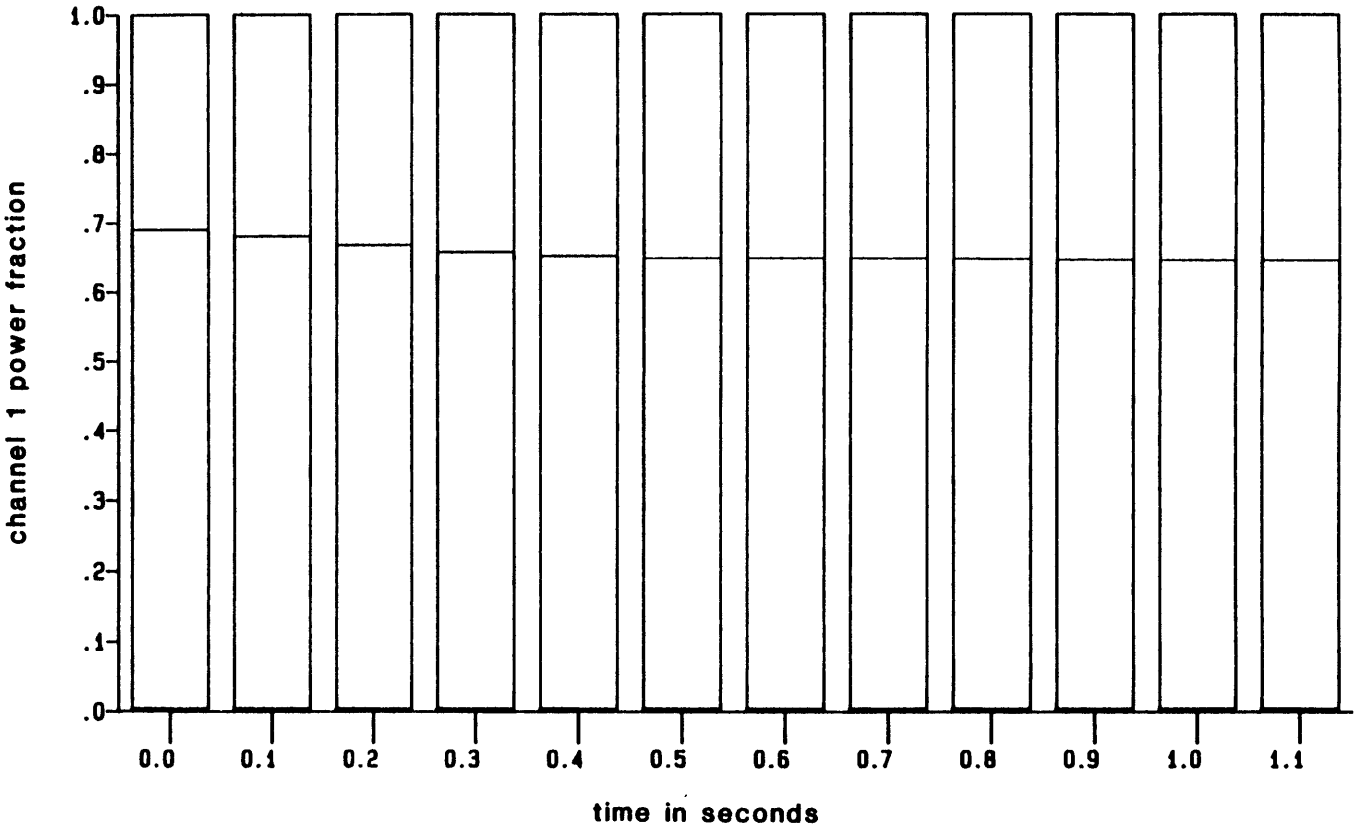

Figure 5.34 BW2C-T Rod Withdrawal, TITAN:

Change in Relative Channel Powers

convected out of the reactor during the transient and the increase in the energy stored in the fuel and coolant at the end of the transient. This is the basis for an energy balance check that was performed on the TITAN results for the rod withdrawal transient. The reactor power and the net rate of fluid energy crossing the reactor boundaries are output parameters calculated by TITAN at each time-step. These were integrated over the 1.1 seconds of transient time (110 time-steps) by assuming a linear variation between each time-step.

The increase in stored energy in the fuel was calculated by integrating the product of fuel density and heat capacity from the initial to the final temperature. The actual algebraic expressions for the temperature-dependent product of fuel density and heat capacity (or cladding density and heat capacity) used in TITAN were integrated for each individual fuel "cell" in each node and multiplied by the appropriate fuel cell volumes. The summation of all the individual fuel cells gave the total increase in fuel stored energy during the transient.

The increase in energy stored in the coolant was calculated for each node using the coolant mixture enthalpy, void fraction, liquid density and vapor density (all of which are output parameters) at the beginning and end of the transient. The energy content of the coolant in a given node was taken to be the product of the mixture enthalpy and the mixture density (see Eq. 4.5). The increase in stored energy, then, is the difference between the final and the initial nodal coolant energy content and the total increase in stored energy is the sum of all the nodal values. Table 5.12 summarizes the results of the energy balance calculation. The difference between the total integrated power

TABLE 5.12

BW2C-T Rod Withdrawal, TITAN: Energy Balance Calculation

Energy convected out of reactor, MW-s	9.459
Energy stored in fuel, MW-s	7.778
Energy stored in coolant, MW-s	-1.948
Net energy deposited in reactor, MW-s	15.289
Total energy produced by transient, MW-s	15.221
"Error" in energy balance, MW-s	0.068
"Error" as percentage of total energy	0.45%

and the total energy stored and convected out of the reactor was less than one half of one percent of the total energy produced. Given that the balance was essentially a "hand" calculation, the error is quite acceptable. This result indicates that the power coupling in TITAN is correct.

5.4.3.3 Modeling Options Sensitivity Studies

A TITAN analysis of a transient such as the BW2C rod withdrawal involves a number of modeling decisions which must be made by the user. Among these decisions are the division of the reactor into nodes and the specification of the nodal dimensions, the choice of a fuel rod model from three available options, the choice of appropriate thermal-hydraulic correlations for critical heat flux and two-phase flow, the optional use of a control rod cusping correction, and the specification of time domain information. Though some guidance in these decisions is available through the experience with QUANDRY and THERMIT (see Chapter 3), the lack of experience with TITAN may make such choices seem somewhat arbitrary. Furthermore, the sensitivity of the results to these modeling decisions is not known. Accordingly, a series of investigations was undertaken to determine the sensitivity of TITAN results to certain of the modeling options. The sensitivity studies were performed for modeling options of particular relevance to the BW2C rod withdrawal analysis. These are:

1. Time-step size,
2. Axial mesh spacing, and
3. Control rod cusping correction model option.

The time-step is a fundamental parameter in the numerical solution of the temporal difference equations. In many cases the time-step size effects the stability, accuracy and cost of code operation. In TITAN, the neutronics and thermal-hydraulics segments use an identical time-step at each point in the analysis and feedback information is exchanged at the end of each time-step. Thus, the time-step size determines the intervals at which feedback is applied. As has been previously discussed, the continuous feedback response of a real reactor must necessarily be approximated by discrete, step-wise feedback. For transients which involve large reactivity insertions and rapid feedback response, the discrete feedback representation may produce inaccurate results if the intervals between feedback exchanges are too large. Furthermore, the time-step size determines the amount of control rod motion during a time-step and, hence, the magnitude of the reactivity insertion. The continuous reactivity insertion resulting from control rod motion is actually approximated by a series of step changes in reactivity. As the time-step size increases, the error associated with this approximation increases. Another source of potential error associated with the time-step size exists in the "kinetic distortion" terms of the neutronics equations. These terms replace the time derivatives of the fluxes by the product of the flux and a frequency obtained from a point kinetics extrapolation. The error associated with these terms may be increased if the reactivity insertion during a given time step is too large. In short, time-steps of inappropriate length may result in inaccurate TITAN analyses. Therefore, the time-step is a particularly appropriate subject for sensitivity investigation.

One solution to the problem of specifying time-steps which will produce acceptable results with confidence is simply to select extremely small time-steps. The various sources of error in the numerical solutions should be diminished as the time interval is reduced, resulting in solutions which, in the limit of zero time-step, approach the solution of the continuous differential equations. Unfortunately, economic considerations render this solution impractical. Furthermore, good solutions can usually be obtained with much less extravagent time-step requirements. The difficulty lies in selecting time-steps which produce satisfactory results at a reasonable cost. Some codes have automatic time-step selection logic options which monitor relevant parameters and select time-steps in accordance with the transient conditions. TITAN contains a somewhat primitive form of automatic time-step control, as was described in Chapter 4. The behavior of the time-step selection logic has bearing on the sensitivity studies, so a brief review of the logic is in order here.

The time-step selection logic in TITAN is designed to give the user considerable flexibility along with an inherent ability to cope with severe analytical demands. The user supplies nominal maximum and minimum time-step sizes for each time domain, as well as a parameter specifying the number of time-steps smaller than the nominal minimum to be allowed during the time domain. The actual time-step used is either the nominal maximum time-step or a time-step equal to the minimum among all nodes of the axial convective transit times, whichever is smaller. The choice of a time-step less than or equal to the minimum axial convective transit time assures (assuming that the axial velocities are always

limiting) that the Courant stability limit of the hydraulics solution is satisfied. This stability limit will often change during the course of a transient as fluid velocities change, especially under two-phase conditions. The neutronics and the fuel rod conduction solutions are fully implicit numerically and therefore stable for any time-step size. This time-step selection logic ensures that, for any reasonable set of time domain information, a stable TITAN analysis can be performed. It does not, however, ensure that the results will be accurate. It also complicates the assessment of time-step sensitivity, since time-steps may vary during the course of a transient. Nevertheless, there is much which can be learned from studying time-step selection in TITAN.

Table 5.13 summarizes the results of several TITAN BW2C-T rod withdrawal analyses with different time-step sizes (labeled "nominal maximum time-steps") and different axial mesh spacings. All of these analyses were performed with the cusping correction model. Cases 1, 2 and 3 involved ten axial nodes with nominal maximum time-step sizes of 0.05, 0.01 and 0.005 seconds, respectively. Cases 4 and 5 involved twenty axial nodes with nominal maximum time-step sizes of 0.01 and 0.005 seconds, respectively. Finally, Cases 6 and 7 involved thirty axial nodes with nominal maximum time-step sizes of 0.01 and 0.005 seconds, respectively. Table 5.13 also indicates the actual maximum and minimum time-steps and the average time-step used in each analysis. For each axial mesh spacing, the analysis using a nominal maximum time-step size of 0.005 seconds will be considered the best result and used as a basis of comparison.

TABLE 5.13

SENSITIVITY OF TITAN BW2C-T ROD WITHDRAWAL TRANSIENT RESULTS TO TIME-STEP AND AXIAL MESH SIZES

PARAMETER	UNIT	VALUE						
Case #	-	1	2	3	4	5	6	7
Number of axial nodes	-	10	10	10	20	20	30	30
Axial mesh size	m	0.1524	0.1524	0.1524	0.0762	0.0762	0.0508	0.0508
Nominal maximum time-step	s	0.0500	0.0100	0.0050	0.0100	0.0050	0.0100	0.0050
Actual maximum time-step	s	0.0265	0.0100	0.0050	0.0100	0.0050	0.0081	0.0050
Average time-step during transient	s	0.0072	0.0100	0.0050	0.0049	0.0048	0.0030	0.0028
Peak power	kw	522,050.	323,000.	272,900.	232,750.	234,050.	214,830.	240,660.
Time of peak power	s	0.1046	0.1300	0.1350	0.1288	0.1350	0.1343	0.1350
Secondary peak power	kw	5616.2	12,622.	14,162.	19,537.	16,944.	13,729.	12,438.
Time of secondary peak power	s	1.1135	0.8500	0.8450	0.7641	0.7841	0.8906	0.9347
Integrated power	MW-s	13.468	15.221	14.894	14.320	14.920	15.224	15.616
Maximum fuel temperature	°K	2720.5	2539.9	2522.8	2531.9	2534.2	2538.7	2541.2

i) Time-Step Effect

The results shown in Table 5.13 demonstrate that the time-step size can have a significant impact on a TITAN analysis. This is particularly true for the analysis having ten axial nodes (Cases 1, 2 and 3), for which the use of different time-step sizes produced substantial differences in the calculated magnitudes and times of both power peaks and in the integrated powers. Figure 5.35 shows the calculated reactor power as a function of time during the rod withdrawal transient for Cases 1, 2 and 3. The figure shows that Case 1 was particularly different from Cases 2 and 3. As indicated in Table 5.13, Case 1 was one in which the specified nominal maximum time-step size was greater than the convective limit throughout the transient. Thus, the time-step used was always equal to the limiting value and "floated" throughout the analysis. This resulted in relatively large time-steps in the early part of the transient and much smaller time-steps later on when increased boiling produced higher vapor velocities. In the other two cases, the specified nominial maximum time-step sizes were always less than the convective limit, so these were the actual time-steps used.

The differences in the results obtained in Cases 1, 2 and 3 are directly attributable to the differences in time-step sizes, particularly in the early part of the transient. The time and magnitude of the first power peak has a profound effect upon the course of the remainder of the transient. It is also during the period of the initial excursion that the time-step sensitivity can be more clearly seen, since the sharp reduction in time-step following the peak in Case 1 blurs the

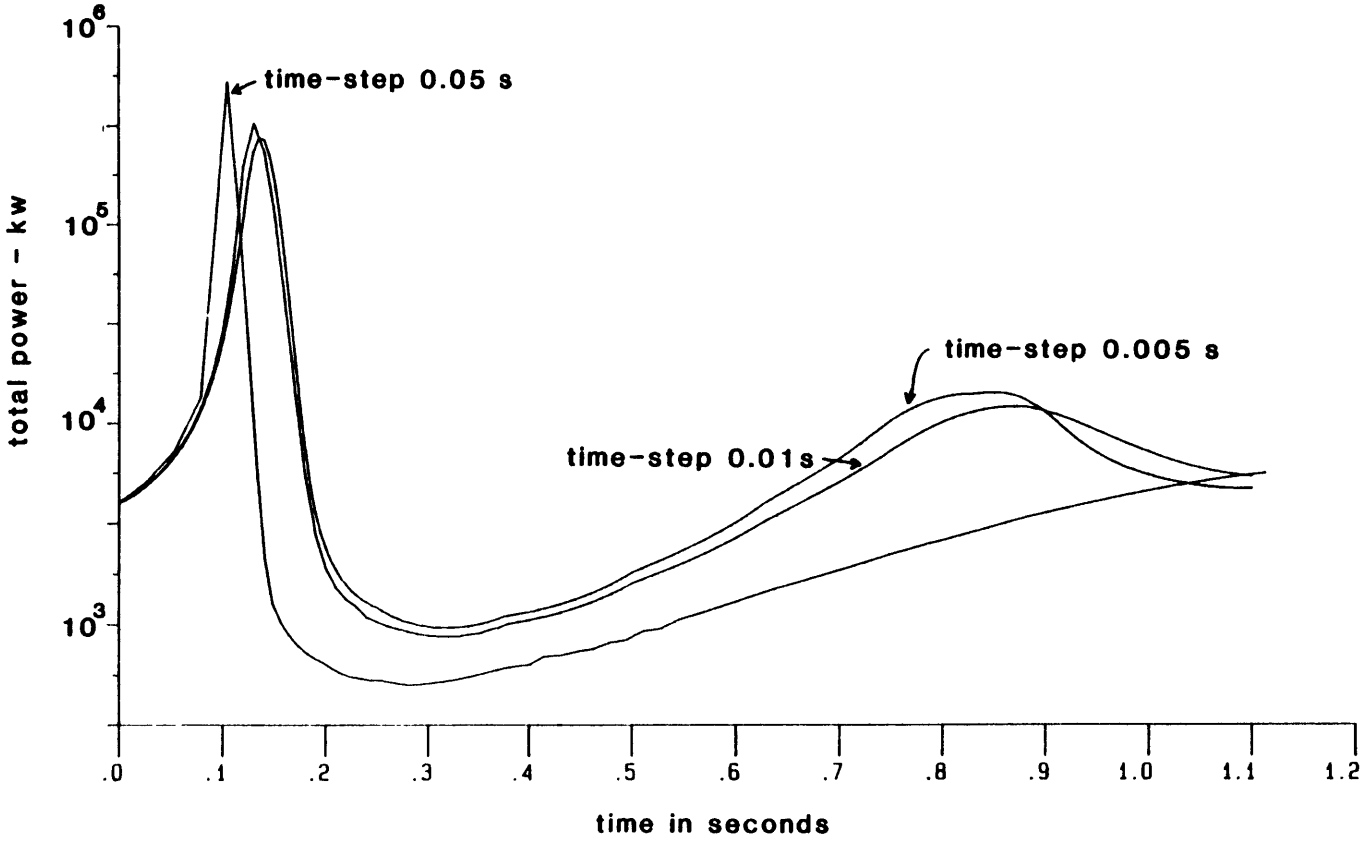

Figure 5.35 BW2C-T Rod Withdrawal, 10 Axial Nodes, TITAN:

Power versus Time for Three Time-step Sizes

distinction between the analyses for the remainder of the transient. An examination of time-step sensitivity during the initial excursion, then, will largely account for the results obtained.

Two effects of reducing the time-step size on the initial excursion have been identified. The first involves the neutronics solution itself. Figure 5.36 shows the power as a function of time for the rod withdrawal as calculated by QUANDRY for time-step sizes of 0.025, 0.01 and 0.005 seconds, with no feedback in each case. The results show that the neutronics solution itself is very sensitive to the time-step size and that a larger time-step produces a more rapid power rise. Both the 0.025s and 0.01s cases were terminated when computer system limits on maximum magnitude of a stored number were exceeded, indicating that the calculated power at the next time-step would have been very large indeed. These results are consistent with those obtained from the TITAN analyses, wherein the case with the largest time-step (Case 1) produced the largest magnitude power excursion at the earliest time and the case with the smallest time-step (Case 3) produced the smallest magnitude power excursion at the latest time.

The second effect involved in reducing the time-step size was the feedback. In Case 1, the time between feedback calculations was relatively large, allowing the larger positive reactivity insertions between each negative reactivity feedback response. This allowed the power to rise higher and faster, as Figure 5.35 shows. It also resulted in hotter fuel, more boiling and, hence, stronger negative feedback to terminate the excursion. As a result, the power decreased more rapidly and to a lower level than in the other two cases. Indeed, Case 1 never attained

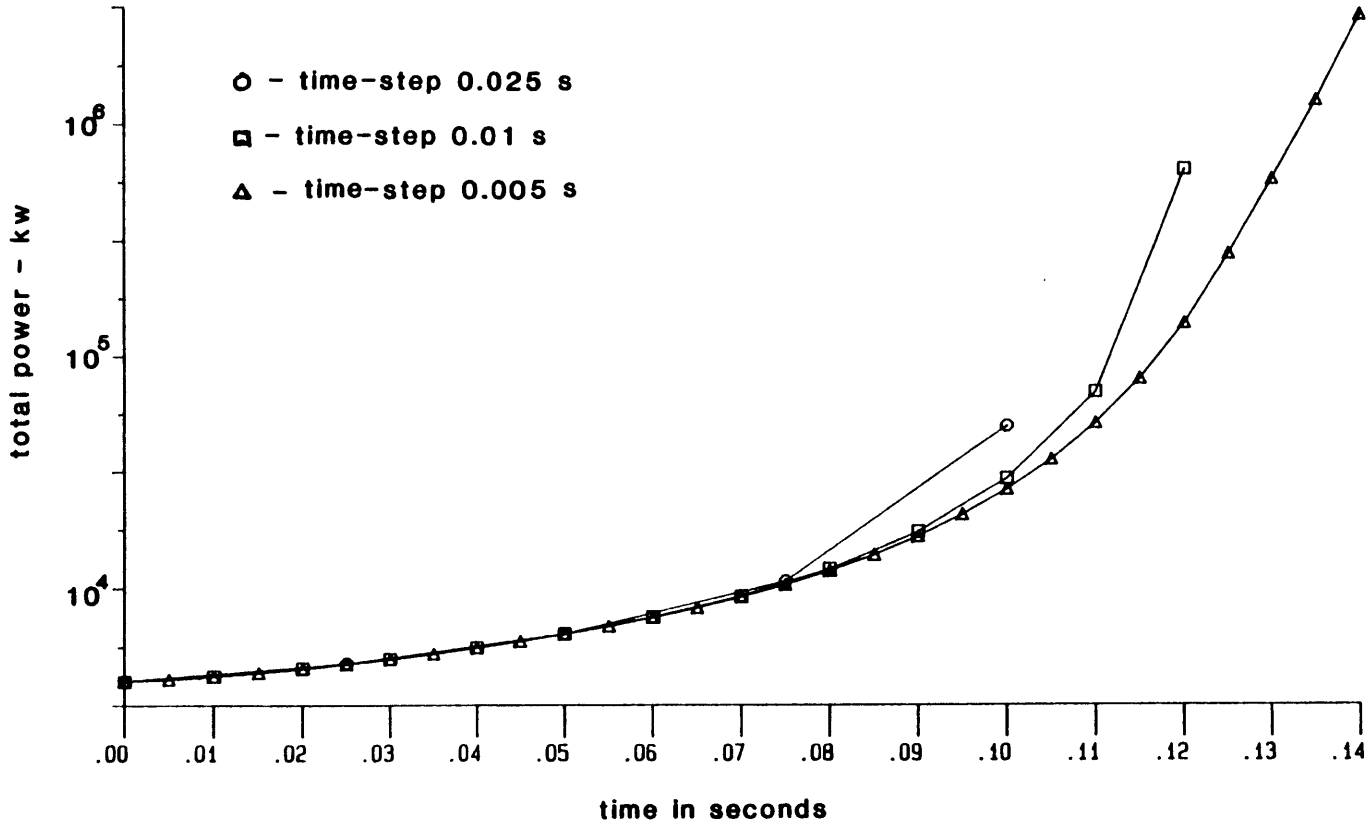

Figure 5.36 BW2C-T Rod Withdrawal, QUANDRY Without Feedback:

Power versus Time for Three Time-step Sizes

the second power peak exhibited in Cases 2 and 3. A similar though much milder effect can be observed in Cases 2 and 3, in which the higher initial peak power (Case 2) produces stronger feedback, lower power following the excursion, and a second peak of lesser magnitude which is delayed in time.

The sensitivity of the results to time-step size was less for a model with twenty axial nodes (Cases 4 and 5) and a model with thirty axial nodes (Cases 6 and 7). Some of the observed effects of smaller time-steps were consistent with those discussed for the ten axial node case; others were not. One consistent trend was that the analyses with shorter time-steps resulted in a later time for the first power peak. Another was that a higher initial peak precedes a second peak which is of lesser magnitude and occurs later. In addition, both the twenty and thirty axial node cases produced a faster rise in power during the initial excursion for the cases with larger time-step sizes. As has been explained, this is characteristic of the neutronics solution and results in the observed earlier peak power. However, the reduction of time-step size did not produce a reduction in the peak power for the twenty and thirty axial node cases. Table 5.13 shows that the peak powers for the twenty axial node model (Cases 4 and 5) differed by less than 0.6%, with the smaller time-step resulting in the higher power. The sensitivity of the peak power to time-step was actually greater for the thirty axial node model, for which the smaller time-step resulted in an increase in power of 12.0%. This result may appear somewhat puzzling, since the reduction in actual time-steps used from Case 6 to Case 7 was less (0.008 to 0.005) than it was from Case 4 to

Case 5 (0.01 to 0.005). The reactor power as a function of time for the initial excursion as calculated with the thirty axial node model with two different time-steps is shown in Figure 5.37. This non-logarithmic plot emphasizes the observed time-step sensitivity. It also clearly shows the large power increases and decreases which occur in one time-step on either side of the peak power. In Case 6, the longer time-steps resulted in power increases of 40 - 50% per time-step at the steepest part. The shorter time-steps of Case 7 limited the power increases to 30 - 35% per time-step. The very abrupt termination of the power rise indicates the dramatic impact of the onset of feedback. Given the extremes in both the rates of power increase and the sudden impact of the feedback, it is not surprising that discrepancies in peak power of the order of 10% were observed. The excellent agreement in peak power seen in Cases 4 and 5 is probably fortuitous. Therefore, no real significance should be attached to the impact of time-step size on the peak powers in these cases.

ii) Axial Mesh Size Effect

The analyses presented in Table 5.13 provide an opportunity to look at the effect of reducing the axial mesh spacing on the BW2C-T rod withdrawal transient. There are several reasons to think that the axial mesh spacing could effect the results. First, this type of sensitivity has already been observed for a simulated turbine trip transient (see Figure 5.29). As was discussed, the increase in the detail with which the thermal-hydraulics is treated affects the feedback. An additional effect is the reduction in the control rod cupsing phenomenon. The

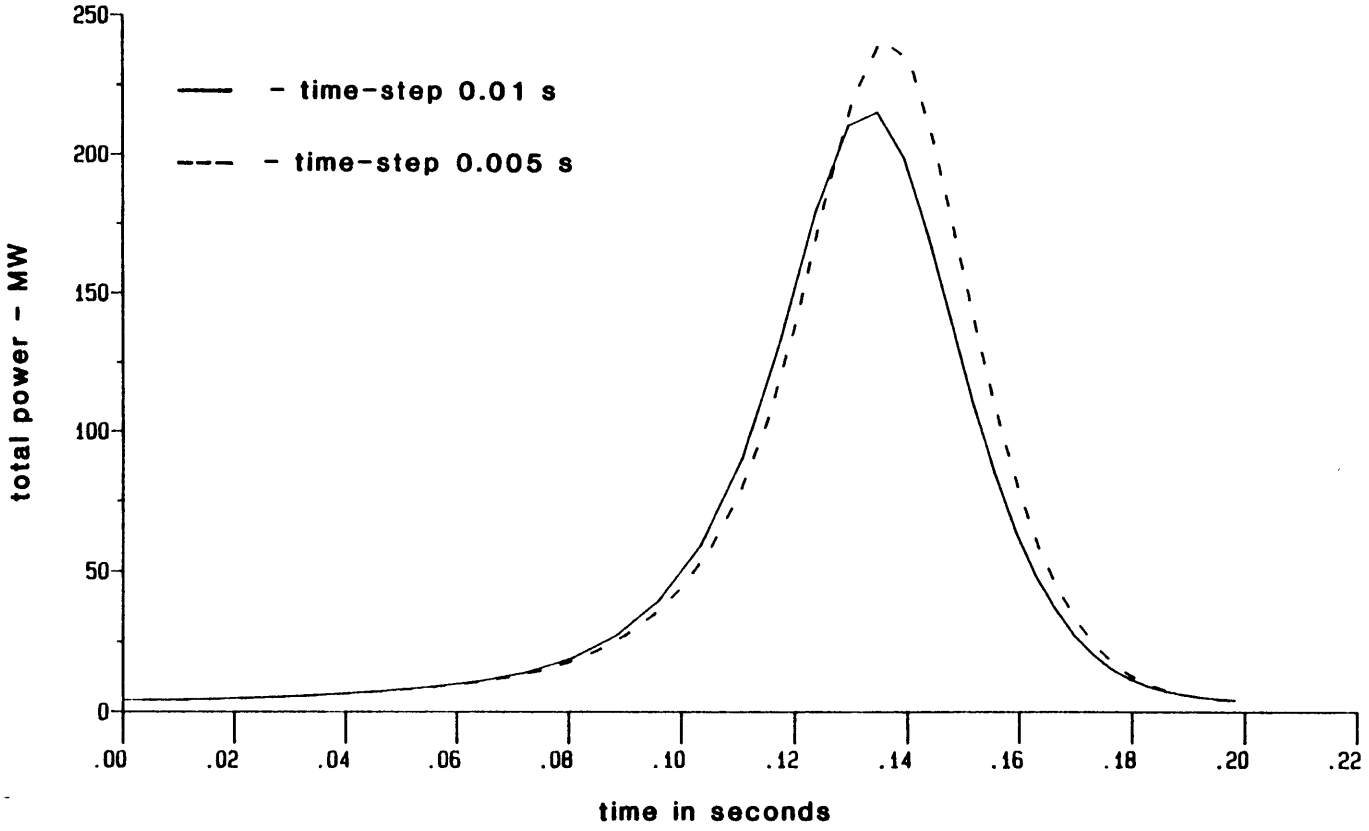

Figure 5.37 BW2C-T Rod Withdrawal, 30 Axial Nodes, TITAN:

Power versus Time for Two Time-step Sizes

cusping phenomenon arises because the motion of a control rod through a node is modeled as a non-spatial perturbation of the homogenized cross sections. Cusping effectively means that the reactivity impact of the control rod withdrawal is undervalued at the beginning and overvalued at the end of the rod motion out of the node. Theoretically, the cusping effect should be reduced as the axial mesh spacing is reduced. Even with the cusping correction model used in these analyses, it is possible that some reduction in cusping could occur as the axial mesh spacing is reduced. Figure 5.38 shows the calculated power as a function of time for models having 10, 20 and 30 axial nodes (Cases 3, 5 and 7, respectively). The maximum time-step size in each case was 0.005 seconds. The results of these three cases were in fairly good agreement. The peak power with 10 axial nodes was 13.4% higher while the 20 axial peak power was 2.7% lower than that with 30 axial nodes. The time of the peak power was the same in each case. None of the other results of Table 5.13 indicate that the basic model with ten axial nodes is improper.

iii) The Cusping Effect

The cusping correction model of TITAN is an option designed to improve the accuracy of the control rod representation. Several additional TITAN analyses of the BW2C rod withdrawal transient without the cusping correction model were performed in order to investigate the impact of the model. Table 5.14 summarizes the results of three pairs of analyses which were identical except for the inclusion of the cusping correction. The table shows that the impact of the model

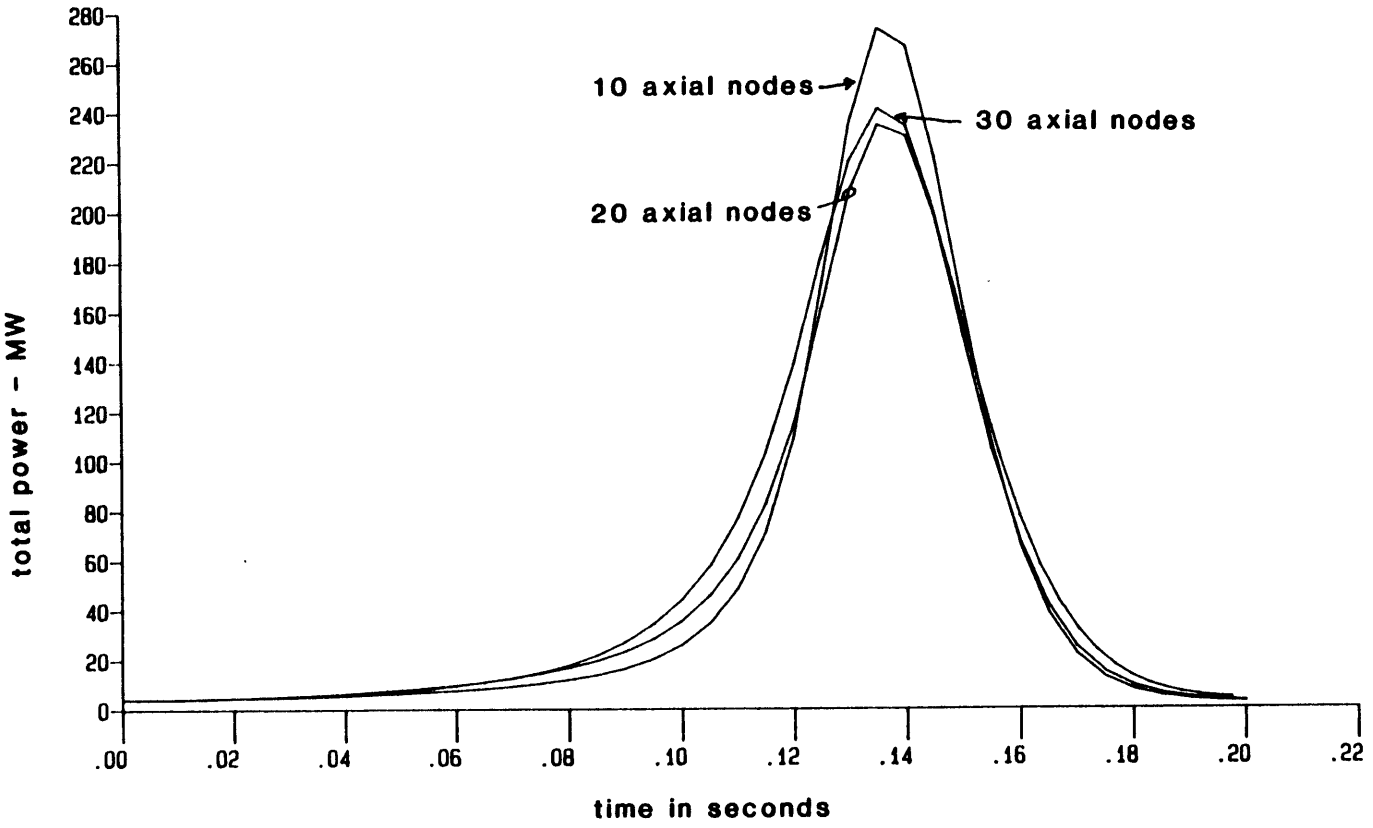

Figure 5.38 BW2C-T Rod Withdrawal, 10, 20 and 30 Axial Nodes, TITAN:

Power versus Time

TABLE 5.14

SENSITIVITY OF TITAN BW2C-T ROD WITHDRAWAL TRANSIENT RESULTS TO CUSPING CORRECTION OPTION/AXIAL MESH SIZE

PARAMETER	UNIT	VALUE					
Number of axial nodes	-	10	10	10	10	20	20
Axial mesh size	m	0.1524	0.1524	0.1524	0.1524	0.0762	0.0762
Cusping correction model	-	yes	no	yes	no	yes	no
Actual maximum time-step	s	0.0265	0.0265	0.010	0.010	0.010	0.010
Peak power	kw	522,050.	6,928,400.	323,000.	296,850.	232,750.	221,200.
Time of peak power	s	0.1046	0.1072	0.1300	0.1300	0.1288	0.1290
Secondary peak power	kw	5616.2	3251.6	12,089.	12,622.	19,537.	20,301.
Time of secondary peak power	s	1.1135	1.1507	0.8700	0.8500	0.7641	0.7590
Integrated power	MW-s	13.468	138.433	15.221	15.123	14.320	14.411

was very significant for the ten axial mode model with a relatively large time-step (0.0265s), but not very significant for the same model with a time step of 0.010s. The analyses with a twenty axial node model and a time-step size of 0.010s were identical for all intents and purposes. The cusping correction, then, would seem to be important for relatively large axial mesh spacings (typical of nodal methods) and large time-steps.

Chapter 6 PWR Control Rod Ejection Analyses

6.1 Introduction

This chapter presents the results of two PWR control rod ejection analyses performed with TITAN. Steady-state results are also discussed. The first control rod ejection transient is identical to one analyzed with MEKIN-B by Brookhaven National Laboratory [C-13]. The second transient is a variation of the BNL problem designed to accentuate three-dimensional effects. These analyses involve challenges and difficulties not present in the test cases of Chapter 5. Therefore, the work in this chapter constitutes a continuation and extension of the development, testing and verification of TITAN.

The PWR control rod ejection accident is caused by a failure in the pressure housing of the control rod drive mechanism. In this event, the rapid depressurization of the volume above the control rod produces a large force which ejects the rod and drive mechanism to a fully withdrawn position. The result is a rapid positive reactivity addition and, hence, a rapid power excursion in the core. The excursion is limited by nuclear feedback (primarily Doppler) and, after a short delay, by the scram of the other control rods. The limiting parameters are maximum local (average) fuel enthalpy, maximum cladding temperature, maximum extent of fuel melting, and peak reactor coolant pressure.

The analyses presented herein address several specific objectives. The first objective was to test TITAN on a problem of realistic size and scope. The previous applications were to a BWR-type problem consisting of only two part-length fuel assemblies. Though this "BW2C" problem was

quite appropriate for code development, debugging, testing and sensitivity studies, TITAN is ultimately intended to be applied to real reactors having many fuel assemblies and more complex geometries. Therefore, it was desirable to demonstrate that TITAN can be successfully applied to a "real" reactor.

An additional concern regarding the application of TITAN to a large problem involves the practical limits of computers and economics. Other three-dimensional coupled codes, particularly those using finite difference neutronics methods, have been subject to very large computer memory requirements and extremely long running times when applied to large problems. Indeed, a major motivation for the development of TITAN was to produce a more economical three-dimensional coupled code. Therefore, the determination of the running time required for the TITAN analysis of a problem of realistic size and scope is also a significant result.

The second objective addressed by the control ejection transients is the further verification of TITAN. The previous transient analyses lacked any independent solutions, so the TITAN results could only be checked for self-consistency and qualitative correctness. The availability of both steady-state and transient analyses by a well known code of comparable capability made these problems ideal for comparison.

The third objective was to exercise certain features of TITAN not used in the previous analyses and to add other features which would improve the code. The most important of these features is the three-dimensional fluid dynamics solution. Thus, a PWR type reactor was called for. The direct moderator heating model was also required for the rod ejection analyses and would be tested in the process. In addition, the analyses

in this chapter required the addition and testing of two new models. The first was the feedback model with quadratic moderator density and control rod position dependence. This model is an improvement over the original linear feedback model in TITAN. The second model added for these analyses was the equilibrium xenon model. The details of both of these models are given in Chapter 4.

The final objective addressed by the PWR control rod ejection analyses was to provide a transient displaying significant spatial changes in the flux. The previous analyses of the BW2C problem exhibited relatively small spatial effects. Since one of the primary advantages of TITAN is its three-dimensional capability, it is desirable to analyze a problem which requires this capability.

6.2 Problem Description

6.2.1 Steady-State

The reactor model used in the BNL MEKIN-B analyses was duplicated to the greatest possible extent for the TITAN analyses. The model is based upon a typical three loop PWR and consists of a full length quarter core, as shown in Fig. 6.1. Each of the forty-seven fuel assemblies is modeled individually, but the lines of symmetry reduce the inner edge assemblies and the central assembly to one-half and one-quarter assembly size, respectively. The locations of the control rods at steady-state are shown in Fig. 6.1 by the shaded regions. Thus, there are three fully inserted control rods and two partially inserted control rods.

Figure 6.2 shows a plan view of the reactor model, including channel

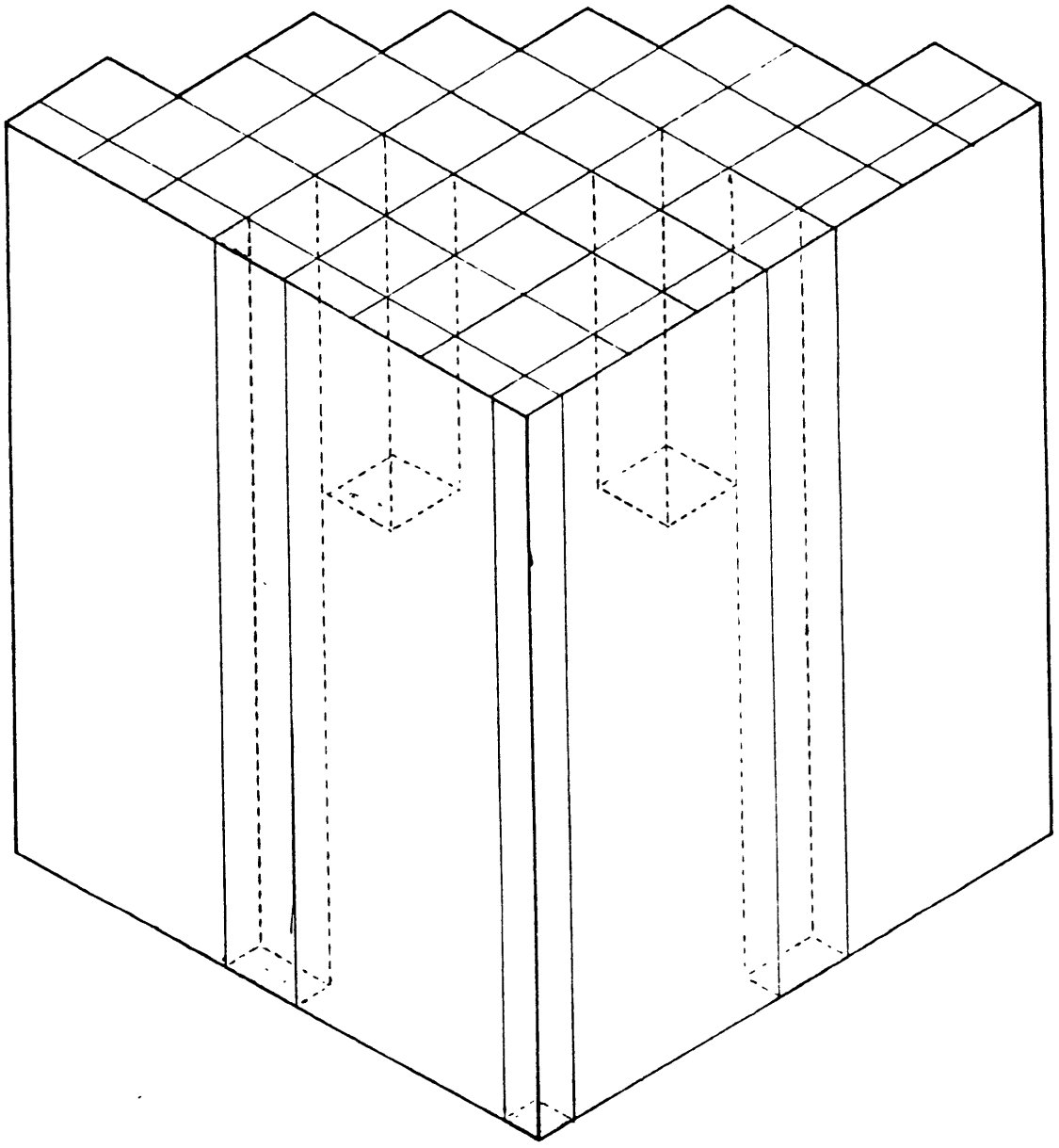

Figure 6.1 Quarter Core PWR Geometry

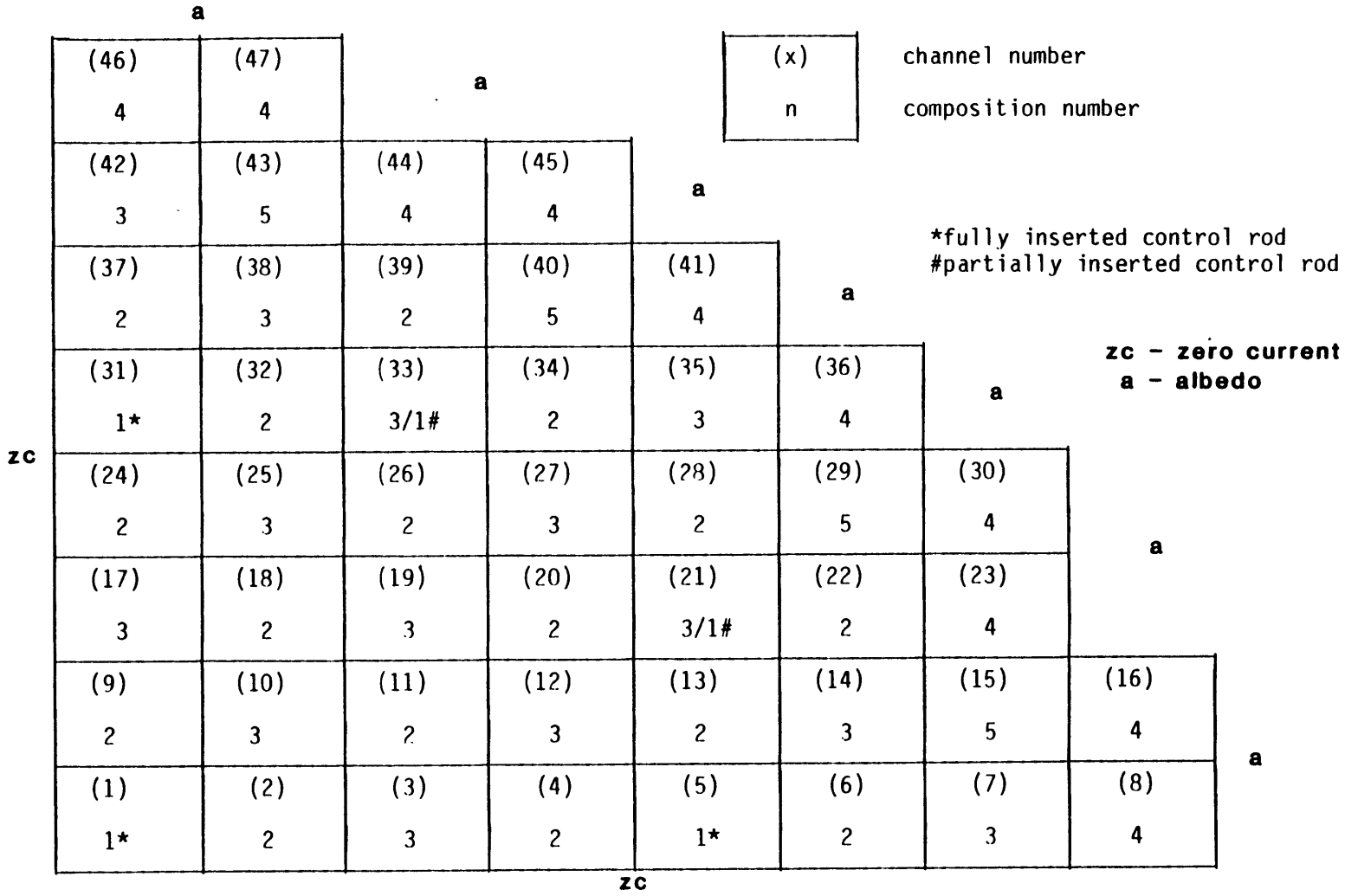

Figure 6.2: Neutronic Boundary Conditions, Channel and Composition Numbers for Quarter Core PWR Problem

numbering convention, neutronic compositions and neutronic boundary conditions. Composition 1 is the same as composition 3 with the addition of a homogeneously distributed control rod. The assembly compositions are uniform axially except where there are partially inserted control rods (channels 21 and 33). The arrangement of fuel assemblies is that of a fresh core with a checkerboard loading pattern.

The nuclear cross sections and feedback coefficients for each composition were produced at BNL using a multi-group, two-dimensional collision probability code. The reference cross sections for each composition are given in Table 6.1. The reflectors and core baffle are not modeled explicitly, but are simulated by albedo boundary conditions. The "interior" vertical surfaces, corresponding to the quarter core lines of symmetry, are modeled by a zero current boundary condition. The values of the horizontal and vertical albedoes and the feedback coefficients for each composition are given in Appendix D.

The reactor model also includes thermal-hydraulic boundary conditions. The reactor inlet is modeled as having a uniform coolant velocity and temperature. At the reactor outlet, a uniform pressure boundary condition is applied. The vertical surfaces are closed to flow and heat transfer.

Table 6.2 summarizes the parameters characterizing the geometry and operating conditions of the steady-state PWR. Additional geometrical and operational parameters are given in Appendix D. In general, these parameters are consistent with the actual reactor upon which the model is based. However, the full power of 2200.0 MW(th) is not consistent

Table 6.1

Reference Nuclear Cross Sections for PWR Problem

Cross Section	Composition 1	2	3	4	5
D_1	1.41049	1.38522	1.30194	1.30711	1.37954
Σ_{R1}	0.29057×10^{-1}	0.26666×10^{-1}	0.26956×10^{-1}	0.26401×10^{-1}	0.26499×10^{-1}
Σ_{21}	0.16467×10^{-1}	0.17316×10^{-1}	0.18401×10^{-1}	0.17325×10^{-1}	0.16840×10^{-1}
$\nu_1 \Sigma_{f1}$	0.48819×10^{-2}	0.58090×10^{-2}	0.49690×10^{-2}	0.64522×10^{-2}	0.65231×10^{-2}
Σ_{f1}	0.18922×10^{-2}	0.22520×10^{-2}	0.19260×10^{-2}	0.25009×10^{-2}	0.25283×10^{-2}
D_2	0.38947	0.39035	0.36544	0.37156	0.39258
Σ_{R2}	0.97647×10^{-1}	0.89259×10^{-1}	0.65934×10^{-1}	0.84521×10^{-1}	0.98429×10^{-1}
$\nu_2 \Sigma_{f2}$	0.864417×10^{-1}	0.10856	0.83647×10^{-1}	0.12551	0.12777
Σ_{f2}	0.35680×10^{-1}	0.44802×10^{-1}	0.34522×10^{-1}	0.51801×10^{-1}	0.52731×10^{-1}

Table 6.2

PWR Geometry and Operating Conditions

Geometry:	
Number of Fuel Assemblies	157
Core Active Length, m	3.6724
Number of Fuel Rods per Assembly	204
Fuel Rod Diameter, mm	10.72
Fuel Assembly Width, m	0.214
Operating Conditions, Power:	
Total Reactor Power, MW(th)	2200.00
Average Linear Heat Generation Rate, kw/m	1.74
Average Power Density, MW/m^3	83.36
Operating Conditions, Thermal-Hydraulic:	
System Pressure, MPa	15.46
Total Core Flow Rate, kg/s	13,290.
Inlet Coolant Temperature, °K	554.80
Operating Conditions, Neutronic:	
Core Burnup, MWd/MTU	≈ 0.0
Soluble Boron Concentration, ppm	825.0
Bank "D" Control Rods, Insertion Depth, m	3.6724
Bank "C" Control Rods, Insertion Depth, m	1.5874
Xenon Microscopic Thermal Neutron Neutron Cross Section, cm^2	2.714×10^{-18}
Xenon + Iodine Yield	0.059
Xenon Decay Constant, 1/S	2.1×10^{-5}

with the control rod configuration shown in Fig. 6.1. Indeed, the actual reactor is limited to approximately 20% power with this control rod configuration. Neverthless, the combination of full power and inserted control rods was selected by BNL in order to produce more adverse power peaking than the actual operating configuration.

The remaining components of the steady-state reactor model are the discretionary choices made by the analyst. The number and type of these options are dependent on the code used. Table 6.3 summarizes the various optional factors in the TITAN and MEKIN-B PWR models. Among the most important of the optional parameters are the mesh spacings. The mesh spacings used in the analyses reflect fundamental differences in the two codes. The TITAN model uses the same mesh spacings for both neutronic and thermal-hydraulics, but MEKIN-B superimposes a separate neutronic mesh upon the thermal-hydraulic model. The nodal neutronics method in TITAN permits a very coarse mesh as shown, but the finite difference neutronic method of MEKIN-B may require a relatively fine mesh to produce accurate results. As a result, the total number of neutronic mesh points (nodes) in the MEKIN-B model is about twenty times that in the TITAN model. The number of thermal-hydraulic nodes in the TITAN model is also less than the MEKIN-B model because of the somewhat larger axial mesh spacings in the TITAN model. The slightly non-uniform axial mesh spacings of the TITAN model allow the partially inserted control rods to occupy an integral number of nodes.

Table 6.3

Modeling Options in TITAN and MEKIN-B PWR Analyses

			TITAN	MEKIN-B
Horizontal Mesh Spacing, cm:	Neutronic		21.402	7.197
	Thermal-Hydraulic		21.402	21.402
Axial Mesh Spacing, cm:	Neutronic	(z = 1-7)	29.786	10.20
		(z = 8-12)	31.748	
	Thermal-Hydraulic	(z = 1-7)	29.786	20.40
		(z = 8-12)	31.748	
Total Number of Mesh Points (Nodes):				
	Neutronic		564	11,916
	Thermal-Hydraulic		564	846
Eigenvalue Convergence Criteria:			1.0×10^{-6}	1.0×10^{-4}
Flux Convergence Criteria:			1.0×10^{-6}	1.0×10^{-4}
Number of Radial Fuel Regions:			4	4
Number of Radial Clad Regions:			1	1
Fuel Thermal Properties:			temperature-dependent	constant
Fuel-Clad Gap Heat Transfer Coefficient, J/m^2-kg-°K			temperature-dependent	constant, h=5678.26
Single-Phase Friction Factor Model:			$0.184\ Re^{-0.2}$	$0.184\ Re^{-0.2}$
Critical Heat Flux Correlation:			W-3*	W-3*
Subcooled Boiling:			yes	no
Two-Phase Model:			two-fluid, MIT interfacial momentum exchange	homogeneous equilibrium, no slip

*Ref. T-5

6.2.2 Control Rod Ejection Transients

The steady-state PWR model described previously forms the basis for two control rod ejection transients. The first transient is initiated by ejecting the central control rod (channel #1) at a constant speed, resulting in a fully withdrawn rod after 0.10 seconds. No scram is modeled. Table 6.4 summarizes the pertinent parameters for the transient calculations. These parameters characterize central control rod ejection analyses performed with TITAN and MEKIN-B. In addition, a second control rod ejection transient was analyzed with TITAN. This transient is initiated by ejecting one of the edge control rods (channel #5) at the same constant speed used for the central control rod ejection. The purpose of this transient is to produce an asymmetric change in the flux shape during the rod ejection, thereby demonstrating the three-dimensional capability of TITAN. The transient parameters of Table 6.4 were also used for the second rod ejection analysis.

6.3 Steady-State Analyses

6.3.1 Results

The quarter core PWR problem was analyzed with TITAN to produce a converged steady-state solution. Table 6.5 presents several of the pertinent parameters characterizing the TITAN convergence and compares them to the corresponding MEKIN-B parameters. The TITAN steady-state calculation was a two-step process, beginning with the convergence of a solution with no channel cross-flow allowed. The final step involved "opening" the channels and completing the analysis with the full three-

Table 6.4

Transient Parameters for Rod Ejection Analyses

Control rod velocity, m/s	36.7
Number of delayed neutron precursor groups	1
Effective delayed neutron fraction	0.00738
Effective delayed neutron decay constant, 1/s	0.4353
Group 1 neutron speed, m/s	1,000,000
Group 2 neutron speed, m/s	4347.8

Table 6.5

Parameters from Steady-State PWR Analyses

Description	TITAN	MEKIN-B
Number of Time-steps	35	—
Time-step Size, s	0.05	
Flow Balance Error, %	0.0688	≈0.0000
Energy Balance Error, %	0.393	0.0004
Neutronic Convergence Criteria Satisfied	yes	no
Reactor Eigenvalue (k_{eff})	0.987113	0.974004
Computer Time, c.p.u. seconds*	5620.19	1286.8
Equivalent Computer Time, Multics cpu-s**	5620.19	≈6434

* TITAN: Multics Honeywell DPS8/70 m
MEKIN-B: CDC 7600

**best estimate of 5 Multics cpu-s per CDC 7600 cpu-s

dimensional hydraulics solution. The feedback parameters were updated and the power shape recalculated throughout this procedure. Convergence of the flux and eigenvalue solutions to the very stringent criteria of Table 6.3 was always obtained. The global flow and energy balances were converged to within 0.1% and 1.0%, respectively. The MEKIN-B analysis produced a thermal-hydraulic solution having a negligible error in the global flow and energy balances. However, the neutronic solution did not satisfy the convergence criteria of Table 6.3 even though the criteria were two orders of magnitude larger than those used in the TITAN analysis. Both TITAN and MEKIN-B calculated a global reactor eigenvalue (k-effective) of less than unity. The TITAN eigenvalue exceeded that of MEKIN-B by 1.3%.

The computing time required for the TITAN and MEKIN-B analyses were comparable, as Table 6.5 shows. The TITAN analysis took advantage of diagonal symmetry in the neutronics calculations and made minor use of the capability of varying the number of thermal-hydraulics time-steps per static neutronics calculation. However, the convergence was by no means optimized with respect to reducing computing time. It is very likely that the computing time required for this analysis, though reasonable, could be significantly reduced with the existing methodology.

The steady-state analyses of the quarter core PWR problem produced thousands of individual results. Obviously, all of these cannot be presented and discussed here. The most important results of these analyses are the power distributions in the core. These will be presented and discussed in detail, especially in Section 6.3.2. Many of the remaining

results of interest are strongly related to the power distribution, particularly fuel temperatures and critical heat flux ratios. Global parameters such as coolant pressure drop and core average feedback parameters are presented and discussed, along with channel parameters such as coolant enthalpy rise and exit flow distribution. Taken together, these results provide a reasonably complete basis for comparing the TITAN and MEKIN-B analyses.

Both TITAN and MEKIN-B produce a fully three-dimensional steady-state power distribution. For purposes of comparison, it is convenient to reduce these distributions to radial and axial power profiles. Figure 6.3 shows the radial power density profiles calculated by TITAN and MEKIN-B. These profiles are produced by dividing the average power density in each fuel assembly by the power density of the average assembly.

The radial profiles produced by TITAN and MEKIN-B are not in good agreement. The TITAN radial profile shows the power to be higher in the core periphery and lower in the core interior than the MEKIN-B profile. In the worst location, the TITAN assembly power prediction exceeds the MEKIN-B assembly power by 46.79%. The average magnitude of the "error" (based upon the MEKIN-B values) in the assembly power predictions is 17.49%. The maximum difference in nodal powers (the MEKIN-B power having been appropriately averaged) was 55.87%. The radial power profiles do not disagree in a random fashion; rather, they show a distinctly different and consistent tilt from the inner to the outer region of the core. Both radial profiles clearly show the presence of the fully inserted control rods. In neither result does the presence of the part-length control

1.401 1.026 36.55	1.142 0.778 46.79			TITAN MEKIN-B Δ%			
1.181 1.107 6.68	1.277 1.118 14.22	1.322 1.059 24.83	0.990 0.717 38.03				
0.984 0.984 -0.02	1.014 1.044 -2.87	1.070 1.029 3.98	1.054 0.964 9.34	0.938 0.715 31.16			
0.482 0.525 -8.21	0.856 0.950 -9.92	0.874 0.959 -8.84	0.999 1.019 -1.96	0.917 0.882 3.99	0.938 0.715 31.16		
0.836 1.036 -19.29	0.881 1.111 -20.71	0.994 1.153 -13.76	0.975 1.119 -12.90	0.999 1.019 -1.96	1.054 0.964 9.34	0.990 0.717 38.03	
0.903 1.208 -25.23	0.983 1.236 -20.48	0.972 1.235 -21.30	0.994 1.153 -13.76	0.874 0.959 -8.84	1.070 1.029 -3.98	1.322 1.059 24.83	
0.824 1.090 -24.39	0.875 1.185 -26.20	0.983 1.236 -20.48	0.881 1.111 -20.71	0.856 0.950 -9.92	1.014 1.044 -2.87	1.277 1.118 14.22	1.142 0.778 46.79
0.448 0.583 -23.12	0.824 1.090 -24.39	0.903 1.208 -25.23	0.836 1.036 -19.29	0.482 0.525 -8.21	0.984 0.984 -0.02	1.181 1.107 6.68	1.401 1.026 36.55

Figure 6.3: PWR Steady-State, TITAN and MEKIN-B:
Normalized Assembly Power Densities

rods make an appreciable impact on the radial power profile. Despite the existence of a few locations where the calculated assembly power densities are in good agreement, the two codes produced radial power shapes which are fundamentally different. This is discussed in detail in later sections.

A comparison of the TITAN and MEKIN-B axial power profiles is shown in Fig. 6.4. These profiles are calculated by dividing the average power density in each radial plane by the core average radial plane power density. The two axial profiles are very similar, especially in view of the substantial disagreement in the radial power profiles. Indeed, when the eighteen radial planes of the MEKIN-B analysis are reduced to twelve planes equivalent to the TITAN model, the maximum difference in planar power density is 5.52% and the average of the magnitudes of the differences is approximately 3%. Both codes predict a strong bottom peak, consistent with the presence of the two partially inserted control rods.

A comparison of selected TITAN and MEKIN-B thermal-hydraulic results for the quarter core PWR problem is given in Table 6.6. Since the two power distributions are significantly different, local values for many of the thermal-hydraulic parameters are also quite different. However, as Table 6.6 shows, global parameters such as the core average moderator temperature and density are in reasonably good agreement. TITAN predicted a significantly lower core average fuel temperature than did MEKIN-B because TITAN used temperature-dependent fuel properties and fuel-to-clad heat transfer coefficients.

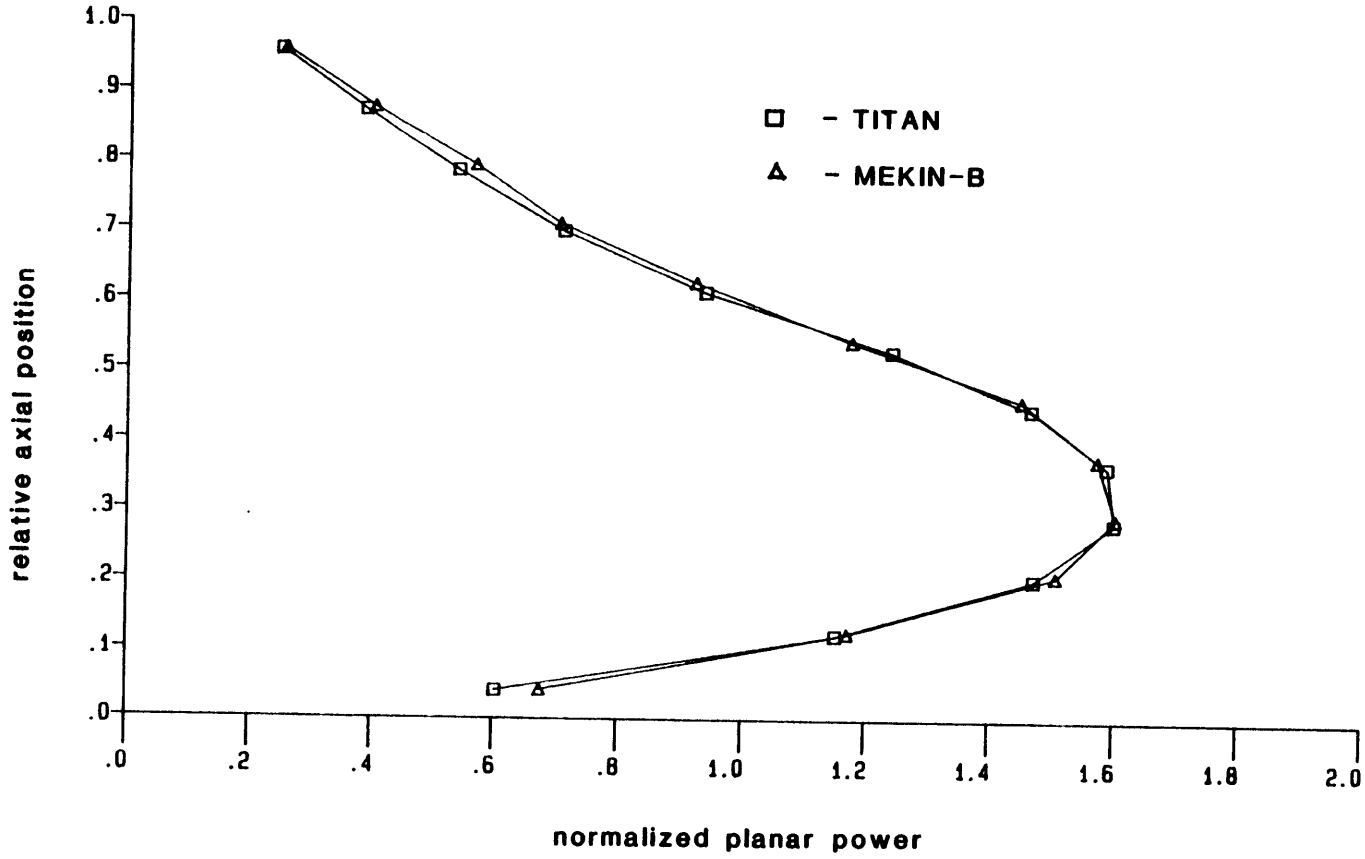

Figure 6.4 PWR Steady-state Axial Power Profile: TITAN and MEKIN-B

Table 6.6

Selected Thermal-Hydraulic Results for Quarter Core PWR Problem

	TITAN	MEKIN-B
Core Average Fuel Temperature, °K	776.61	932.04
Core Average Moderator Temperature, °K	573.81	572.04
Core Average Moderator Density, kg/m^3	724.0	712.0
Core Average Pressure Drop, MPa	0.102	0.155
Maximum Linear Heat Generation Rate, kw/m	3.75	3.39
M.L.H.G.R. Location: (channel #; axial level)	(8,46;4/12)	(19;7/18)
Maximum Pellet Average Fuel Temperature, °K	1065.07	1263.01
Maximum Centerline Fuel Temperature, °K	1506.9	(1)
Maximum Cladding Temperature, °K	613.9	611.76
M.C.T. Location: (channel #; axial level)	(8,46;6/12,7/12)	(19;10/18)
MDNBR	(2)	4.30
MDNBR Location: (channel#; axial level)	(2)	(19;7/18)

Notes:

(1) MEKIN-B centerline temperatures were available for only five channels out of forty-seven, none of which contains the peak power node. The maximum fuel centerline temperature among the five available channels was approximately 1560°K.

(2) No reliable MDNBR calculations were obtained in the TITAN analysis because of a coding error in the W-3 correlation. This has subsequently been corrected.

In addition, the two codes differed considerably in their prediction of core average pressure drop. This is probably due to differences in the models for form losses associated with grid spacers.

The remaining parameters in Table 6.6 are safety-related and strongly dependent on the power distribution. The TITAN analysis produced a somewhat higher local peak power at a different radial location than did MEKIN-B. In keeping with the similarity of the axial power profiles, the axial locations of the peak powers are roughly the same. Despite the lower peak power, the MEKIN-B maximum fuel temperatures were higher than those of TITAN. Thus, the differences in the fuel rod models were more significant with respect to maximum fuel temperature than were the power shape discrepancies. Of course, the power distributions were also affected by the fuel rod models. The differences in power distribution also did not result in significant differences in the peak cladding temperatures, as shown in Table 6.6. The axial locations of the peak cladding temperatures were in good agreement, but the radial locations were not.

The effect of the radial power distributions can be seen clearly in Fig. 6.5, which shows the coolant enthalpy rise for each channel as calculated by TITAN and MEKIN-B. The correspondence between the channel enthalpy rises and the channel powers (Fig. 6.3) is very strong, indicating the effect of flow between channels is small. This is affirmed by Fig. 6.6, which shows the exit coolant mass fluxes for each channel as calculated by TITAN and MEKIN-B. In both analyses the inlet mass fluxes were uniform. The figure shows that the TITAN and MEKIN-B exit mass fluxes

227.29 165.70 37.17	185.65 126.63 46.61			TITAN MEKIN-B Δ%			
190.75 179.42 6.31	218.35 191.05 14.29	214.41 171.52 25.01	160.81 116.62 37.89				
167.92 168.03 -0.07	163.56 169.19 -3.33	182.75 176.17 3.74	179.88 164.54 9.32	152.13 116.16 30.97			
77.76 87.32 -10.95	145.68 162.45 -10.32	141.08 155.70 -9.39	170.27 174.54 -2.45	147.71 143.14 3.19	152.13 116.16 30.97		
142.17 177.56 -19.93	141.76 180.59 -21.50	169.43 197.80 -14.34	157.10 181.75 -13.56	170.27 174.54 -2.45	179.88 164.54 9.32	160.81 116.62 37.89	
145.26 195.94 -25.87	167.45 212.22 -21.10	156.56 200.82 -22.04	169.43 197.80 -14.34	141.08 155.70 -9.39	182.75 176.17 3.74	214.41 171.52 25.01	
140.04 186.40 -24.87	140.57 192.22 -26.87	167.45 212.22 -21.10	141.76 180.59 -21.50	145.68 162.45 -10.32	163.56 169.19 -3.33	218.35 191.05 14.29	185.65 126.63 46.61
78.59 104.76 -24.98	140.04 186.40 -24.87	145.26 195.94 -25.87	142.17 177.56 -19.93	77.76 87.08 -10.70	167.92 168.03 -0.07	190.75 179.42 6.31	227.29 165.70 37.17

Figure 6.5: PWR Steady-state, TITAN and MEKIN-B: Channel Enthalpy Rises, MJ/kg

3133.6 3169.6 -1.14	3133.6 3194.0 -1.89						
3179.1 3161.5 0.56	3084.9 3097.7 -0.41	3144.5 3166.9 -0.71	3148.6 3200.8 -1.63				
3111.1 3114.0 -0.09	3196.8 3169.6 0.86	3106.7 3109.9 -0.10	3108.1 3116.7 -0.28	3153.9 3202.1 -1.51			
3235.1 3218.4 0.52	3125.4 3118.1 0.23	3211.3 3180.4 0.97	3113.9 3113.3 0.02	3205.7 3185.9 0.62	3153.9 3200.8 -1.51		
3124.2 3107.2 0.55	3208.4 3162.8 1.44	3114.1 3095.0 0.62	3201.7 3162.8 1.23	3113.9 3111.3 0.02	3108.1 3116.7 -0.28	3148.6 3200.8 -1.63	
3204.8 3150.6 1.72	3113.6 3084.1 0.96	3200.8 3147.9 1.68	3114.1 3095.0 0.62	3211.3 3180.4 0.97	3106.7 3110.0 -0.10	3144.5 3166.9 -0.71	
3124.1 3101.8 0.72	3208.1 3152.0 1.78	3113.6 3084.1 0.96	3208.4 3162.8 1.44	3125.4 3118.1 0.23	3196.8 3169.6 0.86	3084.9 3097.7 -0.41	3133.6 3194.0 -1.89
3105.9 3126.2 -0.65	3124.1 3101.8 0.72	3204.8 3150.6 1.72	3124.2 3107.2 0.55	3235.0 3218.4 0.52	3111.1 3114.0 -0.09	3179.1 3161.5 0.56	3133.6 3169.6 -1.14

TITAN
MEKIN-B
Δ%

uniform inlet mass flux: 3148.5 kg/m^2-s

Figure 6.6: PWR Steady-State, TITAN and MEKIN B: Channel Exit Mass Fluxes, kg/m^2-s

differed by at most 1.89%. When the channel exit mass fluxes are compared to the inlet mass flux, the maximum change for TITAN and MEKIN-B is 2.75% and 2.29%, respectively. Thus, the cross-flow is not particularly strong and both codes produce similar results.

The steady-state analyses of the quarter core PWR problem by TITAN and MEKIN-B produced distinctly different results. The focus of the disagreement between the two codes is the radial power distribution. There are three possible explanations for the differences, each of which could be wholly or partly responsible:

1. Inconsistencies between TITAN and MEKIN-B,
2. Errors in one or both of the codes, and
3. Inappropriate reactor models.

Each of these possible sources of disagreement are explored in the following section.

6.3.2 Potential Sources of Disagreement

6.3.2.1 Inconsistencies Between TITAN and MEKIN-B

The first of the possible causes of disagreement between TITAN and MEKIN-B are inconsistencies between the physics or numerics of the codes. Of course, there are many differences in the two codes, some of which are potentially significant. Some of these have been previously discussed in Appendix A. However, the basic physical processes are treated very similarly in TITAN and MEKIN-B. Both solve the two-energy-group neutron diffusion equation in three dimensions. Both solve the equations of conservation of mass, momentum and energy for the coolant and the one-

dimensional heat conduction equation for the fuel. Both couple the neutronic and thermal-hydraulic equations via the dependence of nuclear cross sections on fuel temperature, coolant temperature and coolant density. The differences come in some of the specific details of how these basic physical processes are simplified or approximated, in the constitutive relations required to close the equation sets, and in the numerical solution methods. For example, the thermal-hydraulic portions of TITAN and MEKIN-B differ in their treatment of two-phase flow, in the calculation of flow in the horizontal plane, in certain aspects of the fuel-to-coolant heat transfer package, in the available options for the fuel temperature calculations, and in the method and capabilities of the fluid dynamics solution. Since the quarter core PWR problem involves single-phase liquid, no reverse flow or sonic fluid velocities, no critical heat flux or subcooled boiling, and relatively small cross-flows, only the fuel temperature calculation could be a significant contributor to the observed discrepancies. As Table 6.6 shows, the TITAN core average and maximum fuel temperatures are lower than those obtained with MEKIN-B. This undoubtedly had some effect on the power distribution through the Doppler feedback mechanism. However, it is implausible that a combination of the observed discrepancy in radial power shape and the agreement in axial power shape could be the result of inconsistent fuel temperature calculations.

Perhaps the most significant difference between TITAN and MEKIN-B lies in their neutronics portions. TITAN solves a nodal form of the diffusion equations, while MEKIN-B solves a finite difference approximation. The numerical methods used to solve these equations are also

different. However, these methods, when properly applied, should produce very similar results. This has been demonstrated both theoretically and experimentally [S-1]. Therefore, there is no fundamental inconsistency between the neutronics portions of TITAN and MEKIN-B (when properly applied).

The final area of potential inconsistency between TITAN and MEKIN-B is the feedback models. However, the exact feedback model used in MEKIN-B was added to TITAN expressly to perform the quarter core PWR analysis. Furthermore, an equilibrium xenon model was also added to ensure that the two calculations were as consistent as possible. In summary, the results cannot be explained by inconsistencies in TITAN and MEKIN-B. In theory they should be capable of producing very similar results for the quarter core PWR problem.

6.3.2.2 Programming Errors in TITAN or MEKIN-B

The consistency of the physical modeling in TITAN and MEKIN-B could be undermined by the existence of programming errors ("bugs"). It is therefore possible that the differences in the observed results are attributable to such errors. For example, the disparity in radial power shapes suggests that one of the codes might not be handling the horizontal neutronic boundary conditions correctly. Another possibility is that the association of neutronic parameters with node locations was not done properly. A large number of other possible sources of error can also be imagined. The direct way to investigate the spectrum of possible errors is to perform a systematic check of the relevant sections of the

codes. This is a difficult and time-consuming task for codes of the complexity of TITAN and MEKIN-B. In fact, the lack of a copy of MEKIN-B rendered this approach impossible. In the case of TITAN, some checking was performed. The neutronics portion was exercised without any feedback to demonstrate agreement with QUANDRY alone. This showed that no errors were introduced to the neutronics during the programming of TITAN. Furthermore, the new feedback and equilibrium xenon models were carefully checked for errors. Unfortunately, such checking can never practically rule out the possibility of error.

A better approach to the isssue of finding errors in TITAN or MEKIN-B is to test the codes against experiments and other codes, thereby finding errors empirically. There is apparently nothing unique about the quarter core PWR problem, so any errors responsible for the observed results should also produce similar problems in other analyses. When the performance of both TITAN and MEKIN-B in other applications is considered, the likelihood of significant errors seems remote. MEKIN [B-2] and its offspring (SAI-MEKIN [G-3], MEKIN-B [A-1] and BWKIN [M-3]) have been tested, compared with experimental data and analytic results, and used in academic, national laboratory and industrial settings. No problems or errors have been reported which could account for the results obtained in this chapter. TITAN, on the other hand, is a relatively new code which lacks the amount of verification and experience of MEKIN-B. Nevertheless, a comparison of steady-state results for the two channel BW2C problem with those obtained with MEKIN showed good agreement (see Chapter 5). Furthermore, the component parts of TITAN have been well tested and

shown to be reliable (see Chapter 3). Though this does not rule out the possibility of errors contributing to the results, the empirical evidence suggests that the problem may lie elsewhere.

6.3.2.3 Inappropriate Reactor Models

The final possible source of the differences in the TITAN and MEKIN-B results is the "reactor model." In this context, the reactor model means the set of data and modeling options making up the input data for each analysis. For our purposes, the reactor models can be inappropriate in two different senses. The first requirement of the reactor model is that it faithfully represent the actual reactor being analyzed. In this case, the "reactor" is really defined by the MEKIN-B input data. Thus, the first test of appropriateness is simply whether the TITAN input faithfully represents the MEKIN-B input. The second requirement of the reactor model is that the optional aspects of the input be consistent with the requirements of the given computer code. TITAN and MEKIN-B contain approximations which place certain restrictions on the way a reactor can be represented. An inappropriate reactor model can cause the inherent approximations to be poor ones and result in erroneous results. The appropriateness (in both senses) of the reactor models is discussed in the remainder of this sub-section.

The TITAN reactor model should faithfully represent the same "reactor" as the MEKIN-B model. Otherwise, agreement in the analytical results cannot be expected. The careful interpretation and reproduction of the MEKIN-B reactor model was the first step of the process leading to the

results of this chapter. The TITAN model was based upon the actual input used in the MEKIN-B analysis, as supplied by BNL. Much of the data was directly transferable from MEKIN-B to TITAN. Some of the data required transformations, including conversion from English to SI units and the recasting of neutronic albedo boundary conditions into $\overline{\phi} = \overline{\overline{\alpha}}\overline{J}$ form from $\overline{J} = \overline{\overline{B}}\ \overline{\phi}$ form.

The preparation of the input data was checked several times to ensure consistency with the MEKIN-B reactor model. The optional choices in the TITAN model were generally chosen to match those of the MEKIN-B model, as shown in Table 6.3. The most significant differences in the optional aspects of the reactor models are the neutronic mesh spacings. Of course, these should not be the same because of the two different neutronic methods of TITAN and MEKIN-B. The question of whether these mesh spacings are appropriate falls in the second category and is discussed in succeeding paragraphs. Otherwise, the TITAN reactor model seems faithful to the "reactor" as defined by the MEKIN-B input data.

The appropriateness of each reactor model for the given code remains to be examined. The only area of uncertainty in this regard is the choice of neutronic mesh spacings. Since the discrepancies in the steady-state results are primarily related to the horizontal power profile, the appropriateness of the horizontal mesh spacings bears investigation.

The horizontal mesh spacings used in the TITAN reactor model (21.4 cm) are typical for a code having a nodal neutronics method. The

accuracy of the quadratic analytic nodal method has been extensively tested with horizontal mesh spacings of 10-20 cm (see Chapter 3). In particular, five benchmark calculations with horizontal mesh spacings greater than or equal to 20 cm produced maximum assembly power errors of 0.94%, 2.59%, 1.91%, 0.28% and 0.69% [S-1]. Of course, nodal methods were developed specifically to yield accurate results with large mesh spacings, thereby achieving a reduction in computational effort over fine mesh calculations. Finite difference methods, on the other hand, often require relatively small mesh spacings to produce accurate results. For example, MEKIN (neutronics only) required horizontal mesh spacings of 2.0 cm and 2.5 cm respectively, for the 2-D IAEA PWR [A-5] and the 2-D LRA BWR benchmark problems to produce reasonable results. Even with these small mesh spacings, the results were less accurate than QUANDRY results with horizontal mesh spacings of 20 cm and 15 cm, respectively [S-1, H-6]. Similarly, the VENTURE [A-5] finite difference neutronics code was less accurate with a 1.67 cm horizontal mesh spacing than was QUANDRY with a 20 cm horizontal mesh spacing when both codes analyzed the same benchmark problem. In light of these results, the 7.2 cm horizontal mesh spacings of the MEKIN-B quarter core PWR model seem rather large.

A comparison of the horizontal mesh spacings used in the MEKIN-B analysis to those used in previous benchmark calculations raises questions but does not demonstrate the model to be inappropriate. The mesh spacing requirements are rather problem dependent, so one must be careful in judging one problem on the basis of others. However, it is clear from

both empirical and theoretical considerations that finite difference methods cannot be expected to produce accurate results with large mesh spacings for many realistic reactor problems. This is because of the heterogeneity of reactors and the resultant spatial character of the neutron flux. The major approximation inherent in finite difference methods is that spatial flux derivatives are given by the slope of the flux between neighboring points. This approximation is subject to a truncation error which is dependent on the mesh spacing and the spatial behavior of the actual neutron flux. Finite difference methods also have the property that the solution converges to a unique limit as the mesh spacing in reduced [H-3]. As a result, the largest appropriate mesh size for a given problem can be determined empirically by reducing the mesh size until the solution remains unchanged. Barbehenn [B-10] used this approach to study mesh spacing requirements of MEKIN for a series of simple test problems. MEKIN was shown to be most sensitive to horizontal mesh spacing when the reactor is heterogeneous in the horizontal plane (as theory will predict). It was concluded that MEKIN solutions converge to the "correct" solution in an approximately linear manner as the spatial mesh size is reduced. Furthermore, if albedo boundary conditions are used, a horizontal neutronic mesh of 2.5 cm or less is required to give region powers accurate to 1%. These results tend to indicate that the MEKIN-B horizontal mesh of 7.2cm may not be adequate because the reactor is highly heterogeneous in the horizontal plane and also uses albedo boundary conditions. However, the results of Barbehenn do not conclusively show that the

horizontal mesh spacings are the source of the disagreement between TITAN and MEKIN-B. Nevertheless, there is ample reason to suspect that this is the case. Accordingly, a horizontal mesh sensitivity study was performed and is presented in the next section.

6.3.3 Horizontal Neutronic Mesh Spacing Study

The issue of horizontal mesh spacings in both the TITAN and MEKIN-B analyses was investigated directly by a series of calculations with a recent version of QUANDRY [S-5]. This version incorporates discontinuity factors in the nodal solution and has an option which reduces the nodal solution to a solution of the finite difference form of the neutron diffusion equations. Thus, it was possible to compare directly the nodal and finite difference solutions for a given mesh spacing and to determine what mesh spacing is required to produce a spatially converged solution with each method.

Since the most significant discrepancy between the TITAN and MEKIN-B results is the horizontal power distribution, a two-dimensional (x-y) version of the quarter core PWR was used for the mesh spacing sensitivity studies. The two-dimensional model consists of a single horizontal plane from the three-dimensional model, with neutronic compositions and boundary conditions as shown in Fig. 6.2. The two fuel assemblies containing partially inserted control rods in the three-dimensional model are assumed to contain control rods in the two-dimensional model. The discontinuity factors were all given as unity, so the original analytic nodal solution was obtained. All of the two-dimensional analyses were neutronics-only.

The actual horizontal mesh spacings used in the TITAN and MEKIN-B analyses were tested first in the two-dimensional model. Figure 6.7 shows the normalized fuel assembly powers produced with the analytic modal method using a horizontal mesh spacings of 21.6 cm and with the finite difference method using a horizontal mesh spacing of 7.2 cm. The results show the same type of discrepancy as the TITAN and MEKIN-B results. The nodal method predicts higher power in the peripheral fuel assemblies and lower power in the interior fuel assemblies than does the finite difference method. The results strongly imply that the root of the discrepancies seen between TITAN and MEKIN-B is the neutronic model/mesh spacing choice.

In order to clarify the issue, a series of mesh spacing sensitivity studies were performed with both the nodal and finite difference methods. Most of these analyses were performed by Dr. Kord S. Smith of Argonne National Laboratory, Idaho Falls, Idaho [S-11].

Figure 6.8 shows the normalized assembly power results for the analytic nodal method mesh spacing sensitivity study. Steady-state analyses were performed with one, four (2 x 2), nine (3 x 3) and twenty-five (5 x 5) nodes per fuel assembly. The 5 x 5 case was taken to be the reference result and the other results are given in terms of error with respect to the reference. Figure 6.8 shows that the nodal method exhibited some sensitivity to horizonatal mesh spacing in reducing from 21.6 cm to 10.8 cm, but was essentially spatially converged at that point. The maximum assembly power error for the case corresponding to the TITAN model (one node per fuel assembly)

21.6 cm nodal
7.2 cm finite difference

2.173 1.366	1.695 1.010						
1.690 1.365	1.761 1.336	1.627 1.167	1.081 0.725				
1.195 1.079	1.145 1.075	1.053 0.921	1.008 0.850	0.868 0.634			
0.443 0.506	0.698 0.828	0.428 0.464	0.760 0.782	0.800 0.739	0.868 0.634		
0.687 1.099	0.680 1.110	0.685 1.001	0.691 0.913	0.760 0.782	1.008 0.850	1.081 0.725	
0.747 1.401	0.799 1.400	0.749 1.287	0.685 1.001	0.428 0.464	1.053 0.921	1.627 1.167	
0.686 1.307	0.725 1.411	0.799 1.400	0.680 1.110	0.698 0.828	1.145 1.075	1.761 1.336	1.695 1.010
0.365 0.682	0.686 1.307	0.747 1.401	0.687 1.099	0.443 0.506	1.195 1.079	1.690 1.365	2.173 1.366

Figure 6.7: Two-Dimensional PWR Steady-State, QUANDRY, No Feedback: Transverse Power Profile, Nodal and Finite Difference Methods, Original Mesh Spacings

2.85	0.29						
0.18	-0.58						
-0.09	-0.45						
2.112	1.690						
1.75	2.48	2.16	-0.78				
0.20	0.21	0.01	-0.61				
-0.01	-0.10	-0.18	-0.43				
1.661	1.718	1.592	1.089				
0.51	1.39	2.68	3.54	0.47			
0.28	0.30	0.34	0.21	-0.65			
0.10	0.08	0.05	-0.14	-0.59			
1.189	1.129	1.026	0.973	0.864			
-0.96	-1.80	-0.36	2.05	5.31	0.47		
0.15	0.14	0.23	0.42	0.43	-0.65		
0.21	0.20	0.17	0.12	-0.05	-0.59		
0.448	0.706	0.430	0.744	0.760	0.864		
-4.81	-4.42	-3.04	-0.82	2.05	3.54	-0.78	
-0.03	-0.08	0.07	0.18	0.42	0.21	-0.61	
0.38	0.34	0.33	0.22	0.12	-0.14	-0.43	
0.722	0.711	0.706	0.696	0.744	0.973	1.089	
-6.68	-6.08	-4.63	-3.04	-0.36	2.68	2.16	
-0.21	-0.10	-0.12	0.07	0.23	0.34	0.01	
0.43	0.45	0.37	0.33	0.17	0.05	-0.18	
0.800	0.851	0.786	0.706	0.430	1.026	1.592	
-7.26	-6.81	-6.08	-4.42	-1.18	1.39	2.48	0.29
-0.19	-0.23	-0.10	-0.08	0.14	0.30	0.21	-0.58
0.48	0.45	0.45	0.34	0.20	0.08	-0.10	-0.45
0.741	0.778	0.851	0.711	0.706	1.129	1.718	1.690
-6.88	-7.26	-6.68	-4.81	-0.96	0.51	1.75	2.85
-0.21	-0.19	-0.21	-0.03	0.15	0.28	0.20	0.18
0.49	0.48	0.43	0.38	0.21	0.10	-0.01	-0.09
0.392	0.741	0.800	0.722	0.448	1.189	1.661	2.112

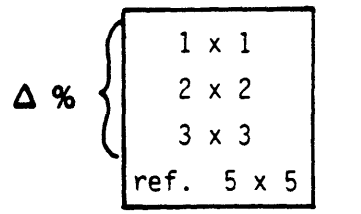

Figure 6.8
Two-dimensional PWR Steady-state, QUANDRY, No Feedback: Transverse Power Profile, Nodal Method with Four Mesh Spacings

was 7.26%. The magnitude of this error is much larger than any previously observed in other benchmark problems. This indicates that the two-dimensional problem is particularly challenging one, so that the previously established standards of accuracy for the analytic nodal method may not hold.

The combination of a checkerboard fuel pattern, fully inserted control rods and albedo boundary conditions is probably responsible for the unprecedented nodal mesh spacing sensitivity. It is of some consolation that the maximum error occurred at a relatively low power location, while the errors at the high power locations were always conservative. Furthermore, the fact that the nodal method produces a spatially converged solution with four nodes per assembly means that a reasonable revision of the TITAN model could be done if very accurate results were desired.

The reference horizontal power shape of Fig. 6.8 is obviously quite different from the power shape obtained with the finite difference method and a 7.2 cm mesh spacing (see Fig. 6.7). It remains to be seen whether this difference is because the finite difference mesh spacing is inadequate. As previously stated, the finite difference method should produce solutions which converge to a limit as the mesh spacing is reduced. A series of finite difference analyses with decreasing mesh spacing was performed to determine the power shape sensitivity and the limiting power shape. Figure 6.9 shows the assembly power errors for seven different finite difference solutions of the steady-state two-dimensional PWR problem. The assembly power errors are calculated with respect to the 5 x 5 nodal reference powers of Figure 6.8.

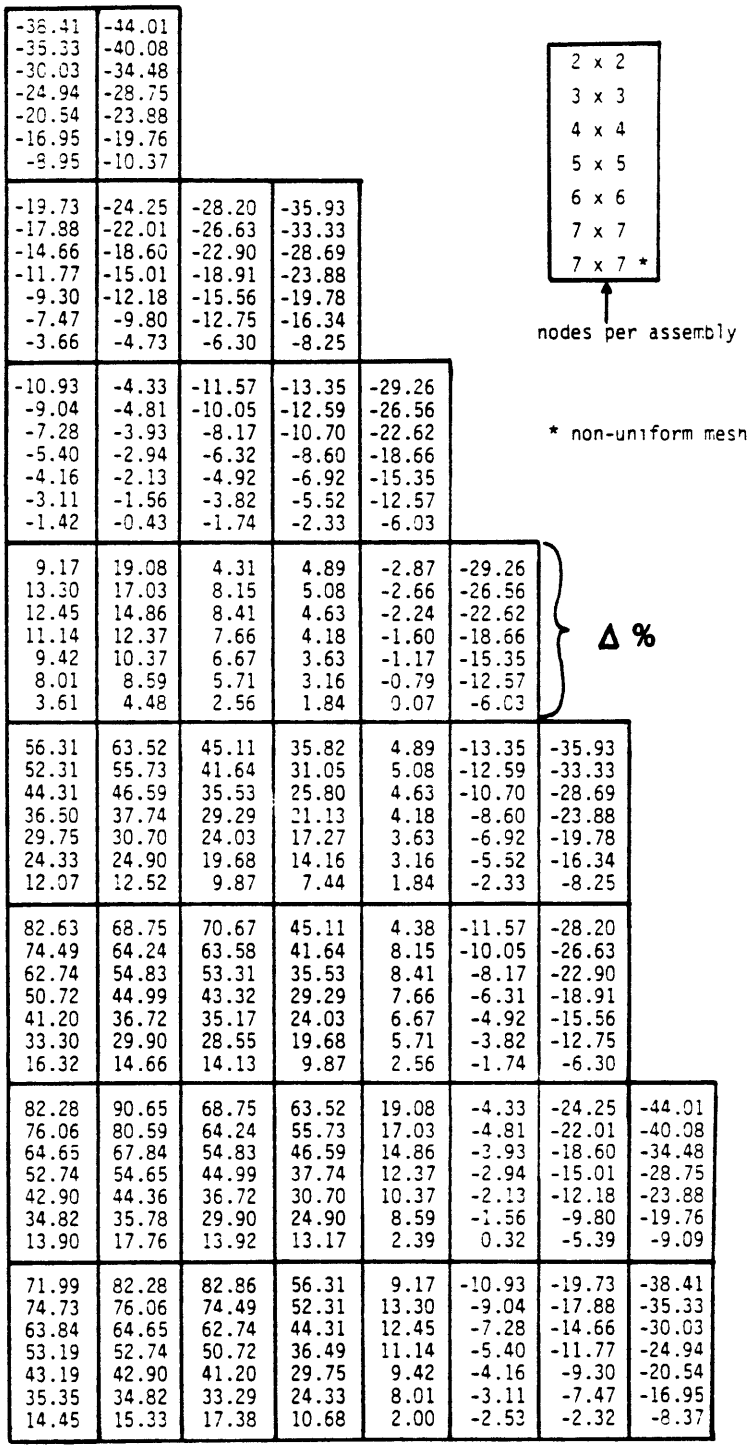

-38.41	-44.01						
-35.33	-40.08						
-30.03	-34.48						
-24.94	-28.75						
-20.54	-23.88						
-16.95	-19.76						
-8.95	-10.37						
-19.73	-24.25	-28.20	-35.93				
-17.88	-22.01	-26.63	-33.33				
-14.66	-18.60	-22.90	-28.69				
-11.77	-15.01	-18.91	-23.88				
-9.30	-12.18	-15.56	-19.78				
-7.47	-9.80	-12.75	-16.34				
-3.66	-4.73	-6.30	-8.25				
-10.93	-4.33	-11.57	-13.35	-29.26			
-9.04	-4.81	-10.05	-12.59	-26.56			
-7.28	-3.93	-8.17	-10.70	-22.62			
-5.40	-2.94	-6.32	-8.60	-18.66			
-4.16	-2.13	-4.92	-6.92	-15.35			
-3.11	-1.56	-3.82	-5.52	-12.57			
-1.42	-0.43	-1.74	-2.33	-6.03			
9.17	19.08	4.31	4.89	-2.87	-29.26		
13.30	17.03	8.15	5.08	-2.66	-26.56		
12.45	14.86	8.41	4.63	-2.24	-22.62		
11.14	12.37	7.66	4.18	-1.60	-18.66		
9.42	10.37	6.67	3.63	-1.17	-15.35		
8.01	8.59	5.71	3.16	-0.79	-12.57		
3.61	4.48	2.56	1.84	0.07	-6.03		
56.31	63.52	45.11	35.82	4.89	-13.35	-35.93	
52.31	55.73	41.64	31.05	5.08	-12.59	-33.33	
44.31	46.59	35.53	25.80	4.63	-10.70	-28.69	
36.50	37.74	29.29	21.13	4.18	-8.60	-23.88	
29.75	30.70	24.03	17.27	3.63	-6.92	-19.78	
24.33	24.90	19.68	14.16	3.16	-5.52	-16.34	
12.07	12.52	9.87	7.44	1.84	-2.33	-8.25	
82.63	68.75	70.67	45.11	4.38	-11.57	-28.20	
74.49	64.24	63.58	41.64	8.15	-10.05	-26.63	
62.74	54.83	53.31	35.53	8.41	-8.17	-22.90	
50.72	44.99	43.32	29.29	7.66	-6.31	-18.91	
41.20	36.72	35.17	24.03	6.67	-4.92	-15.56	
33.30	29.90	28.55	19.68	5.71	-3.82	-12.75	
16.32	14.66	14.13	9.87	2.56	-1.74	-6.30	
82.28	90.65	68.75	63.52	19.08	-4.33	-24.25	-44.01
76.06	80.59	64.24	55.73	17.03	-4.81	-22.01	-40.08
64.65	67.84	54.83	46.59	14.86	-3.93	-18.60	-34.48
52.74	54.65	44.99	37.74	12.37	-2.94	-15.01	-28.75
42.90	44.36	36.72	30.70	10.37	-2.13	-12.18	-23.88
34.82	35.78	29.90	24.90	8.59	-1.56	-9.80	-19.76
13.90	17.76	13.92	13.17	2.39	0.32	-5.39	-9.09
71.99	82.28	82.86	56.31	9.17	-10.93	-19.73	-38.41
74.73	76.06	74.49	52.31	13.30	-9.04	-17.88	-35.33
63.84	64.65	62.74	44.31	12.45	-7.28	-14.66	-30.03
53.19	52.74	50.72	36.49	11.14	-5.40	-11.77	-24.94
43.19	42.90	41.20	29.75	9.42	-4.16	-9.30	-20.54
35.35	34.82	33.29	24.33	8.01	-3.11	-7.47	-16.95
14.45	15.33	17.38	10.68	2.00	-2.53	-2.32	-8.37

Figure 6.9 Two-dimensional PWR Steady-state, QUANDRY, No Feedback: Transverse Power Profile, Finite Difference Method with Seven Mesh Spacings

The first six finite difference results are for uniform horizontal mesh spacings with four (2 x 2), nine (3 x 3), sixteen (4 x 4), twenty-five (5 x 5), thirty-six (6 x 6) and forty-nine (7 x 7) neutronic mesh points per fuel assembly. The final finite difference result is for a tailored horizontal mesh spacing of 1.50 cm at the edge and 3.72 cm in the interior of each fuel assembly, a total of forty-nine mesh points per assembly. Figure 6.9 shows very significant mesh spacing sensitivity. The errors in assembly powers are very large for all but the tailored 7 x 7 case, ranging from 36% to more than 90%. These errors were almost universally reduced with each reduction in horizontal mesh spacing, indicating that the finite difference solution does indeed approach the reference nodal solution in the limit. The use of a very fine horizontal mesh at the edge of the fuel assemblies produced a significant increase in the rate of the spatial convergence. Even with this type of mesh refinement, the finite difference method was less accurate than the analytic nodal method with one node per fuel assembly. This indicates that the finite difference method may require a very small mesh spacing indeed to achieve accuracies comparable to the nodal method.

The results of the two-dimensional mesh spacing sensitivity study are summarized in Table 6.7. This shows the contrast between the nodal and finite difference methods clearly. The errors in assembly powers resulting from the finite difference method with the mesh spacing of the MEKIN-B model are very large, an order of magnitude larger on average and at maximum than those of the nodal method with the mesh spacing of the TITAN analysis. The assembly

Table 6.7

Summary of Two-Dimensional Neutronic Mesh Spacing Sensitivity Study

Horizontal Mesh Spacing, cm	Nodes per Fuel Assembly ixj (total)	Analytic Nodal Method			Finite Difference Method		
		K eff	maximum assembly power error,* |%|	average magnitude assembly power errors*,%	K eff	maximum assembly power error,* |%|	average magnitude assembly power errors*: %
21.60	1x1 (1)	1.006090	7.26	2.70	___	___	___
10.80	2x2 (4)	1.004559	0.65	0.26	0.997780	90.65	33.40
7.20	3x3 (9)	1.004400	0.59	0.26	0.997009	80.59	30.85
5.40	4x4 (16)	___	___	___	0.997550	67.84	26.27
4.32	5x5 (25)	1.004469	0.00	0.00	0.998312	54.65	21.55
3.60	6x6 (36)	___	___	___	0.999150	44.36	17.62
3.09	7x7 (49)	___	___	___	0.999900	35.78	14.37
3.72/1.50	7x7**(49)	___	___	___	1.002100	17.76	6.92

* Errors calculated with respect to 5x5 nodal solution
**non-uniform mesh: 1.50 cm at assembly boundaries, 3.72 in interior

power errors of the nodal method with one neutronic node per fuel assembly are larger than expected, but smaller than those achieved with the finite difference method with the smallest mesh spacing tested. This result is consistent with the previous static benchmark problems analyzed with QUANDRY and finite difference methods.

The results of the mesh spacing sensitivity study are very significant for interpreting the TITAN and MEKIN-B analyses of the quarter core PWR problem. The implication is that both the TITAN and MEKIN-B analyses contain neutronic solutions which are not spatially converged, resulting in errors in the calculation of the horizontal power distribution. The magnitudes of these errors are not known precisely, since the effects of the axial dimension and the thermal-hydraulic feedback were not included in the mesh spacing sensitivity study. However, the errors associated with the finite difference method and the MEKIN-B mesh spacing are so large that it must be concluded that the model is inappropriate for the quarter core PWR analysis. Furthermore, the fact that the mesh spacing error explains the discrepancy between the TITAN and MEKIN-B results lends support to the validity of the TITAN result. The error associated with the TITAN model is tolerable, through larger than expected.

6.3.4 Resolution

The results of the horizontal mesh spacing sensitivity study seem to show that the MEKIN-B reactor model is not adequate for the quarter core PWR problem. However, the BNL report [C-13] did give some justification for the reactor model in the form of a comparison with measured reactor data. The reactor model was identical to

that of the control rod ejection analysis except for the position of the control rods. A MEKIN-B analysis of the "real" reactor produced assembly powers which had maximum and average errors of 9.56% and 3.75%, respectively, when compared to the measured data. Furthermore, the magnitude andlocation of the peak assembly power were well predicted. Since the control rod configuration was different in the actual reactor, the BNL report stated that the comparison with measured data did not validate the reactor model for the control rod ejection problem. However, the accuracy apparently achieved with the model does challenge the conclusion that the horizontal mesh spacing of the MEKIN-B model was not adequate.

The apparent good performance of MEKIN-B with a 7.2 cm horizontal mesh spacing could be related to the positions of the control rods and their impact on the power distribution. In the actual (quarter core) reactor, two control rods were fully withdrawn an the other three were approximately 80% withdrawn. The horizontal power shape for this configuration was much more smoothly varying than that of the control rod ejection problem. As a result, the error associated with using a coarse horizontal mesh in a finite difference neutronics method should be less than in the control rod ejection problem. However, it is not clear that this explanation alone is sufficient to account for the apparent dramatic inconsistency in accuracy between the MEKIN-B analyses.

A second explanation for the inconsistency in the performance of the MEKIN-B reactor model is that the comparisons are fundamentally different. In the mesh spacing sensitivity study, two different solution methods were used to solve the same set of partial differential equations,

subject to the same boundary conditions. The conclusion was that a finite difference method is very inaccurate with a 7.2 cm mesh spacing for the problem analyzed. For the same problem, the analytic nodal method with a 21.6 cm mesh spacing was much more accurate, though still subject to non-negligible error. This is a very different comparison from one in which a MEKIN-B result is shown to match measured reactor data fairly well. The fact that the analytical result was close to the measured data does not prove that the reactor model was adequate and that the basic equations were well-solved. Indeed, the mesh spacing sensitivity study would imply that the calculated horizontal power distribution would converge to a different result as the mesh spacing is decreased, thereby changing (and probably degrading) the apparent match with the measured data.

The most likely explanation for MEKIN-B results which compared well with measured reactor data in spite of a neutronics solution which was probably not spatially converged is compensating errors. The existence and nature of such errors is speculative because of incomplete information on the preparation of the reactor data. However, one possibility is that the albedo boundary conditions used on the outside vertical surfaces are not physically realistic and compensate for the error in the finite difference solution. The albedos should account for the effect of the water reflector and core baffle. Kalambokas [K-10] and Parsons [P-3] studied the replacement of reflectors by albedo boundary conditions and produced analytical expressions for calculating albedos. The values of non-diagonal albedos such as those used in the MEKIN-B and TITAN

analyses are primarily dependent on the properties of the reflector. Unfortunately, the properties of the quarter core PWR reflector and the method by which the albedos were determined were not reported and the possibility of error cannot be investigated directly. However, it is possible to do some comparisons which may give reason to question the albedos used. Table 6.8 shows a comparison of a set of albedos calculated by Barbehenn using the expressions of Kalambokas for a "typical" PWR reflector and baffle to the albedos used in the MEKIN-B analyses. The two albedo sets are distinctly different, particularly in the contribution of the fast flux to the thermal current. This is more than two orders of magnitude higher for the MEKIN-B reflector than for the "typical" PWR reflector. Perhaps the albedos used in the MEKIN-B analysis of the actual reactor serve to compensate for the errors associated with the horizontal mesh spacing.

The differences in the TITAN and MEKIN-B analyses of the quarter core PWR problem illustrate one of the primary advantages of TITAN. MEKIN-B is capable of producing accurate results if adequate mesh spacings are used, but this is often impractical. The BNL reactor model was as detailed as the available computer memory capacity (CDC-7600) would allow. To model the quarter core PWR with a horizontal mesh spacing of 2.1 cm would have increased the accuracy considerably but also would have increased the number of neutronic mesh points from approximately 11,900 to approximately 70,650. Thus, it was practically impossible to produce an accurate result with MEKIN-B. The analytic nodal method allows problems of

Table 6.8

Comparison of PWR Albedo Boundary Conditions

	MEKIN-B	Barbehenn
α_{11}	0.39	0.105
α_{22}	0.70	0.203
α_{21}	-0.90	-0.0067

where: $J_1 = \alpha_{11}\ \phi_1$

$J_2 = \alpha_{21}\ \phi_1 + \alpha_{22}\ \phi_2$

realistic size to be analyzed accurately with far fewer mesh points than is possible with a finite difference method. Thus, TITAN is a substantial improvement over MEKIN and other codes of its type.

6.4 Transient Analyses

6.4.1 Null Transient

The first transient analysis using the quarter core PWR steady-state was a null transient involving the "ejection" of a "non-perturbing control rod." The purpose of this analysis was to demonstrate that the steady-state solution was well converged and would therefore remain stable under transient conditions when no perturbation was applied. Figure 6.10 shows the total reactor (quarter core) power as a function of time during the null transient. The results show a slight rise in power followed by a decrease to a quasi-steady power level slightly greater than the nominal steady-state value. The maximum change in total reactor power form the nominal power of 550 MW(th) was 0.22 MW(th), or 0.04%. This is a very small change which can be neglected in comparison to the power excursions expected from the control rod ejection analyses to follow. The spatial stability of the steady-state solution was also maintained during the null transient. The maximum change in normalized fuel assembly power was -0.045%. In summary, the null transient analysis indicates that the steady-state solution was well converged and suitable for the control rod ejection analyses.

6.4.2 Center Control Rod Ejection

This analysis was performed with TITAN to compare to results produced with MEKIN-B. Figure 6.11 shows the total (quarter core) reactor power as a function of time during the first 1.0 second of the accident. The power excursion predicted by TITAN is significantly milder than that produced by MEKIN-B. Both codes show a rapid power increase during the

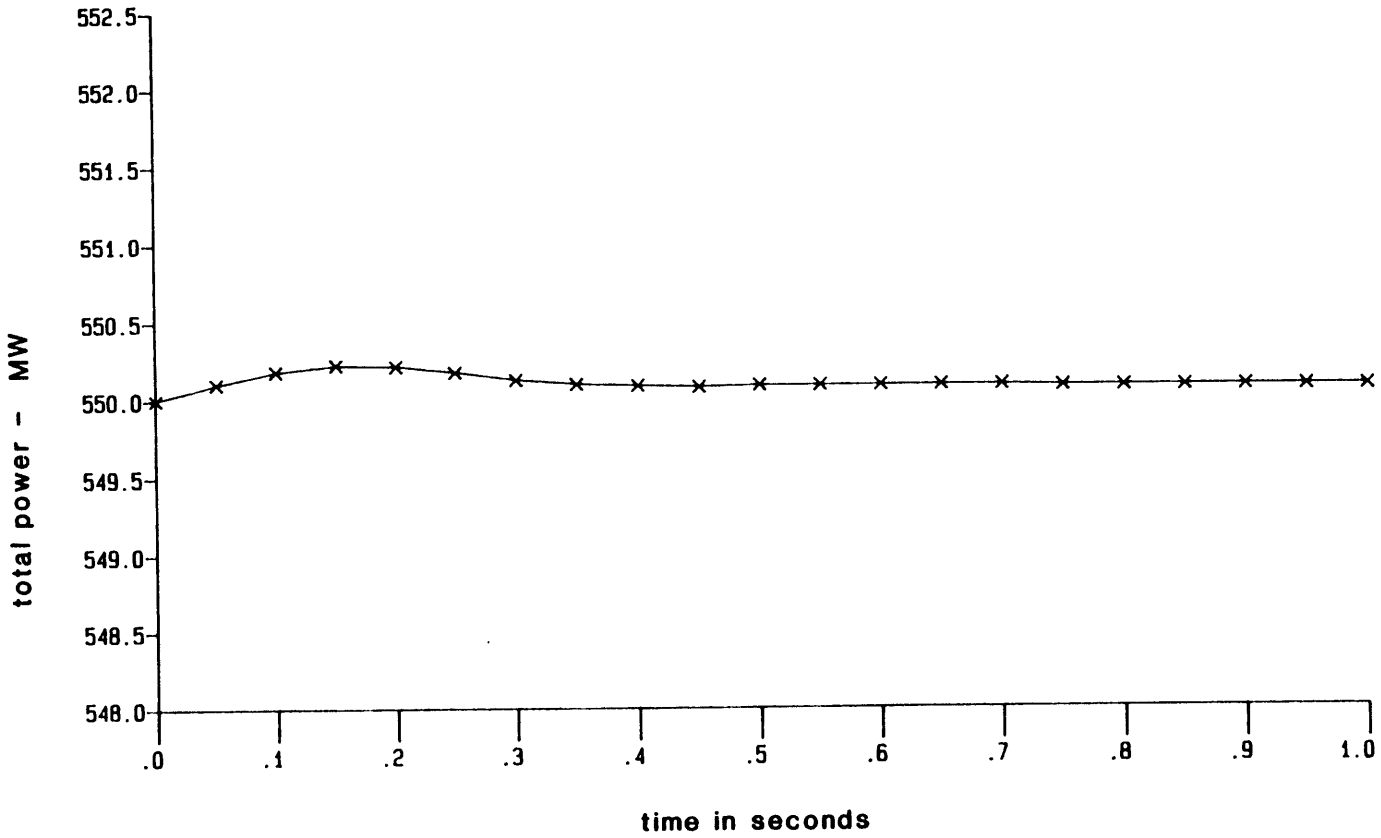

Figure 6.10 PWR Null Transient, TITAN: Power versus Time

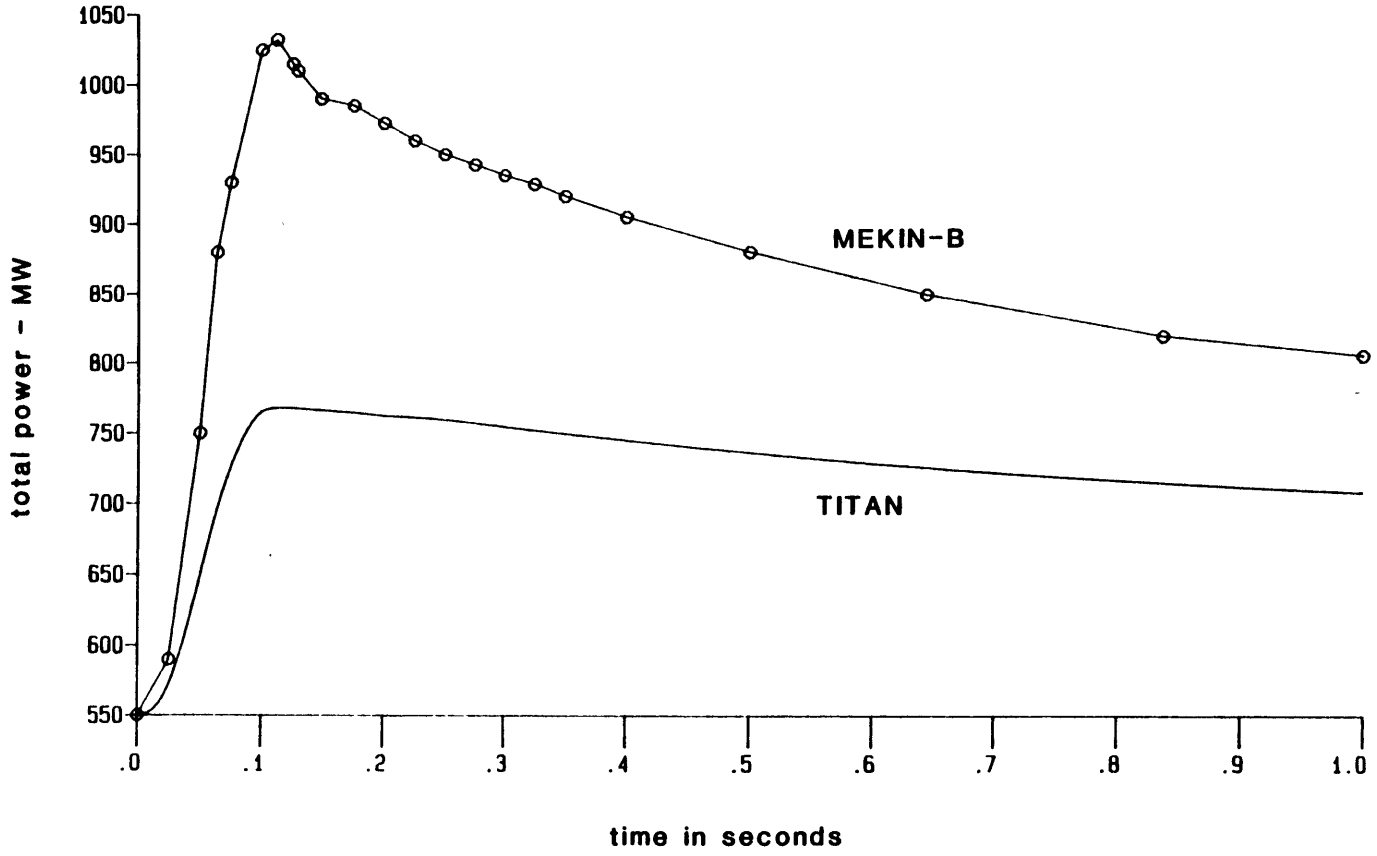

Figure 6.11 PWR Center Rod Ejection, TITAN and MEKIN-B:

Power versus Time

first 0.1 seconds, the period during which the control rod is being ejected. This is followed by a monotonic decrease in total power during the remaining 0.90 seconds. In the case of the MEKIN-B analysis, the decrease in power is somewhat faster immediately after the peak and slower as time goes on. The power decay predicted by TITAN is rather linear and less rapid than that of MEKIN-B. No scram was modeled in either case. Table 6.9 presents some of the parameters characterizing the power histories of the TITAN and MEKIN-B analyses. The time of the power peaks are very close, but the magnitude of the MEKIN-B power rise is more than twice as large as that of the TITAN analysis. These discrepancies are the result of the different steady-state solutions used. The static worth of the central control rod is nearly twice as great in the MEKIN-B analysis than it is in the TITAN analysis. In the TITAN analysis, the control rod is ejected from a relatively low flux region. Thus, the disagreements in the transient results are reasonable in light of the disparate steady-state solutions.

An additional element of interest in the center control rod ejection is the three-dimensional nature of the transient. The event was expected to produce the kind of spatial changes which could only be captured by a code such as TITAN. Figure 6.12 shows the normalized fuel assembly powers at the beginning and the end of the transient as well as at approximately the time of the peak power. The results clearly show the effect of the control rod ejection in that the relative power in the center of the core increases significantly while the relative power in the core exterior decreases. This is emphasized in Figure 6.13, which

Table 6.9

Selected Parameters from TITAN and MEKIN-B

Analyses of a Center Control Rod Ejection Transient

	TITAN	MEKIN-B
Power History		
Maximum Reactor Power (1/4 core), MW(th)	768.16	1032.5
Time of Maximum Power, s	0.116	0.112
Integrated Power (0.0 - 1.0s), MW-s	723.63	871.33
Ejected Control Rod Worth, % $\frac{\Delta K}{K}$	0.153	0.280
Fuel		
Maximum*(pellet-averaged) Fuel Temperature, °K	1087.75	1434.82
Time of Maximum Fuel Temperature, s	1.0	3.9
Maximum Fuel Temperature at 1.0s, °K	1087.75	1341.76
Maximum Fuel Enthalpy, cal/g (MJ/kg)	-	82.0 (0.343)
Maximum Cladding Temperature, °K	614.27	624.22
Time of Maximum Cladding Temperature, s	1.0	3.9
Maximum Cladding Temperature at 1.0s, °K	614.27	620.87
Coolant		
Maximum Local Void Fraction, %	0.0	0.0
Minimum Coolant Subcooling, °K	20.35	-
Maximum Cladding Superheat, °K	-1.0	-
Computational Requirements		
Number of Time Steps	80	-
Computer Time, Multics cpu-s	2371.46	-
cpu-s/node/time-step	0.0526	-
Computer Time, IBM 370/168 equivalent**	877.44	

* Maxima for 1.0s and 3.9s of transient time, respectively.

**1 MULTICS cpu-s ~ 0.37 IBM cpu-s

1.401 1.253 1.262	1.142 1.023 1.032	time =	0.00 s 0.12 s 1.00 s				
1.181 1.067 1.073	1.277 1.155 1.162	1.322 1.202 1.210	0.990 0.902 0.910				
0.984 0.909 0.914	1.014 0.938 0.943	1.070 0.988 0.993	1.054 0.973 0.978	0.938 0.865 0.873			
0.482 0.479 0.480	0.856 0.840 0.842	0.874 0.838 0.841	0.999 0.845 0.949	0.917 0.855 0.860	0.938 0.865 0.873		
0.836 0.930 0.923	0.881 0.952 0.947	0.994 1.024 1.022	0.975 0.958 0.959	0.999 0.845 0.949	1.054 0.973 0.978	0.990 0.902 0.910	
0.903 1.141 1.123	0.983 1.187 1.170	0.972 1.082 1.073	0.994 1.024 1.022	0.874 0.838 0.841	1.070 0.988 0.993	1.322 1.202 1.210	
0.824 1.343 1.308	0.875 1.237 1.211	0.983 1.187 1.170	0.881 0.952 0.947	0.856 0.840 0.842	1.014 0.938 0.943	1.277 1.155 1.162	1.142 1.023 1.032
0.448 1.332 1.287	0.824 1.343 1.308	0.903 1.141 1.123	0.836 0.930 0.923	0.482 0.479 0.480	0.984 0.909 0.914	1.181 1.067 1.073	1.401 1.253 1.262

Figure 6.12: PWR Center Control Rod Ejection, TITAN:
Change in Transverse Power Profile

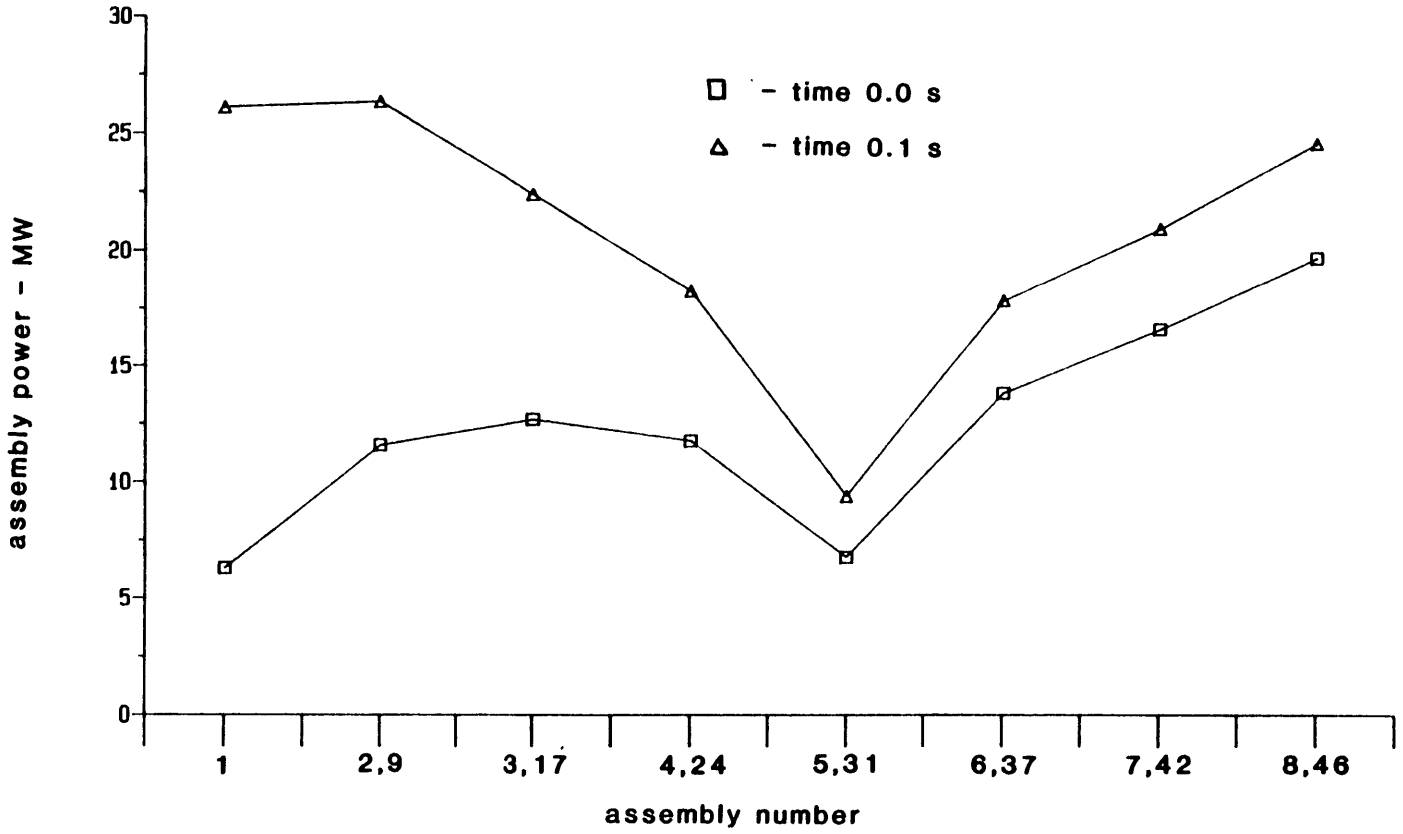

Figure 6.13 PWR Center Rod Ejection: Change in Edge Assembly Powers

shows the assembly powers along the quarter core lines of symmetry at two times during the transient. It is clear that the control rod ejection produces substantial changes in the horizontal power shape. Figure 6.14 shows the average axial power shape at two times during the control rod ejection. The change in axial power shape is less pronounced than that of the radial power shape. The results of the TITAN analysis show a slight shift in power toward the upper part of the core. The basic axial power shape is not changed by the control rod ejection because the partially inserted control rods remain in place. Thus, the main spatial effect of the control rod ejection is to produce a radial flux tilt toward the center of the core.

Fuel and coolant parameters from the TITAN and MEKIN-B analyses are also presented in Table 6.9. The maximum fuel and cladding temperatures from MEKIN-B were higher than those from TITAN. The maximum fuel and cladding temperatures occurred at the end of the calculated transient time in both analyses. Since the TITAN analysis ended at 1.0 seconds and the MEKIN-B analysis continued to 3.9 seconds, Table 6.9 also compares the fuel and cladding temperatures at 1.0 seconds. Once again, the MEKIN-B temperatures exceeded the TITAN temperatures. This is primarily the result of the larger power excursion (and greater integral energy deposition) of the MEKIN-B analysis. In addition, differences in the fuel rod models contribute to the higher MEKIN-B fuel temperatures (as was also observed in the steady-state results). The maximum fuel temperatures from both analyses are not the absolute maxima associated with the control rod ejection since the temperatures were increasing when the

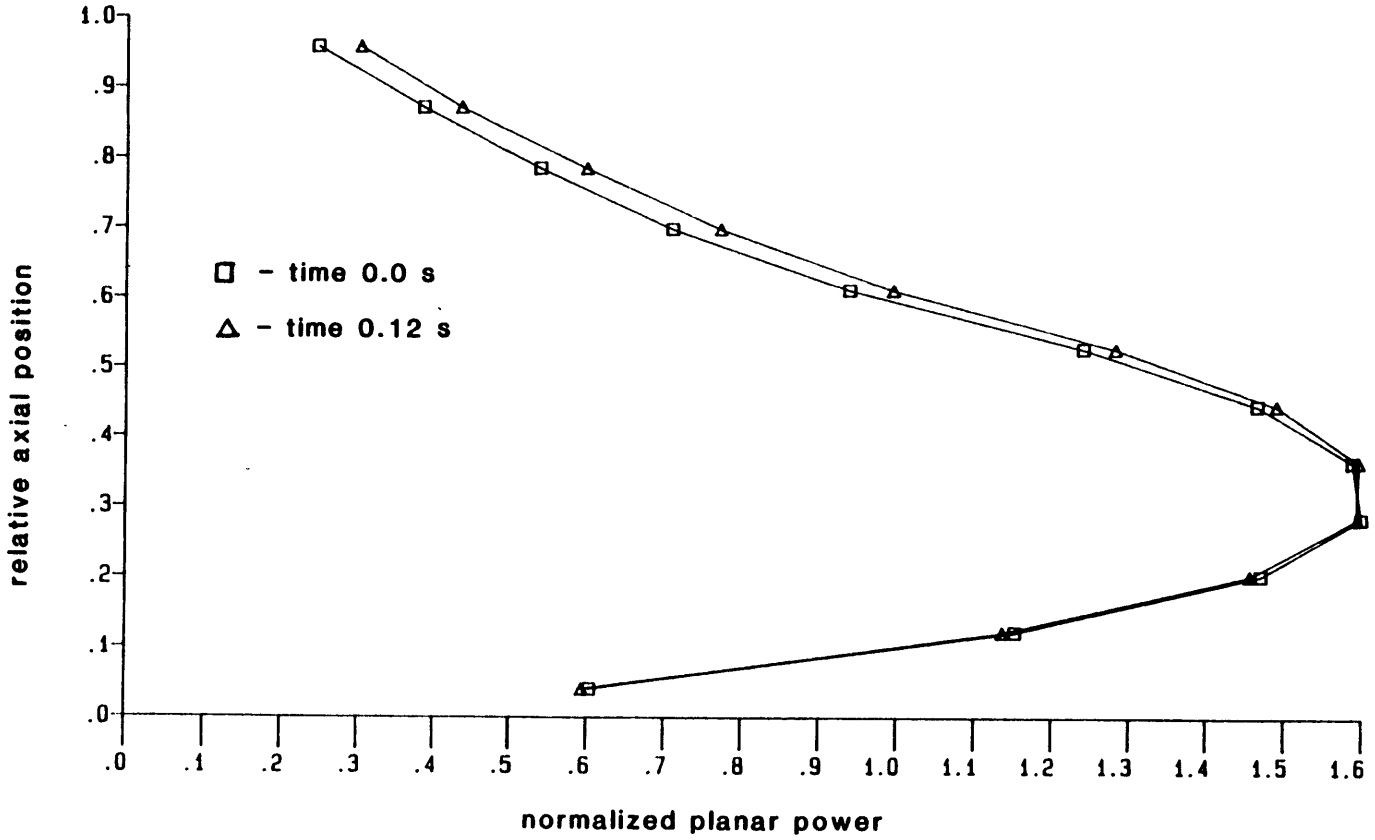

Figure 6.14 PWR Center Rod Ejection, TITAN:

Change in Axial Power Profile

analyses were terminated.

Table 6.9 also shows that no boiling was predicted by either code. The TITAN analysis showed substantial coolant subcooling and cladding surface temperatures below the saturation temperature in all nodes. (The corresponding MEKIN-B information was unavailable.) However, it is quite possible that subcooled boiling or even bulk boiling would occur later in the transient when more of the stored energy has been conducted into the coolant.

Finally, Table 6.9 shows the computer time required for the center control rod ejection analysis. Approximately 40 minutes of MULTICS cpu time were required, which is equivalent to about 13 minutes on an IBM 370/168. This is slightly less per node and time step than was required for the BW2C problem (see Table 5.11). Apparently the use of diagonal symmetry in the neutronics more than compensated for the additional effort expended in analyzing three-dimensional fluid dynamics. In any event, the computational requirements are reasonable and could be reduced with modest effort.

6.4.3 Edge Control Rod Ejection

A second control rod ejection transient was analyzed with TITAN. The purpose of this analysis was to produce even greater spatial changes than the center control rod ejection analysis. To accomplish this, one of the edge control rods (located in channel #5) was ejected, producing an asymmetric change in flux shape. Figure 6.15 shows the total (quarter core) reactor power as a function of time during the first 1.0 second of

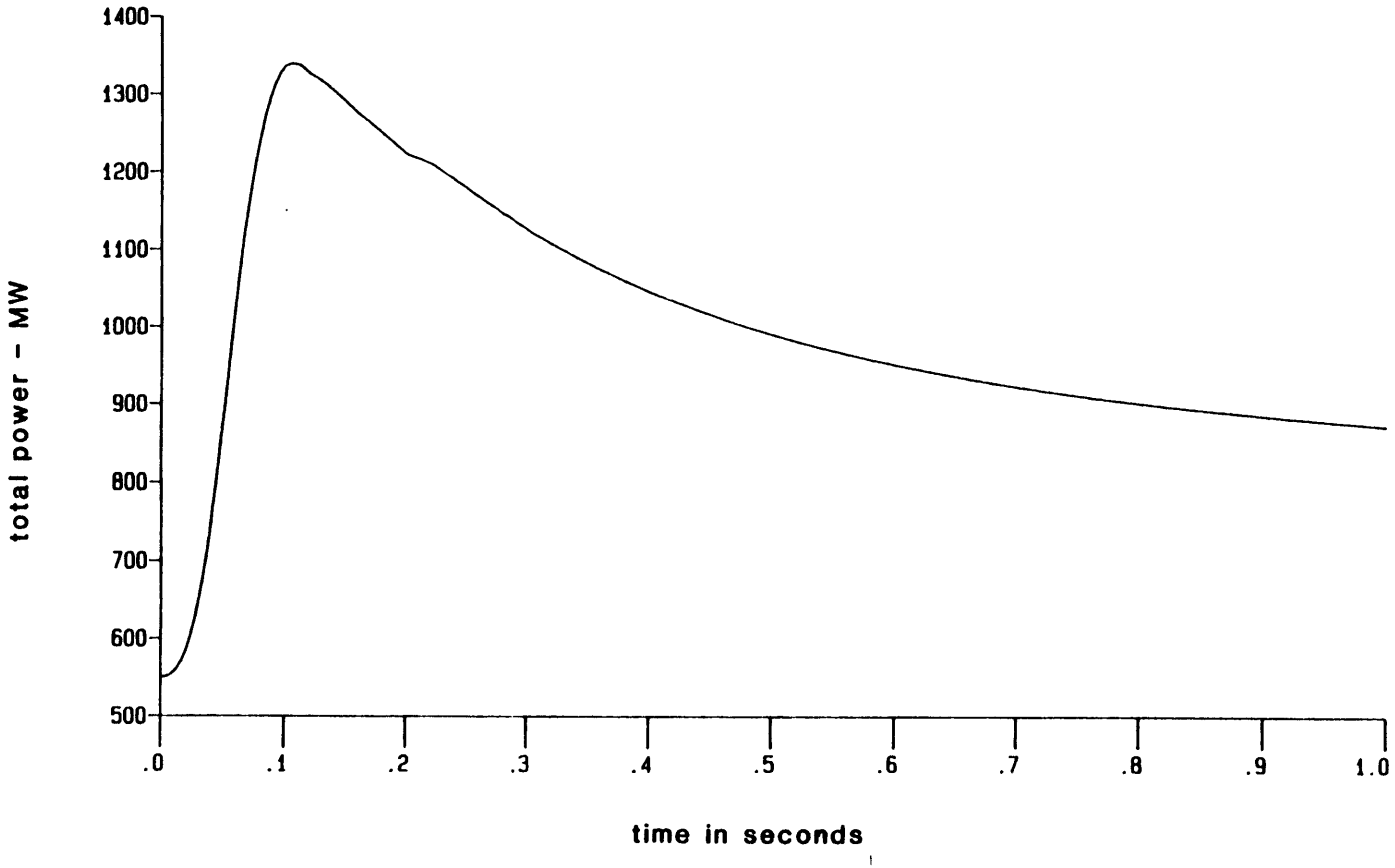

Figure 6.15 PWR Edge Rod Ejection, TITAN: Power versus Time

the edge control rod ejection. The power excursion is significantly larger than that of the center control rod ejection. The time of the peak power is slightly earlier than in the center control rod ejection and the subsequent power decay is more rapid. Table 6.10 presents selected parameters from the edge control rod ejection analysis. The power excursion is greater than in the center control ejection because of the greater reactivity worth of the edge control rod. The regions in which the edge control rods are located have higher flux levels than the center of the core, hence the higher reactivity worth of the control rods.

The larger power excursion resulting from the edge control rod ejection produces a larger integral energy deposition, as shown in Table 6.10. This, in turn, produced higher fuel and cladding temperatures. No boiling was predicted, but the minimum coolant subcooling was less than in the other transient. Furthermore, the cladding surface temperatures were greater than the coolant saturation temperatures in several nodes. The occurrence of subcooled or bulk boiling during later stages of the transient is therefore more probable than for the central control rod ejection.

The power history shown in Figure 6.15 has an unexpected change in slope during the power decay. This occurs at 0.22 seconds into the transient and is followed by a resumption of the original slope. This change in slope is not a physical effect, but the result of the tandem coupling scheme used in TITAN. The change in slope occurred because the time-step was increased from 0.01s to 0.02s with the neutronic portion

Table 6.10

Selected Parameters from TITAN Edge Control Rod Ejection Analysis

Power History	
Maximum Power (1/4 core), MW(th)	1339.2
Time of Maximum Power, s	0.104
Integrated Power (0.0-1.0s), MW-s	1005.44
Edge Control Rod Worth, % ΔK/K	0.445
Fuel	
Maximum* (pellet-averaged) Fuel Temperature, °K	1190.96
Time of Maximum Fuel Temperature, s	1.0
Maximum Cladding Temperature, °K	631.4
Time of Maximum Cladding Temperature, s	1.0
Coolant	
Maximum Void Fraction, %	0.0
Minimum Coolant Subcooling, °K	12.31
Maximum Cladding Superheat, °K	13.10
Computational Requirements	
Number of Time-Steps	80
Computer Time, Multics cpu-s	3364.80
cpu-s/node/time-step	0.0746
Computer Time, equivalent IBM 370/168 cpu-s*	1244.98

*1 MULTICS cpu-s ~ 0.37 IBM 370/168 cpu-s

* Maximum during first 1.0 s

**1 MULTICS cpu-s ~ 0.37 IBM 370/168 cpu-s

of the calculation "leading" in the tandem procedure. The thermal-hydraulic feedback contribution to the first neutronic calculation with the longer time-step was calculated in the previous shorter time-step. Since the control rod ejection was completed earlier in the transient, there was no other reactivity change. Thus, the reactivity change associated with a time increment of 0.01s was actually applied over a time increment of 0.02s, resulting in the observed change in the rate of the power decay. In subsequent time-steps, the size of the neutronic and thermal-hydraulic time-steps was identical and the power decay proceeded normally.

The spatial effects of the edge control rod ejection are shown in Figures 6.16, 6.17, and 6.18. Figure 6.16 shows the normalized fuel assembly powers at 0.0, 0.10, and 1.0 seconds into the transient. The radial power tilt is across the diagonal line of symmetry rather than from outside to inside. This is emphasized in Figure 6.17, which shows the change in assembly powers along the two interior "edges" of the quarter core. Prior to the rod ejection, the assembly powers along these edges are symmetric. After the control rod along the "bottom edge" is ejected, the relative power rises sharply in the area near the ejected rod and falls in the area far from the ejected rod. Figure 6.18 shows the change in the core average axial power shape during the edge control rod ejection. As in the center rod ejection, the change in axial power shape is small. On the whole, the edge control rod ejection transient produces substantial spatial changes. The importance of the spatial changes in both control rod ejection transients is investigated in Chapter 7.

1.401 1.003 1.095	1.142 0.820 0.898	time =	0.00 s 0.10 s 1.00 s				
1.181 0.860 0.933	1.277 0.938 1.015	1.322 0.999 1.073	0.990 0.769 0.822				
0.984 0.740 0.799	1.014 0.772 0.829	1.070 0.837 0.890	1.054 0.859 0.901	0.938 0.800 0.832			
0.482 0.390 0.416	0.856 0.699 0.741	0.874 0.734 0.768	0.999 0.874 0.900	0.917 0.842 0.853	0.938 0.906 0.906		
0.836 0.736 0.768	0.881 0.782 0.813	0.994 0.912 0.936	0.975 0.935 0.945	0.999 1.002 0.993	1.054 1.098 1.066	0.990 1.058 1.025	
0.903 0.839 0.864	0.983 0.932 0.954	0.972 0.975 0.984	0.994 1.075 1.066	0.874 1.000 0.974	1.070 1.231 1.171	1.322 1.498 1.416	
0.824 0.799 0.818	0.875 0.878 0.891	0.983 1.079 1.076	0.881 1.134 1.106	0.856 1.282 1.222	1.014 1.345 1.261	1.277 1.539 1.425	1.142 1.335 1.247
0.448 0.446 0.457	0.824 0.852 0.862	0.903 1.039 1.031	0.836 1.247 1.206	0.482 1.316 1.241	0.984 1.480 1.376	1.181 1.460 1.345	1.401 1.644 1.520

Figure 6.16: PWR Edge Control Rod Ejection, TITAN:
Change in Transverse Power Profile

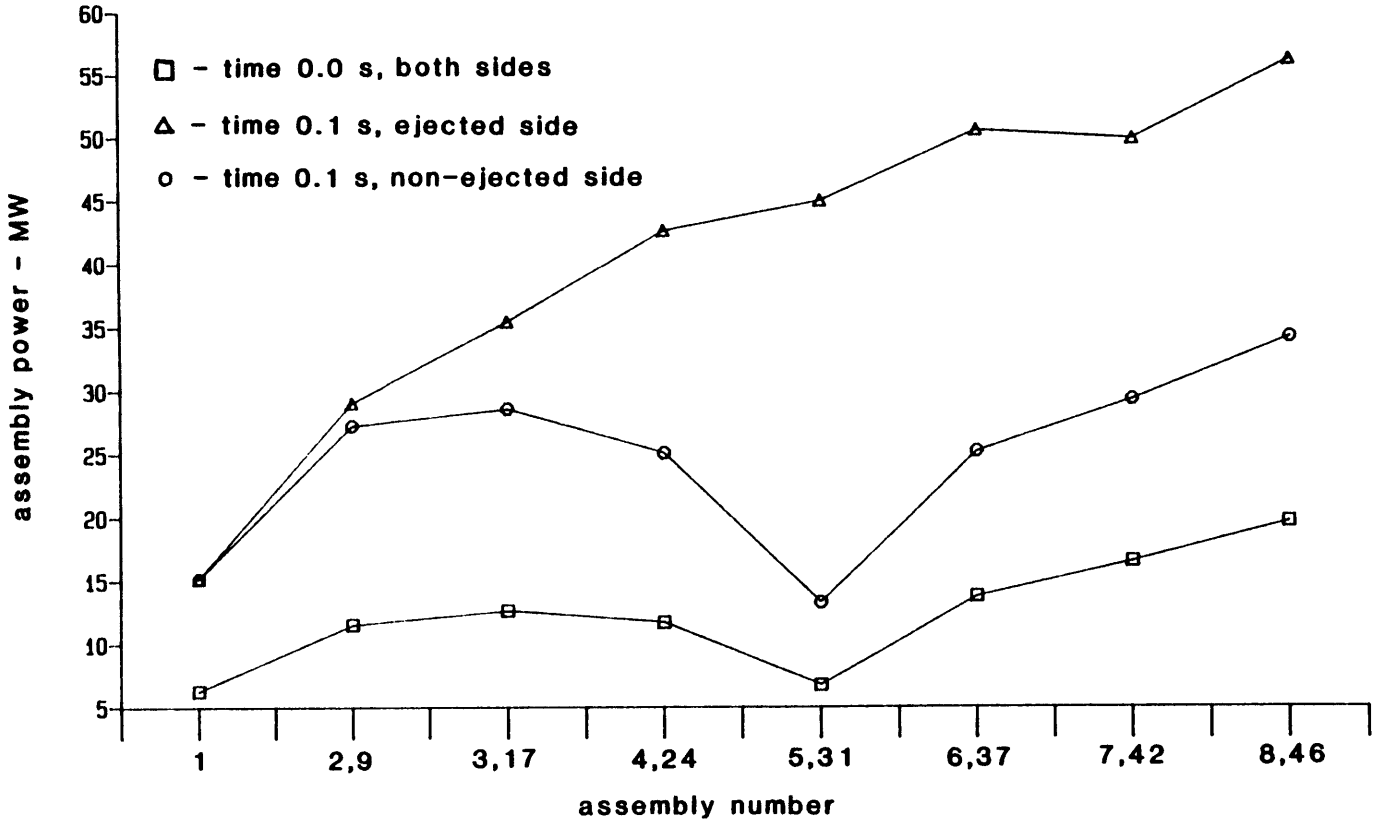

Figure 6.17 PWR Edge Rod Ejection, TITAN:

Change in Edge Assembly Powers

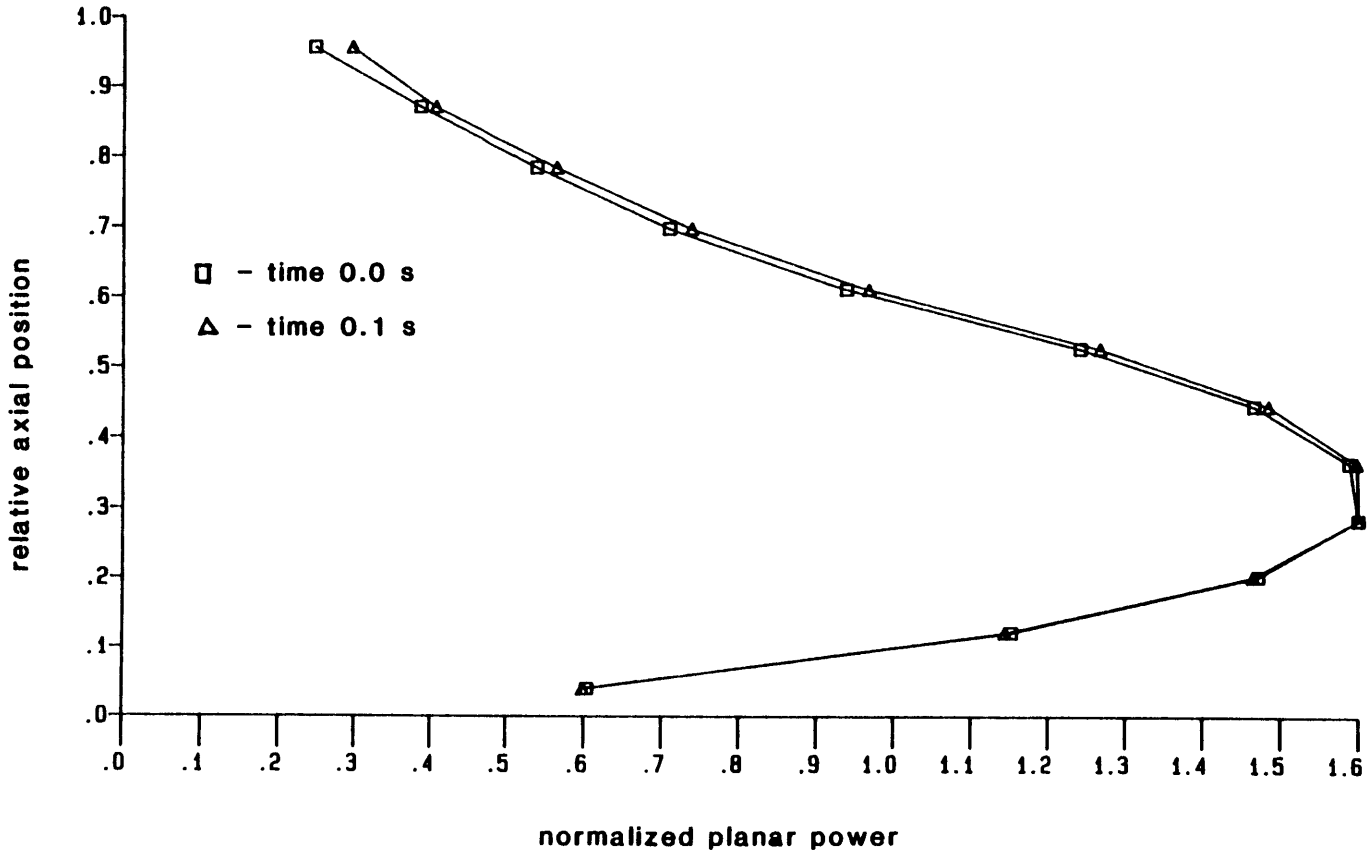

Figure 6.18 PWR Edge Rod Ejection, TITAN:

Change in Axial Power Profile

Table 6.10 shows that the computational effort required for the edge control rod ejection analysis was about 40% greater than for the center rod ejection. The edge rod ejection required about 56 minutes of MULTICS cpu time, which is equivalent to about 21 minutes of IBM 370/168 cpu time. There were two reasons for the increased computer time. First, the neutronic diagonal symmetry option could not be used and every neutronic node was included in the calculations. Second, the power excursion was more severe and therefore required some additional computational effort. Nevertheless, the computing requirements were reasonable for a three-dimensional coupled analysis of a full-size quarter core reactor.

6.5 Summary

This chapter presented the two PWR control rod ejection transients analyzed by TITAN. These analyses showed that TITAN can successfully analyze a problem of realistic size and scope with a reasonable amount of computer time. In the process, the equilibrium xenon model, the direct moderator heating model and the quadratic feedback model were exercised. Both rod ejection transients exhibited significant three-dimensional spatial effects, thereby demonstrating one of the major advantages of TITAN. The importance of these three-dimensional effects are investigated in Chapter 7.

The results of the TITAN control rod ejection analyses were compared to the results obtained with MEKIN-B. The two codes produced significantly

different results for both the steady-state and the transient. Sensitivity studies regarding the horizontal mesh spacings lend support to the TITAN steady-state results and raise doubts about the MEKIN-B results. However, in the absence of reliable reference solutions for the problem, the degree of accuracy of the TITAN analyses cannot be defined. Nevertheless, the comparison with MEKIN-B did show the advantages of TITAN in analyzing realistic reactor transients.

CHAPTER 7 COMPARISON OF POINT KINETICS AND THREE-DIMENSIONAL NEUTRONICS FOR PWR CONTROL ROD EJECTION TRANSIENTS

7.1 Introduction

This chapter presents the results of coupled point kinetics/thermal-hydraulics analyses of two PWR rod ejection transients. The two rod ejection transients were based upon the same quarter core PWR control rod ejections analyzed with TITAN in Chapter 6. The results obtained with point kinetics are compared to those obtained with the three-dimensional neutronics of TITAN.

The purpose of this chapter is to investigate the importance of three-dimensional neutronics in the analysis of reactivity transients involving significant spatial effects. The existence of strong spatial effects in the two PWR control rod ejection transients has already been demonstrated by the TITAN analyses of Chapter 6. The review of the conclusions of other investigators in Chapter 2 showed that a point kinetics representation may not be adequate when significant spatial changes occur, when the core is large and loosely coupled, or if the reactivity insertion produces a super-prompt-critical reactor. Neither of the PWR control rod ejection transients are of the super-prompt-critical variety, but both involve a full scale (quarter core) power reactor. Thus, the application of point kinetics and three-dimensional neutronics to the two transients provides an interesting test of the importance of higher order methods such as TITAN.

The analyses presented in this chapter were performed with THERMIT-3 [D-4], a core dynamics code combining a point kinetics model

with the thermal-hydraulics code THERMIT. (See discussion in Sec. 3.4 and App. A). THERMIT-3 is ideal for comparing to TITAN because the thermal-hydraulics portions of the two codes are essentially identical. Thus, any differences in the transient results are attributable to the neutronics portions of the codes.

Chapter 7 is organized into five sections, including this introduction. Section 2 presents the calculations required to produce the reactor model for the THERMIT-3 analyses and discusses some important aspects of the point kinetics analyses. Section 3 presents the steady-state results, while Section 4 discusses the transient results (including comparisons with the TITAN steady-state and transient results). A summary of the chapter is given in Section 5.

7.2 The Point Kinetics Reactor Model

The THERMIT-3 quarter core PWR model is based upon that used in the TITAN analyses in Chapter 6. The geometry and the thermal-hydraulics parameters and options are identical to those used previously. However, the neutronic portion of the THERMIT-3 model is quite different because of the nature of point kinetics (see Chapter 2 for a discussion of point kinetics). THERMIT-3 requires the specification of several parameters, including: time-independent power distribution; the prompt-neutron lifetime; reactivity feedback coefficients for fuel temperature, moderator temperature and moderator density (or void fraction); and coefficients for a polynomial expression of applied reactivity as a function of time. The calculation of all necessary neutronic parameters is given in this section.

The original version of THERMIT-3 was modified to enhance the control rod ejection analyses. First, void fraction was replaced by moderator density as a feedback parameter. This makes the THERMIT-3 analyses more consistent with the TITAN analyses. Second, the order of the polynomial function for applied reactivity was increased from three to six. This permits a more accurate representation of the control rod ejection reactivity curve. No other substantive changes were made to the original THERMIT-3 code.

Unlike the three-dimensional neutronics of TITAN, the point kinetics model of THERMIT-3 assumes that the power shape is known and is time-independent. This power shape is specified by a transverse and an axial power profile. These profiles are assumed to describe both the steady-state and transient power distributions. Since the TITAN analyses of the quarter core PWR were performed previously, the steady-state power distribution is known. However, the three-dimensional power distribution cannot be captured exactly by the two THERMIT-3 power profiles. The transverse power profile was taken to be the TITAN normalized assembly power distribution, shown in Fig. 7.1. As a result, the power deposited in each channel at steady-state was identical in both the TITAN and THERMIT-3 analyses. The axial profile was the average axial profile from the TITAN analysis. This profile is shown in Fig. 7.2, along with the actual axial profiles from two selected channels. One difficulty in producing a single representative axial power profile is the presence of two partially inserted control rods. As Fig. 7.2 shows, the actual axial profile in the two assemblies containing partially inserted control rods is significantly different

1.40	1.14						
1.18	1.28	1.32	0.99				
0.98	1.01	1.07	1.05	0.94			
0.48	0.86	0.87	1.00	0.92	0.94		
0.84	0.88	0.99	0.97	1.00	1.05	0.99	
0.90	0.98	0.97	0.99	0.87	1.07	1.32	
0.82	0.87	0.98	0.88	0.86	1.01	1.28	1.14
0.45	0.82	0.90	0.84	0.48	0.98	1.18	1.40

Figure 7.1: PWR Normalized Assembly Powers:
THERMIT-3 Transverse Power Profile

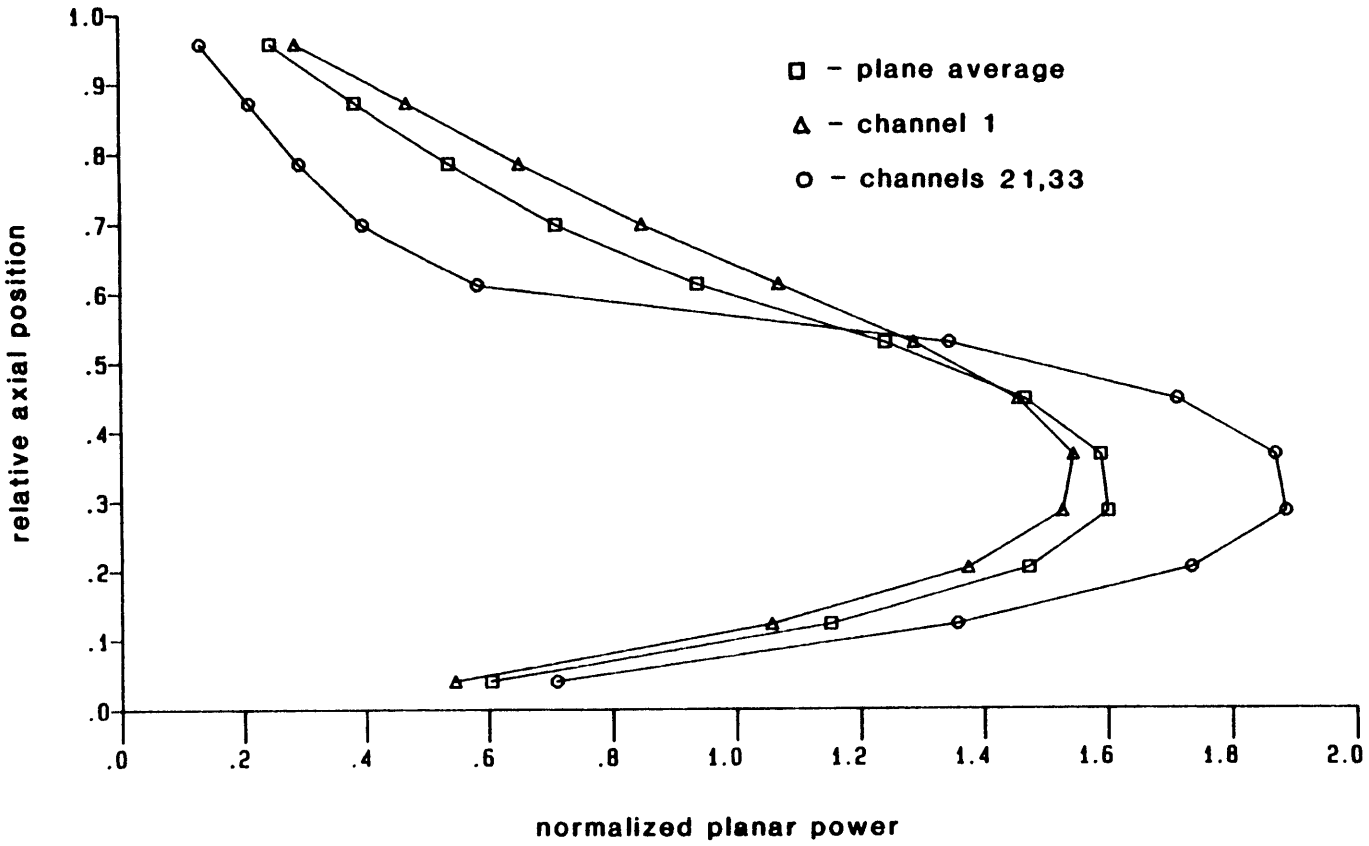

Figure 7.2 PWR Steady-state Axial Power Profile, TITAN:

Average(THERMIT-3) versus Individual Channels

from the average profile. However, the actual axial profile of one of the other (axially uniform) assemblies is reasonably similar to the average profile. The effect of using a single axial power profile is an inaccurate representation of the steady-state power distribution, particularly in the two assemblies having partially inserted control rods. The errors in nodal powers for the axially uniform assemblies are as high as 18%, while the errors in the nodal powers for the two partially controlled assemblies range from 8% to 90%. Most of the nodal powers are within 10% of the reference powers. Fortunately, the larger errors are found in the upper (low power) portions of the core, so that the maximum fuel temperatures and enthalpies should not be significantly effected.

The prompt-neutron lifetime, Λ, is a fundamental parameter in the point reactor kinetics equations. The formal definition of the prompt-neutron lifetime is given by Henry [H-3] as follows (for one fissionable species):

$$\Lambda \equiv \frac{\int dV \int dE\ W(\vec{r},E)\ \frac{1}{v(E)}\ \phi(\vec{r},E,t)}{\int dV \int dE\ W(\vec{r},E)\chi(E) \int dE'\ \nu\Sigma_f(\vec{r},E',t)\phi(\vec{r},E',t)} \qquad (7.1)$$

where

V = reactor core volume

E, E' = neutron energy

$\vec{r}$ = position vector

W = weight function (importance or adjoint flux)

v = neutron speed

ϕ = neutron flux density

χ = fission neutron spectrum

ν = average number of neutrons produced per fission

Σ_f = macroscopic fission cross section.

This expression was applied to the steady-state quarter core PWR results of TITAN in order to calculate the prompt-neutron lifetime. The expression can be simplified because the TITAN fluxes and cross sections are constant in a given node. In addition, the fluxes and cross sections are already integrated over the thermal and fast parts of the neutron energy spectrum. Therefore, the following simplifications can be made:

$$\int_0^{E_c} \phi(\vec{r},E,t)\, dE = \phi_1(\vec{r},t) \tag{7.2}$$

$$\int_{E_c}^{\infty} \phi(\vec{r},E,t)\, dE = \phi_2(\vec{r},t) \tag{7.3}$$

$$\int_0^{E_c} \nu\Sigma_f(r,E,t)\, dE = \nu_1\Sigma_{f_1}(\vec{r},t) \tag{7.4}$$

$$\int_{E_c}^{\infty} \nu\Sigma_f(\vec{r},E,t)\, dE = \nu_2\Sigma_{f_2}(\vec{r},t) \tag{7.5}$$

$$\frac{\int_0^{E_c} \frac{\phi(\vec{r},E,t)}{v(E)}\, dE}{\int_0^{E_c} \phi(\vec{r},E,t)\, dE} = \frac{1}{v_1} \tag{7.6}$$

$$\frac{\int_{E_c}^{\infty} \frac{\phi(\vec{r},E,t)}{v(E)}\, dE}{\int_{E_c}^{\infty} \phi(\vec{r},E,t)\, dE} = \frac{1}{v_2} \tag{7.7}$$

$$\int_0^{\infty} \chi(E)dE = 1 \tag{7.8}$$

where E_c = cutoff neutron energy for the thermal neutron group.

The usual method for calculating the prompt-neutron lifetime includes using the adjoint flux as the weighting function. Unfortunately, QUANDRY does not solve the adjoint equations and some other weight function had to be chosen. In the absence of any other more appropriate function, the functions were chosen to be unity. Finally, the time-dependence of the prompt-neutron lifetime is neglected, since THERMIT-3 assumes it to be constant. Therefore, steady-state fluxes and reference cross sections were used to evaluate the prompt-neutron lifetime. When Eq. 7.2-7.8 and the weight functions are substituted and Eq. 7.1 is integrated over the reactor volume node-wise, it yields:

$$\Lambda = \frac{\sum_{i=1}^{564} \left[\frac{1}{v_1} \phi_1 + \frac{1}{v_2} \phi_2 \right];}{\sum_{i=1}^{564} \left[\nu_1 \Sigma_{f_1} \phi_1 + \nu_2 \Sigma_{f_2} \phi_2 \right];} \tag{7.9}$$

Equation 7.9 was evaluated, yielding a value of 1.8038×10^{-5} s for Λ.

Time-dependent reactivity insertions resulting from the two control rod ejections had to be calculated for the THERMIT-3 analyses. QUANDRY was used to determine the static reactivity worth of removing the two control rods. The reference cross sections were used and feedback was omitted. This approach is identical to that of the adiabatic approximation [H-4], in which account is taken of changes in the flux shape caused by the perturbation while the effect of delayed neutrons is neglected. The usual way of generating point kinetics reactivities using first-order perturbation theory involves an integration over the unperturbed steady-state flux shape. The method used in this work should produce much more accurate control rod reactivities than first-order perturbation theory. Indeed, the increased accuracy of the adiabatic method has already been discussed in Sec. 2.2.3.2. It must emphasized that the THERMIT-3 analyses were not strictly consistent with the adiabatic approximation because, as will be discussed, the method of calculating reactivity feedback coefficients was not that of the adiabatic approximation.

The two control rod ejection reactivity curves were produced by determining the change in static eigenvalue as the control rods were withdrawn from the core one axial mesh spacing at a time. Thirteen three-dimensional static neutronic calculations were required for each control rod ejection analysis. It is only the efficiency of QUANDRY that makes such an approach practical. The static eigenvalues and the resulting control rod position reactivities for the center and edge control rods are given in Tables 7.1 and 7.2, respectively.

Table 7.1

Center Control Rod Ejection Reactivities

Rod Insertion Distance	Transient Time	Static Eigenvalue	Control Rod Reactivity	Polynomial Fit Reactivity
m	s		$(\Delta k/k) \times 10^4$	
3.6724	0.0	1.012075	-	0.04
3.3549	0.0083	1.012101	0.26	0.25
3.0374	0.0167	1.012174	0.98	0.94
2.7200	0.0250	1.012338	2.60	2.63
2.4025	0.0333	1.012590	5.09	5.13
2.0850	0.0417	1.012880	7.95	7.95
1.7871	0.0500	1.013148	10.60	10.57
1.4893	0.0583	1.013354	12.64	12.63
1.1914	0.0667	1.013492	14.00	13.96
0.8936	0.0750	1.013559	14.66	14.70
0.5957	0.0833	1.013604	15.11	15.07
0.2979	0.0917	1.013620	15.27	15.31
0.0000	0.1000	1.013626	15.32	15.39

Table 7.2

Edge Control Rod Ejection Reactivities

Rod Insertion Distance	Transient Time	Static Eigenvalue	Control Rod Reactivity	Polynomial Fit Reactivity
m	s		$(\Delta k/k) \times 10^4$	
3.6724	0.0	1.012075	-	0.14
3.3549	0.0083	1.012136	0.60	0.46
3.0374	0.0167	1.012371	2.92	2.94
2.7200	0.0250	1.012952	8.67	8.81
2.4025	0.0333	1.013806	17.10	17.13
2.0850	0.0417	1.014726	26.19	26.05
1.7871	0.0500	1.015507	33.91	33.84
1.4893	0.0583	1.016040	39.18	39.27
1.1914	0.0667	1.016340	42.14	42.28
0.8936	0.0750	1.016478	43.50	43.49
0.5957	0.0833	1.016540	44.12	43.98
0.2979	0.0917	1.016565	44.36	44.50
0.0000	0.1000	1.016575	44.46	44.94

The control rod reactivities were fitted to a sixth order polynomial using a routine which minimizes the maximum error. The reactivity values produced by the polynomial fits are also shown in Tables 7.1 and 7.2. The agreement with the calculated static reactivity worths is excellent. The reactivity curves and the polynomials for the center and edge control rod ejections are shown in Figs. 7.3 and 7.4, respectively. They show that the polynomial functions are well behaved in the intervals between the calculated reactivities.

Thermal-hydraulic feedback was modeled as a linear function of fuel temperature, moderator temperature and moderator density in the THERMIT-3 analyses. A reactivity coefficient for each type of feedback was calculated with QUANDRY. Table 7.3 shows the values of the feedback parameters corresponding to the reference cross sections. A static QUANDRY analysis was performed with an off-reference cross section set corresponding to each off-reference feedback parameter value shown. The off-reference cross sections were calculated with the cross section coefficients and feedback equations used in the TITAN analyses. The change in a particular feedback parameter was applied uniformly throughout the core. The control rods were assumed to be in the steady-state configuration. The resultant reactivity feedback coefficients are also given in Table 7.3

In THERMIT-3, these coefficients are divided by the total number of nodes and multiplied by the change in the appropriate feedback parameter in each node. These are summed up to give the total reactivity effect of the feedback. This approach allows nodal or region-averaged reactivity feedback coefficients to be specified. There

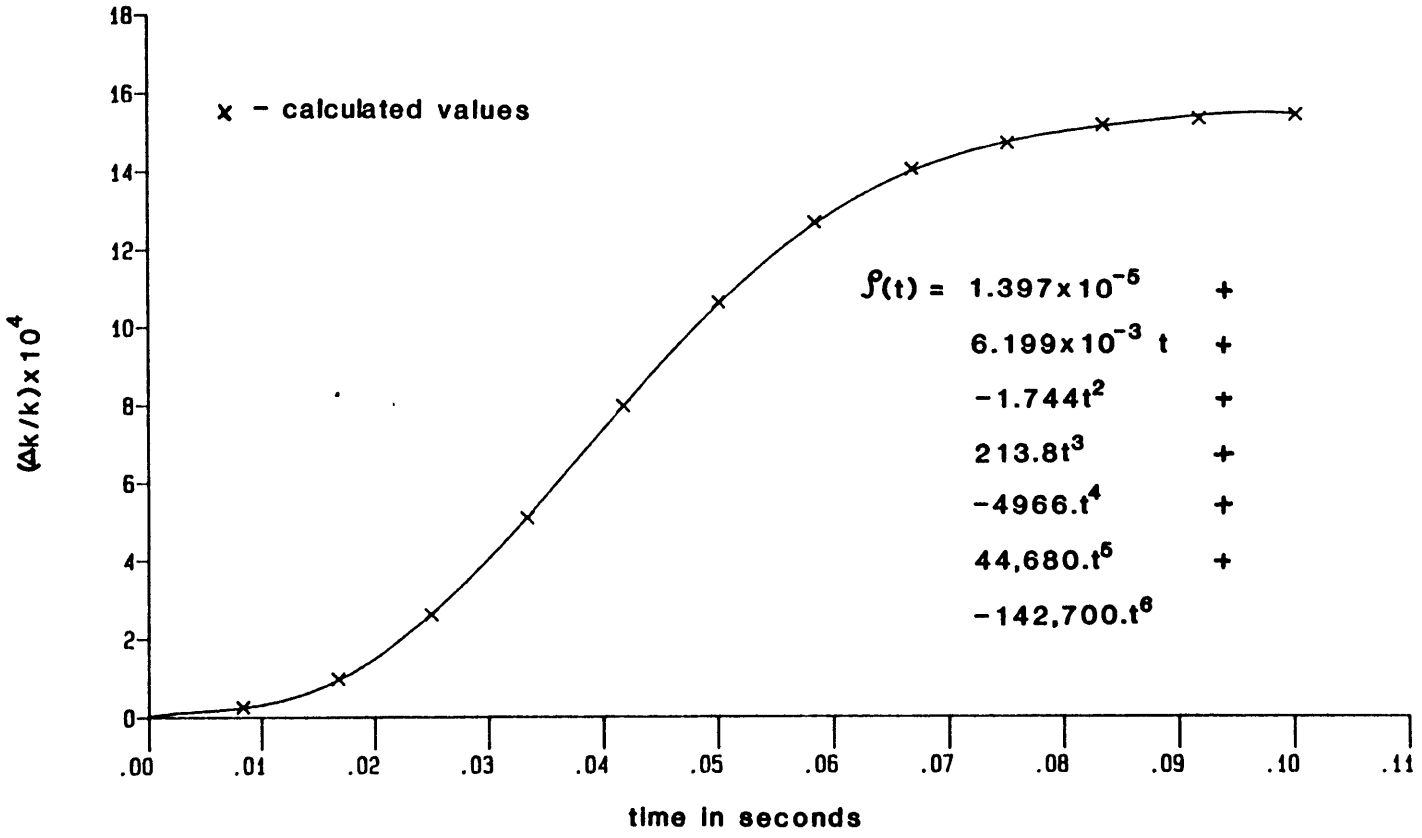

Figure 7.3 PWR Center Rod Ejection Reactivity Curve

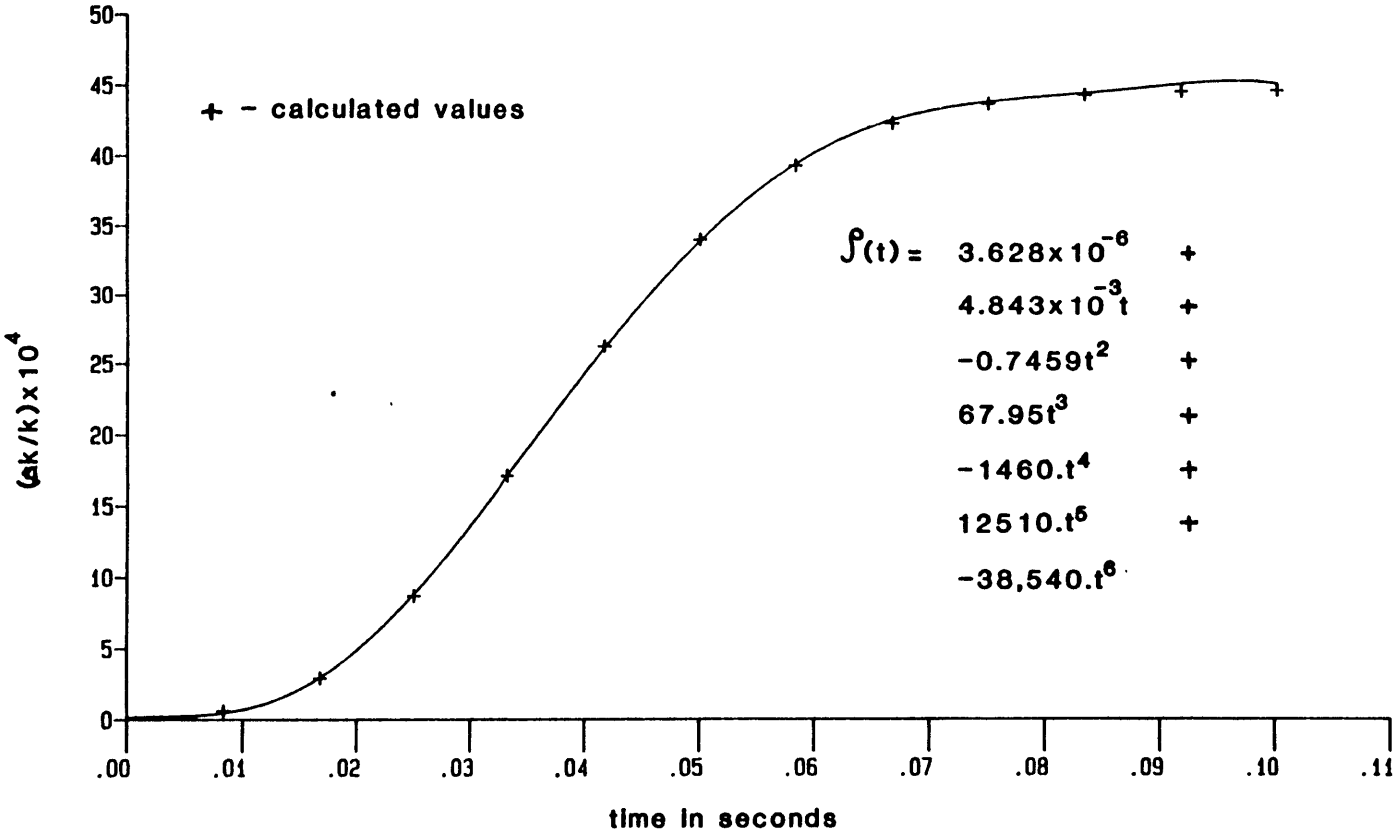

Figure 7.4 PWR Edge Rod Ejection Reactivity Curve

Table 7.3

THERMIT-3 PWR Reactivity Feedback Coefficients

	Fuel Temperature	Moderator Temperature	Moderator Density
Reference Feedback Parameters	942.5°K	575.0°K	723.2 kg/m^3
Off-Reference Feedback Parameters	1042.5°K	610.0°K	643.2 kg/m^3
Off-Reference Eigenvalue	1.009177	1.009715	1.005566
$\Delta k/k$	-0.0117	-0.0111	-0.0064
Reactivity Feedback Coefficient	$-2.8634 \times 10^{-5}/°K$	$-6.6624 \times 10^{-5}/°K$	$8.0392 \times 10^{-5}/(\frac{kg}{m^3})$

is also an option for flux-squared weighting of the nodal contributions to the reactivity feedback. In this case, core-averaged reactivity feedback coefficients with no weighting were used and the procedure described above reduces to determining the product of the core-average reactivity feedback coefficient and the core-averaged change in the feedback parameter.

The approach used to generate reactivity feedback coefficients for the THERMIT-3 analyses is a standard technique used for point kinetics analyses. In the adiabatic method, reactivity feedback coefficients are generated which include the effect of changes in the flux shape caused by the perturbation, neglecting delayed neutrons. This approach requires three additional static QUANDRY analyses for each control rod position during the control rod ejections, a total of seventy-two in all. In addition, THERMIT-3 does not accept time-dependent reactivity feedback coefficients and therefore required modifications to perform an adiabatic point kinetics analysis. As a result, the reactivity feedback coefficients were not determined in the manner of the adiabatic approximation. The THERMIT-3 analyses, therefore, used a hybrid point kinetics method consisting of adiabatic control rod reactivity curves with more approximate reactivity feedback.

7.3 Steady-State Results

The THERMIT-3 steady-state analysis produced results very similar to the TITAN steady-state analysis. THERMIT-3 assumes an initially critical reactor with a known power distribution, so no neutronic calculations are performed in the steady-state analysis. The few differences between the TITAN and THERMIT-3 results were because of

disagreements in the axial power shapes, as discussed previously. Table 7.4 shows a comparison of the maximum fuel and cladding temperatures from the TITAN and THERMIT-3 analyses. The THERMIT-3 maximum fuel temperature was greater than the TITAN maximum fuel temperature, but the maximum cladding temperature was lower. The locations of these maximum temperatures were the same or very close in both cases. The largest discrepancy in fuel temperatures was 122.8°K and occurred in the fuel assemblies with partially inserted control rods. These differences in steady-state fuel temperatures must be considered in evaluating the transient results.

7.4 THERMIT-3 Control Rod Ejection Results

A coupled point kinetics/thermal-hydraulics analysis of the center and edge control rod ejections was performed with THERMIT-3. The steady-state solution was used as the starting point in each case and the analyses were run to 1.0 seconds. Figure 7.5 shows a comparison of the THERMIT-3 and TITAN center rod ejection reactor power as a function of time. The three-dimensional analysis produced a stronger power excursion than the point kinetics analysis. Selected results from the THERMIT-3 and TITAN analyses are presented in Table 7.5. The table shows that the time of the maximum power was somewhat earlier in the THERMIT-3 analysis. The maximum fuel temperature (through 1.0 seconds) was higher in the THERMIT-3 case despite the smaller power excursion and lower integrated power. There are two reasons for this. In the first place, the maximum steady-state fuel temperature was greater for THERMIT-3 because of differences in the power distribution. In addition, changes in the flux shape in the TITAN analysis produced a smaller

Table 7.4

THERMIT-3 and TITAN Steady-state PWR Fuel Temperatures

	THERMIT-3	TITAN
Maximum Fuel Temperature, °K	1581.42	1506.94
Location of Maximum Fuel Temperature: Channel, Axial Level	8,4 46,4	8,5 46,5
Maximum Cladding Temperature, °K	611.17	613.94
Location of Maximum Cladding Temperature: Channel, Axial Level	46,6	46,6
Fuel Temperature at Location of Maximum Disagreement, °K	1070.2	1193.0
Location of Maximum Disagreement: Channel, Axial Level	21,4	21,4

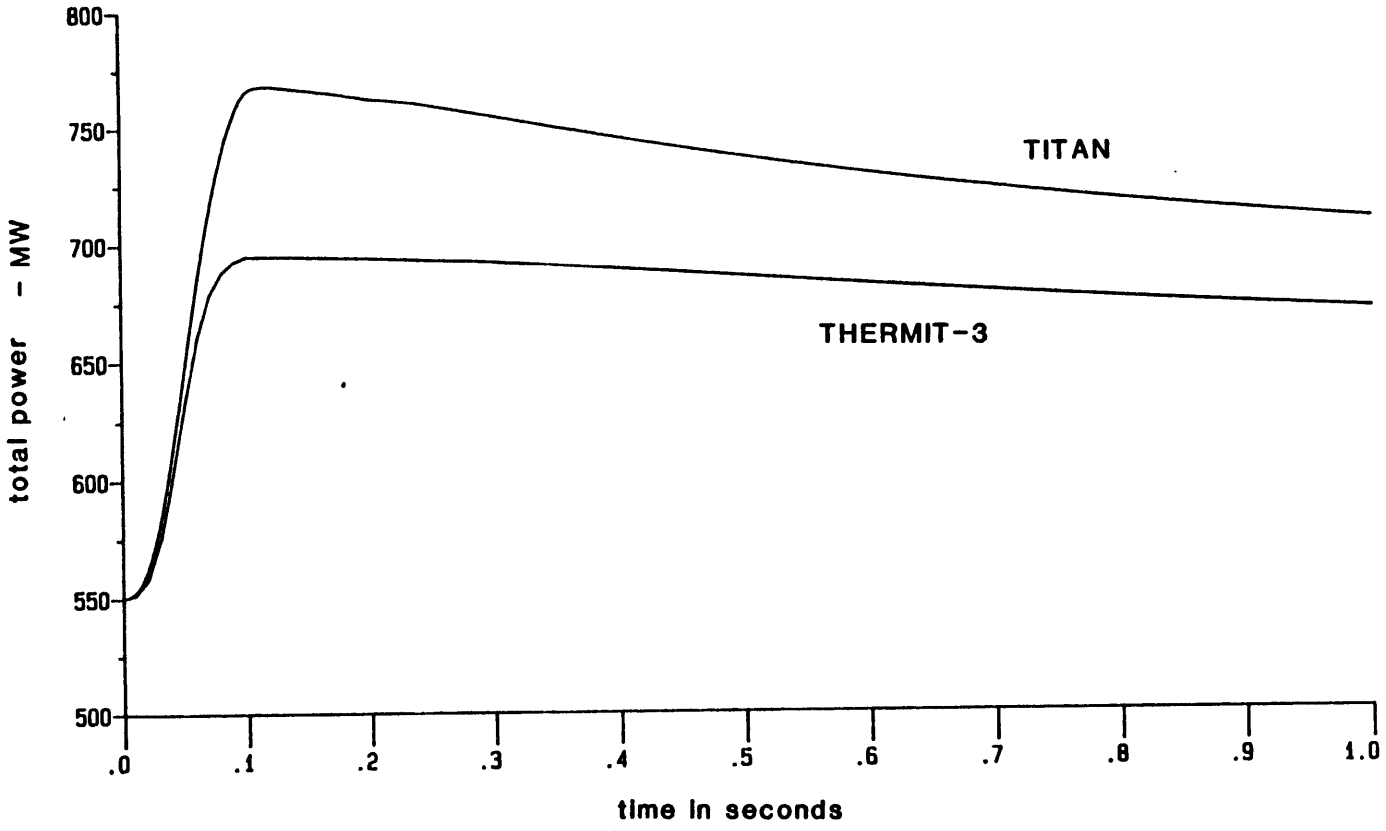

Figure 7.5 PWR Center Rod Ejection, TITAN and THERMIT-3:

Power versus Time

Table 7.5

THERMIT-3 Center Control Rod Ejection Results

	THERMIT-3	TITAN
Maximum Power, kw	694.95	768.16
Time of Maximum Power, s	0.100	0.116
Maximum Power Rise, kw	144.95	218.16
Integrated Power, MW-s	677.41	723.63
Maximum* Fuel Temperature, °K	1622.33	1537.61
Location: Channel, Axial Level	8,5 46,5	8,4 46,4
Maximum* Cladding Temperature, °K	615.43	617.29
Location: Channel, Axial Level	8,6 46,6	8,6 46,6
Computer Time Required, MULTICS cpu-s	2753.10	2731.46
Number of Time-steps	178	80
cpu-s/time-step/node	0.0274	0.0526

*maximum during calculation time of 1.0 s

increase in fuel temperature at the hot spot than was predicted by THERMIT-3. This demonstrates that three-dimensional effects are very important in any attempt to evaluate the true margin between analytical results and design limits. The maximum cladding surface temperature was higher in the TITAN analysis, but the increase was actually smaller than in the THERMIT-3 analysis. This is also a spatial effect.

The THERMIT-3 analysis required more computer time than the TITAN analysis. This result is, in part, a function of choices made regarding time-step size and frequency of neutronic calculations. In both cases the time-step size was increased during the latter stages of the analysis, during which the power was slowly decreasing. However, THERMIT-3 required smaller time-steps than TITAN to produce accurate results for the power decay portion of the transient. As a result, more than twice as many time-steps were calculated in the THERMIT-3 analysis than in the TITAN analysis. Thus, THERMIT-3 was really more efficient than TITAN on a per-time-step basis. Nevertheless, a direct comparison of the total computer time requirements of TITAN and THERMIT-3 is meaningful because the computer time expended was required by the analyses. Therefore, it is significant that the additional capability afforded by the three-dimensional neutronics of TITAN did not require more computer time than THERMIT-3.

A comparison of the THERMIT-3 and TITAN power histories for the edge control rod ejection is shown in Fig. 7.6. Unlike the center rod ejection, the THERMIT-3 excursion was slightly larger than the TITAN excursion. However, Table 7.6 shows that the results were generally very similar. The maximum powers differed by less than 5% and the

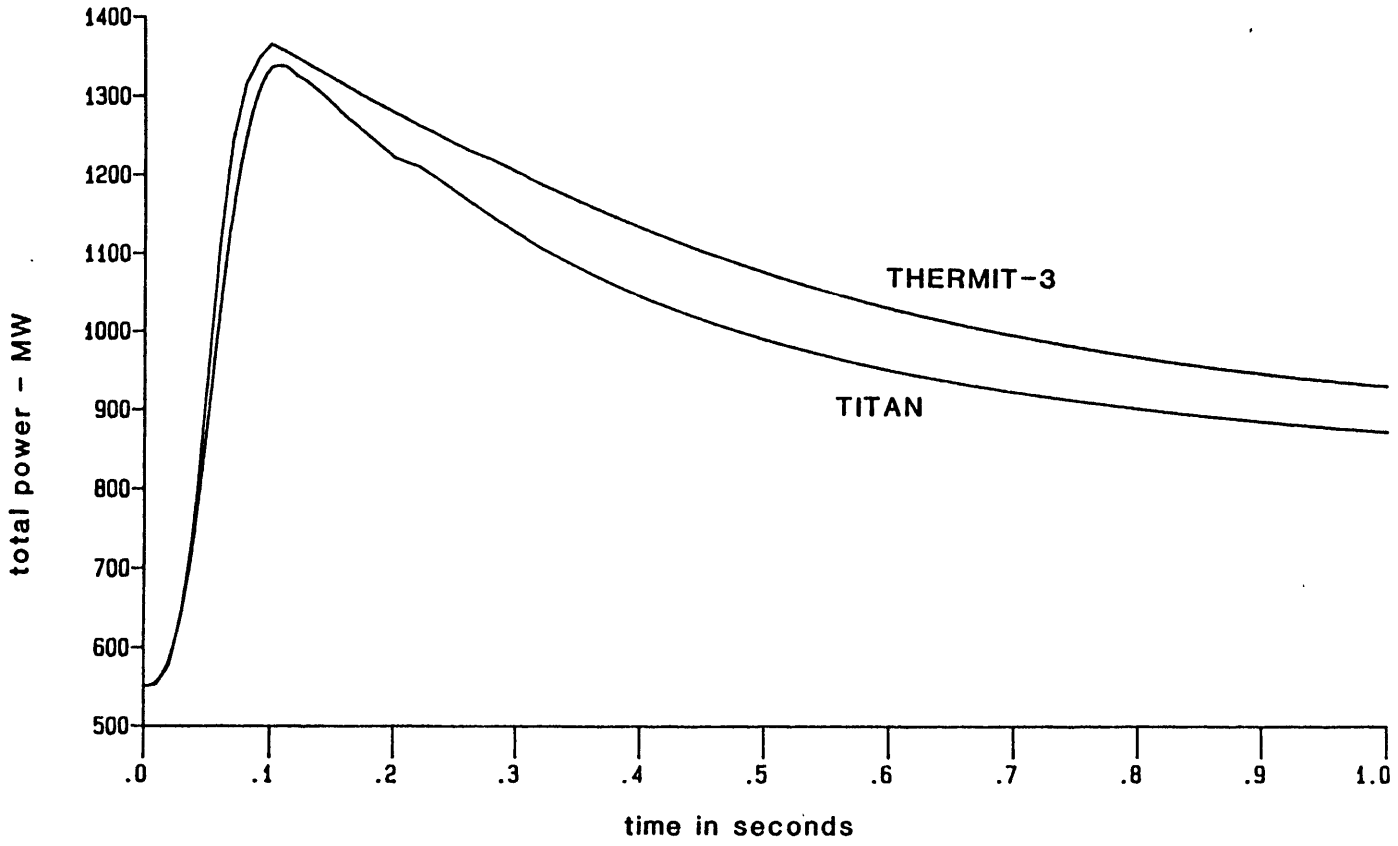

Figure 7.6 PWR Edge Control Rod Ejection, TITAN and THERMIT-3:

Power versus Time

Table 7.6

THERMIT-3 Edge Control Rod Ejection Results

	THERMIT-3	TITAN
Maximum Power, kw	1366.47	1339.2
Time of Maximum* Power, s	0.100	0.104
Maximum Power Rise, kw	816.47	789.2
Integrated Power, MW-s	1071.26	1005.44
Maximum* Fuel Temperature, °K	1747.54	1678.94
Location: Channel, Axial Level	8,5 46,5	8,4 46,4
Maximum* Cladding Temperature, °K	625.45	631.37
Location: Channel, Axial Level	8,6 46,6	8,6 46,6
Computer Time Required, MULTICS cpu-s	4129.30	3364.80
Number of Time-steps	178	80
cpu-s/time-step/node	0.0411	0.0746

*maximum during calculation time of 1.0 s

times of the maximum powers were within four milliseconds of each other. Once again the maximum fuel temperature (through 1.0 seconds) was higher and the maximum cladding surface temperature lower in the THERMIT-3 analysis. However, when the differences in the steady-state conditions are taken into account, the increase in fuel temperature at the hot spot was actually larger in the TITAN analysis. This is a result of a shift in power toward the vicinity of the ejected rod, seen only in the TITAN analysis. Even so, the higher initial fuel temperature and the slightly larger power excursion combined to produce a higher maximum fuel temperature in the THERMIT-3 analysis. However, the point kinetics analysis produced a lower maximum cladding surface temperature that did TITAN. This could be significant if sufficient surface temperature "superheat" was present to produce subcooled boiling or even DNB. However, neither of these was predicted to occur. Finally, the computing time required for the THERMIT-3 analysis was again greater than for the TITAN analysis.

7.5 Summary

Two control rod ejection transients were analyzed with THERMIT-3, a coupled point kinetics/thermal-hydraulics code having a thermal-hydraulics model essentially identical to that of TITAN. The THERMIT-3 results were compared to the TITAN results of Chapter 6. The point kinetics method produced a smaller power excursion than TITAN for the center control rod ejection, and a slightly larger excursion than TITAN for the edge control rod ejection. Correspondingly, the integrated energy deposition for the TITAN analyses was larger for the center control rod ejection and smaller for the edge control rod

ejection. Thus, it seems that the point kinetics method used in the THERMIT-3 analyses does not always provide conservative results for the power history and the integrated energy deposition. The fact that THERMIT-3 produced better agreement with TITAN for the edge control rod ejection transient is difficult to explain in light of the more severe flux tilting observed in the TITAN analysis (see Chapter 6). The combination of the adiabatic approach for control rod reactivities and a less rigorous method for reactivity feedback somehow produced these unexpected results. There is some consolation in the fact that the more approximate methods typically used for the reactivity determination would, in all probability, lead to less accurate results. These results do (at least) illustrate the potential problem of interpreting the results of transient analyses with point kinetics.

The primary goal of the control rod ejection analyses with TITAN and THERMIT-3 was to compare the total reactor power histories prior to scram. Accordingly, the analyses were terminated after 1.0 seconds of transient time had elapsed. The determination of safety-related parameters such as maximum fuel temperature and enthalpy requires an analysis of longer duration. Even so, a comparison of the calculated fuel temperatures does have value. The THERMIT-3 analyses consistently produced higher maximum (centerline) fuel temperatures than the TITAN analyses, in part because of higher steady-state fuel temperatures. Because the integrated power was greater, it is possible that an extended TITAN center control rod ejection analysis would ultimately show a higher overall maximum fuel temperature than an extended THERMIT-3 analysis.

Another important conclusion is that the THERMIT-3 analyses actually required more computer time than the TITAN analyses. Of course, THERMIT-3 is not representative of most coupled codes using point kinetics because of the complexity of its thermal-hydraulics. However, it is significant that the substantial improvement in accuracy offered by three-dimensional nodal neutronics does not require any additional computational effort. In light of the difficulties associated with producing good results using point kinetics, there seems to be a strong incentive for using a three-dimensional nodal neutronics method instead.

Another important conclusion is that the THERMIT-3 analyses actually required more computer time than the TITAN analyses. Of course, THERMIT-3 is not representative of most coupled codes using point kinetics because of the complexity of its thermal-hydraulics. However, it is significant that the substantial improvement in accuracy offered by three-dimensional nodal neutronics does not require any additional computational effort. In light of the difficulties associated with producing good results using point kinetics, there seems to be a strong incentive for using a three-dimensional nodal neutronics method instead.

code THERMIT and the three-dimensional nodal neutronics code QUANDRY were available and well-suited for incorporation in a coupled code. Both codes had been extensively tested and shown to be reliable. Of particular importance was the high degree of accuracy and computational efficiency of the QUANDRY nodal method. The capabilities of these two codes are such that a coupled code based upon them would have the potential of being more generally applicable and physically rigorous than existing coupled codes. Furthermore, this state-of-the-art code could be more computationally efficient than the existing codes of comparable capability. Thus, QUANDRY and THERMIT were chosen as the main constituents of TITAN.

The first major task of this work was the development and implementation of a coupling methodology for QUANDRY and THERMIT. This methodology must produce a unified code capable of generating steady-state solutions as well as analyzing a variety of transients. The numerical solutions of QUANDRY and THERMIT dictated that separate procedures be developed for the steady-state and transient modes of operation. The coupling methodologies for both modes are based on the tandem approach, in which the neutronics and thermal-hydraulics equations are solved separately with the feedback information exchanged as necessary. Some form of tandem coupling was used in all the coupled codes reviewed. Furthermore, a tandem approach was particularly appropriate for TITAN because the utility of the QUANDRY and THERMIT components is strongly dependent on preserving their solution techniques.

The steady-state coupling methodology combines the direct solution method of the static nodal neutronic equations of QUANDRY with the transient approach to steady-state fluid dynamics solution of THERMIT to produce a converged coupled solution. This approach takes advantage of the speed of the QUANDRY static solution in that a number of these solutions are performed during a single TITAN convergence. The convergence of the coupled solution is simple to assess and straightforward to obtain because a complete neutronics solution is performed each time. The resulting power distribution and eigenvalue is therefore consistent with the thermal-hydraulics solution (within the limits of the feedback models). The convergence of the coupled solution can therefore be monitored by observing the convergence of the thermal-hydraulics model. This methodology was implemented and proved to be effective in generating steady-state solutions.

The TITAN transient coupling methodology is a staggered tandem approach with alternating neutronic and thermal-hydraulic time-steps. The nuclear cross sections are updated after each thermal-hydraulic time-step and the power distribution is updated after each neutronic time-step. The staggered procedures differentiate between transients which are initiated by neutronics and those which are initiated by thermal-hydraulics. The type of initiation determines which segment will lead and which will follow during each time-step. For the initial implementation, there is a one-to-one correspondence between neutronic and thermal-hydraulic time-steps and the same time-step size is used for each segment. Of course, the time scales for neutronic and thermal-hydraulic phenomena are often quite different and therefore the

appropriate time-step size for the two segments may be quite different. However, the restriction of one time-step size for both neutronics and thermal-hydraulics was acceptable for the initial development of TITAN.

The TITAN development effort also included the addition of several models and extensions to existing models:

1) A second nuclear cross section model with quadratic coolant density and control rod position dependence was added to the linear model originally used in QUANDRY.
2) A model for direct moderator heating was added to the thermal-hydraulics solution. The amount of direct heating is assumed to vary linearly with moderator density.
3) An optional equilibrium xenon model was added to the steady-state mode. This enhances the calculation of the steady-state power distribution.
4) The control rod cusping correction model was extended to allow its use in modeling reactors without axial reflectors. All of these new and enhanced models were tested and used in the applications reported previously.

8.1.2 Code Applications

TITAN was applied to two distinctly different problems, both in terms of reactor type and problem size. The first application was a boiling water two channel (BW2C) problem which had the virtue of small size and an existing steady-state solution. The BW2C problem was the primary vehicle for debugging and testing TITAN. Numerous steady-state and transient analyses of the BW2C problem were performed.

The second application was a quarter core PWR problem based on a real reactor. Reference solutions for the steady-state and for a control rod ejection transient were available for the PWR problem. Thus, TITAN was applied to the steady-state and transient analysis of a PWR problem of realistic size and the accuracy and economy of the solutions were assessed.

Numerous steady-state analyses based on the BW2C problem were performed with TITAN. Some additional analyses were also performed with QUANDRY and the results compared to TITAN. The TITAN and QUANDRY results were compared to a reference solution produced by the MEKIN code [R-11]. These steady-state analyses led to several interesting conclusions.

1) The steady-state TITAN solution was in good agreement with the MEKIN solution, particularly the power distribution. Some disagreement in fuel rod temperatures was attributable to differences in the fuel thermal properties used. This result demonstrates the effectiveness of the TITAN coupling methodology in producing an accurate steady-state solution.

2) A QUANDRY analysis using a simple feedback model did not produce good agreement with TITAN and MEKIN. This demonstrates the importance of a rigorous thermal-hydraulics model in a coupled code.

3) The sensitivity of the steady-state TITAN results to axial mesh spacing was examined. It was found that reducing the axial mesh spacing produced little change in the solution, thereby demonstrating that the typical node size used in QUANDRY and

THERMIT analyses is appropriate for TITAN.

4) The steady-state TITAN results were shown to be insensitive to increasing the number of thermal-hydraulic time-steps per static neutronic calculation from one to eight. However, the computer time required for the convergence was quite sensitive to this ratio, decreasing by a factor of ≈ 4.7 as the neutronic calculation frequency was decreased.

5) The sensitivity of the steady-state solution to the choice of fuel rod model was also examined. It was found that fuel centerline temperatures were very sensitive to the model employed. A fuel model with constant fuel thermal properties and a constant gap coefficient predicted the highest temperatures, while a fuel model with temperature-dependent fuel properties and gap coefficients predicted the lowest temperatures. The power distribution and most other parameters were rather insensitive to the choice of fuel rod model. Therefore, the choice of fuel rod model can be important if fuel temperatures are expected to be limiting.

The BW2C problem was also used as the basis for a number of transient analyses. These analyses were used for testing and sensitivity studies, but, given the absence of any transient reference solution, not for assessing the accuracy of TITAN. The transients analyzed included null transients, simulated turbine trip transients and control rod withdrawal transients. These analyses led to a number of conclusions.

1) Null transients with both neutronic and thermal-hydraulic "initiation" were analyzed and the steady-state solution was essentially maintained. This indicated that the steady-state solution was properly converged and showed that both modes of the transient coupling methodology operate correctly.

2) The analysis of a pair of simulated turbine trip transients further demonstrated the proper operation of the transient coupling methodology for thermal-hydraulic initiation. The results obtained were in qualitative agreement with the expected behavior of a reactor following a turbine trip.

3) The effect of reducing the axial mesh spacing on the results of a simulated turbine trip was also investigated. The results showed a slight sensitivity of the time-dependent total reactor power and maximum fuel temperature to reducing the axial mesh spacing. The reduction in axial mesh spacing did increase the computer time required approximately linearly with the increase in the number of nodes. Therefore, there was little incentive to use reduced axial mesh spacings for these analyses.

4) A number of analyses were performed in which the rapid withdrawal of a control rod from one of the fuel assemblies produced a super-prompt critical reactivity insertion and a resultant rapid rise in cure power. The power excursion was terminated by feedback alone. The rod withdrawal analyses further demonstrated the proper operation of the transient coupling methodology for neutronic initiation. Unfortunately, no reference solution exists to which the TITAN results could be compared. However, the results were investigated for qualitative correctness and internal consistency. This included a QUANDRY analysis

without feedback to determine the fundamental response of the reactor to the rod withdrawal. The correspondence of the power history and the time-dependent core-average feedback parameters was also used to explain the results. Finally, an energy balance was performed over the course of the transient to demonstrate proper coupling of the neutronic and thermal-hydraulic segments. In light of these investigations, the TITAN results seem to be reasonable.

5) The sensitivity of the rod withdrawal results to axial mesh spacing, time-step size and the cusping correction model were investigated. The power history results were shown to be very sensitive to time-step size. The results were not very sensitive to axial mesh spacing when the time-step was small, but some sensitivity was observed for large time-steps. Similarly, the cusping correction was very important when the analysis involved relatively large time-steps and axial mesh spacings. The results indicate that additional work on the time-step selection and control is needed.

The applications of TITAN to the quarter core PWR problem included a steady-state analysis and two control rod ejection transients. A MEKIN-B solution for the steady-state reactor and the center control rod ejection was used as a basis for comparison. A TITAN analysis of an interior control rod ejection transient was also performed. These analyses produced a number of interesting results.

1) The steady-state TITAN results were compared with the MEKIN-B solution and showed a fundmental disagreement in the horizontal power profiles. The MEKIN-B horizontal power shape was depressed at the core periphery and peaked in the middle. Conversely, the TITAN horizontal

power shape was depressed in the center and peaked at the core periphery. As a result, other parameters such as fuel temperatures and coolant enthalpies did not agree well. However, the reactor eigenvalues and axial power shapes were in good agreement.

2) The disagreement in horizontal power shape between TITAN and MEKIN-B led to an investigation of the horizontal mesh spacings used in the two analyses. A second generation version of QUANDRY was used to determine the effect of reducing horizontal mesh spacing in a two-dimensional (planar) representation of the quarter core PWR for nodal and finite difference solutions of the static neutronics equations without feedback. This investigation showed that the horizontal mesh spacing used in the MEKIN-B analysis was not adequate for the quarter core PWR. Assembly power errors of up to 80% were observed for the finite difference solution with the MEKIN-B mesh spacings. It was also observed that the finite difference solution approached the nodal reference solution as the mesh spacing was successively reduced.

3) The nodal method with the same mesh spacing as the TITAN model (one node per assembly) showed larger errors than were expected from previous experience with QUANDRY. The maximum error in assembly power was 7.3%, which, while higher than expected, was tolerable. Furthermore, a reduction of the error to less than 1% was achieved by having four nodes per fuel assembly.

4) The horizontal mesh sensitivity study provided a reasonable explanation for the discrepancies in the TITAN and MEKIN-B steady-state results. The actual errors in the TITAN and MEKIN-B analysis may be larger or smaller than those observed in the sensitivity study, but it

is clear that a finite difference method would require a very small (and very expensive) horizontal mesh spacing to achieve accuracy equal to the TITAN result for the quarter core PWR. This is a strong demonstration of a major advantage of TITAN over finite difference-based codes such as MEKIN.

5) The TITAN and MEKIN-B transient results for the center control rod ejection reflected the inconsistencies in the steady-state solutions. The TITAN power excursion was milder than that predicted by MEKIN-B, with a maximum power rise about 50% below the MEKIN-B value. This is directly attributable to the discrepancy in the steady-state power shapes. Since the TITAN analysis produced a depressed flux level in the center of the core, the worth of the ejected control rod was significantly less than for the MEKIN-B analysis. The transient did produce significant spatial changes in the neutron flux and power, in the form of a shift toward the center of the core.

6) A second quarter core PWR control rod ejection transient was analyzed with TITAN. In this case, a higher reactivity worth control rod located on the quarter core boundary was ejected. This produced a larger power excursion and significant asymmetric changes in the spatial distribution of flux and power. No MEKIN-B solution is available for this case.

7) The computer running time requirements for the TITAN analyses were all quite reasonable. The steady-state BW2C analyses required 2-10 minutes of MULTICS cpu time. The transient analyses required 1-10 minutes of MULTICS cpu time. The quarter core PWR problem involved many more nodes and therefore required substantially more computer time.

The steady-state convergence required 92 minutes of cpu time. The center and edge control rod ejection analyses required 40 and 56 minutes of MULTICS cpu time, respectively. These transient computer time requirements translate to a usage rate of 0.05 to 0.075 cpu-s/node/time-step. The time-step sizes were generally limited by the time scales of the reactivity insertions rather than by numerical stability limits. The TITAN running times were produced with a non-optimized first generation version. Significant reductions can probably be achieved with the existing methodology by selecting different convergence strategies or by improvements to the code.

8.1.3 Investigation of Point Kinetics and Three-Dimensional Kinetics

The final task in this work was to investigate the importance of three-dimensional neutronics in the analysis of reactivity transients involving significant spatial effects. This was done by analyzing the two quarter core PWR control rod ejection transients with THERMIT-3, which couples THERMIT to a point kinetics model. This was an interesting test because both transients exhibit significant spatial effects which only a three-dimensional neutronics method can really model. Furthermore, the point kinetics and three-dimensional neutronics models are coupled to (essentially) identical thermal-hydraulics models, so the results will directly indicate the impact of the neutronics models.

The reactivity curves required for the THERMIT-3 analyses were generated with QUANDRY using the adiabatic approach, which accounts for changes in flux shape caused by the removal of the rod but neglects the effect of delayed neutrons. Core average reactivity feedback coefficients were generated by applying the effect of uniform changes in each of the feedback parameters to the steady-state reference cross sections and determining the reactivity change.

The results of the THERMIT-3 analyses of the center and edge control rod ejections were compared to the TITAN analyses for the same transients. Some surprising results were obtained.

1) THERMIT-3 produced a smaller power excursion than TITAN for the center rod ejection, resulting in a lower maximum and integrated power. Therefore, point kinetics was not conservative for this case.

2) In contrast, the THERMIT-3 and TITAN results for the edge control rod ejection were actually in rather good agreement, though THERMIT-3 predicted slightly larger maximum and integrated powers than did TITAN. Point kinetics was therefore nominally conservative for this case.

3) The particular point kinetics method used in these analysis did not produce results which differed from TITAN in a consistent manner. The point kinetics results for the transient having greater spatial changes (i.e., the edge rod ejection) were actually closer to the TITAN results. This is at odds with expectations on based theoretical considerations. Therefore, it is not possible to draw a general conclusion about the effect of three-dimensional analysis on these transients.

4) The point kinetics results do demonstrate some of the difficulties associated with lower order methods. Since it cannot be assumed that this point kinetics method produces conservative results, the interpretation and use of the results requires extreme caution. Furthermore, the preparation of the necessary reactivity curves and feedback coefficients made the process of analyzing reactor transients with THERMIT-3 more complicated than with TITAN. The point kinetics analysis was aided by the existence of a full three-dimensional coupled steady-state solution (for the power shape and neutron generation time) and the capability of performing three-dimensional static reactivity calculations. These three-dimensional calculations in support of the point kinetics analyses are not typical and probably account for the rather good results obtained.

5) A final point about the TITAN and THERMIT-3 control rod ejection analyses is that the computer time requirements of the point kinetics analyses were greater than required by TITAN. This was because more frequent feedback exchanges were required to produce physically meaningful results with THERMIT-3. Thus, twice as many time-steps were used by THERMIT-3 to analyze the same transient for the same duration.

8.2 Recommendations for Future Work

The current work completes the initial development, testing and validation of TITAN. There remain several additional areas of potentially fruitful work which should be pursued. Some of these are given in this section in the approximate order of their importance.

1) The reliability and accuracy of TITAN should be assessed further. Comparisons of TITAN results with measured reactor data are particularly

important. Additional comparisons to analytical results can also be helpful.

2) Steps should be taken to improve the computational efficiency of the steady-state mode of TITAN. The steady-state procedures can be modified to use one continuous static neutronic solution in the convergence rather than several, as discussed in Section 4.3.3.1. This approach, if successful, could reduce the steady-state computational requirements significantly. Furthermore, the thermal-hydraulics portion could be modified to take advantage of diagonal symmetry when it is present. The neutronics part currently has this capability.

3) The computational efficiency of the transient mode could also be improved. The restriction of equal time-step sizes for the neutronics and thermal-hydraulics portions during transients should be removed. This would give more flexibility and allow the time-step sizes to be chosen as appropriate for neutronics and thermal-hydraulic time scales. As a result, some unnecessary calculations required by the current approach could be eliminated. The easiest first step is to allow the user to specify the time-step sizes during each time domain. Of course, the problems associated with the Courant stability limit still must be respected. A more advanced approach is to automate the time-step selection process within the code. This is not a straightforward problem because, as has been shown, the results may be very sensitive to the time-step size.

4) The one-to-one coupling between neutronic and thermal-hydraulic control volumes should be replaced by a more general geometry specification. This would allow lumping of thermal-hydraulic regions

while maintaining the usual neutronic detail. This would reduce computational costs for both steady-state and transient modes and permit larger problems to be analyzed. It is also desirable to have neutronics-only nodes for modeling reflectors.

5) The initialization procedures for the fluid dynamics arrays should be extended to provide void fractions. The nodal enthalpies from the simple thermal-hydraulics model could be converted to approximate void fractions by assuming homogeneous equilibrium flow with no slip. In addition, a simple pressure drop calculation could be added to the model to improve the void fraction calculation and to allow initialization of the nodal pressures.

6) The existing time-step logic (or any improved logic added in the future) must be improved to account for occasions when the hydraulic pressure solution does not converge the first time. Currently, the code automatically cuts the time-step size and repeats the pressure iteration. However, the reduced time-step is not used by the neutronics portion and the two get out of phase with each other.

7) The control rod cusping correction model currently is strictly valid only for a uniform axial mesh. This should be extended to allow cusping corrections for non-uniform axial meshes. The "hard-wired" uniform mesh polynomial coefficients in the model can easily be replaced by the actual polynomial coefficients for the mesh used.

8) The restart capabiity should be extended to allow transient restarts. This involves adding additional variables to the dump and restart routines.

9) Modelling fission product decay heat should be considered, particularly for events which last tens of seconds.

There are also several areas of academic interest which should be pursued. The sensitivity of transient results to the fuel rod model option should be investigated. The importance of the two-fluid model in transients with significant boiling could be investigated by forcing TITAN to simulate a homogeneous equilibrium model. The impact of cross-flow on PWR transients can also be investigated. The generality and flexibility of TITAN makes it an ideal tool for computational experiments like these.

The implementation of these suggestions in the future will enhance the already substantial capabilities of TITAN. As a result, the status of TITAN as one of the most advanced publicly available coupled neutronics/thermal-hydraulics codes will be maintained.

Appendix A - Review of Coupled Neutronics/Thermal-Hydraulics Codes

A.1 Introduction

This appendix presents a review of the capabilities of many of the existing coupled neutronics/thermal-hydraulics codes. Public codes for both LWRs and LMFBRs are included, as well as a few proprietary codes. The review is not exhaustive, but provides an overview of the various methods used. Specifically excluded from this appendix are steady-state core simulators and neutronics codes coupled to adiabatic fuel rod models. Thirty-three codes are reviewed herein.

The discussion is organized according to the capabilities of the neutronic and thermal-hydraulic models of the coupled codes. The codes are presented in four groups corresponding to the spatial detail of their neutronic models as follows:

1. point kinetics
2. one-dimensional kinetics
3. two-dimensional kinetics
4. three-dimensional kinetics.

Within each of these categories, the codes are arranged in approximate order of increasing sophistication of their

thermal-hydraulics models, as follows:

1. single-phase flow, lumped heat capacity models
2. two-phase flow, lumped heat capacity models
3. homogeneous equilibrium models
4. advanced two phase models
5. system or loop codes.

The descriptions of each code include the following topics, as appropriate:

1. geometry
2. reactor types
3. coupling method/strategy
4. feedback models
5. two-phase flow treatment
6. direct moderator/ structural heating models
7. boundary conditions
8. special features and capabilities.

A.2 Coupled Codes with Point Kinetics

A.2.1 NOWIG [Y-2]

The NOWIG code combines a point kinetics model with a very simple non-boiling thermal-hydraulics model. The thermal-hydraulics model assumes one-dimensional single-phase water coolant. No pressure drop is calculated; therefore, the reactor is assumed to be at a uniform user-supplied reference pressure. The reactor is subdivided

into thermal-hydraulic channels for which the average coolant temperature and average fuel temperature are calculated. User-supplied flow fractions determine the coolant flow through the hydraulically isolated channels. A lumped capacity technique is used to calculate the average fuel temperature in each channel. In this model the fuel is assumed to have an infinite thermal conductivity, resulting in a uniform temperature throughout the fuel. The cladding and film drop heat flow resistances are modeled, but no fuel-clad gap is considered. Direct moderator heating is modeled as a user-supplied fraction of the channel fission power.

NOWIG assumes that problems begin with an equilibrium state. The steady state flux shapes and temperatures can be generated by some other means and input to NOWIG or the code can generate the steady-state temperature distribution given the equilibrium flux distributions and corresponding adjoint flux distributions.

Transients are initiated by specified changes in the material nuclear properties, changes in the core inlet temperature and changes in the coolant flow rate. The inlet temperature and coolant flow rate can be varied linearly during the course of the transient. No provision is made for more general forcing functions.

The modeling of reactivity transients with NOWIG

differs markedly from the usual point kinetics method in which a time-dependent reactivity function must be specified. NOWIG uses two group macroscopic cross sections to determine the time-dependent reactivity and prompt neutron lifetime. This approach permits a direct and easy comparison with more sophisticated neutronics models. Control rod motions are modeled as changes to the cross sections of a given composition for all channels containing that composition. All channels containing a given neutronic composition are considered to operate in concert with respect to control rod motion. There can be as many different control rod "banks" as there are material compositions. The control rod "banks" may all be withdrawn simultaneously or in a sequence determined by composition number. All control rods move at the same constant velocity and must be initially inserted the same distance into the core. The control rod contributions to the channel cross sections (and, hence, to the total reactivity) are weighted by the fractions of the channel length affected by the presence of a control rod.

The thermal-hydraulic feedback in NOWIG is also handled differently from other point kinetics codes reviewed. As has been mentioned, the thermal-hydraulics model calculates the average fuel temperature and the average coolant temperature in each channel. The average coolant temperatures are transformed into average coolant densities with the aid of built-in fluid property tables and the user-supplied reference pressure. The average coolant densities and fuel

temperatures are then used to calculate the cross sections for the channels according to a model which represents them as linear functions of coolant density and the square root of fuel temperature. This model is like the linear feedback models used in many other more sophisticated coupled codes. It requires a set of reference cross sections, a reference fuel temperature and coolant density, and a set of partial derivatives of the cross sections with respect to coolant density and the square root of fuel temperature for each material composition. In particular, the fast group absorption cross sections, the fast group fission cross sections, and the fast-to-thermal group scattering cross sections are modeled as functions of fuel temperature and coolant density, while the remaining cross sections are modeled as functions of coolant density only.

A.2.2 FORE [G-1], FORE-II [F-1] and "FORE-III" [H-1]

FORE is one of the oldest coupled codes reviewed, having been reported in 1962. FORE-II is an upgraded version of FORE which was reported in 1966. Both codes were developed for fast reactor applications, though their generality (and simplicity) would permit any reactor to be modeled provided the limitations of the models could be tolerated.

FORE combines a point kinetics model with a two channel thermal-hydraulic model. The point kinetics model is a standard one, with the time-dependent reactivity being specified

in tabular form and a linear interpolation performed between table points. The feedback effects modeled are the fuel Doppler (temperature) effect and the thermal expansion of core materials (both dimensional and density effects). The reactivity change associated with the Doppler effect is based on a weighted global average temperature. The contribution of each core region is weighted according to the square of its power density. A user-supplied fraction of the fission energy is assumed to be generated in the clad, structure and coolant.

The thermal-hydraulic model of FORE is interesting because it is a combination of a rather primitive formulation (by today's standards) and a number of special models motivated by fast reactor concerns. The code calculates the time-dependent temperature distributions in two channels representing average and peak core conditions. The channels are cylindrical and are made up of annular rings corresponding to the fuel (up to nine rings), fuel-clad gap, clad and coolant (one ring each). These channels are divided into one to five vertical sections. Heat transfer and temperature calculations for each channel, beginning with the section at the core inlet and proceeding through the channel in the direction of the coolant flow. The flow in each channel is strictly one-dimensional and the channels do not communicate with each other. No pressure

drop is calculated and axial heat conduction is neglected. Much of the flexibility of FORE is due to the lack of built-in models in the heat transfer calculation. The fuel gap and the fuel-coolant heat transfer coefficients are user-supplied constants. The fuel properties are modeled to be a function of fuel temperature according to a quadratic polynomial relation with user-supplied coefficients. A limitation of the code is that two-phase flow cannot be modeled. Both the core inlet temperature and flow remain constant during a transient.

Two unusual features of the thermal-hydraulic model are the fuel melting correction and the representation of structural material in the core. Fuel melting is represented as a correction to the average fuel temperatures corresponding to the heat of fusion of the fuel. This reduces the Doppler feedback when the melting temperature is exceeded since not all the energy produced is being converted to sensible heat. No relocation of melted fuel is modeled, however.

The second interesting feature is the inclusion of structural material in the temperature calculation of the channel sections. This structural material is assumed to be in contact with the coolant and has an internal heat generation due to gamma and neutron heating. The structure is modeled as a lumped capacity having a uniform temperature throughout. This temperature is calculated using the same

heat transfer coefficient as that used for the fuel and coolant.

The FORE-II code was based on the same fundamental models as the FORE code with the relaxation of some of the limitations of the latter and the addition of several models. The point kinetics model was retained and augmented with a control rod model and a decay heat model. Additional feedback models accounting for fuel rod bowing and deformation and coolant voiding were incorporated. The void feedback model of FORE-II is not a traditional mechanistic model; rather it is an attempt to account for an important phenomenon which is beyond the capabilities of the code. The model consists of a user-specified reactivity insertion table which is triggered by the calculation of certain coolant, cladding and fuel temperatures. A simultaneous user-defined reduction of the heat transfer coefficient completes the void "feedback" treatment. The apportionment of gamma and neutron heating among the different core materials is estimated according to the relative masses of the materials.

Most of the improvements incorporated in FORE-II involved the thermal-hydraulics portion of the code. FORE-II models three channels each of which may be divided axially into seven or fewer calculational sections. Each channel can have a distinct axial power profile. The geometry of

the channels is the same as that of FORE, except that up to ten fuel rings may be modeled. The fuel rod calculation is more sophisticated in FORE-II. The one-dimensional conduction equation is solved with a finite difference technique for both steady-state and transient calculations. A fuel-clad gap heat transfer coefficient model allows the gap heat transfer to vary in space and in time. The fuel temperature calculation can be performed for fuel which has a "void" at the center. The radial variation of heat generation within the fuel can be modeled as well as the expansion of fuel and clad. The heat transfer from fuel rod to coolant is defined by a flexible function of coolant conductivity, hydraulic diameter, Reynolds number and Prandtl number. A simple pressure drop calculation is performed for the three channels, including friction and orificing losses. The inlet flow rate and temperature are allowed to vary with time in FORE-II, thus adding additional categories of transients which may be addressed.

A third coupled code based on the FORE model has been developed [H-1] ("FORE-III": no name was given for the code). The point kinetics model and one-dimensional non-boiling thermal-hydraulics model are the main components of the code. This code is not limited to two or three thermal-hydraulic channels and has the capability of modeling other core components such as radial blankets, bypass regions

and plenum regions. Each of the parallel, individually orificed flow channels are connected to common inlet and outlet plena. An integral momentum equation was added to the thermal-hydraulics model to permit the calculation of flow stagnation and reversal. With this formulation, any single-phase compressible coolant can be modeled. The core boundary conditions can be modeled as combinations of the time-dependent inlet and exit pressure and coolant flow rate.

A.2.3 CHIC-KIN [R-1] and PARET [O-1]

Another early coupled neutronics/thermal-hydraulics code was CHIC-KIN [R-1]. It consists of a fairly detailed single channel thermal-hydraulic model coupled to a point kinetics neutronic model. A reactivity feedback scheme incorporates the effects of moderator density changes, moderator temperature changes, fuel expansion and fuel temperature changes. The feedback effects are spatially weighted according to user-specified weighting functions. Direct moderator heating is modeled as a constant fraction of the reactor power.

The thermal-hydraulics model represents the reactor core by a single fuel element with a single coolant channel. Fluid dynamics are represented by a momentum integral model which allows zero flow initial conditions, flow reversal and internal pressure buildup. The two-phase

flow is treated by a homogeneous equilibrium model. A subcooled boiling void fraction model is also included. The fuel element model allows a detailed spatial representation by axial and radial sectionalization. Transients may be initiated by reactivity insertion, changes in inlet enthalpy or temperature, changes in inlet flow rate or core pressure drop or changes in system pressure.

PARET [O-1] is an expanded version of CHIC-KIN which couples a point kinetics model to a four channel thermal-hydraulics model. Each of the four channels represents the average behavior of a specified radial annulus of the core and contains a fuel rod and its associated coolant. The feedback model allows for separate weighting of the Doppler and moderator effects. The neutronic model extrapolates reactivity between thermal-hydraulic calculations and iterates if the extrapolation is significantly in error when the next thermal-hydraulic calculation is performed.

The PARET thermal-hydraulic model has several improvements on that found in CHIC-KIN. Temperature-dependent thermal properties may be specified for the fuel, gap, clad and coolant. Heat transfer correlations for subcooled convective-conductive, nucleate boiling, transition boiling and stable film boiling regimes are included in PARET. Two-phase friction correlations and an improved void fraction model for subcooled boiling were added to the CHIC-KIN model.

A.2.4 NAIADQ [D-3]

The NAIADQ code [D-3] combines a standard point kinetics model with a one-dimensional nonequilibrium thermal-hydraulics model. The feedback effects of fuel expansion, moderator density and moderator temperature are modeled. The reactor core is represented by a single channel having average power and flow rate. The fuel model assumes plate fuel and only solves for the fuel surface temperature. It is the treatment of two-phase flow in NAIADQ that is unusual. The code assumes homogeneous flow, but allows the two phases to be at different temperatures. In particular, the vapor is assumed to be at saturation while the liquid is allowed to superheat. This model is apparently a mechanistic subcooled boiling model which moves away from the lumped parameter approach used in all the other coupled codes reviewed (see Sec 2.1.4). When water adjacent to the fuel reaches saturation, the heat transfer is calculated with a surface boiling correlation. The increase in heat transfer results in the rapid propagation of superheated liquid into the coolant. Vapor is assumed to be generated at a nonequilibrium rate in the expanding superheated layer. The mass exchange between phases is specified by a differential equation. In addition to this advanced model for subcooled boiling, the hydraulic solution in NAIADQ allows for flow reversal.

A.2.5 THERMIT-3 and THIOD-K [D-4]

THERMIT-3 and THIOD-K are two recently developed coupled codes that are strongly related to the current work. A point kinetics model was coupled to THERMIT and THIOD via a reactivity feedback loop and the resultant codes were named THERMIT-3 and THIOD-K, respectively. The GAPOTKIN [H-7] point kinetics model was used in both codes. This model solves the space-independent kinetics equations for a very general form of the reactivity function. The reactivity is specified as dependent on time to simulate control rod motion, as well as dependent on thermal-hydraulic parameters such as void fraction, coolant temperature and fuel temperature. Either core-averaged reactivity coefficients or region-averaged reactivity coefficients may be specified. If region-averaged coefficients are specified, the codes generate core-averaged coefficients using a flux-squared weighting scheme. THIOD-K extrapolates reactivity linearly between thermal-hydraulic calculations when the time-step size is large. This was not found to be necessary in THERMIT-3 because the time-steps are limited in size by the hydraulic solution. The thermal-hydraulics of THERMIT-3 are discussed in Section 3.3.1.

A.2.6 FREADM-1 [F-3]

The FREADM-1 code [F-3] couples a point kinetics

model to a rather detailed thermal-hydraulics model of a tank-type sodium-cooled primary loop. The kinetics model can simulate control rod motion through specified reactivity insertions. The feedback effects modeled are fuel and coolant temperatures, local Doppler, sodium voiding and fuel redistribution. The Doppler coefficients for a given bundle type are dependent on the extent of the voiding within that bundle type. Parabolic fits to static calculations determine the void reactivity effect.

FREADM-1 models a reactor core with annular or cylindrical coaxial regions, each of which is represented by a separate bundle type. Each bundle type is subdivided into a maximum of nine axial sections, each having up to ten radial fuel nodes, a clad node and a coolant node. Two independent primary loops of different sizes may also be modeled. Each loop contains a pump and a heat exchanger. A cover gas model and a check valve model are also included. The code computes temperature distributions in each bundle type assuming temperature-dependent fuel properties but constant properties for the clad and coolant, as well as constant gap and fuel-coolant heat transfer coefficients. The fuel temperature calculation accounts for the heat of fusion when fuel melting is predicted. The fuel model also can include a central void region. Heat transfer to the coolant is assumed to stop when coolant voiding occurs.

The hydraulics model assumes one-dimensional flow through isolated channels. The time-dependent pressures and flow accelerations are calculated by solving a momentum equation for each channel section. Pressure losses due to friction, spacers, velocity and gravity are modeled. Sodium voiding is initiated when a specified fuel or coolant temperature limit is reached. The voids are assumed to occur in a slug flow regime. Perturbations in the coolant flow rate and inlet temperature to one or more bundle types may be used to initiate reactor transients.

The coupling of neutronics and thermal-hydraulics in FREADM-1 involves some interesting features designed to decrease the computational effort. A much smaller time-step is used for the neutronics calculation than for the detailed thermal-hydraulics calculation. A simple model is used to estimate changes in fuel temperatures between heat transfer calculations in order to determine when the new heat transfer calculation should be performed. The actual time-step used is controlled by the amount of voiding previously calculated, the fractional power change, the estimated fuel temperature, the estimated reactivity change and/or proximity (in time) to an elapsed time trigger. A detailed thermal-hydraulics calculation is performed when the estimated change in the average fuel temperature in a channel section exceeds a specified value, or whenever a

specified maximum number of neutronics steps have been performed since the last thermal-hydraulics calculation. This time-step/coupling controller logic can produce acceptable transient results more economically than a coupling strategy which uses a single constant time-step for both neutronics and thermal-hydraulics.

A.2.7 SAS1A [C-3], SAS2A [D-7] and SAS3A [S-3]

The SAS codes have been developed to assess the consequences of severe accidents in liquid metal fast breeder reactors. The codes calculate reactor response to perturbations in power and/or flow resulting from a specified reactivity insertion or coolant flow reduction. The codes are designed to analyze severe accidents, including fuel deformation, melting and core disassembly. As a result, the thermal-hydraulics calculation is very detailed and contains many specific models to handle the extreme conditions of such accidents. Sodium boiling and related hydraulic phenomena are explicitly modeled in the SAS codes. The fuel rod model includes the effects of melting and calculates the transient stresses and strains of the fuel and cladding. Radial and axial expansion of the fuel are modeled, as well as the effects of fuel slumping following melting. Conversely, the neutronics model utilized is a standard point kinetics approximation to the neutron diffusion and precursor equations. This model

will permit control rod motion to be simulated and accounts for feedback from fuel temperature (Doppler broadening), sodium voiding, axial and radial fuel rod expansion, and the slumping of melted fuel. The codes can generate the steady-state thermal-hydraulic conditions needed for the transient calculation.

As their names suggest, there is a progression in time and capability in the three SAS codes reviewed. The previous description applies to all three versions. In what follows, some of the pertinent features of SAS1A are presented first, followed by the changes incorporated in SAS2A and SAS3A.

The SAS1A code models a reactor core as a single average channel which is divided into as many as two hundred axial segments. The transient temperatures in the fuel and coolant are calculated for each of these axial segments. One-dimensional radial heat transfer is assumed in both the fuel and the coolant. Coolant temperatures are calculated for each segment in succession following the direction of the flow. Sodium boiling is modeled in two different regimes. A slip-flow homogeneous equilibrium model is used until the occurence of very high void fractions following a flow reversal and coolant ejection. A slug model is used in the second regime. Neither subcooled boiling nor liquid superheat are modeled; boiling begins when the bulk temperature reaches the saturation temperature

and the two phases remain at saturation. The boiling heat transfer model assumes that a liquid film remains in contact with the channel wall. A time-dependent flow rate may be specified, but the inlet temperature is assumed to be constant.

The fuel rod model in SAS1A is quite sophisticated for a core dynamics code. In addition to calculating the thermal state of the fuel, the model calculates the mechanical behavior as a function of time and space. The fuel rod model includes the temperature dependence of fuel thermal conductivities and heat capacities in calculating a fuel rod having a central void. The dimensional changes due to thermal expansion are modeled and the impact on the fuel-clad gap heat transfer coefficients is included. The reactivity effect of radial and exial expansion is also included. It should be noted that the geometry for the hydraulic calculation is not affected by these expansion calculations and remains constant throughout the transient. The fuel temperature calculation includes latent heat absorption where melting is calculated to occur. The dimensional changes associated with fuel melting are calculated and the reactivity impact of fuel slumping is included.

The SAS2A code has several improvements and additions to SAS1A. SAS2A can accomodate up to ten flow channels.

This requires specification of a radial power shape. Different fuel and cladding properties can be used in each channel. An improved sodium boiling model allows multiple bubbles and slug ejection as well as voiding caused by the release of fission product gas. A given channel may have up to nine gas bubbles, separated by liquid slugs, at any time. An integral momentum equation is solved for liquid-filled channels or for individual liquid slugs. Axial pressure gradients within the bubbles are calculated by the model. The direct deposition of fission energy in the cladding and coolant is modeled as specified fractions of the power produced in the node.

SAS2A has been developed with additional boundary condition capability such that certain aspects of primary loop behavior can be approximated. The time-dependent coolant exit pressure is specified by a tabular forcing function. The time-dependent inlet pressure can be controlled by a simple pump model for which the time-dependent pump head is specified. The time-dependent pump head is determined from a cubic polynomial with specified coefficients or from a specified tabular forcing function. The pressure drop across the core is calculated from the pump head and a time-independent gravity head. The time-dependent coolant flow rate can be specified in place of the pump model. Finally, the time-dependent coolant inlet temperature is specified in tabular form.

The SAS3A code contains several additions and improvements to SAS2A, all of which involve the thermal-hydraulics calculation. A complete loop model has been added which contains a pump, heat exchanger and piping. The loop model is connected to inlet and outlet plena, providing time-dependent pressure boundary conditions for the core model. The pump pressure history is specified by the user. The fuel rod model was enhanced by the addition of models for calculating fuel restructuring, fuel swelling, cladding swelling and fission gas release/retention at steady-state. This obviates the need for auxiliary calculations with a detailed fuel performance code. Models for fuel-coolant interaction and cladding and fuel motion were added for transient calculations. Finally, the multi-bubble sodium boiling model was modified to allow the treatment of a moving sodium film.

A.3 Coupled Codes with One-Dimensional Neutronics

A.3.1 WIGL2 [H-2], WIGL3 [V-1]

WIGL2 and WIGL3 are core dynamics codes which couple a one-dimensional neutronics model to a simple non-boiling thermal-hydraulics model. The neutronics model solves the time-dependent one-dimensional, two-group neutron diffusion and delayed precursor equations for either radial or axial problems. Zero, one or six delayed neutron precursor

groups may be selected. A radial problem is one in which the flux does not vary spatially along the axial dimension. Similarly, an axial problem is one in which the flux does not vary spatially in the transverse direction. For either type of problem, control rod motion may be simulated as changes to the cross sections of selected neutronic compositions.

The coupling between neutronics and thermal-hydraulics includes feedback due to transient xenon concentration, fuel temperature and coolant temperature. Changes in these parameters are converted to changes in the macroscopic cross sections of the neutronic compositions. The moderator temperatures are converted to density and moderator density coefficients are used to modify the cross sections. The temperatures and xenon concentrations are calculated for average regions consisting of a thermal-hydraulic region having a single neutronic composition.

The thermal-hydraulics model is a one-dimensional non-boiling method like that already described for NOWIG. It does not calculate a pressure drop, has a lumped capacity fuel rod model, and cannot handle flow reversal. For a radial problem, the thermal-hydraulic model consists of parallel isolated flow channels for which average temperatures and xenon concentrations are calculated. For an axial type problem, the thermal-hydraulic model consists

of a single channel divided into axial segments.

Transients are initiated by specified changes in inlet coolant temperature, coolant flow rate, or control rod positions. WIGL2 requires that the initial conditions be supplied as input. WIGL3 has a steady-state calculation which includes feedback contributions.

A.3.2 ALMOS [F-2]

The ALMOS code [F-2] combines a one-dimensional neutron kinetics model with a one-dimensional thermal-hydraulics model which includes the loop as well as the core. The neutronics portion of ALMOS uses a nodal method to solve the time-dependent one-dimensional two group neutron diffusion and delayed neutron precursor equations with six delayed groups. The spatial dependence of the flux within a node is expressed by a second-order polymial. Alternatively, the code can use a point kinetics approximation. For the one-dimensional formulation, moderator and Doppler feedback are represented by temperature- and density-dependent cross sections. The point kinetics approximation uses nonlinear reactivity feedback functions.

The thermal-hydraulics model of ALMOS solves the one-dimensional hydrodynamic equations for the core and primary loop. The two-phase model assumes thermodynamic equilibrium with either variable or constant slip between the vapor and liquid. The core is modeled as several parallel coolant

channels. The fuel rod model solves the radial conduction equation assuming temperature-dependent fuel conductivity. Direct deposition of heat in the coolant is also modeled. These models are supplemented by safety and control system models which allow the prediction of large amplitude BWR transients.

A.3.3 RETRAN-02 [M-2]

RETRAN-02 [M-2] is sophisticated systems code for the analysis of light water reactor transients. It couples a flexible one-dimensional thermal-hydraulics model to a one-dimensional neutronics model. The neutronics model uses the space-time factorization method to solve the time-dependent one-dimensional two-group neutron diffusion equations. In this approach, it is assumed that the flux behavior may be separated into a time-dependent amplitude function and a shape function which varies more slowly with time. This method is also known as the quasistatic method. A new amplitude (power) is calculated at each time-step, but the spatial shape is calculated intermittently according to certain internal and specified criteria. When the spatial shape is not calculated for a new time-step, an estimate of the current shape function is made by extrapolating the shape functions of the previous two time-steps. The flux shape is calculated in the axial direction with either vacuum surface zero flux, extrapolated boundary zero flux

or zero current boundary conditions. A point kinetics model is available as an alternative to the one-dimensional formulation. The neutronics model can calculate a steady state power shape prior to the transient analysis. This steady state calculation does not involve iterations with the thermal-hydraulics portion. The initial power shape is therefore calculated using the reference cross sections. Care must be taken that the reference cross sections correspond to the initial thermal-hydraulic state. Feedback is determined by using the changes from this initial thermal-hydraulic state in a generalized polynomial expression for the cross sections. The polynomial involves the three feedback parameters: moderator density, moderator temperature and fuel temperature. Control rod motion is modeled by time-dependent changes in the cross sections. Additional features of the neutronics model include a decay heat model and density-weighted direct moderator heating.

The thermal-hydraulics model in RETRAN-02 solves the mass, energy, and momentum balance equations for a tube-and-tank (or node-junction) mesh. In this formulation, the mass and energy equations and the equation of state are applied to volumes while the momentum equation is applied to junctions connecting the volumes. These volumes and junctions can be used to construct a thermal-hydraulic

model for the core and other components within the plant. The hydrodynamic solution treates two-phase flow by assuming thermodynamic equilibrium with slip between the vapor and liquid. A dynamic slip model uses a differential equation to determine the appropriate time-dependent slip ratio. An average fuel rod is modeled in each core volume, with heat transfer to the coolant controlled by a boiling curve. Sixteen different heat transfer regimes are modeled, including subcooled boiling. A metal-water reaction model is included. The boundary conditions for the core calculation are provided by the loop model as an integral part of the transient analysis.

A.3.4 COSTANZA-CYLINDRICAL [A-2]

COSTANZA-CYLINDRICAL [A-2] is a one-dimensional core dynamics code for LMFBR analysis. The neutronic model solves the time-dependent one-dimensional, two-group neutron diffusion and delayed precursor equations for an infinite cylinder. The reactor is modeled by up to ten concentric annuli, each of which may have a separate flow channel modeled. These annuli are divided axially into a maximum of twenty axial regions. A constant axial power shape is specified for each channel. Control rod movement in each region is modeled as a time-dependent diffused poison, specified in tabular form. The average fuel temperature and coolant temperature in each region

provides the neutronic feedback. The thermal-hydraulics model considers one-dimensional single-phase flow in each of the hydraulically isolated channels. The fuel rod model solves the one-dimensional conduction equation for the fuel, gap and cladding by a finite difference technique. Two different models for the gap heat transfer coefficient are available. Transients may be initiated by control rod movement, or by specified ramp or tabular time-dependent inlet coolant velocity and/or temperature.

A.4 Coupled Codes with Two-dimensional Neutronics

A.4.1 TWIGL [Y-3]

The TWIGL code [Y-3] combines a two-dimensional neutronics model with a simple non-boiling thermal-hydraulics model. The time-dependent two-dimensional, two-group neutron diffusion and delayed precursor equations for an x-z or r-z geometrical mesh. The cross sections are assumed to vary linearly with changes in fuel temperature, coolant temperature and coolant density. The thermal-hydraulic model is a one-dimensional multi-channel formulation having the same assumptions as that in NOWIG, WIGL2 and WIGL3. Transients are initiated by specified time-dependent variations in the cross sections, coolant inlet temperature or flow rate. Transient problems are assumed to start from equilibrium conditions. This can either be generated by TWIGL or input by the user.

A.4.2 ADEP [D-5]

The ADEP code [D-5] combines a one- or two-dimensional neutronics model with a one-dimensional non-boiling thermal-hydraulics model. This flexible formulation allows a reactor core to be modeled in x, r, x-y, or r-z coordinates with an arbitrary number of mesh points. Zero flux boundary conditions are assumed at all external boundaries. The core is divided into a number of calculational regions, each of which contains a single neutronic composition and for which the average fuel and coolant temperatures are calculated. The region cross sections are assumed to vary linearly with changes in the coolant temperature and the square root of the fuel temperature. The thermal-hydraulic model is a one-dimensional non-boiling model based on that of WIGL2, etc. The cross sections in each region can be perturbed during a transient by a specified linear rate of change.

A.4.3 COSTANZA(R,Z) [V-2]

COSTANZA(R,Z) [V-2] is a two-dimensional version of the COSTANZA-CYLINDRICAL code discussed in section A.3.4. The time-dependent two-dimensional, two-group neutron diffusion and delayed precursor equations are solved by a finite difference method for an r-z geometrical core representation. As in COSTANZA, the core is modeled by up to ten concentric rings, each of which contains a

representative flow channel. These rings are divided into an arbitrary number of uniformly spaced axial mesh points. The neutronic regions are overlaid with vertical control regions, each of which has an independent control rod bank. The control rod banks are modeled by an equivalent diffused poison and a linear interpolation resolves control rod motion within a control zone. Changes in the average fuel and coolant temperature are used to modify the cross sections according to a quadratic relationship. The fuel and coolant temperatures are calculated at every axial mesh point, so the feedback resolution is quite high.

The thermal-hydraulics model assumes single-phase liquid or gas. The fuel rod in each channel is divided into concentric rings having a specified constant radial power distribution. An implicit finite difference solution to the time-dependent conduction and fluid energy conservation equations is performed to give the temperature distribution in the fuel and coolant at each axial mesh point in each channel. In addition to control rod motion, transients may be initiated by specified time-dependent flow rates and/or inlet temperatures.

A.4.4 RADYVAR [K-2]

The RADYVAR CODE [K-2] is similar to the COSTANZA (R,Z) code just described. It models a reactor core in r-z geometry with up to twenty annular zones, each having

a coolant channel. The code solves the time-dependent two-dimensional, few group neutron diffusion and delayed precursor equations for an r-z geometry using a variational technique. A maximum of six energy groups and six delayed neutron groups may be used. The radial zones are divided axially into a fine mesh for the neutronics solution and into a maximum of ten axial zones for the thermal-hydraulics and feedback calculation. The boundaries of the axial zones must coincide with the locations of neutronic mesh points.

The feedback model includes the effects of changes in coolant density and fuel temperature as well as radial and axial expansion of the fuel. The thermal-hydraulics model assumes one-dimensional single-phase flow in isolated channels. Up to ten nodes can be modeled in the fuel. The coolant flow rate in each channel is assumed to be a constant during the transient calculation.

2.4.5 COTRAN [P-2]

COTRAN [P-2] is a core dynamics code designed to analyze the BWR control rod drop accident. A finite-difference solution to the time-dependent two-dimensional one-group neutron diffusion and delayed precursor equations is performed for an r-z geometry. The feedback effects of changes in fuel temperature and coolant void fraction are modeled, as well as direct moderator heating.

The thermal-hydraulics model solves the fluid mass,

energy and momentum equations coupled with the fuel rod conduction model. Two-phase flow is handled by a homogeneous equilibrium model. No pressure drop is calculated, so a spatially uniform reference pressure is used.

A.4.6 BNL-TWIGL [D-6]

BNL-TWIGL [D-6] is a two-dimensional core dynamics code with a two-phase thermal-hydraulics model. The code solves the time-dependent two-dimensional two-group neutron diffusion and delayed precursor equations in r-z geometry with a finite difference methodology. Either zero flux or zero current boundary conditions may be used. Control rods are represented by local changes in the cross sections. Multiple control rods may be modeled per channel, each represented by an axially varying density or weight factor. The feedback parameters used are moderator density, moderator temperature, and fuel temperature.

The thermal-hydraulics model assumes one-dimensional homogeneous equilibrium flow with slip. A slip correlation is provided to calculate the relative phasic velocities needed in this formulation. A mixture mass equation and liquid and vapor energy equations are solved for each node. No momentum equation is solved, so the entire reactor is assumed to be at the same pressure. A subcooled boiling model is included. A single fuel rod is modeled in each node and the average fuel temperature is calculated. The

direct deposition of energy in the cladding and coolant is also modeled.

A.4.7 FX2-TH [S-2]

The FX2-TH code[S-2] was developed for transient LMFBR analysis but is applicable to any reactor with single-phase coolant. The code combines a two-dimensional neutron kinetics model with a one-dimensional non-boiling thermal-hydraulics model The two-dimensional neutronics solution can be reduced to one dimension, enabling a reactor core to be modeled in x, r, x-y, r-z, or θ-r coordinates. The time-dependent, two-group neutron diffusion and delayed precursor equations are solved by the improved quasistatic method, in which the point kinetics equations are solved with a periodic recalculation of the spatial flux shape. The macroscopic cross sections for each reactor region are modified by changes in the region average fuel and coolant temperatures.

The thermal-hydraulic model assumes one-dimensional single-phase flow through a number of hydraulically isolated flow channels. These flow channels are usually taken to be the size of a fuel assembly and contain one fuel rod with gap, cladding and associated coolant. For an r-z representation, the flow channels are divided axially into thermal-hydraulic regions. The main purpose of the thermal-hydraulic model is to calculate average fuel and coolant

temperatures for each of these regions. The hydrodynamics solution solves the continuity and energy equations, but not the momentum equation. As a result, no pressure drop is calculated and flow reversal is not allowed. The fuel rod model solves the radial conduction equation assuming a uniform radial heat generation profile and temperature-dependent fuel properties. All of the power produced is assumed to be deposited in the fuel. The heat transfer between fuel and coolant is modeled by a general correlation of Reynolds and Prandtl numbers with specified coefficients and exponents. This permits different single-phase coolants to be modeled. A time-dependent core mass flow rate can be specified via a quadratic forcing function.

A.5 Coupled Codes with Three-Dimensional Neutronics

A.5.1 QUANDRY [S-1]

QUANDRY is a coupled three-dimensional neutronics/thermal-hydraulics code that is fundamental to the current work. It combines a three-dimensional nodal neutronics model with a very simple non-boiling thermal-hydraulics model. A more complete discussion of QUANDRY is presented in Chapter 3, Section 3.2.

A.5.2 MEKIN [B-2], MEKIN-B [A-1], BWKIN [M-3]

MEKIN [B-2] is a three-dimensional light water reactor transient analysis code with feedback. MEKIN was developed at M.I.T. under EPRI sponsorship to be a benchmark code for

verifying the analyses of simpler codes. MEKIN is particularly important for the current work, since it will provide a basis for the assessment of TITAN. As a result, MEKIN will be described in somewhat greater detail than the other codes.

MEKIN operates in a tandem fashion, with information being exchanged between individual neutronic and thermal-hydraulic solution schemes. Both steady-state and transient problems can be analyzed. The neutronic portion utilizes a finite difference solution to the three-dimensional neutron diffusion equations, either in one or two energy groups. Full, half, and quarter core symmetric sections may be modeled with fuel assembly sized volumes (divided axially) of equal dimensions. The neutronic solution accepts zero flux, zero current, or albedo boundary conditions. A transient can be initiated by a perturbation of the base cross sections. In addition, a scram can be simulated during a transient, initiated by overpower, reactor period, or elapsed time. The thermal-hydraulic model is based upon the code COBRA III C/MIT [B-11], a steady-state and transient code capable of both subchannel analysis and lumped channel calculations. This model allows a three-dimensional thermal-hydraulic model with either open or closed flow channels, but requires a uniform axial mesh. Steady-state inlet conditions of coolant flow rate and

enthalpy (or temperature) may be specified for each channel. During a transient, the time-dependence of inlet conditions must be the same for all channels. Core outlet pressure may vary during a transient. Under two-phase conditions, the coolant is modeled as a single fluid with the two phases well mixed (at equilibrium) and uniformly distributed throughout each other. The inclusion of slip ratio correlations allows the vapor and liquid phases to move at different speeds. The code permits a choice of two-phase void fraction models. A one-dimensional finite difference fuel rod model allows an arbitrary number of nodes in the fuel pellet, one node in the clad, and assumes constant material properties. Correlations are included for the forced convection to subcooled water and nucleate boiling heat transfer regimes. The solution method is a semi-explicit marching-type scheme which allows any value of time-step size and axial mesh size without numerical instabilities. The coupling logic begins with the calculation of cross sections for each calculational volume which are appropriate for the current thermal-hydraulic parameters. A neutronic calculation is then performed, taking into account any external neutronic perturbations. The fluxes thus calculated are then used to determine new volumetric heat generation rates, the thermal-hydraulic portion is updated, and a complete thermal-hydraulic calculation (one time-step

in a transient calculation) is performed, including any externally supplied thermal-hydraulic perturbations. An updated set of cross sections for the new thermal-hydraulic conditions is then generated, and the cycle is repeated. In the steady-state this process continues until selected convergence criteria are satisfied. For a transient calculation, one such cycle is used per time-step. The cross section calculation is based on a linear variation with respect to changes in fuel temperature, moderator temperature, and moderator density. The reference cross sections and their partial derivatives are constants supplied by the user.

MEKIN has undergone a considerable amount of investigation [C-5, L-6, R-5, V-4, C-14, G-3, L-7, V-5, C-13] and assessment. As a result, many of its operational characteristics and limitations have been documented. Some of these limitations are inherent in the models and were recognized when the code was developed, while others have been discovered through experience. Many of the inherent limitations are due to the thermal-hydraulics model. Two such limitations are the lack of a pressure drop boundary condition option and the inability to calculate a reverse flow situation. The mathematical model neglects sonic velocity propagation and as a result only transients in which the time scale is greater than the time for a sonic wave to pass through the channel may be analyzed. Treating

the coolant as a single homogeneous fluid is quite adequate for single-phase, low quality, and very high quality two-phase flow. However, it is much less appropriate for annular flow regimes that are often encountered in BWR analyses. The assumption of equilibrium between the phases may result in inaccurate results when extreme power transients are analyzed. Many of the thermal-hydraulic models employed by MEKIN were originally devised for sub-channel analysis, rather than for the lumped channel application typical of a MEKIN analysis. Thus it has been observed that a large channel model provides accurate prediction of hot channel parameters only if the hot assembly is divided into several smaller channels [R-5].

The major disadvantage associated with the neutronics portion of MEKIN is the high cost associated with the fine mesh finite difference solution technique. A fully-converged neutronics solution requires a tight neutronic mesh size (on the order of 2 cm.), resulting in the necessity for a small neutronic time-step. It has been estimated that the calculation of a full core PWR rod ejection transient, with accurate neutronic convergence, would require <u>months</u> of computer time [L-7]! Even modeling a partial core could take days of continuous computer time. Thus it is that the primary application of MEKIN is the calculation of small three-dimensional benchmark problems, rather than the analysis of transients needed for licensing.

MEKIN-B [A-1] is a slightly modified version of MEKIN developed at Brookhaven National Laboratory. The changes made can be characterized as enhancements or refinements of existing capabilities. A new feedback model has been added which represents the coolant density (or void) contribution with quadratic dependency rather than linear, as in the original MEKIN model. The new model also allows the void feedback effect to be dependent on the presence or absence of control rods. The Doppler effect is taken to be linearly dependent on changes in the square root of the average fuel temperature in this new model. An acceleration scheme has been added to the neutronic/thermal-hydraulic coupling for the steady-state calculation. MEKIN-B has added capability to calculate the departure from nucleate boiling ratio for a PWR and the thermal margin for a BWR. Other improvements to the original MEKIN are an improved subcooled boiling, the incorporation of temperature-dependent thermal conductivity and specific heat, and the calculation of fuel enthalpy.

BWKIN [M-3] is the Babcock and Wilcox version of MEKIN. A major modification to MEKIN allows hundreds or thousands of cross section sets to be specified, so that each node can have its own base composition. This permits accurate representation of cases which are not at beginning of life. The feedback model has been enhanced to allow a non-linear representation of cross section response

to changes in fuel temperature, moderator density, etc. Finally, the flexibility of the inlet boundary condition specification has been enhanced such that a number of spatially distributed transient forcing functions can be specified.

A.5.3 HERMITE [R-2]

HERMITE [R-2] is a proprietary multi-dimensional space-time dependent coupled code developed by Combustion Engineering (C.E.) as a benchmark code. HERMITE is a very flexible code, in that the neutronic and thermal-hydraulic portions can be used independently or coupled with feedback. The neutronics portion solves the time-dependent neutron diffusion and precursor equations with from one to four energy groups in one, two or three dimensions. A linear finite element method utilizing Hermite polynomials is the primary solution technique. The solution method allows arbitrary mesh spacings and zero flux or zero current boundary conditions. A 2 x 2 array of mesh elements per fuel assembly is usually required for analyzing C.E. reactors. A full core can be modeled, as well as half and quarter core symmetry sections. In addition to steady-state and transient analyses, HERMITE can also perform depletion calculations. A decay heat model has been added to HERMITE [W-4]. An alternate neutronics model based on the nodal expansion method has also been added to HERMITE [R-12]. This method solves a one-dimensional diffusion

equation for each spatial dimension in each node using polynomials derived by a weighted residual method. A neutron balance condition links the nodes together. The nodal method is designed to be more accurate and economical than the original finite element method. Feedback is accomplished by means of a linear cross section model which accounts for any combination of fuel temperature, moderator temperature, moderator density and soluble boron concentration.

The thermal-hydraulic model solves a three-dimensional, variable area coolant continuity, lateral and axial momentum and energy conservation equations for a homogeneous mixture. The core may be modeled with open or closed channels for which coolant inlet conditions of flow and enthalpy or temperature may be individually prescribed. On option, an inlet pressure distribution/total inlet flow boundary condition uses a special iterative procedure to adjust the inlet flows after each iteration. The code will also accept inlet and outlet pressure distribution boundary conditions. A finite difference fuel rod model allows an arbitrary number of nodes in the fuel and cladding and includes temperature-dependent material properties. Important constitutive relations include several two-phase void fraction models and models for nucleate boiling and forced convection to subcooled water heat transfer regimes.

During a transient calculation, channel inlet conditions may vary independently and core-wide ambient pressure may also vary. HERMITE has been under development for more than nine years and is clearly a very flexible and sophisticated code for the calculation of reactor transients.

A.5.4 CRONOS [K-3]

The CRONOS code [K-3] is the core dynamics module of an integrated PWR analysis package called NEPTUNE. CRONOS combines a three-dimensional finite element neutron kinetics model with a one-dimensional homogeneous equilibrium thermal-hydraulics model. The reactor is modeled as a group of cylindrical vertical channels which are subdivided axially. Cross sections are stored in tables as functions of moderator density and fuel temperature for each composition. The cross sections corresponding to the calculated conditions in each region are obtained by interpolation. The thermal-hydraulics model assumes no cross-flow between the channels. It is almost a standard homogeneous equilibrium model with a mixture mass conservation equation, a mixture energy balance equation, and a vertical momentum balance equation. However, a second energy equation for the liquid enables subcooled boiling to be treated.

A.5.5 ANTI [L-4]

ANTI [L-4] is a fully three-dimensional core dynamics code. The time-dependent three-dimensional one-group neutron diffusion and delayed precursor equations are solved for a coarse mesh representation of a nuclear reactor core. The calculational nodes are usually obtained by subdividing a fuel element axially. The average one-group flux in each of these nodes is calculated assuming that the diffusion between nodes can be accurately modeled by coupling coefficients determined from specified input factors. Two-group cross sections are required for the calculation of feedback effects, but these are collapsed to one-group cross sections prior to the flux calculation. The nodal neutron balance equations are solved by a predictor-corrector method in which the fluxes and power distributions at the advanced time-step are predicted by linear extrapolation from previous time-steps. The balance equations are integrated by a first order backward difference formula and the calculated results are compared to those obtained by the linear extrapolation. If the difference is too large, the time-step size is reduced and the process is repeated. This continues until an acceptable agreement has been obtained. Albedo boundary conditions are used. Control rod motion is represented by time-dependent changes to the local cross sections.

Feedback effects of changes in fuel temperature, moderator temperature and moderator density are modeled. An equilibrium xenon model is provided for the steady-state calculation. The direct deposition of fission energy in the coolant is modeled.

The thermal-hydraulics representation uses a drift flux model with cross-flow and turbulent mixing between parallel channels. The number of channels is limited to ten, so several fuel assemblies are usually lumped together in one channel. One average fuel rod is modeled for each channel, having up to eight fuel nodes, a gap node and a cladding node. All fuel rods are identical in geometry and material properties. One-dimensional radial heat conduction is assumed. The fuel rod and hydrodynamics equations are solved in a fully implicit manner, allowing relatively large time-steps to be used. Time-dependent boundary conditions at the core inlet and outlet must be specified.

A.5.6 RAMONA3B [W-1]

RAMONA3B [W-1] is a three-dimensional coupled neutronics/thermal-hydraulics code designed for analyzing the transient behavior of boiling water reactors. A reactor core is modeled as a number of parallel flow channels plus a bypass channel. Each coolant channel corresponds to one or more fuel assemblies. The code can model a full core or one-half, one-quarter, or one-eighth

symmetric sections. RAMONA3B also models the reactor loop, including the riser region, steam dome, downcomer, jet pump, lower plenum and the steam line out to the turbine. An automatic control system can be used to control the feedwater flow rate, drive pump, steam line valves and control rods.

The neutronics model is based upon a nodal formulation of the time-dependent three-dimensional two-group neutron diffusion and delayed precursor equations in Cartesian coordinates. Each fuel bundle is divided into twenty-four axial nodes. The neutron balance equations are solved in a fast flux coarse mesh formulation with asymptotic thermal flux, also known as the 1½ group method. Core boundaries are treated by albedo boundary conditions. The two-group cross sections used in the calculation are functions of fuel and moderator temperature and void fraction. The presence or absence of control rods and, on option, equilibrium xenon also affect the cross sections. The cross section model allows for corrections to account for such things as spacer grids, reactivity curtains, exposure and void history at each node in the core.

The thermal-hydraulics model of RAMONA3B involves not only the core but also important components of the vessel and loop. The loop model makes RAMONA3B a dedicated boiling water reactor code. The one-dimensional

conservation equations are solved assuming non-homogeneous, non-equilibrium two-phase flow. A separate liquid and vapor mass equation and a mixture energy equation are solved for each node. An integral momentum equation is solved for each channel, accounting for gravity and losses due to spacers, area changes (specified loss coefficients) and friction in the channel and loop. As a result, a single time-dependent system pressure is used in the equation of state. The equations are solved so that the flow direction can be either positive or negative. The two mass equations are related by a slip model in which the vapor velocity is equal to a slip ratio times the liquid velocity plus a bubble-rise velocity. Several correlations for the slip ratio are available to the user. The two phases are not assumed to be in thermal equilibrium, though the vapor is assumed to be at the saturation temperature. The amount of vapor in a node varies with pressure and heat content. Models for surface evaporation/condensation and bulk evaporation/condensation are included; subcooled boiling can therefore be modeled. A fuel rod conduction model is used for every neutronic node. The fuel rod is modeled by several fuel nodes, a gap, and cladding. All of the fuel rods must have the same geometry and material properties.

A.6 Summary

Thirty-three coupled neutronics/thermal-hydraulics codes have been reviewed. The codes span a wide range of capabilities and many show a disparity between the capabilities of their component nodels. Many of the codes use point kinetics and are therefore limited to transients for which an assumption of time-independent spatial behavior is appropriate. Others are limited to single-phase coolants. None of the codes reviewed have the potential for rigor and generality of application that the TITAN code promises.

A few important similarities were also observed among the codes reviewed. All of the neutronics models rely on diffusion theory (or something derived from it). There is a general consistency in using fuel temperature, coolant temperature and coolant density (or void fraction) as feedback parameters. All of the codes use a lumped parameter approach to the calculation of coolant temperature and pressure distributions. Finally, all of the codes use some type of tandem coupling scheme, either with a reactivity loop or a cross section model connecting the neutronics and thermal-hydraulics portions of the calculation.

APPENDIX B: QUANDRY MULTICS CONVERSION

Before the development of TITAN could begin, it was necessary to convert QUANDRY from an IBM 370/168 computer to the MULTICS Honeywell computer. This conversion was accomplished and a number of sample problems were run to demonstrate that the MULTICS version faithfully reproduces results obtained with the original QUANDRY. This was found to be the case, allowing for slight differences in the accuracy of the computers and round-off error.

The conversion involved many changes to the original source code. However, none of the changes involved the physics or numerics of QUANDRY. The essential structure of the code was not changed, nor were the input and output functions modified. The important changes required by the MULTICS conversion were as follows:

(1) Removal of IBM data management package - This useful feature would not work on MULTICS because it included some coding written in IBM assembler. The coding for calculating and assigning container array pointers was also deleted.

(2) Explicit dimensioning of all arrays - All arrays are explicitly dimensioned as appropriate for the problem of interest and in accordance with the storage requirements of each subscripted variable. The container array "G " was deleted.

(3) Addition of several common blocks - These included named common blocks to hold and dimension the integer and real variable arrays.

(4) Removal of all entry points - This was the most complicated part of the conversion. In the IBM QUANDRY, entry points were sometimes used to

transfer large numbers of variable addresses from one subroutine to another. This was done by calling a subroutine in the normal manner with a lengthy argument list and immediately returning to the first subroutine. The subroutine just called would then be entered again by means of an entry point immediately following the first "return" statement. This entry point would have an argument list also, thereby transferring additional variable addresses into the called subroutine. This technique is apparently a way of getting around the limitation on the number of arguments allowed for a subroutine. Unfortunately, this procedure did not work on MULTICS because the addresses of the variables from the original call to the subroutine are not retained when the entry point is used. Therefore, all of the entry point usage was eliminated from the MULTICS version of QUANDRY.

(5) Creation of subroutine RODMOV - In one case, the removal of entry points required the creation of a "new" subroutine. The entry point RODMOV was removed from subroutine PURTO and a subroutine RODMOV was created. Some changes to the argument lists of both subroutines was required, but the workings of the subroutines themselves were not affected.

(6) Reduction of argument list lengths for several subroutines - MULTICS allows fewer subroutine arguments than does IBM, so there were several cases where the number of arguments had been reduced. This was accomplished by deleting unnecessary arguments and by using common blocks.

(7) Addition of simple two-phase thermal-hydraulics - A simple steady-state two-phase thermal-hydraulics model [K-9] was added, replacing the existing single-phase model. The existing transient single-phase thermal-hydraulics model was retained. Therefore, the MULTICS version of QUANDRY can perform static calculations for a BWR but is limited to single-phase coolant for transients.

(8) Addition of function subprograms for hyperbolic functions - It was necessary to calculate double precision hyperbolic cosine, sine and tangent internally, since MULTICS FORTRAN does not support these functions directly. These are calculated in the standard way using exponentials.

The resulting MULTICS QUANDRY works well with no degradation in results. Input data can be used interchangeably between the IBM and MULTICS versions.

Appendix C

Parameters for the Boiling Water Two Channel Problem

Contents:

Table C.1

BW2C Cross Sections

Cross Section	Composition Number 1	2	3	4	5	6	7
D_1	1.4116	1.4115	1.4263	1.4259	1.4261	1.4117	1.4115
Σ_{r1}	0.026684	0.026676	0.026991	0.026983	0.027000	0.026685	0.026675
Σ_{21}	0.016792	0.016814	0.019527	0.019495	0.019490	0.016807	0.016821
$\nu_1 \Sigma_{f1}$	0.0046877	0.0047043	0.0046510	0.0046663	0.0046169	0.0047033	0.0047224
Σ_{f1}	0.0018253	0.0018320	0.0018110	0.0018171	0.0017968	0.0018315	0.0018390
D_2	0.40163	0.40171	0.38887	0.38902	0.38849	0.40151	0.40168
Σ_{r2}	0.067356	0.066530	0.048297	0.049027	0.049430	0.067045	0.066622
$\nu_2 \Sigma_{f2}$	0.069901	0.71751	0.060233	0.067000	0.058840	0.070965	0.72351
Σ_{f2}	0.028899	0.029664	0.024902	0.025095	0.024326	0.029339	0.029912

Reference fuel temperature 922.0 °K
Reference moderator temperature 559.0 °K
Reference moderator density 739.87 kg/m^3

Table C.2

BW2C Cross Section Feedback Coefficients

Composition #1,3

	Type of Feedback		
	Moderator Density	Moderator Temperature	Fuel Temperature
	ρ_m	T_m	T_f
$\frac{\partial D_1^{-1}}{\partial x}$	-0.59009	-4.3067×10^{-4}	-1.7066×10^{-6}
$\frac{\partial \Sigma_{r1}}{\partial x}$	7.2196×10^{-4}	-1.4856×10^{-6}	3.3454×10^{-7}
$\frac{\partial \Sigma_{21}}{\partial x}$	0.022044	-2.2537×10^{-5}	-2.3491×10^{-7}
$\frac{\partial \nu_1 \Sigma_{f1}}{\partial x}$	6.0058×10^{-4}	-7.9119×10^{-7}	-3.4044×10^{-9}
$\frac{\partial \Sigma_{f1}}{\partial x}$	2.3388×10^{-4}	-3.0808×10^{-7}	-1.3256×10^{-9}
$\frac{\partial D_2^{-1}}{\partial x}$	-0.17111	-1.7206×10^{-3}	1.6717×10^{-5}
$\frac{\partial \Sigma_{r2}}{\partial x}$	7.6037×10^{-3}	-8.7008×10^{-6}	-3.7707×10^{-8}
$\frac{\partial \nu_2 \Sigma_{f2}}{\partial x}$	7.3853×10^{-3}	-6.1346×10^{-6}	-7.1430×10^{-8}
$\frac{\partial \Sigma_{f2}}{\partial x}$	3.0533×10^{-3}	-2.5362×10^{-6}	-2.9531×10^{-8}

$x = \rho_m, T_m, T_f$

Table C.3

BW2C Cross Section Feedback Coefficients

Composition #2

Type of Feedback

	Moderator Density ρ_m	Moderator Temperature T_m	Fuel Temperature T_f
$\frac{\partial D_1^{-1}}{\partial x}$	-0.59079	-4.3034×10^{-4}	-1.6877×10^{-6}
$\frac{\partial \Sigma_{r1}}{\partial x}$	7.2332×10^{-4}	-1.4747×10^{-6}	3.3505×10^{-7}
$\frac{\partial \Sigma_{21}}{\partial x}$	0.022046	-2.2528×10^{-5}	-2.3321×10^{-7}
$\frac{\partial \nu_1 \Sigma_{f1}}{\partial x}$	6.2719×10^{-4}	-8.0629×10^{-7}	-2.5533×10^{-9}
$\frac{\partial \Sigma_{f1}}{\partial x}$	2.4425×10^{-4}	-3.1400×10^{-7}	-9.9430×10^{-10}
$\frac{\partial D_2^{-1}}{\partial x}$	-0.17210	-1.7247×10^{-3}	1.2263×10^{-6}
$\frac{\partial \Sigma_{r2}}{\partial x}$	7.5460×10^{-3}	-8.5581×10^{-6}	-8.6205×10^{-9}
$\frac{\partial \nu_2 \Sigma_{f2}}{\partial x}$	7.9765×10^{-3}	-6.3854×10^{-6}	-5.5320×10^{-8}
$\frac{\partial \Sigma_{f2}}{\partial x}$	3.2976×10^{-3}	-2.6399×10^{-6}	-2.2871×10^{-8}

$x = \rho_m, T_m, T_f$

Table C.4

BW2C Cross Section Feedback Coefficients

Composition #4,6

Type of Feedback

	Moderator Density ρ_m	Moderator Temperature T_m	Fuel Temperature T_f
$\frac{\partial D_1^{-1}}{\partial x}$	-0.59160	-4.3000×10^{-4}	-1.7101×10^{-6}
$\frac{\partial \Sigma_{r1}}{\partial x}$	7.4554×10^{-4}	-1.4982×10^{-6}	3.3454×10^{-7}
$\frac{\partial \Sigma_{21}}{\partial x}$	0.022024	-2.2487×10^{-5}	-2.3533×10^{-7}
$\frac{\partial \nu_1 \Sigma_{f1}}{\partial x}$	6.2374×10^{-4}	-8.1312×10^{-7}	-3.4044×10^{-9}
$\frac{\partial \Sigma_{f1}}{\partial x}$	2.4289×10^{-4}	-3.1663×10^{-7}	-1.3257×10^{-9}
$\frac{\partial D_2^{-1}}{\partial x}$	-0.17247	-1.7199×10^{-3}	1.7575×10^{-6}
$\frac{\partial \Sigma_{r2}}{\partial x}$	7.3583×10^{-3}	-8.3914×10^{-6}	-2.7840×10^{-8}
$\frac{\partial \nu_2 \Sigma_{f2}}{\partial x}$	8.4158×10^{-3}	-6.6338×10^{-6}	-8.8094×10^{-8}
$\frac{\partial \Sigma_{f2}}{\partial x}$	3.4794×10^{-3}	-2.7426×10^{-6}	-3.6419×10^{-8}

$x = \rho_m, T_m, T_f$

Table C.5

BW2C Cross Section Feedback Coefficients

Composition #5

Type of Feedback

	Moderator Density ρ_m	Moderator Temperature T_m	Fuel Temperature T_f
$\frac{\partial D_1^{-1}}{\partial x}$	-0.59076	-4.3061×10^{-4}	-1.6732×10^{-6}
$\frac{\partial \Sigma_{r1}}{\partial x}$	7.2775×10^{-4}	-1.4722×10^{-6}	3.3425×10^{-7}
$\frac{\partial \Sigma_{21}}{\partial x}$	0.022060	-2.2545×10^{-5}	-2.3363×10^{-7}
$\frac{\partial \nu_1 \Sigma_{f1}}{\partial x}$	5.7695×10^{-4}	-7.8278×10^{-7}	-5.9576×10^{-9}
$\frac{\partial \Sigma_{f1}}{\partial x}$	2.2454×10^{-4}	-3.0465×10^{-7}	-2.3186×10^{-9}
$\frac{\partial D_2^{-1}}{\partial x}$	-0.17121	-1.7206×10^{-3}	2.6220×10^{-7}
$\frac{\partial \Sigma_{r2}}{\partial x}$	7.1591×10^{-3}	-8.7958×10^{-6}	-7.4789×10^{-8}
$\frac{\partial \nu_2 \Sigma_{f2}}{\partial x}$	6.7151×10^{-3}	-5.9628×10^{-6}	-1.4129×10^{-7}
$\frac{\partial \Sigma_{f2}}{\partial x}$	2.7762×10^{-3}	-2.4652×10^{-6}	-5.8411×10^{-8}

$x = \rho_m, T_m, T_f$

Table C.6

BW2C Cross Section Feedback Coefficients

Composition #7

	Type of Feedback		
	Moderator Density	Moderator Temperature	Fuel Temperature
	ρ_m	T_m	T_f
$\frac{\partial D_1^{-1}}{\partial x}$	-0.59148	-4.3029×10^{-4}	-1.7110×10^{-6}
$\frac{\partial \Sigma_{r1}}{\partial x}$	7.3512×10^{-4}	-1.4783×10^{-6}	3.3412×10^{-7}
$\frac{\partial \Sigma_{21}}{\partial x}$	0.022020	-2.2505×10^{-5}	-2.3533×10^{-7}
$\frac{\partial \nu_1 \Sigma_{f1}}{\partial x}$	6.4344×10^{-4}	-8.1643×10^{-7}	-3.4045×10^{-9}
$\frac{\partial \Sigma_{f1}}{\partial x}$	2.5059×10^{-4}	-3.1795×10^{-7}	-1.3259×10^{-9}
$\frac{\partial D_2^{-1}}{\partial x}$	-0.17249	-1.7233×10^{-3}	1.7459×10^{-6}
$\frac{\partial \Sigma_{r2}}{\partial x}$	7.4998×10^{-3}	-8.4464×10^{-6}	-2.5331×10^{-8}
$\frac{\partial \nu_2 \Sigma_{f2}}{\partial x}$	8.6044×10^{-3}	-6.7088×10^{-6}	-9.1068×10^{-8}
$\frac{\partial \Sigma_{f2}}{\partial x}$	3.5574×10^{-3}	-2.7736×10^{-6}	-3.7650×10^{-8}

$x = \rho_m, T_m, T_f$

Table C.7

BW2C Albedo Sets

Albedo boundary conditions are z-directed and applied at the top of each channel to simulate the neutronic effect of the missing portions of the assemblies.

	Channel 1	Channel 2
AL 1	112.00	105.23
AL 2	0.00	0.00
AL 3	13.776	25.582
AL 4	10.00	10.00
ALRATIO	-1.00	-1.00

The following matrix defines AL 1, AL 2, AL 3, AL 4:

$$\begin{bmatrix} \phi_1 \\ \phi_2 \end{bmatrix}_s = \begin{bmatrix} AL\ 1 & AL\ 2 \\ AL\ 3 & AL\ 4 \end{bmatrix} \cdot \begin{bmatrix} J_1 \\ J_2 \end{bmatrix}_s$$

where "s" indicates the fluxes and leakages are defined at the node surface.

ALRATIO is defined as the ratio of the transverse leakage in the boundary node to the transverse leakage in the adjacent non existent "node" beyond the reactor boundary.

Table C.8

Parameters for QUANDRY Thermal-hydraulic Model, BW2C Problem

Specific heat of fuel:	3.3495×10^6 ergs/gm - °K
Specific heat of moderator:	5.2550×10^7 ergs/gm - °K
Density of fuel:	10.2518 gm/cm^3
Initial core coolant flow rate (reference case):	3.1703×10^4 gm/s
Initial core coolant flow rate (test case):	2.0841×10^4 gm/s
Fuel-coolant heat transfer coefficient:	2.0×10^7 ergs/cm^2 - s - °K
Cladding conductivity/conduction length:	1.0188×10^6 ergs/cm^2 - s - °K
Surface area of cladding/coolant volume:	2.6379 cm^{-1}
Coolant volume fraction:	0.5529
Coolant inlet temperature:	548 °K
Direct moderator heat deposition fraction:	0.0164
Coolant pressure:	7.1361×10^6 Pa
Partial derivative of the product of coolant density and enthalpy with respect to coolant temperature:	1.60×10^7 ergs/cm^3 - °K

Note: units given are those required by the model.

Table C.9

Transient Parameters for BW2C Problem

Control rod velocity - m/s	1.219
Number of delayed neutron groups	1
Effective delayed neutron fraction	0.00725
Effective delayed neutron decay constant, 1/s	0.076719
Group 1 neutron speed, m/s	1,000,000.
Group 2 neutron speed, m/s	4545.

Cross Section Changes for Control Rod Withdrawal

	Composition #1	Composition #7
ΔD_1	0.0147	0.0145
$\Delta \Sigma_{r1}$	3.0700×10^{-4}	3.0200×10^{-4}
$\Delta \Sigma_{21}$	2.7350×10^{-3}	2.7140×10^{-3}
$\Delta \nu_1 \Sigma_{f1}$	-3.6725×10^{-5}	-4.6799×10^{-5}
$\Delta \Sigma_{f1}$	-1.4251×10^{-5}	-1.8226×10^{-5}
ΔD_2	-0.012760	-0.012620
$\Delta \Sigma_{r2}$	-0.019059	-0.018612
$\Delta \nu_2 \Sigma_{f2}$	-9.6689×10^{-3}	-1.06572×10^{-2}
$\Delta \Sigma_{f2}$	-3.9974×10^{-3}	-4.40630×10^{-3}

Appendix D

Parameters for the Quarter Core PWR Problem

Contents:

Table D.1

PWR Fuel Rod Model Data

Fuel rod radius, m	5.36×10^{-3}
Cladding thickness, m	6.17×10^{-4}
Fuel/cladding gap thickness, m	8.255×10^{-5}
Fraction of fuel theoretical density	1.00
Fraction of Pu O_2 in fuel	0.0
Fuel contact pressure, Pa	0.0
Gap roughness, m	4.4×10^{-6} (default value)
Gap gas pressure, Pa	0.0 *
Gap helium fraction	1.0
Fuel burnup, MWd/MTU	0.0

* this means no small gap correction to gas conductivity

Table D.2

PWR Cross Section Feedback Coefficients

Composition #1

	Type of Feedback		
	Moderator Density *	Moderator Temperature	Fuel Temperature
	ρ_m	T_m	$\sqrt{T_f}$
$\frac{\partial D_1}{\partial x}$	-1.0857	6.6667×10^{-7}	3.2094×10^{-4}
$\frac{\partial \Sigma_{r1}}{\partial x}$	0.030664	1.0475×10^{-6}	2.1624×10^{-5}
$\frac{\partial \Sigma_{21}}{\partial x}$	0.025979	9.8533×10^{-7}	-1.5555×10^{-5}
$\frac{\partial \nu_1 \Sigma_{f1}}{\partial x}$	1.9103×10^{-3}	4.5067×10^{-8}	-3.3662×10^{-7}
$\frac{\partial \Sigma_{f1}}{\partial x}$	7.4043×10^{-4}	1.7468×10^{-8}	-1.3047×10^{-7}
$\frac{\partial D_2}{\partial x}$	-0.8562	8.2573×10^{-5}	8.2731×10^{-5}
$\frac{\partial \Sigma_{r2}}{\partial x}$	0.02746	-2.9649×10^{-5}	-3.2371×10^{-5}
$\frac{\partial \nu_2 \Sigma_{f2}}{\partial x}$	0.024124	-4.3945×10^{-5}	-8.4328×10^{-5}
$\frac{\partial \Sigma_{f2}}{\partial x}$	9.9562×10^{-3}	-1.8137×10^{-5}	-3.4803×10^{-5}

$x = \rho_m, T_m, \sqrt{T_f}$ * quadratic density coefficients = 0.0

Table D.3

PWR Cross Section Feedback Coefficients

Composition #2

Type of Feedback

	Moderator Density * ρ_m	Moderator Temperature T_m	Fuel Temperature $\sqrt{T_f}$
$\frac{\partial D_1}{\partial x}$	-1.3014	5.2000×10^{-5}	3.4804×10^{-4}
$\frac{\partial \Sigma_{r1}}{\partial x}$	0.030296	9.5973×10^{-7}	2.0277×10^{-5}
$\frac{\partial \Sigma_{21}}{\partial x}$	0.026945	8.7200×10^{-7}	-1.5590×10^{-5}
$\frac{\partial \nu_1 \Sigma_{f1}}{\partial x}$	1.7627×10^{-3}	6.1200×10^{-8}	-2.4748×10^{-8}
$\frac{\partial \Sigma_{f1}}{\partial x}$	6.8321×10^{-4}	2.3721×10^{-8}	-9.5922×10^{-8}
$\frac{\partial D_2}{\partial x}$	-0.91469	7.1080×10^{-5}	6.8110×10^{-5}
$\frac{\partial \Sigma_{r2}}{\partial x}$	0.036362	-3.3197×10^{-5}	-3.0832×10^{-5}
$\frac{\partial \nu_2 \Sigma_{f2}}{\partial x}$	0.029581	-5.1253×10^{-5}	-9.3069×10^{-4}
$\frac{\partial \Sigma_{f2}}{\partial x}$	0.012208	-2.1153×10^{-5}	-3.8412×10^{-5}

$x = \rho_m, T_m, \sqrt{T_f}$ * quadratic density coefficients = 0.0

Table D.4

PWR Cross Section Feedback Coefficients

Composition #3

Type of Feedback

	Moderator Density * ρ_m	Moderator Temperature T_m	Fuel Temperature $\sqrt{T_f}$
$\frac{\partial D_1}{\partial x}$	-1.2549	6.6667×10^{-7}	3.2094×10^{-4}
$\frac{\partial \Sigma_{r1}}{\partial x}$	0.031151	1.0475×10^{-6}	2.1624×10^{-5}
$\frac{\partial \Sigma_{21}}{\partial x}$	0.028164	9.8533×10^{-7}	-1.5555×10^{-5}
$\frac{\partial \nu_1 \Sigma_{f1}}{\partial x}$	1.5168×10^{-3}	4.5067×10^{-8}	-3.3662×10^{-7}
$\frac{\partial \Sigma_{f1}}{\partial x}$	5.8792×10^{-4}	1.7468×10^{-8}	-1.3047×10^{-7}
$\frac{\partial D_2}{\partial x}$	-0.88789	8.2573×10^{-5}	8.2731×10^{-5}
$\frac{\partial \Sigma_{r2}}{\partial x}$	0.031439	-2.9649×10^{-5}	-3.2371×10^{-5}
$\frac{\partial \nu_2 \Sigma_{f2}}{\partial x}$	0.018529	-4.3945×10^{-5}	-8.4328×10^{-5}
$\frac{\partial \Sigma_{f2}}{\partial x}$	7.6471×10^{-3}	-1.8137×10^{-5}	-3.4803×10^{-5}

$x = \rho_m, T_m, \sqrt{T_f}$ * quadratic density coefficients = 0.0

Table D.5

PWR Cross Section Feedback Coefficients

Composition #4

Type of Feedback

	Moderator Density * ρ_m	Moderator Temperature T_m	Fuel Temperature $\sqrt{T_f}$
$\frac{\partial D_1}{\partial x}$	-1.3307	5.3333×10^{-7}	2.9598×10^{-4}
$\frac{\partial \Sigma_{r1}}{\partial x}$	0.030308	9.2347×10^{-7}	2.0895×10^{-5}
$\frac{\partial \Sigma_{21}}{\partial x}$	0.027113	8.5200×10^{-7}	-1.5051×10^{-5}
$\frac{\partial \nu_1 \Sigma_{f1}}{\partial x}$	1.8757×10^{-3}	7.0800×10^{-8}	5.3490×10^{-8}
$\frac{\partial \Sigma_{f1}}{\partial x}$	7.2703×10^{-4}	2.7442×10^{-8}	2.0732×10^{-8}
$\frac{\partial D_2}{\partial x}$	-0.90324	7.0360×10^{-5}	5.6485×10^{-5}
$\frac{\partial \Sigma_{r2}}{\partial x}$	0.037899	-3.3735×10^{-5}	-3.1639×10^{-5}
$\frac{\partial \nu_2 \Sigma_{f2}}{\partial x}$	0.032123	-5.7853×10^{-5}	-1.0149×10^{-4}
$\frac{\partial \Sigma_{f2}}{\partial x}$	0.013257	-2.3877×10^{-5}	-4.1885×10^{-5}

$x = \rho_m, T_m, \sqrt{T_f}$ * quadratic density coefficients = 0.0

Table D.6

PWR Cross Section Feedback Coefficients

Composition #5

Type of Feedback

	Moderator Density * ρ_m	Moderator Temperature T_m	Fuel Temperature $\sqrt{T_f}$
$\frac{\partial D_1}{\partial x}$	-1.3159	4.2667×10^{-6}	3.3306×10^{-4}
$\frac{\partial \Sigma_{r1}}{\partial x}$	0.030006	9.0453×10^{-7}	2.0264×10^{-5}
$\frac{\partial \Sigma_{21}}{\partial x}$	0.026494	8.1467×10^{-7}	-1.5419×10^{-5}
$\frac{\partial \nu_1 \Sigma_{f1}}{\partial x}$	1.9720×10^{-3}	7.1733×10^{-8}	-9.9848×10^{-9}
$\frac{\partial \Sigma_{f1}}{\partial x}$	7.6433×10^{-4}	2.7804×10^{-8}	-3.8701×10^{-9}
$\frac{\partial D_2}{\partial x}$	-0.91319	6.5693×10^{-5}	5.7341×10^{-5}
$\frac{\partial \Sigma_{r2}}{\partial x}$	0.039742	-3.4748×10^{-5}	-3.0210×10^{-5}
$\frac{\partial \nu_2 \Sigma_{f2}}{\partial x}$	0.036296	-5.6760×10^{-5}	-1.0063×10^{-4}
$\frac{\partial \Sigma_{f2}}{\partial x}$	0.014980	-2.3426×10^{-5}	-4.1532×10^{-5}

$x = \rho_m, T_m, \sqrt{T_f}$ * quadratic density coefficients = 0.0

Table D.7

PWR Albedo Sets

	x,y - directed	z - directed (bottom)	z - directed (top)
AL 1	2.5641	7.6923	7.6923
AL 2	0.00	0.00	0.00
AL 3	3.2967	0.9615	9.7371
AL 4	1.4286	12.50	12.6582
ALRATIO *	-1.00	-1.00	-1.00

The following matrix defines AL 1, AL 2, AL 3, AL 4:

$$\begin{bmatrix} \phi_1 \\ \phi_2 \end{bmatrix}_s = \begin{bmatrix} AL\ 1 & AL\ 2 \\ AL\ 3 & AL\ 4 \end{bmatrix} \cdot \begin{bmatrix} J_1 \\ J_2 \end{bmatrix}_s$$

where "s" indicates the fluxes and leakages are defined at the node surface.

* see Table C.7 for definition of ALRATIO.

REFERENCES

A-1 A. Aronson et al., "MEKIN-B: The BNL Version of the LWR Core Dynamics Code MEKIN," BNL-NUREG Informal Report 28071, Brookhaven National Laboratory (1980).

A-2 A. Agazzi, G. Forti, E. Vincenti, "COSTANZA - Cylindrical, A Cylindrical One Dimensional Dynamics Code for Liquid-Cooled Multi-Channel Nuclear Reactors," EUR 3171.e (1966).

A-3 L. Agee, R. Duffey, S. Banerjee, "Multi-Fluid Models for Transient Two-Phase Flow," NP-618-SR, Electric Power Research Institute (1978).

A-4 A. Acona et al., "Coarse Mesh Techniques for Multidimensional Core Analysis," CONF-780401, Proc. ANS Topical Meeting 'Advances in Reactor Physics,' Gatlinburg, Tennessee, 145 (1978).

A-5 Argonne Code Center: Benchmark Problem Book, ANL-7416, Supplement 2, Argonne National Laboratory (1977).

B-1 D. Billington, "CYCLOPS - A Program for the Solution of the Few Group, One Dimensional Neutron Kinetics Equations with Temperature Feedback, "in Proc. of the Joint NEACRP/CSNI Specialists' Meeting on New Developments in Three-Dimensional Neutron Kinetics and Review of Kinetics Benchmark CAlculations, Garching, F.D.R., 355 (1975).

B-2 R. Bowring, "MEKIN: MIT-EPRI Nuclear Reactor Core Kinetics Code, RP 227, Program Development Notes," CCM-1, Electric Power Research Institute (1975).

B-3 S. Bian, G. Malan, G. Schwenk, "Multidimensional Analysis of PWR Accidents Using the BWKIN (MEKIN) Code," Trans. Am. Nucl. Soc., 34, 315 (1980).

B-4 S. Bian, "Application of Reactivity Weighting to Rod Ejection Accident Analysis in a Pressurized Water Reactor," Nuclear Technology, 41, 401 (1978).

B-5 A. Birkhofer, A. Schmidt, W. Werner, "Comparison of Two- and Three-Dimensional Calculations of Super Prompt Critical Excursions," Nuclear Technology, 24, 7 (1974).

B-6 F. Bennewitz, H. Finnemann, M. Wagner, "Higher Order Corrections in Nodal Reactor Calculations," Trans. Am. Nucl. Soc., 22, 250 (1975).

B-7 A. Basset, Hydrodynamics, Dover Publications Inc., New York (1961).

B-8 T. Bjornard, "Blowdown Heat Transfer in a Pressurized Water Reactor," Ph.D. Thesis, Department of Nuclear Engineering, M.I.T. (1977).

B-9 E. Burns, E. Lim, "MEKIN Simulations of the Peach Bottom - 2 Turbine Trip Experiments," SAI-147-79-PA, Science Applications, Inc. (1979).

B-10 C. Barbehenn, "Neutronic Sensitivity Studies on MEKIN, An Accident Analysis Computer Code for Nuclear Reactors," Nuclear Engineer/ S.M. Thesis, Department of Nuclear Engineering, M.I.T. (1977).

B-11 R. Bowring, P. Moreno, "COBRA IIIC/MIT Computer Code Manual," CCM-4, Electric Power Research Institute (1976).

C-1 H. Cheng, D. Diamond, "Effect of Thermal-Hydraulic Feedback on the BWR Rod Drop Accident," Trans. Am. Nucl. Soc., 33, 474-475 (1979).

C-2 A. Casadei, P. Turinsky, "Subcooled Boiling and Open Channel Effects in PWR Neutronics Calculations," Trans. Am. Nucl. Soc., 32, 718-720 (1979).

C-3 J. Carter et al., "SAS1A, A Computer Code for the Analysis of Fast-Reactor Power and Flow Transients," ANL-7607, Argonne National Laboratory (1970).

C-4 W. Cadwell, A. Henry, A. Vigilotti, "WIGLE - A Program for the Solution of the Two-Group Space-Time Diffusion Equations in Slab Geometry," WAPD-TM-416, Bettis Atomic Power Laboratory (1964).

C-5 A. Cook, "Light Water Reactor Kinetics Analysis with Feedback: An Investigation of the Computer Code MEKIN," Ph.D. Thesis, Department of Nuclear Engineering, M.I.T. (1978).

C-6 R. Crowther, et al., "Reactivity Feedback Modeling and Effects for BWRs," Trans. Am. Nucl. Soc., 32, 724 (1979).

C-7 S. Congdon, R. Linford, "Peach Bottom Turbine Trip Simulation with a One-Dimensional Transient Model," Trans. Am. Nucl. Soc., 30, 219 (1978).

C-8 H. Cheng, D. Diamond, "Thermal-Hydraulic Effects on Center Rod Drop Accident in a Boiling Water Reactor," BNL-NUREG Informal Report 28109, Brookhaven National Laboratory (1980).

C-9 H. Cheng, D. Diamond, "Analyzing the Rod Drop Accident in a Boiling Water Reactor," Nuclear Technology, 56, 40 (1981).

C-10 H. Cheng, M. Lu, D. Diamond, "Effect of Pressure and Flow on the BWR Rod Drop Accident," Trans. Am. Nucl. Soc., 38, 441 (1981).

C-11 J. Collier, Convective Boiling and Condensation, McGraw-Hill Book Company, Limited, London, 65-67 (1972).

C-12 H. Cheng, M. Lu, D. Diamond, "A Space-Time Analysis of Void Reactivity Feedback in Boiling Water Reactors," Nuclear Technology, 41, 229 (1978); also BNL-NUREG-23501, Brookhaven National Laboratory (1977).

C-13 H. Cheng et al., "The Use of MEKIN-B for Light Water Reactor Transient Calculations," BNL-NUREG-28785 (Informal Report), Brookhaven National Laboratory (1980).

C-14 H. Cheng et al., "A Dynamic Analysis of BWR Scram Reactivity Characteristics," BNL-NUREG-50584, Brookhaven National Laboratory (1976).

D-1 J. Duderstadt, L. Hamilton, Nuclear Reactor Analysis, John Wiley and Sons, Inc., New York, 556-565 (1976).

D-2 D. Diamond, "Light Water Reactor Coupled Neutronic and Thermal-Hydraulic Codes," NUREG/CP-0034, Vol. 2, Proc. Am. Nucl. Soc. Topical Meeting: Advances in Reactor Physics and Core Thermal Hydaulics, Kiamesha Lake, New York, 736-751 (1982).

D-3 A. Dalton, "Simulation of Self-Limiting Power Transients in Enriched Nuclear Reactor Cores Using a Thermodynamic Non-equilibrium Axial Flow Model for the Water Coolant," NUREG/CP-0034, Vol. 2, Proc. Am. Nucl. Soc. Topical Meeting: Advances in Reactor Physics and Core Thermal Hydraulics, Kiamesha Lake, New York, 793 (1982).

D-4 D. Dube, "Development of a Fully Implicit Two-Fluid, Thermal-Hydraulic Model for Boiling Water Reactor Transient Analysis," Ph.D. Thesis, Department of Nuclear Engineering, M.I.T. (1980).

D-5 R. Denning, "ADEP, One- and Two-Dimensional Few-Group Kinetics Code," BMI-1911, Battelle Memorial Institute (1971).

D-6 D. Diamond, "BNL-TWIGL, A Program for Calculating Rapid LWR Core Transients," BNL-NUREG-21925, Brookhaven National Laboratory (1976).

D-7 F. Dunn et al., "SAS2A LMFBR Accident-Analysis Computer Code," ANL-8138, Argonne National Laboratory (1974).

D-8 G. Dubois, "The Importance of Flux Shape Changes in Space-Time Kinetics Calculations," in Proc. of the Joint NEACRP/CSNI Specialists' Meeting on New Developments in Three-Dimensional Neutron Kinetics and Review of Kinetics Benchmark Calculations, Garching, F.D.R., 281-320 (1975).

D-9 D. Delp et al., "FLARE: A Three-Dimensional Boiling Water Reactor Simulator," GEAP-4598, General Electric Company (1964).

D-10 L. Dresner, Resonance Absorption in Nuclear Reactors, Pergamon Press Inc., New York, 26-60 (1960).

F-1 J. Fox, B. Lawler, H. Butz, "FORE II, A Computational Program for the Analysis of Steady-State and Transient Reactor Performance," GEAP-5273, General Electric Company (1966).

F-2 W. Frisch, S. Langenbuch, P. Peternell, "The Significance of Fast Moderator Feedback Effects in a Boiling Water Reactor During Severe Pressure Transients," Nuclear Science and Engineering, 64, 843-848 (1977).

F-3 D. Freeman et al., "The FREADM-1 Code: A Fast Reactor Excursion and Accident Dynamics Model," GEAP-13608, General Electric Company (1970).

F-4 D. Ferguson, "Multidimensional Reactor Dynamics Today: An Overview," CONF 750413-P2, Vol. 6, Proc. Conference on Computational Methods in Nuclear Engineering, Charleston, S.C., VI-49 (1975).

F-5 W. Frisch et al., "Necessity and Feasibility of Space-Time-Dependent LWR Calculations," Trans. Am. Nucl. Soc., 20, 461 (1975).

G-1 P. Greebler, D. Shever, N. Walton, "FORE - A Computational Program for the Analysis of Fast Reactor Excursions," GEAP-4090, General Electric Company (1962).

G-2 G. Greenman, K. Smith, A. Henry, "Recent Advances in an Analytic Nodal Method for Static and Transient Reactor Analysis," Proc. Am. Nucl. Soc. Topical Meeting on Computational Methods in Nuclear Engineering, Vol. 1, Williamsburg, Va., 3-49 (1979).

G-3 T. Gozani, H. Kirch, E. Lim, "Dynamic Analysis of Scrammed Power Reactors Interim Informal Report," SAI/SR-147-PA, Science Applications, Inc. (1976).

H-1 K. Hornyik, "Models, Methods and Digital Computer Programs for Analyses in Reactor Dynamics with Emphasis on Fast Breeder Reactors and Compressible Single-Phase Coolants," EURFNR 652 (1968).

H-2 A. Henry, V. Vota, "WIGL2, A Program for the Solution of the One-Dimensional, Two-Group, Space-Time Diffusion Equations Accounting for Temperature, Xenon and Control Feedback," WAPD-TM-532, Bettis Atomic Power Laboratory (1965).

H-3 A. Henry, Nuclear-Reactor Analysis, The M.I.T. Press, Cambridge, MA, 120-124 (1975).

H-4 A. Henry, N. Curlee, "Verification of a Method for Treating Neutron Space-Time Problems," Nuclear Science and Engineering, 4, 727-744 (1958).

H-5 J. Holzer, R. Habert, E. Pilat, "Consistency Considerations in the Use of Point Kinetics for BWR Application," EPRI-WS-80-150, Proc. First International RETRAN Conference, Electric Power Research Institute (1981).

H-6 A. Henry, R. Sims, "A Coarse-Mesh Nodal Diffusion Method Based on Response Matrix Considerations," MITNE-197, Department of Nuclear Engineering, M.I.T. (1977).

H-7 K. Hansen, P. Koch, "GAPOTKIN: A Point Kinetics Code for the Univac 1108," GA-8204, General Atomics, Inc. (1967).

I-1 Indiana and Michigan Electric Company "Donald C. Cook Nuclear Plant, Preliminary Safety Analysis Report," Vol. III, Sec. 14.1.4, pp. 14.1-12.

I-2 M. Ishii, "Foundations of Various Two-Phase Flow Models and Their Limitations," EPRI-WS-81-212, Electric Power Research Institute (1981).

I-3 Iowa Electric Light and Power Company, "Preliminary Safety Analysis Report, Duane Arnold Energy Center," (1968).

J-1 S. Johnson, E. Gyftopoulos, M. Radd, "Effects of Flux-Shape Changes on Power-Excursion Behavior," Trans. Am. Nucl. Soc., 8, 221 (1965).

J-2 J. Jackson et al., "TRAC-P1A: An Advanced Best-Estimate Computer Program for PWR LOCA Analysis," NUREG/CR-0665 (1979).

J-3 O. Jones, "Advances in LWR Thermal Hydraulics" NUREG/CP-0034, Vol. 1, Proc. Am. Nucl. Soc. Topical Meeting: Advances in Reactor Physics and Core Thermal Hydraulics, Kiamesha Lake, New York, 58 (1982).

K-1 J. Kelly, S. Kao, M. Kazimi, "THERMIT-2: A Two-Fluid Model for Light Water Reactor Subchannel Transient Analysis," MIT-EL-81-014, M.I.T. Energy Laboratory (1981).

K-2 G. Kessler, "RADYVAR, Program for the Processing of the Place-Dependent Dynamics of Fast Breeder Reactors with the Aid of the Kantorowitsch Variation Process," EURFNR-682 (1968).

K-3 A. Kavenoky, J. Latard, "The Neutron Kinetics and Thermal-Hydraulic Transient Computational Module of the Neptune System: CRONOS," NUREG/CP-0034, Vol. 2, Proc. Am. Nucl. Soc. Topical Meeting: Advances in Reactor-Physics and Core Thermal Hydraulics, Kiamesha Lake, New York, 781 (1982).

K-4 R, Kern, et al., "PWR Core Response for a Steamline Break Accident - Sensitivity Studies," Trans. Am. Nucl. Soc., 34, 496 (1980).

K-5 J. Kelly, M. Kazimi, "Development and Testing of the Three Dimensional, Two-Fluid Code THERMIT for LWR Core and Subchannel Applications," MIT-EL 79-046, M.I.T. Energy Laboratory (1979).

K-6 J. Kelly, M. Kazimi, "Development of the Two-Fluid Multi-Dimensional Code THERMIT for LWR Analysis," A.I.Ch.E. Symposium Series on Heat Transfer, No 199, Vol. 76, Orlando, Fla., 149 (1980).

K-7 J. Kelly, M. Kazimi, "Interfacial Relations for Two-Fluid Vapor-Liquid Flow: A Simplified Regime-Map Approach," Nuclear Science and Engineering, 81, 305 (1982).

K-8 S. Kao, M. Kazimi, "Critical Heat Flux Predictions in Rod Bundles," Nuclear Technology, 60, 7 (1983).

K-9 H. Khalil, "A Static, Two-Phase, Thermal Hydraulic Feedback Model for the Nodal Code QUANDRY," MITNE-235, Department of Nuclear Engineering, M.I.T. (1980).

K-10 P. Kalambokas, A. Henry, "The Replacement of Reflectors by Albedo-Type Boundary Conditions," MITNE-183, Department of Nuclear Engineering, M.I.T. (1975).

L-1 J. Lamarsh, Introduction to Nuclear Engineering, Addison-Wesley, Reading, MA, 275 (1975).

L-2 J. Lamarsh, Introduction to Nuclear Reactor Theory, Addison-Wesley, Reading, MA, 73 (1972).

L-3 E. Lewis, Nuclear Power Reactor Safety, John Wiley and Sons, New York, 157-205 (1977).

L-4 A. Larsen, "The Three-Dimensional PWR Transient Code ANTI; Rod Ejection Test Calculation," RISO-M-2209 (1980).

L-5 G. Lellouche, D. Diamond, M. Levine, "Application of Reactivity Weight Factors to Reactor Transients," BNL-16650, Brookhaven National Laboratory (1972).

L-6 D. Lanning et al., "The Sensitivity of Light Water Reactor Transient Calculations to Numerical Parameters and Models: A Study of the Computer Code MEKIN," Summary Report, Research Project 811, submitted to Electric Power Research Institute, Department of Nuclear Engineering, M.I.T. (1978).

L-7 D. Lanning, A. Henry, "Experience with the MEKIN Computer Code," Trans. Am. Nucl. Soc., 32, 720 (1979).

L-8 S. Langenbuch, W. Maurer, W. Werner, "Simulation of Transients with Space-Dependent Feedback by Coarse Mesh Flux Expansion Method," in Proc. of the Joint NEACRP/CSNI Specialists' Meeting on New Developments in Three-Dimensional Neutron Kinetics and Review of Kinetics Benchmark Calculations, Garching, F.D.R., 173 (1975).

L-9 S. Langenbuch, W. Maurer, W. Werner, "Coarse-Mesh Nodal Diffusion Method for the Analysis of Space-Time Effects in Large Light Water Reactors," Nuclear Science and Engineering, 63, 437 (1977).

L-10 R. Lawrence, "A Nodal Green's Function Method for Multidimensional Neutron Diffusion Theory Calculations," Ph.D. Thesis, University of Illinois, Urbana, IL (1979).

M-1 F. Motley, T. Morita, "Coupled Nuclear-Thermal Hydraulic Code for Prediction of Core Behavior During Steam Line Break Transient," Trans. Am. Nucl. Soc., 34, 316 (1980).

M-2 J. McFadden et al., "RETRAN-02 - A Program for Transient Thermal-Hydraulic Analysis of Complex Fluid Flow Systems," EPRI-NP-1850, Electric Power Research Institute (1981).

M-3 G. Malan, W. Herwig, "BWKIN Development and Validation," Trans. Am. Nucl. Soc., 41, 608 (1982).

M-4 L. Moberg, J. Naser, J. Rasmussen, "RAMONA Analysis of the Peach Bottom Turbine Trip Tests," Trans. Am. Nucl. Soc., 34, 503 (1980).

M-5 P. MacDonald, L. Thompson, "MATPRO" VERSION 09, A Handbook of Materials Properties for Use in the Analysis of Light Water Reactor Fuel Rod Behavior," TREE-NUREG-1005, E.G. and G., Idaho, Inc. (1976).

O-1 C. Obenchain, "PARET - A Program for the Analysis of Reactor Transients," IDO-17282 (1969).

P-1 J. Park et al., "The Interaction of Neutronics and Thermal-Hydraulics in the Evaluation of BWR Stability," NUREG/CP-0034, Proc. Am. Nucl. Soc. Topical Meeting: Advances in Reactor Physics and Core Thermal Hydraulics, Vol. 1, Kiamesha Lake, New York, 209 (1982).

P-2 D. Pruitt, "COTRAN: A Coupled Neutronic and Thermal-Hydraulic Transient Analysis Code," Trans. Am. Nucl. Soc., 41, 602 (1982).

P-3 D. Parsons, "The Replacement of Reflectors and Baffles in Nodal Calculations by Albedo Boundary Conditions," Ph.D. Thesis, Department of Nuclear Engineering, M.I.T. (1984).

R-1 J. Redfield, "CHIC-KIN: A FORTRAN Program for Intermediate and Fast Transients in a Water-Moderated Reactor," WAPD-TM-479, Bettis Atomic Power Laboratory (1965).

R-2 P. Rohan, S. Wagner, S. Ritterbusch, "HERMITE, A Multi-Dimensional Space-Time Kinetics Code for PWR Transients," CENPD-188, Combustion Engineering Co. (1976).

R-3 P. Rohan, S. Wagner, "Development and Application of Coupled Neutronic/Thermal-Hydraulic Models," Trans. Am. Nucl. Soc., 32, 716 (1979).

R-4 D. Risher, "An Evaluation of the Rod Ejection Accident in Westinghouse Pressurized Water Reactors Using Spatial Kinetics Methods," WCAP-7588, Rev. 1-A, Westinghouse Electric Corporation (1975).

R-5 T. Rodack, L. Wolf, "Sensitivity Study of the Assembly Averaged Thermal Hydraulic Models of the MEKIN Computer Code in Power Transients," MITNE-206, Department of Nuclear Engineering, M.I.T. (1977).

R-6 W. Reed et al., "THERMIT: A Computer Program for Three-Dimensional Thermal-Hydraulic Analysis of Light Water Reactor Cores," EPRI NP-2032, Electric Power Research Institute (1981).

R-7 W. Reed, H. Stewart, L. Wolf, "Applications of the THERMIT Code to 3D Thermal Hydraulic Analysis of LWR Cores," BNL-25484, Brookhven National Laboratory (1979).

R-8 C. Robinson, J. Eckard, "A Higher Order Difference Method for Diffusion Theory," Trans. Am. Nucl. Soc., 15, 297 (1972).

R-9 W. Rivard, M. Torrey, "Numerical Calculation of Flashing from Long Pipes Using a Two-Fluid Model," LA-6104-MS, Los Alamos National Laboratory (1975).

R-10 J. Robinson, "An Analysis of the CHF Prediction Capabilities of THERMIT Under Steady State PWR Conditions," Special Problem Report, Department of Nuclear Engineering, M.I.T. (1981).

R-11 F. Rodriguez-Vera, "Some Benchmark Calculations by Using the Computer Code MEKIN," S.M./Nuclear Engineer Thesis Prospectus, Department of Nuclear Engineering, M.I.T. (1981).

R-12 P. Rohan, S. Wagner, "PWR Spatial Kinetics at Combustion Engineering," Trans. Am. Nucl. Soc., 41, 606 (1982).

S-1 K. Smith, "An Analytic Nodal Method for Solving the Two-Group, Multidimensional, Static and Transient Neutron Diffusion Equations," S.M./Nuclear Engineer Thesis, Department of Nuclear Engineering, M.I.T. (1979).

S-2 R. Shober, T. Daly, D. Ferguson, "FX2-TH: A Two-Dimensional Nuclear Kinetics Code with Thermal-Hydraulic Feedback, ANL-78-97, Argonne National Laboratory (1978).

S-3 M. Stevenson et al., "Current Status and Experimental Basis of the SAS LMFBR Accident Analysis Code System," CONF-740401-P3, Proc. Fast Reactor Safety Meeting, Beverly Hills, CA, 1303 (1974).

S-4 B. Sun, D. Earles, S. Johnson, "Local Reactivity Feedback in PWR Steamline Break Evaluations," Trans. Am. Nucl. Soc., 34, 498 (1980).

S-5 K. Smith, "Spatial Homogenization Methods for Light Water Reactor Analysis," Ph.D. Thesis, Department of Nuclear Engineering, M.I.T. (1980).

S-6 K. Smith, A. Henry, R. Loretz, "Determination of Homogenized Diffusion Theory Parameters for Coarse Mesh Nodal Analysis," in Proc. Am. Nucl. Soc. Topical Meeting: 1980 Advances in Reactor Physics and Shielding, Sun Valley, Idaho, 294 (1980).

S-7 R. Shober, A. Henry, "Non-linear Methods for Solving the Diffusion Equation," MITNE-196, Department of Nuclear Engineering, M.I.T. (1976).

S-8 R. Shober, "A Nodal Method for Solving Transient Few-Group Neutron Diffusion Equations," ANL-78-51, Argonne National Laboratory (1978).

S-9 C. Stewart et al., "COBRA-IV: The Model and the Method," BNWL-2214, Battelle Pacific Northwest Laboratories (1973).

S-10 H. Bruce Stewart, Brookhaven National Laboratory, personal communication (1980).

S-11 Kord S. Smith, Argonne National Laboratory - West, Idaho Falls, Idaho, personal communication (1984).

T-1 T. Thompson J. Beckerley, The Technology of Nuclear Reactor Safety, Volume 1, The M.I.T. Press, Cambridge, MA, p. 11-124 (1973).

T-2 L. Tong, J. Weismann, Thermal Analysis of Pressurized Water Reactors, 2nd ed., The American Nuclear Society, La Grange Park, IL, 33-36, 382-384 (1979).

T-3 C. Tsai, "Assessment of THERMIT Application to Initial Phase of LWR Core Uncovery," S.M. Thesis, Department of Nuclear Engineering, M.I.T. (1982).

T-4 C. Tsai et al., "Development and Quarter Core PWR Rod Ejecton Accident Application of the TITAN Code: Final Report: 1982-1983," MIT-EL 83-007, M.I.T. Energy Laboratory (1983).

T-5 L. Tong, "Prediction of Departure from Nucleate Boiling for an Axially Non-Uniform Heat Flux Distribution," Journal of Nuclear Energy, Pts. A and B, 21 (1967).

V-1 A. Vota, N. Curlee, A. Henry, "WIGL3; A Program for the Steady-State and Transient Solution of the One-Dimensional, Two-Group, Space-Time Diffusion Equations Accounting for Temperature, Xenon, and Control Feedback," WAPD-TM-788, Bettis Atomic Power Laboratory (1969).

V-2 E. Vincenti, A. Clusaz, "COSTANZA (R,Z)," EUR4673e (1971).

V-3 R. Varga, Matrix Iterative Analysis, Prentice-Hall, Englewood Cliffs, NJ (1962).

V-4 J. Valente, "Multidimensional Modeling of the Rod Drop Accident," S.M./Nuclear Engineer Thesis, Department of Nuclear Engineering, M.I.T. (1975).

V-5 M. Van Haltern, "A Sensitivity Study of Thermal-Hydraulic Correlations in the Computer Code MEKIN," S.M. Thesis, Department of Nuclear Engineering, M.I.T. (1980).

W-1 W. Wulff et al., "RAMONA-3B: A Computer Code with Three-Dimensional Neutron Kinetics for BWR System Transients," BNL-NUREG to be pubished, Brookhaven National Laboratory (1982).

W-2 E. Wachspress, Iterative Solution of Elliptic Systems and Applications to the Neutron Diffusion Equations of Reactor Physics, Prentice-Hall, Englewood Cliffs, NJ (1966).

W-3 M. Wagner et al., "Validation of the Nodal Expansion Method and the Depletion Program MEDIUM-2 by Benchmark Calculations and Direct Comparison with Experiment," Atomkernenergie, Bd. 30, Lfg. 2. (1977).

W-4 S. Wagner, P. Rohan, J. Youngblood, "Design Analysis Using Coupled Neutronics and Thermal-Hydraulic Models," CONF-780401, Proc. Am. Nucl. Soc. Topical Meeting: Advances in Reactor Physics, Gatlinburg, TN, 319 (1978).

Y-1 J. Yasinsky, "Notes on Nuclear Reactor Kinetics," WAPD-TM-960, Bettis Atomic Power Laboratory (1970).

Y-2 J. Yasinsky, "NOWIG - A Program to Solve the Point Kinetics Approximation to the One-Dimensional, Two-Group Diffusion Equations with Temperature Feedback," WAPD-TM-806, Bettis Atomic Power Laboratory (1968).

Y-3 J. Yasinsky, M. Natelson, L. Hageman, "TWIGL - A Program to Solve the Two-Dimensional, Two-Group, Space-Time Neutron Diffusion Equations with Temperature Feedback," WAPD-TM-806, Bettis Atomic Power Laboratory (1968).

Y-4 J. Yasinsky, A. Henry, "Some Numerical Experiments Concerning Space-Time Reactor Kinetics Behavior," Nuclear Science and Engineering, 22, 171 (1965).

Y-5 J. Yasinsky, "On the Use of Point Kinetics for the Analysis of Rod-Ejection Accidents," Nuclear Science and Engineering, 39, 241 (1970).

Z-1 B. Zolotar, "A Consistent Modeling Procedure for Utility BWR Analysis," Trans. Am. Nucl. Soc., 32, 717 (1979).

NOMENCLATURE

Abbreviations, Acronyms	Meaning
ATWS	Anticipated Transient Without Scram
BWR	Boiling Water Reactor
BW2C-R, BW2C-T	Boiling Water Two Channel, -Reference, -Test
$\underline{\underline{B}}$	albedo matrix, current form
cal	calories
CHF	Critical Heat Flux
CHFR	Critical Heat Flux Ratio
cm	centimeters
cpu, c.p.u.	central processing unit
D_1, D_2	diffusion constants, fast and thermal groups
DNB	Departure from Nucleate Boiling
DNBR	Departure from Nucleate Boiling Ratio
eV	electron volts
ft	foot, feet
°F	degrees Fahrenheit
g	grams
GW	gigawatt
HEM	homogeneous equilibrium model
j, J	joules
$\bar{J}$	nodal neutron leakage vector
°K	degrees Kelvin
kg	kilograms
kj	kilojoules

Nomenclature continued

Abbreviations, Acronyms	Meaning
kw	kilowatts
LMFBR	Liquid Metal Fast Breeder Reactor
LWR	Light Water Reactor
m	meters
M.C.T.	Maximum Cladding Temperature
MDNBR	Minimum Departure from Nucleate Boiling Ratio
MJ	megajoules
M.L.H.G.R.	Maximum Linear Heat Generation Rate
mm	millimeters
MPa	megapascals
ms	milliseconds
MTU, M.T.U.	Metric Tons of Uranium
MW	megawatts
MWd	megawatt-days
MW(th)	megawatts-thermal
P_o	initial power level
ppm	parts per million
Pa	pascals
PSAR	Preliminary Safety Analysis Report
psi	pounds per square inch
PWR	Pressurized Water Reactor
q"	heat flux
s, S	seconds
SI	International System of units

Nomenclature continued

Abbreviations, Acronyms	Meaning
T	temperature
t	time
v, V	velocity
V	volume
W	watts

Greek

α	void fraction
$\underline{\underline{\alpha}}$	albedo matrix, flux form
Δ	difference
ν_1, ν_2	average number of neutrons emitted per fission, fast and thermal groups
ϕ, $\overline{\phi}$	neutron flux, neutron flux vector
ρ	density
ρ	reactivity
σ	microscopic neutron cross section
Σ	macroscopic neutron cross section
Σ_{r1}, Σ_{r2}	removal cross section, fast and thermal groups
Σ_{21}	scattering cross section, fast to thermal group
Σ_{f1}, Σ_{f2}	fission cross section, fast and thermal groups

Nomenclature continued

subscripts	Meaning
c	coolant
eff	effective
f	fuel
ℓ	liquid
msfb	minimum stable film boiling
v	vapor

BIOGRAPHICAL NOTE

The author was born in Atlanta, Georgia and spent the next twenty-two years in Atlanta, Cordele and Macon, Georgia. He is the son of an accountant and an office worker and has two younger brothers. The author was graduated with honors from Central High School, Macon, Georgia, in 1972, where he was President of the Honorary Society, captain of the Math Team and College Bowl Teams and played in the band. He was a National Merit Finalist and Scholarship Recipient and a Governor's Honors participant. The author was named a Presidential Scholar by President Nixon and honored in a White House ceremony in June, 1972.

The author attended the Georgia Institute of Technology, where he initially majored in physics. He was elected to the national freshman academic honorary Phi Eta Sigma during his first year there. He changed majors to nuclear engineering after two years in order to pursue a more applied course of study and, ironically, to avoid the necessity of a graduate degree. The author was graduated summa cum laude with a Bachelor's of Nuclear Engineering in 1976, having been elected to the national honoraries Tau Beta Pi (engineering), Phi Kappa Phi (academic), and Omicron Delta Kappa (leadership).

In 1976 the author was awarded the John W. Simpson Westinghouse Fellowship of the American Nuclear Society. As a result, he worked for the Nuclear Fuels Division of Westinghouse Electric Company in the summer of 1976.

The author entered the Massachusetts Institute of Technology in the fall of 1976. He was awarded the Sherman Knapp Fellowship for the academic year 1978-1979 by the Department of Nuclear Engineerng and subsequently worked for the Safety Analysis Group of Northeast Utilites Service Company in the summer of 1979. The author received the S.M./Nuclear Engineer's degree from M.I.T. in 1980, having completed a thesis on the thermal-hydraulic design of an ultra-tight pitch PWR core. While at M.I.T., he served as Secretary of the ANS Student Branch and received two citations from the Nuclear Engineering Department for public information contributions. He authored or co-authored four M.I.T. energy lab reports, three conference parpers and one journal article as well as two theses. He was elected to the scientific research society Sigma Xi and the nuclear engineering honorary Alpha Nu Sigma. The author received the Sc.D. degree in Nuclear Engineering in 1984.